STUDY ON APPLICABILITY OF SPHERICAL SHAPED EAF SLAG FINE AGGREGATE IN CONCRETE

ROY SUSHANTA

STUDY ON APPLICABILITY OF SPHERICAL SHAPED EAF SLAG FINE AGGREGATE IN CONCRETE

By

ROY SUSHANTA

A Dissertation Submitted to Nagoya University

In Partial Fulfillment of the Requirements for

The Degree of Doctor of Engineering

Department of Civil Engineering

Graduate School of Engineering, Nagoya University

Nagoya, Japan

ABSTRACT

Electric Arc Furnace (EAF) oxidizing slag is a steel manufacturing by-product. Utilization of EAF slag in concrete as replacement of aggregates is attracting increased popularity due to several reasons such as safe and environment friendly disposal of industrial wastes that contain heavy metals, encounter the problem of depletion of natural aggregate stock for rapid infrastructural development etc.

Recently, a new production method has been developed where slag granules are formed by passing of high-pressure cold air through the molten slag and the slag particles thus obtained become spherical in shape. Due to spherical shape, it is expected that the problems of workability and durability of concrete due to the application of conventional angular shaped EAF slag aggregates can be solved. In addition, because of high particle density chances of obtaining concrete of improved mechanical properties by incorporating spherical shaped EAF slag are high. To validate the above possibilities, a thorough study on the applicability of the newly developed spherical shaped EAF slag fine aggregates in concrete is necessary. Therefore, this study aims to investigate the applicability of spherical shaped EAF slag fine aggregates in concrete at different slag replacement ratio and W/C ratio.

In order to facilitate the study, all physical properties of the newly developed EAF slag were tested. The results indicate that spherical shaped EAF slag possesses higher sphericity (0.92), lower void ratio, larger particle density (3.6g/cc) and lower water absorption than that of angular shaped EAF slag and natural sand.

Based on the material properties, mix proportions were designed for two different W/C, slump and air content of 0.4, 5cm, 5% and 0.6, 12cm, 5% respectively with an aim to investigate the utilization possibility of such material in concrete pavement and normal concrete respectively. From the mix proportions it was confirmed that spherical shaped EAF slag concrete requires 16% lesser mix water and cement than angular shaped EAF slag concrete. Study on the fresh concrete behaviors revealed that spherical shaped EAF slag concrete at higher slag replacement ratio and W/C imparts higher bleeding although corresponding particle settlement due to segregation is very low to negligible.

In so far as the mechanical properties of slag concrete are concerned, spherical shaped EAF slag fine aggregates are found to be advantageous in concrete at lower W/C, slump and air content of 0.4, 5cm and 5% as they impart higher strength and elastic

modulus than normal concrete. In contrary, at higher W/C, slump and air content of 0.6, 12cm and 5% normal concrete showed improved behavior than slag concrete. Regarding durability properties, due to stronger particle resistance, spherical shaped EAF slag concrete showed approximately half of drying shrinkage in comparison to normal concrete when all sand is replaced by spherical slag. In addition, water absorption and air permeability of such concrete are found to be lower than normal concrete.

During thermal change, spherical shaped EAF slag fine aggregate concrete demonstrated improved material stability by showing superior behavior such as lower thermal expansion, thermal conductivity, thermal diffusivity and specific heat than normal concrete. The mechanisms behind such behaviors were clarified as lower porosity, higher particle density and lower moisture content and mineralogical compositions. Improved freezing and thawing resistance of spherical shaped EAF slag concrete is observed up to 200 freezing-thawing cycles, beyond which resistance deteriorates due to lower air retention capacity of such concrete.

Under high temperature exposure, spherical shaped EAF slag concrete showed lower mass loss than normal concrete due to lower volume of cement pastes. Up to a heating exposure of 500°C, spherical shaped EAF slag concrete manifested improved residual elastic modulus and similar to slightly improved residual compressive strength than normal concrete. Image analysis results by DICM confirmed the damage of concrete due to heating in the form of compression closing cracks occurred by heating process and it was proved that the degradation of elastic modulus and compressive strength of concrete due to high temperature heating is dictated by the extent of compression closing cracks.

Regarding water proofing, spherical shaped EAF slag concrete showed improved behavior than normal concrete as the reduction of compressive strength of such concrete under water during static compression test was much lower in comparison to normal concrete. Similarly, concrete produced by spherical shaped EAF slag fine aggregates of higher slag replacement ratio experienced higher fatigue life due to slower damage accumulation than normal concrete under water at lower stress level.

In a nutshell, this study revealed some important findings through the confirmation of the applicability of spherical shaped EAF slag fine aggregates in concrete especially at lower W/C and slump of 0.4 and 5cm. Utilization of this newly developed by-product material in concrete should solve many structural problems and durability concerns and ensure environmentally safe, sustainable and economic construction.

ACKNOWLEDGEMENTS

First of all, I would like to express my deepest gratitude to Almighty Lord Krishna for the immense blessings in bringing out this study successful.

I owe the great debt of gratitude and appreciation to my supervisor Professor Hikaru Nakamura, for his incredible ideas, earnest guidance, personal encouragement, invaluable suggestions and continuous support throughout this study. I felt myself enriched with insightful discussions and splendid motivations in several occasions.

I owe a special debt of gratitude to Assistant Professor Taito Miura for his timely support, patience and understanding and effective ideas during the experimental works related to this study. I would also like to express my heartfelt gratitude to Associate Professor Yoshihito Yamamoto for his advice and important suggestions to improve significant part of this work. Sincere gratitude is also due to the examination committee, Professor Kazuo Tateishi, and Associate Professor Ryo Yoshida for their precious time in providing vital suggestions for the improvement of this dissertation.

Thanks are due to the staff, former and present students of concrete laboratory for their support during administrative as well as experimental works. I am delighted to have many unforgettable memories with them in these three years. I wish my deepest appreciation to Dr. Rodolfo Mendoza, Mr. Takahiro Nanri, Shun-yuan Chi, Naoki Oshima and Atik Sarraz for their excellent support during the laborious days of casting. I am particularly thankful to my tutor Mr. Hirotaka Ishiguro and foreign student advisor Mrs. Hiroko Kawahara for their help in sorting out the daily life difficulties.

I acknowledge the scholarship support from JASSO in the early period of this study. In addition, I am grateful to the Ministry of Education, Culture, Sports, Science and Technology (MEXT-Monbukagakusho) for the Super Global University (SGU) scholarship without which continuation of this study would have been difficult.

Last but not the least, I would like to express my deepest gratitude to my parents for preparing me intellectually and spiritually for this important stage of my life. This effort is humbly dedicated to them. Special appreciation to my younger brother for his nice support in taking care of our parents while I am in Japan. Heartfelt thanks to my lovely wife Tandra for her invaluable help in taking care of our daughter, Samyukta and son, Shashwata. Her moral support, sacrifice and continuous love helped me to concentrate on my research.

Table of Contents

List of Tables

List of Figures

1 General Introduction

1.1 Background

In this era of industrial revolution, generation of post-production waste, often called as 'industrial by-product' is inevitable. From production to disposal, by-product materials are the cause of concern for the respective industries due to several reasons. Firstly, by-product materials often contain hazardous/toxic elements which are difficult to dispose in an environment friendly manner. Secondly, due to the difficulty in disposal, large amount of storage spaces are required for the dumping of such materials which in turns increases the operation cost. Thirdly, rapid increase in the production of primary products triggers the production of 'by-product' materials and demands for even larger storage facilities. In order to address the above problems it is necessary to find an eco-friendly and sustainable solution to dispose the by-product materials.

There is a popular saying that ***'One man's trash is another man's treasure'***. Based on this concept, taking out the waste from one production process and use it into another as a primary resource is the best possible option for the safe disposal of by-product materials as this approach can solve the previously mentioned problems. According to the world business council for sustainable development (WBCSD) and the US environmental protection agency (EPA), this process is termed as 'By-product synergy'

Iron/steel making industry might be considered as an ideal situation where the concept of 'by-product synergy' can be effectively utilized. It is fact that, steel is the most commonly consumed metals on earth followed by aluminum and copper. Due to the increased consumption and subsequent demand, production of crude steel is increasing significantly. According to world steel association (WSA, 2018), around 1.712 billion tons of crude steel was produced in 2018 which is 4.9% higher than that produced in 2017.

It has been projected that this production will reach up to 1.752 billion tons in 2020 (WSA, 2018).

The production of crude steel results in formation of different types of 'Slag' depending on the production process and type of raw materials (Nippon Slag Association). Here, the word 'Slag' refers to a siliceous melt which is produced when scrap iron or, iron ore is melted in the furnace and refined. During heating in the furnace, the impurities (silica, alumina, non-ferrous components) in the iron ore or scrap iron form oxides and float on top of the molten steel because of having relatively lower specific gravity than steel. These floated oxides along with other impurities (i.e. ash from coke used as reducing material, limestone used as auxiliary material) are collected and cooled down to form 'Slag' (Juckes, 2011). Similarly, 'Slag' can be obtained from the production process of non-ferrous metals such as copper and ferrous-nickel alloy and termed as 'Copper Slag (CS)', and 'Ferronickel Slag (FNS)' respectively. A detail flow chart depicting classification of different types of slag is provided in Figure 1-1.

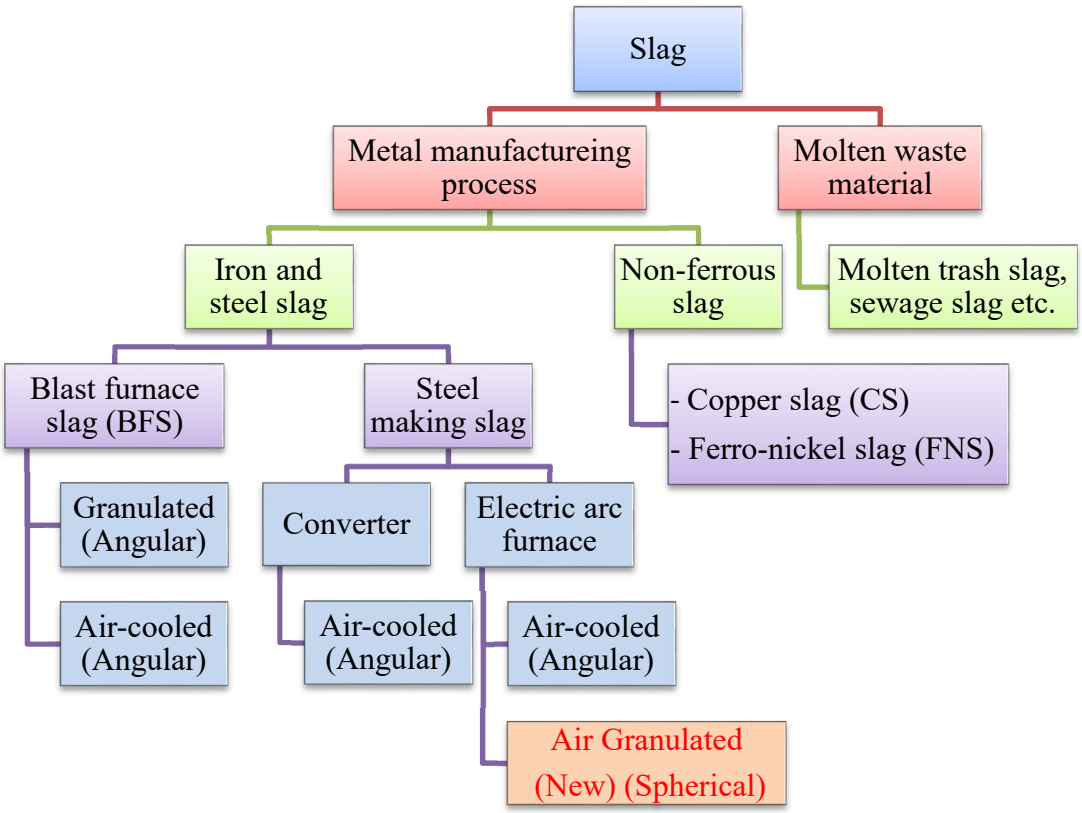

Figure 1-1 Classification of slag with particle shape

Among the iron and steel making slags, 'Blast Furnace Slag (BFS)' and 'Electric Arc Furnace Slag (EAFS)' are two common variants. Despite the difference in furnace, the former type is produced during the production of pig iron from iron ore while the latter type is produced during the production of steel from scrap. Another type of slag known as 'Converter Slag' is also common which is produced during the conversion of pig iron to steel with a mix of scrap steel in the converter. It is clear from the production process flow as depicted in Figure 1-2 that the highly produced type of slag is blast furnace slag (290 kg/ton of pig iron) followed by converter slag (110 kg/ton of steel) and electric arc furnace slag (70kg/ton of steel) since iron ore contains more impurities such as non-ferrous components and the production of pig iron is much higher than steel (Nippon Slag Association). Although the slag produced in the electric arc furnace are lesser in quantity, their constituents are however different from the other two types due to the refining of iron in many stages.

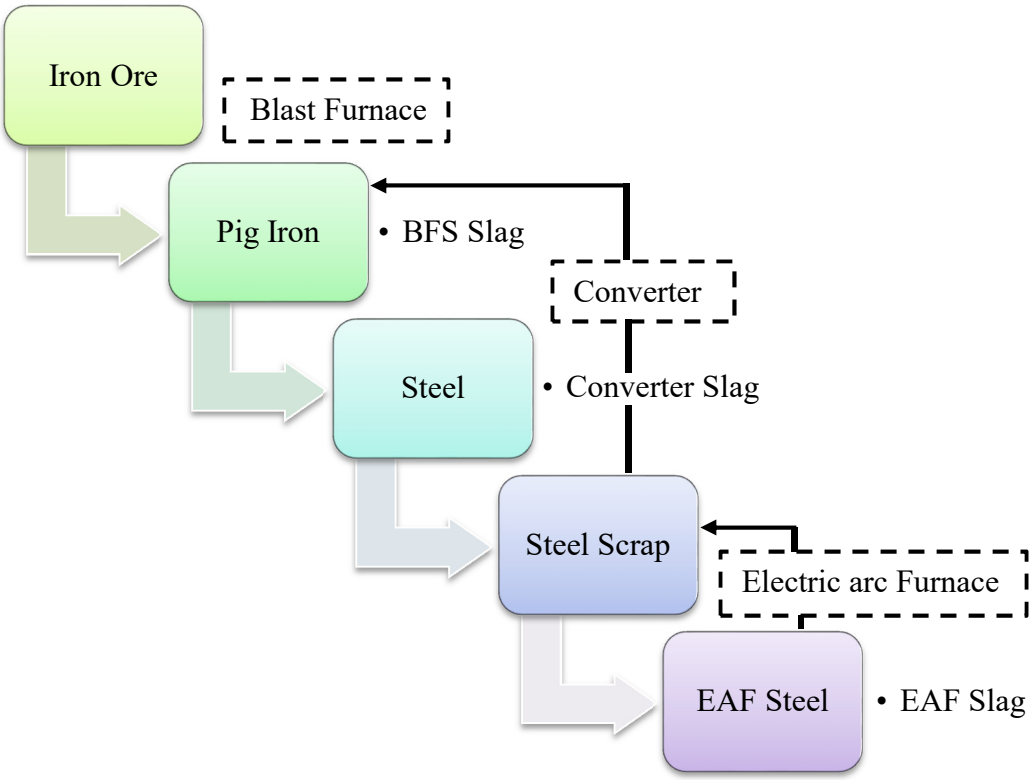

Figure 1-2 Slag production process flow

It has been estimated that 25% of total crude steel is produced in the electric furnace and the rate of production is expected to increase rapidly due to the rapid increase in steel scrap globally (WSA, 2018). This indicates the chance of gradual increase in EAF slag. Sustainable utilization of EAF slag has become a concern to the steel manufacturers due to several reasons. Firstly, recycling of EAF slag by back-feeding them into the process is limited as mixing impurities will consume more energy and make the removal task even difficult (Juckes, 2011). Secondly, because of having large amount of metal oxides in EAF slag, it is difficult to dispose them in an environment friendly manner (Sekaran et al., 2015). Thirdly, dumping of such materials as landfill element is expensive and adversely affects the porosity and permeability of soil (Jukes, 2011, Sekaran et al., 2015).

According to JSCE guidelines for concrete (No. 1, 2004) EAF slag is composed of stable minerals such as CaO, SiO_2 similar to the dicalcium silicate phase and possesses the characteristic feature of high density. In addition, Alizadeh et al. (2003) confirmed that the low percentage of amorphous silica along with higher ferric oxide in EAF slag reduces the pozzolanic activities of EAF slag in comparison to blast furnace slag and therefore is more applicable to concrete as replacement of aggregates. It is fact that the rapid infrastructural development globally demands for over 10 billion tons of concrete annually (Meyer, 2009) which triggers the depletion of natural aggregate stock. This has financial consequences as well as several environmental impacts such as loosening of water holding strata, erosion of river bank etc. (Prabhu et al., 2014, Dash et al., 2016). In this context, utilization of EAF slag as partial or full replacement of aggregate in concrete would be the best possible option considering the concept of 'by-product synergy' as discussed earlier.

Several studies utilized EAF slag as replacement of both coarse and/or, fine aggregates in concrete (Maslehuddin et al., 2003, Pellegrino et al., 2009, Manso et al., 2006, Coppola et al., 2016, Rondi et al., 2016, Qasrawi, 2014). The outcome of those studies indicate that utilization of EAF slag in concrete as replacement of aggregate up to a certain slag replacement ratio is advantageous since it enhances the mechanical properties of concrete. It is fact that, EAF slag aggregates utilized in those studies are of conventional angular or distorted shape (as marked in Figure 1-1) due to their production process. Ideally, such aggregates are produced by smashing of large slag chunks of EAF

slag which are formed due to slow cooling in air or rapid cooling quenching in water (Figure 1-3, Nippon Slag Association). It has been further pointed out in the previous studies that the workability of concrete produced by angular shaped EAF slag aggregate is much lower than normal concrete especially at higher slag replacement ratio due to the less ball bearing effect because of angular shape and higher water amount is required to improve the workability. This indicates a potential risk of degradation of durability properties of such concrete such as shrinkage.

Recently, a new production method (detail method is discussed in section 1.2) has been developed, adopting which a new type of EAF slag is obtained (Figure 1-1 highlighted in red). The newly developed EAF slag particles are spherical shaped fine aggregates and possess high density. From these features, it is expected that the former problems of lower workability and poor durability of concrete associated with the use of angular shaped EAF slag aggregates can be solved without hampering the mechanical properties. In this background, in order to confirm their applicability in concrete a thorough study on all the properties of concrete by utilizing spherical shaped EAF slag fine aggregates by replacing natural sand at different replacement ratio is necessary.

1.2 Production method of spherical shaped EAF slag

It has already been discussed that the specific gravity of molten slag, which contains oxides of many non-ferrous metals along with ash and limestone, is lower than that of molten iron/steel. As a result, slag particles float on top of the molten iron/steel. In the conventional slag (either BF, Converter or EAF) production method, these molten slag is separated and collected. Two different cooling methods are generally adopted in cooling the molten slag. The first method is to cool the hot molten slag slowly by placing them in the cooling yard where sufficient air is blown to achieve proper cooling. In the second method, rapid cooling quenching is applied to the molten slag by blowing cold water through them. The former method is applied to all types of slag (BF, Converter and EAF) with an aim to utilize the produced material in road base course and as aggregates in concrete while the latter method is used only for producing ground granulated blast furnace slag with a target of utilizing them as raw material for slag cement and fine

aggregates in concrete. For both the methods, crusher/grinder is used to smash the air/water cooled large slag lumps and the crushed materials are then sieved through screen to separate the coarse (> 4.75mm) and fine aggregates (< 4.75mm) respectively. Figure 1-3 depicts the conventional production method of all types of slag under discussion.

(a) Production process of air-cooled BF/Converter/EAF slag (shape: angular)

(b) Production process of granulated BF slag (shape: angular)

Figure 1-3 Production process of conventional slag

Recent improvement in the production method of EAF slag lies in the cooling process. In this method, a high pressure cold air is blown through the molten slag. As a result, slag particles instantly form spherical shape and gets deposited in the air cooled area. Flow of cold air/water is passed through the deposited slag particles to ensure sufficient cooling. Slag particles thus formed are finer in size (< 4.75mm) and do not require any further crushing and screening. Figure 1-4 shows the real time production photos of spherical shaped EAF slag (courtesy: Hoshino sansho Co. Ltd.). Although most of the current production lines do not have the facility, however it appears that a minor modification in the cooling process will enable the production of spherical shaped EAF slag fine aggregates. The detail production method is however under the patent and jurisdiction of Hoshino sansho Co. Ltd., Japan.

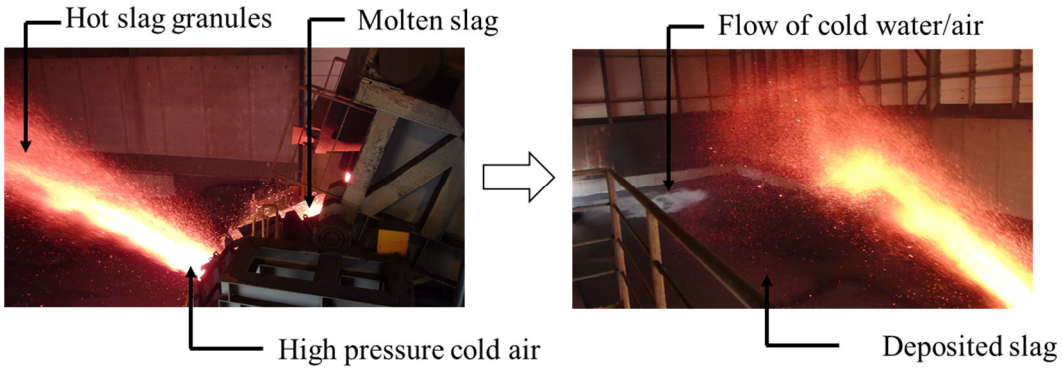

Figure 1-4 Production process of new spherical shaped EAF slag fine aggregate (courtesy: Hoshino sansho Co. Ltd.)

1.3 Literature review

1.3.1 Effect of shape of fine aggregates on the fresh, physical, mechanical and durability properties of mortar and normal concrete

The effect of shape of fine aggregates on the fresh, physical and mechanical properties of mortar and/or concrete were examined in several studies (Neville, 2010, Cepuritits et al., 2016, Belhadj et al., 2014, Cortes et al., 2008, Quiroga and flower, 2003). Most of those studies concluded that the change in shape of aggregate significantly influences the workability and strength of concrete. The former of which happens primarily due to the change in shape of fine aggregates while the latter is due to the change in shape of coarse aggregates respectively (Neville, 2010).

Cortes et al. (2008) conducted a study on the rheological and mechanical properties of mortar mix having sand of different shape. They concluded that a larger volume of paste will be required to attain adequate flowability and strength when angular shaped fine aggregates are used instead of spherical shaped aggregates of same grading. Neville (2010) pointed out that the shape of fine aggregate particles influences the concrete mix water requirement significantly. He described that the void contents (loose or rodded condition) in angular shaped particles are higher than that of rounded shaped particles which demand for more mix water during concreting. Figure 1-5 shows a relationship of mixing water content and void content in reference to Neville, 2010 which clearly depicts the fact as discussed above.

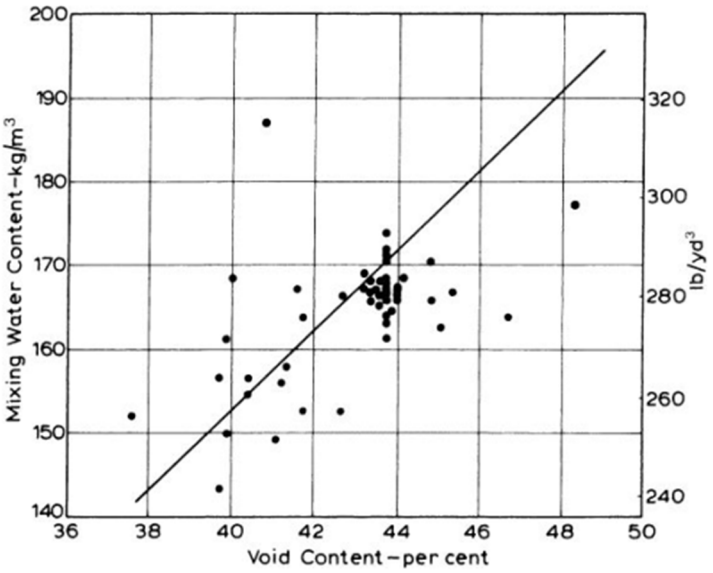

Figure 1-5 Relationship between void content of sand (loose condition) and water requirement of concrete (after Neville, 2010)

Galloway (1994), Hudson (1999) and Kalcheff (1977) indicate that the bleeding of concrete is strongly affected by the shape, gradation and water absorption capacity of aggregates as uniformly graded rounded shaped particles of lower water absorption tends to have higher bleeding. Influence of shape of fine aggregates on the fresh concrete density is negligible as the latter is strongly dependent on the density of individual aggregates. Similar to fresh concrete density, settlement and segregation of aggregates in the concrete mix is strongly related to the particle density and the effect is more pronounced for the case of coarse aggregates of higher density (Neville, 2010). Belhadj et al. (2014) in their study on the effect of shape of sand on the mechanical properties of concrete observed that the concrete produced by angular shaped sand particles exhibits superior mechanical properties and pertains more resistance to crack propagation than that of rounded shaped sand particles provided that all the particles have good granular distribution.

The influence of shape of aggregate on the durability properties of concrete such as shrinkage, water absorption and air permeability has been discussed in several studies (Shilstone, 1990, Forster, 1994, Washa, 1998, Ahmed, 1989, Zhang and Zong, 2014). Shilstone (1990) discussed that spherical or cubical particles produce higher strength and lower shrinkage in comparison to flaky and elongated particles. Washa (1998) and Ahmed

(1989) identified the lower water absorption of aggregates and lower fine contents in the aggregate mix as two important factors that reduces the shrinkage of concrete. Zhang and Zong (2014) pointed out water absorption of concrete as an indicator of durability and concluded that the water absorption of concrete is primarily influenced by the water absorption of aggregates.

1.3.2 Influence of EAF slag aggregates on the fresh, physical, mechanical and durability properties of concrete

Several research works have been reported till date where the utilization possibilities of EAF slag aggregates in concrete were examined (Rondi et al., 2016, Sekaran et al., 2015, Maslehuddin et al., 2003, Faleschini et al., 2016, Arribas et al., 2015, Pellegrino et al., 2009, Coppola et al., 2016, Qasrawi et al., 2008). Some of those studies were carried out by utilizing slag as partial or full replacement of only coarse aggregates in concrete (Sekaran et al., 2015, Faleschini et al., 2016, Arribas et al., 2015) while some of them utilized both coarse and fine slag aggregates simultaneously (Rondi et al. 2016, Pellegrino et al., 2009, Monosi et al., 2016, Sezer et al., 2015, Coppola et al., 2016). However, study on the utilization of EAF slag as replacement of only fine aggregates in concrete is very few (Qasrawi et al., 2008). In addition, all the previously reported studies were conducted by utilizing angular shaped EAF slag aggregates in concrete since formation of spherical shaped EAF slag aggregates are very recent and only utilized and reported by Roy et al. (2018, 2019). Most of the above mentioned studies indicate that up to a certain slag replacement ratio, it is advantageous to replace natural aggregates (either coarse and/or fine) by EAF slag since such concrete exhibits improved physical and mechanical properties.

Maslehuddin et al. (2003) in their study replaced coarse limestone aggregates by EAF slag for five different slag replacement ratio of 0.45, 0.50, 0.55, 0.60, 0.65 at a water to cement (W/C) ratio of 0.4 and concluded that the utilization of EAF slag as coarse aggregate in concrete improves the physical, mechanical and durability properties of concrete. Similar findings were reported by Faleschini et al. (2016) with an added information that the shape and texture of EAF slag coarse aggregates is the reason of superior tensile strength due to better bond of slag particles with surrounding mortar in comparison to normal coarse aggregates. The quality of slag-cementitious matrix ITZ

(Interfacial Transition Zone) was observed by Arribas et al. (2015) and they found them better than that of natural aggregate-cementitious matrix. They identified this phenomena as the cause of improved mechanical properties of EAF slag coarse aggregate concrete.

Both coarse and fine EAF slag were utilized in concrete by Pellegrino et al. (2009). They replaced gravel and sand at a slag replacement ratio of 0.0, 0.5 and 1.0 for four different W/C ratio cases of 0.47, 0.49, 0.53 and 0.55. It was concluded that higher fine content in EAF slag reduces the workability and strength in comparison to the lower case although no significant changes were observed in chemical and mineralogical structure before and after durability tests. Manso et al. (2006) added with the similar finding that higher porosity and absorption is expected due to the complete replacement of both fine and coarse aggregates by EAF slag. Similar to slightly increasing shrinkage behavior was reported by Coppola et al. (2016) and Rondi et al. (2016) when natural aggregates were completely replaced by EAF slag.

Qasrawi et al. (2008) in their study replaced natural sand by EAF slag at a slag replacement ratio of 0.0, 0.15, 0.30, 0.5 and 1.0 for the W/C of 0.38, 0.45 and 0.62. They reported that the workability of slag concrete is reduced with the increase in slag ratio although compressive and tensile strength increases up to a slag ratio of 0.3 in comparison to normal concrete.

1.3.3 Thermal properties and freezing and thawing resistance of concrete produced by different types of slag as aggregates

Very few studies have been reported where the thermal properties of concrete produced by EAF slag aggregates have been examined (Patel, 2008, Santamaria et al., 2018). Barra et al. (2016) utilized EAF slag and granite in the asphalt concrete mix and confirmed that steel slag mix shows lower thermal conductivity than that of granite mix. Laughlin (2012) conducted a study on the mechanical and thermal properties of concrete cast by copper slag (CS). The study revealed that utilization of materials formed at higher temperature tend to provide lower thermal conductivity in concrete. Fernandez et al. (2015) in their study on the thermo-physical properties of two different types of EAF slag aggregate produced by rapid and slow cooling observed that the values of specific heat

of different types of slag at lower temperature (below 250°C) is similar due to their similar mineralogical compositions.

Patel (2008) and, Santamaria et al. (2018) investigated the freezing and thawing resistance of concrete produced by conventional angular shaped EAF slag as replacement of either coarse or both coarse and fine aggregates respectively. Patel (2008) observed satisfactory performance of slag concrete in resisting freezing and thawing up to 75% replacement of gravel by EAF slag while Santamaria et al. (2018) observed neither benefit nor excessive detrimental effects in resisting freezing and thawing of slag concrete in aqueous environment.

1.3.4 Behavior of normal and different types of slag concrete under high temperature exposure

In an event of fire, concrete structures undergo rapid temperature changes with the generation of heat flow into its exposed surface. This results in cracking and spalling of concrete and subsequent degradation of mechanical and durability properties due to the formation of temperature, moisture and pore pressure gradient within the concrete mass (Khoury, 2000, Caggiano et al., 2018). Kodur et al. (2003) investigated the high temperature influence on concrete produced by carbonate and siliceous aggregate. They concluded that concrete having higher specific heat (carbonate) performs better and resists the spalling of concrete under high temperature exposure. Zhang et al. (2000) confirmed that lightweight aggregate concrete exhibit remarkable thermal resistance over normal weight concrete due to lower thermal expansion and thermal conductivity although such concrete are highly susceptible to drying shrinkage (Hamad, 2014, Sherin et al., 2018). Similarly, limestone aggregate concrete can resist higher drying shrinkage although their performance during high temperature exposure is not satisfactory (Inoue et al., 2010, Maruyama et al., 2016).

Performance of concrete subjected to high temperature is dependent on the physicochemical and subsequent microstructural changes in the cement paste, aggregates and thermal incompatibility between aggregate and cement paste inside the concrete matrix (Khoury, 2000, Kodur, 2014, Kizilkanat et al., 2013). At 20°C-200°C, along with the evaporation of physically bound water, dehydration of ettringite, decomposition of C-

S-H gel happens in cement paste which releases more water and causes mass loss (Hager, 2013, Zhang and Scherer, 2011, Tantawy, 2017, Zhang, 2011). When the heating exposure is 400°C-500°C, decomposition of $Ca(OH)_2$ happens, which removes the chemically bound water from the cement paste (Hager, 2013, Fernandes et al., 2017) and causes shrinkage of the paste. At the heating temperature of 800°C-1000°C, calcium carbonate decomposes and releases CO_2 which further causes mass loss (Hager, 2013). It has been discussed by Ma et al. (2015) that at higher temperature, concrete starts to cracking due to the imbalance of decomposition of hydration products, shrinkage of cement matrix and expansion of coarse aggregates.

Studies on the high temperature influence of slag concrete is very few (Kodur, 2014, Khaliq and Kodur, 2012, Poon, et al., 2011, Chen and Liu, 2004). It is apparent that concrete incorporating slag exhibits superior strength at ambient temperature due to the formation of denser microstructure although this denser microstructure turns out to be adverse when the same concrete is subjected to high temperature. The governing reason is that concrete having denser microstructure is highly impermeable and under high temperature it allows very little moisture to escape resulting in build-up of pore pressure and rapid development of micro cracks leading to faster deterioration of strength. Saha et al. (2019) reported similar result by utilizing FNS slag as complete replacement of natural sand. They observed a higher reduction in the residual compressive strength in comparison to normal mortar when the heating temperature is 600°C and 800°C although at ambient temperature FNS slag mortar showed the opposite behavior. Sun et al. (2019) reported that ferronickel slags produced in blast furnace impart higher residual compressive strength than those produced in electric arc furnace.

1.3.5 Fatigue performance of normal and slag concrete at dry and submerged condition

The fatigue performance of concrete at dry and submerged condition has been reported in several studies (Lantsoght, et al., 2016, Onoue, and Matsushita, 2012). Lantsoght et al. (2016) indicate several factors such as maximum and minimum stress level, rate of loading, time dependent effects at higher stress level (>80%) and loading frequency at higher stress level (>75%) which influence the fatigue strength of concrete

under uniaxial compression. They concluded that variables like W/C, cement content, entrained air, curing condition and age at loading appears to be not influencing the fatigue strength of concrete. Onoue and Matsushita (2012) investigated the degradation of fatigue strength of concrete under submerged condition in different types of liquid. They identified that liquid penetration lowers the interfacial energy to nucleate micro-cracks. Due to liquid penetration, strain rate increases which eventually decreases the fatigue strength of concrete.

Farooq, et al. (2017) attempted to clarify the fatigue compression behavior of mortar at dry and submerged condition. They utilized blast furnace slag as complete replacement of natural sand and concluded that BFS mortar exhibits higher fatigue life than normal mortar in air although the behavior in water is similar to normal mortar. Similar study was conducted by Onoue, et al. (2014) where fatigue characteristics of concrete produced by three different types of steel making slags (hot metal pretreatment slag, converter slag and polished hot metal pretreatment slag) were investigated in submerged condition. Results indicate that concrete produced by polished hot metal pretreatment slag exhibit improved fatigue performance due to particle restraint in micro-crack nucleation.

1.4 Expected merits and demerits of utilizing spherical shaped EAF slag in concrete

Expected merits:

It is evident from literature review that utilization of the newly developed spherical shaped EAF slag fine aggregates in concrete as partial or full replacement of natural sand has several merits as given below.

1. Fresh behavior such as workability of concrete can be improved because of the spherical shape of particles (Polat et al., 2013).
2. Under same slump, air content and water to cement ratio (W/C), significant reduction in water and cement content is possible because of excellent ball bearing effect of spherical shaped particles.

3. The reduction of water and cement requirement will pertain environmental sustainability due to the utility of by-product materials and reduction of CO_2 emission along with construction economy (Meyer, 2009).
4. Due to lower water and cement requirement, concrete produced by spherical shaped EAF slag aggregate is expected to exhibit improved durability properties such as lower drying shrinkage (Neville, 2010).
5. It has already been discussed that, EAF slag possesses high density. This feature indicates the possibility of obtaining concrete of superior mechanical properties since high density aggregates in concrete increases the compressive and flexural strength of concrete in reference to Iffat, 2015 and Vidha et al., 2015.
6. It is expected that concrete incorporating spherical shaped EAF slag fine aggregate will pertain improved thermal properties than natural aggregate concrete since study of Laughlin (2012) already confirmed that concrete having particles formed at higher temperature exhibit lower thermal conductivity.

Expected demerits:

Some demerits are also expected if spherical shaped EAF slag fine aggregate is used in concrete which are listed below.

1. When the replacement ratio of EAF slag is high, it might be difficult to avoid segregation and bleeding due to particle shape and higher particle density.
2. Although the tendency of particle settlement can be improved by means of increasing viscosity of cement paste by using admixtures such as silica fume, the change in mechanical properties of concrete due to spherical shape is uncertain.

1.5 Study objective and research significance

Utilization of iron/steel making slag as replacement of aggregates in concrete are not new. Many previous studies reported several merits of utilizing slag in concrete, mostly of which are related to the strength gain of concrete, although workability and durability of such concrete are still a matter of concern. As a result, applicability of such materials in concrete is limited. In order to address those problems, recently, a new type of EAF slag fine aggregate has been developed by changing the cooling process of

production (section 1.2). The newly developed materials are spherical in shape and possesses high density. The literature review (section 1.3) suggests several merits and demerits of using spherical shaped fine aggregates in concrete instead of angular shaped aggregates which are listed in section 1.4. Similar performance is expected if the newly developed slag particles are utilized in concrete. In this context, a thorough study is necessary to confirm the applicability of the spherical shaped EAF slag fine aggregates in concrete.

The prime objective of this study is to investigate the performance of concrete produced by spherical shaped EAF slag fine aggregate by replacing natural sand at different slag replacement ratio. Initially, target is to investigate such concrete at different water to cement ratio (W/C), slump, air content for fundamental (fresh behavior, mechanical properties) and durability properties at ambient condition. Performance of such concrete will also be tested in severe environmental condition such as freezing and thawing, high temperature exposure, and static and dynamic fatigue at dry and wet condition to confirm their wider applicability.

The research is significantly important as the improved performance of the newly developed material in concrete will solve many problems related to the workability, durability and thermal properties of concrete. Most importantly, this will enable the fulfillment of sustainable development goal (SDG) target 12 and 13 for respective industries. According to SDG goal 12, an eco-friendly production line should be established where reduction of industrial wastes can be done by recycling. For the manufacturing process this has always been a challenge. As discussed earlier, if the newly developed material can be utilized in concrete it will fulfill the requirement of recycling by the concept of 'by-product synergy', where waste of one industry can be turned out to primary resources to others. At the same time, by reducing the water and cement requirement for concreting, CO_2 emission can also be reduced which will fulfill the SDG goal target 13 for industries that demands for urgent action in fighting 'climate change' by reducing global CO_2 emission.

1.6 Organization of dissertation

The outline of this study is depicted as flow diagram in Figure 1-6. Overall, this experimental study consists of two parts. The first part (chapter 1,2) introduces a newly developed EAF slag fine aggregate along with its production process, physical properties and expected merits and demerits if utilized in concrete as replacement of natural aggregate. The second part (chapter 4,5,6,7) investigates the applicability of this material in concrete with four distinct experimental programs that covers fundamental and durability properties, thermal properties, high temperature influence and water proofing capacity by static and dynamic fatigue test. A brief description of the dissertation content follows.

Chapter 1 starts with the research background and motivation of this study. In this chapter, a newly developed spherical shaped EAF slag fine aggregate is introduced along with its production method and expected performance in concrete. This chapter also includes the review of related key literatures, significance and objective of this study and the dissertation outline along with detail experimental program.

In Chapter 2, all physical properties of the newly developed as well as conventional EAF slag fine aggregate, natural sand, and gravel are discussed with experimental results. In addition, a detail qualitative and quantitative analysis of the shape of the newly developed material is also provided.

Chapter 3 introduces the fresh behavior of concrete produced by spherical shaped EAF slag fine aggregates along with justification of choosing different experimental parameters such as water to cement ratio (W/C), slump, air content etc. Based on the considerations of experimental parameters and subsequent trial tests, mix proportions are proposed along with the method of obtaining minimum water content for spherical shaped EAF slag concrete. The final part of this chapter discusses the probable particle settlement characteristics of EAF slag concrete due to segregation.

In chapter 4, applicability of spherical shaped EAF slag in concrete is investigated at different W/C ratio, slump and air content. Both mechanical and durability properties of concrete are examined and discussed. The mechanism of improved mechanical properties of spherical shaped EAF slag concrete is further discussed by using Digital Image Co-Relation Method (DICM).

Chapter 5 investigates the stability of spherical shaped EAF slag fine aggregate in concrete during temperature change. In doing so, basic thermal properties such as thermal expansion, thermal conductivity, thermal diffusivity and specific heat of slag concrete are investigated and discussed. In the end, performance of EAF slag fine aggregate concrete in resisting freezing and thawing action is discussed with related experimental results.

In chapter 6, a thorough study on the high temperature influence of concrete produced by spherical shaped EAF slag is presented with all experimental results. Degradation of both physical and mechanical properties of normal and slag concrete are introduced. The degradation mechanism is discussed after subsequent image analysis by DIC method.

Chapter 7 investigates the water proofing capacity of spherical shaped EAF slag concrete. The results of static compression test in air and in water is introduced and the fatigue performance of normal and spherical shaped EAF slag concrete under water has been discussed with related mechanism.

Finally, chapter 8 concludes with major findings and includes recommendations for future study.

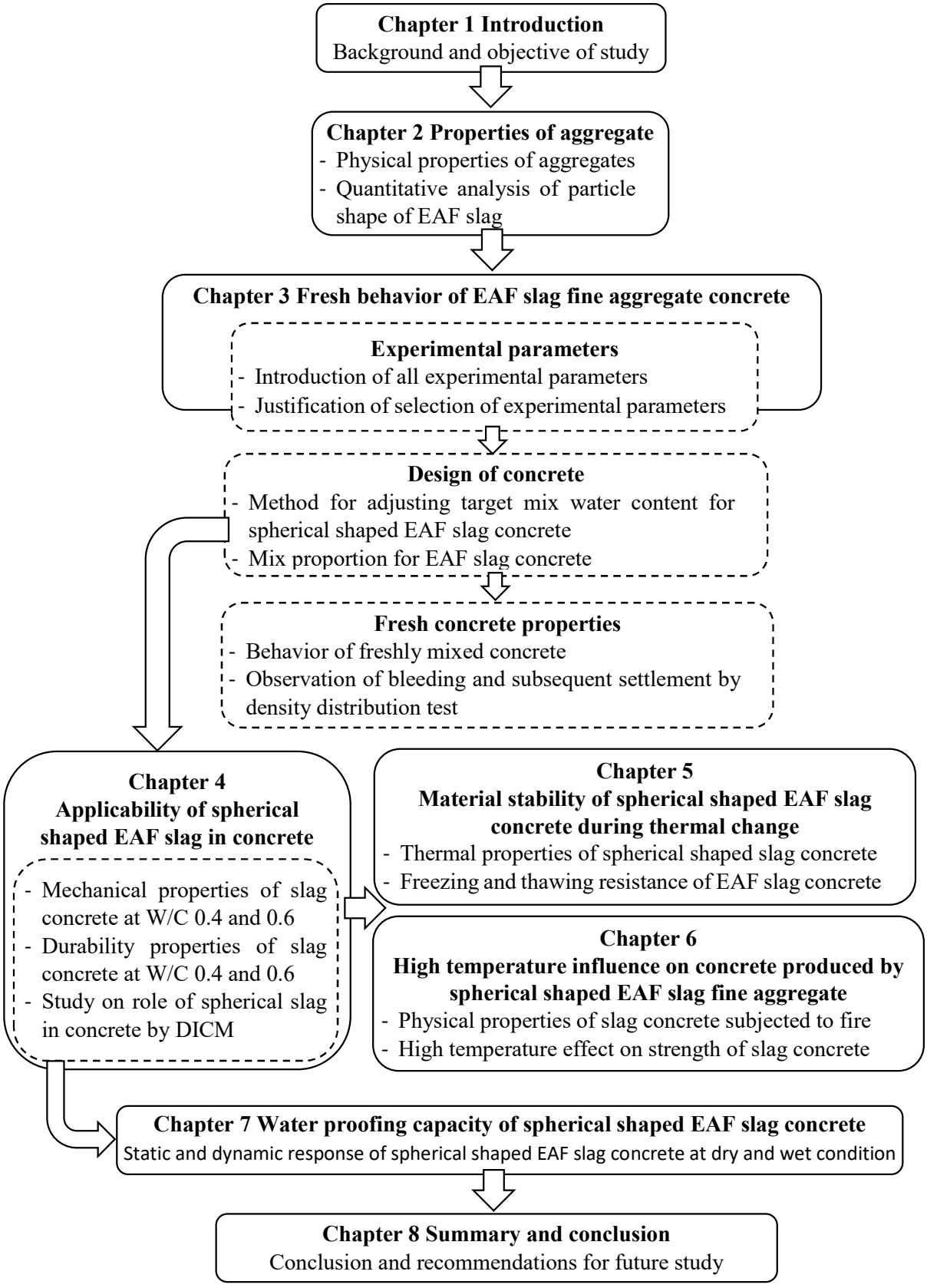

Figure 1-6 Organization of dissertation

1.7 Experimental program and material series

Figure 1-7 depicts the total experimental plan as conducted in this study with individual experimental programs. As can be seen from Figure 1-7, total experimental plan comprises of four major experimental programs that covers the investigation of all important properties ranging from fundamental to fatigue characteristics of concrete produced by spherical shaped EAF slag fine aggregates. The outcome of each of the experimental program is reported in different chapters as mentioned in section 1.6.

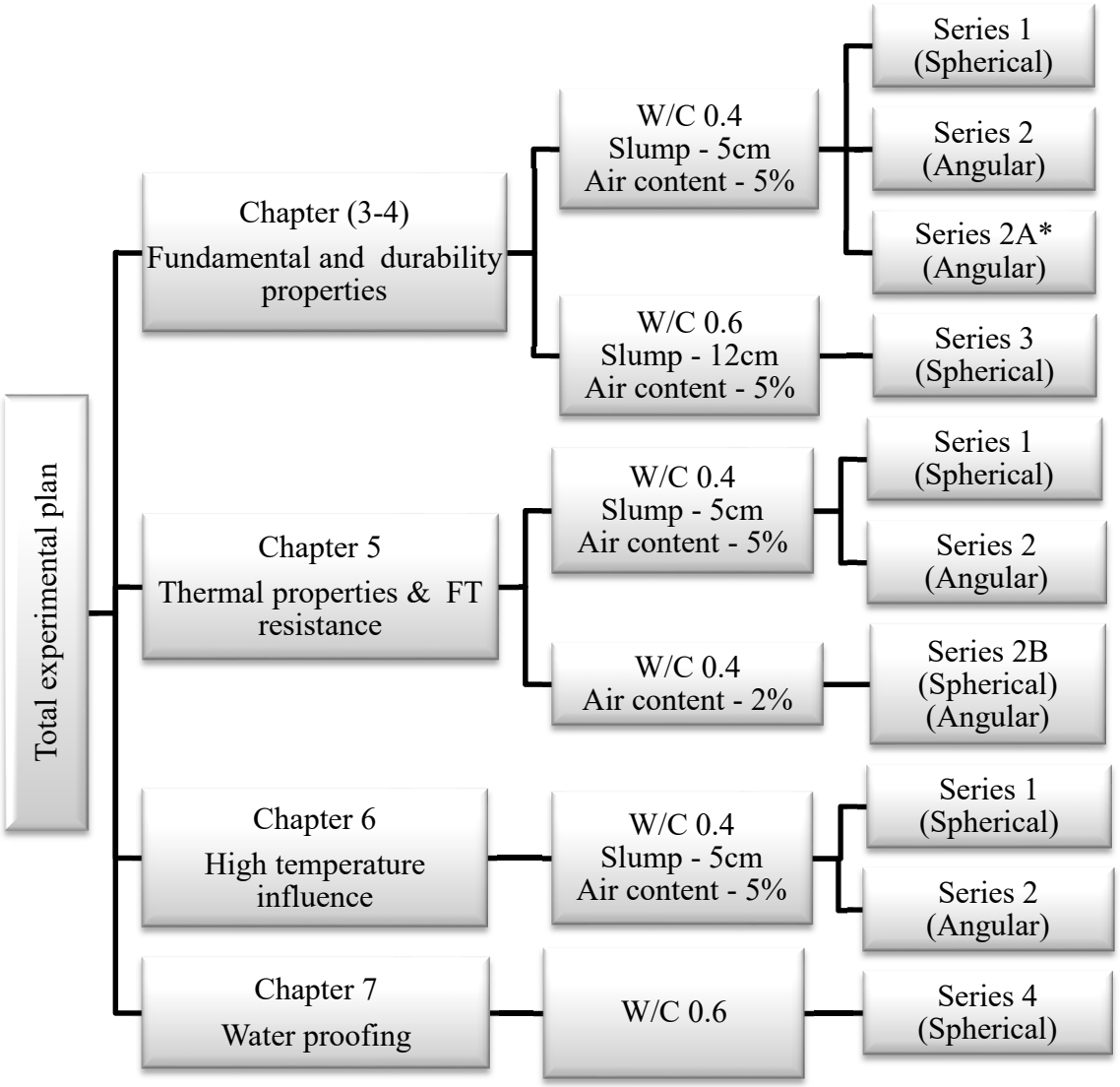

Figure 1-7 Experimental plan with individual series

In the first part (chapter 3-4), fundamental properties such as fresh concrete behavior, mechanical and durability properties of concrete produced by spherical shaped EAF slag fine aggregates were investigated. Properties of concrete were studied primarily under two different sets of parameters such as water to cement ratio (W/C), slump and air content of 0.4, 5cm and 5% and 0.6, 12cm and 5% respectively. The reasons for choosing the above experimental parameters are discussed in detail in chapter 3 (section 3.2). Under the former set of W/C 0.4, two experimental series (series 1 and 2) were planned by utilizing spherical and angular shaped EAF slag fine aggregates respectively while for the W/C of 0.6, single experimental series (series 3) was planned for spherical shaped EAF slag concrete. The reason behind this choice was to evaluate the wider utilization possibility of spherical shaped EAF slag and at the same time identify the variation of concrete properties if EAF slag of different shapes are utilized under same W/C, slump and air content. Series 2A as shown in Figure 1-7 is additional to series 2 which were prepared by angular shaped EAF slag concrete with the same mix proportions of spherical shaped EAF slag concrete of series 1. The purpose was to validate the fresh concrete behaviors of spherical slag concrete.

The second part (chapter 5) of the experimental plan aimed to investigate the basic thermal properties as well as freezing and thawing resistance capacity of EAF slag concrete. In order to facilitate the plan, two different experimental series were undertaken by using spherical and angular shaped EAF slag fine aggregates at W/C, slump and air content of 0.4, 5cm and 5% respectively. Series 2B is different from the former two series as the consideration for air content for this series was much lower (2%) than the former two. The purpose of series 2B was to identify the influence of low air content of normal and slag concrete on the freezing and thawing resistance.

In the third part (chapter 6) of experimental plan, influence of high temperature on the degradation of physical and mechanical properties of EAF slag concrete was planned to investigate. To achieve the purpose, specimens were prepared under two different experimental series by using spherical and angular shaped EAF slag at a volume replacement ratio of 0.0, 0.3, 0.5 and 1.0 for the W/C, slump and air content of 0.4, 5cm and 5% respectively.

Finally, water proofing capacity (chapter 7) of spherical shaped EAF slag fine aggregate concrete are planned to investigate under both static and dynamic loading

condition. Water to cement ratio was considered as 0.6 and concrete specimens were produced by replacing natural sand with spherical shaped EAF slag fine aggregates at a volume replacement ratio of 0.0, 0.3 and 0.5.

2 Properties of aggregate

2.1 Introduction

In order to confirm the applicability of the newly developed spherical shaped EAF slag fine aggregate in concrete, four distinct experimental plans were undertaken. For each of the experimental plans, concreting was done by Ordinary Portland cement (OPC), gravel (maximum size = 20mm) and three different types of fine aggregates. Of the three types, two are EAF oxidizing slag aggregates of spherical (newly developed) and angular shape while the rest is natural sand which was replaced by the former two types of slag. Figure 2-1 depicts the spherical and angular shaped EAF slag aggregates as utilized in this study. Chemical composition of slag aggregate and physical properties of all types of aggregate is discussed in detail in the following subsections of this chapter. Moreover, an attempt of differentiating the particle shape of EAF slag aggregates is presented at the end of this chapter.

(a) Spherical (b) Angular

Figure 2-1 Shape of EAF slag fine aggregates (Roy et al., 2019)

2.2 Chemical composition of slag aggregate

Chemical composition of EAF oxidizing slag aggregate as utilized in this study is listed in Table 2-1. In fact, these results are obtained from the slag manufacturer, Hoshino Shanso Co. Ltd. In order to get a clear idea about the difference in composition of other slag types, chemical composition of blast furnace, converter, copper and ferronickel slag as reported by other researchers (NSA, Ma, et al., 2018, Saha, et al., 2018) are listed in Table 2-2. It is fact that chemical constituents of slag varies because of the type of raw materials and process of production, however, Table 2-2 is useful in understanding the scope of application of these materials based on their constituents.

Table 2-1 Chemical composition of EAF oxidizing slag

Composition (%)	FeO	CaO	SiO_2	Al_2O_3	MnO	MgO	Cr_2O_3	P_2O_5	TiO_2	Others
	22.5	22.5	16.3	15.1	9.4	5.6	4.6	0.2	1.0	2.8

Courtesy: Hoshino Sansho Co. Ltd.

Table 2-2 Chemical composition of OPC and different types of slag

Slag type	FeO	CaO	SiO_2	Al_2O_3	MnO	MgO	Cr_2O_3	P_2O_5	TiO_2	Others
BFS*	0.4	41.7	33.8	13.4	0.3	7.4	-	<0.1	-	0.8
Converter*	17.4	45.8	11.0	1.9	5.3	6.5	-	1.7	-	0.06
OPC*	3.0	64.2	22.0	5.5	-	1.5	-	-	-	2.0
Copper**	56.2	5.9	17.9	6.6	-	4.7	-	0.18	-	1.7
FNS***	11.9	0.4	53.3	2.7	-	31.6	1.08	-	-	0.22

* Nippon Slag Association; BFS – Blast furnace slag; OPC- Ordinary Portland cement
** Ref: Ma et al., 2018
*** Ref: Saha et al., 2018; FNS – Ferronickel slag

It is clear from Table 2-1 and Table 2-2 that the major components of slag are oxides of different foreign metals or ions present in the raw materials. However, there is a distinct difference in composition between EAF and BF slag. The major components for the latter type is limestone (CaO), silica (SiO_2) and alumina (Al_2O_3) which are similar to the compositions of ordinary Portland cement (OPC). In addition, presence of iron oxide (FeO) is very low. The main compositional difference between EAF and BF slag lies in the presence of more iron oxide (FeO) and comparatively less limestone (CaO) and Silica (SiO_2) in EAF slag with good amount of alumina (Al_2O_3) and Manganese (MnO). Other slag types such as copper and ferronickel are rich in iron oxide (FeO) and silica (SiO_2) respectively.

The presence of more iron oxide (FeO) in EAF slag is responsible for its relatively dark appearance. In addition, the pozzolanic activity of EAF slag is much lower to none than that of BF slag which is due to the presence of relatively lower amount of amorphous silica (SiO_2) and higher iron oxide (FeO) in reference to Alizadeh et al., (2003). As a result, in concrete EAF slag is only suitable for utilizing as replacement of aggregates whereas, blast furnace slag can be considered for the replacement of both aggregates and cement.

2.3 Physical properties of aggregate

2.3.1 Gradation of natural sand and slag aggregate

In order to evaluate the particle size distribution of natural sand and both spherical and angular shaped EAF slag fine aggregates, sieve analysis was conducted by the procedure as described in JIS A1102 (2014). Each test was conducted three times for each type of aggregate and the average of the three tests were considered. For each case, fineness modulus (FM) was also computed. Gradation curves obtained by the experiment are shown in Figure 2-2. Standard particle distribution range for fine aggregates as prescribed in JSCE guidelines for concrete (No. 16, 2010) is also shown in the same figure.

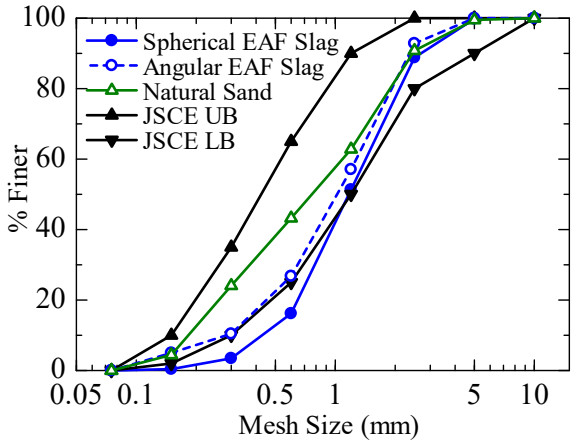

Figure 2-2 Gradation of fine aggregate (Roy et al., 2018)

It can be seen from the figure that the gradation curves of spherical and angular shaped EAF slag are comparable although they are different from that of natural sand to be replaced. The gradation curve of natural sand shows a well graded trend while this

trend is uniform for spherical and angular shaped EAF slag. In addition, the presence of larger particles in the spherical slag mix is more and part of the corresponding gradation curve of spherical slag is out of the JSCE limits for fine aggregates. It is fact that JSCE limits for fine aggregates are for sand particles and do not related to any adverse effect with spherical slag of current gradation.

The fineness modulus of spherical and angular shaped EAF slag is computed as 3.40 and 3.08 respectively which is much higher than that of natural sand (2.80) to be replaced. This tendency might be related to the slag production process. As described in section 1.2, spherical shaped EAF slag is produced by the blow of high pressure cold air through the molten slag whereas angular slag is produced by the smashing of naturally cooled large slag lumps therefore, presence of higher fine contents in case of angular slag is quite obvious. Similarly, presence of larger sized particles in higher quantity in spherical slag mix might be related to the speed of air blown through the molten slag. In this study, materials as obtained from the manufacturer were directly utilized without altering the gradation. This is to understand the behavior of spherical and angular shaped EAF slag at their production condition and to promote economic use.

2.3.2 Density and water absorption of gravel, sand and slag concrete

Similar test methods for measuring the density and water absorption of fine aggregates as described in JIS A1109 were used to evaluate the density and water absorption of spherical and angular shaped EAF slag. For each type of EAF slag, three representative tests were conducted and the average of those test results was considered. Results for density and water absorption of gravel and sand were taken from the supplier's test data. Table 2-3 shows the experimental results related to density and water absorption of all types of aggregate.

Table 2-3 Density and absorption of aggregates

Aggregate	Density (g/cc)	Absorption (%)
Gravel	2.60	1.16
Natural Sand	2.55	1.57
EAF Slag (Spherical)	3.60	0.53
EAF Slag (Angular)	3.85	0.76

It is evident from Table 2-3 that both spherical and angular shaped EAF slag aggregates exhibit very high particle density in comparison to natural sand (2.55 g/cc), gravel (2.60 g/cc) and even cement (3.15 g/cc). This might be due to the fact that slag particles are mostly composed of oxides of heavy metals. A slightly higher density of angular slag in comparison to spherical slag might be due to the presence of higher fine contents in angular slag.

For the case of water absorption, both types of slag exhibit much lower values than natural sand. Among the two types of slag, spherical shaped EAF slag exhibits the lowest water absorption which might be due to the lower fine contents compared to angular slag.

2.4 Investigation on difference in particle shape of EAF slag

2.4.1 Investigation by laser scanning

It has already been discussed in chapter 1 that the newly developed EAF slag fine aggregate particles are spherical in shape due to their unique manufacturing process. Figure 2-1 also depicts the difference in shape of the two types of EAF slag. However, in order to obtain more clear and accurate idea about the difference in shape of EAF slag particles, laser scanning of individual slag particles of each shape was conducted and the results are depicted in Figures 2-3(a) and 2-3(b).

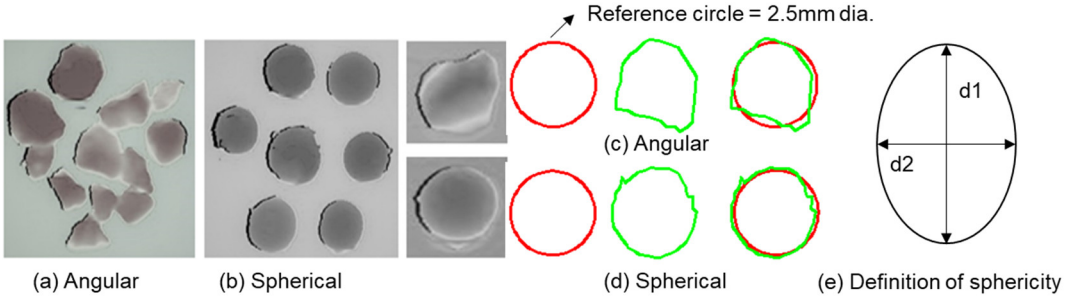

Figure 2-3 Difference in particle shape observed by laser scanning (Roy et al., 2018)

From these figures, clear difference in the shape of particles can be visualized. In addition, from each shape group, several particles retained in the 2.5mm sieve were

further scanned and compared with a reference circle of 2.5mm diameter. The comparison results for angular and spherical shaped slag particles are depicted in Figure 2-3(c) and 2-3(d) respectively. It is clear that the particles are qualitatively distinguishable based on their shape. The spherical shaped particles show matching similarity with the reference circle of 2.5mm diameter in comparison to the angular shaped particles.

Now, to evaluate the particle shape of spherical and angular shaped EAF slag quantitatively, attempts were taken to measure the sphericity (S) of slag particles. Here, the term 'sphericity' is defined as the ratio of particle width (d2) to particle length (d1) in the orientation showing the largest projected area of the particles as shown in Figure 2-3(e). Krumbein and Sloss (1951) proposed the sphericity equation which is provided in Eq. 2.1. Clearly, sphericity (S) tends to 1.0 indicates the particles to be more spherical.

$$\text{Sphericity, } S = \frac{d2}{d1} \tag{2.1}$$

For the calculation of sphericity, six representative particles from each slag type were chosen. For accuracy of measurement, only larger sized particles retained in the 2.5mm sieve were taken into consideration. Each of the chosen particles were then scanned by laser and sphericity of each of them were computed by Eq. 2.1. Table 2-4 shows the sphericity of all measured particles. The average sphericity of spherical and angular shaped slag particles are found as 0.92 and 0.74 respectively, which clearly differentiates the shape of two types of slag quantitatively.

Table 2-4 Particle sphericity

	Spherical	Angular
Sphericity	0.98	0.81
	0.88	0.59
	0.93	0.87
	0.91	0.73
	0.90	0.90
	0.93	0.53
Average =	0.92	0.74

2.4.2 Maximum and minimum void content

In the previous section, the difference in shape of the two types of slag was confirmed. Based on the above result, a relationship between particle shape and void content is required to establish which will provide an idea in selecting the minimum water content of slag concrete while designing concrete of varying aggregate shapes for particular slump, air content and water cement ratio. It has already been discussed in chapter 1 (section 1.3.1) that void content in the angular shaped particles are higher than rounded particles which demands for higher mix water content and vice versa (Neville, 2010).

The tests related to the maximum (e_{max}) and minimum (e_{min}) void ratio were carried out for natural sand and both types of EAF slag as per ASTM D4253-14 (2014) and ASTM D4254-14 (2014) respectively. Here, the values of e_{max} represents the maximum void ratio in the aggregate at loose or no tamping condition whereas, e_{min} represents the minimum void ratio in the aggregate at rodded or tamping condition. The index void ratio (I_e) is the difference between e_{max} and e_{min}. For each type of aggregate, three representative tests were conducted and average of the three results was considered. Experimental results for all tested cases are listed in Table 2-5.

Table 2-5 Maximum and minimum void ratio of aggregates (Roy et al., 2018)

Sl. No.	Aggregate Type	$e_{max,}$ loose	Average $e_{max,}$ loose	$e_{min,}$ rodded	Average $e_{min,}$ rodded	$I_e = e_{max} - e_{min}$
1	Spherical EAF Slag	0.4902	0.4905	0.4745	0.4769	0.0136
2		0.4887		0.4808		
3		0.4926		0.4753		
4	Angular EAF Slag	0.5552	0.5552	0.4809	0.4824	0.0728
5		0.5559		0.4831		
6		0.5545		0.4831		
7	Natural Sand	0.4064	0.4045	0.3620	0.3616	0.0429
8		0.4053		0.3642		
9		0.4019		0.3587		

It is evident from Table 2-5 that the maximum, minimum and Index void ratio are larger for the case of angular particles than those of spherical particles which is consistent with the observations of Neville, 2010 and Zheng and Hryciw (2016) that the angular, non-spherical and uniform sands tend to have larger values of e_{max} and e_{min}. However, the

values of e_{max} and e_{min} of natural sand as utilized in this study were measured lesser than spherical and angular slag. This can be attributed to the fact that although the particles of natural sand are rounded, they are not uniformly graded, which is consistent with the findings of particle size distribution (Figure 2-2) as discussed in section 2.3.1.

A relationship between sphericity and maximum void ratio of spherical and angular shaped EAF slag particles are shown in Figure 2-4. It can be seen from the figure that, for 19.6% decrease in sphericity, maximum void ratio, e_{max} of angular slag particles increases up to 13.2%. Approximate estimation from Neville (2010) shows that, 1% increase in maximum void content of sand, requires an increment of 1.2% mix water during concreting. This implies to a reduction of approximately 16% of mix water if spherical shaped sand particles having sphericity similar to spherical slag (0.92) is used instead of angular shaped sand particles of sphericity 0.74. This calculation provides an important relationship between sphericity and mix water requirement for concreting that for every 1% reduction of sphericity, mix water requirement increases by 0.82%. It is fact that, mix water requirement is dependent on several factors such as type and gradation of fine aggregates however, the above finding is useful in predicting the trial mix water for slag concrete. In the next chapter, verification of the above mentioned relationship between sphericity and mix water requirement for EAF slag concrete will be examined.

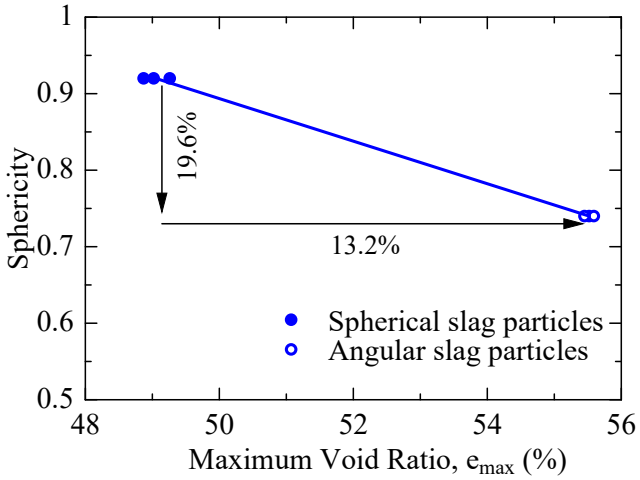

Figure 2-4 Sphericity and maximum void ratio relationship

2.5 Procedure to saturate spherical shaped EAF slag aggregates

Accurate estimation of mix water for spherical shaped particles is very important as the fresh concrete behaviors such as slump, air content, bleeding etc. are completely dependent on appropriate mix water. A little more than the required water can make the mix flow able while a little less can turn it to non-workable. In addition, physical properties of spherical shaped EAF slag particles indicate that the water absorption capacity of such material is very low. Therefore, because of spherical shape, if extra water is present around the slag particles they will either quickly evaporate or contribute to the mix water rather than being absorbed by slag. To overcome the above mentioned problems, slag particles are required to be saturated and moisture content of the saturated spherical slag particles are required to be measured and subsequently adjusted from the initial mix water.

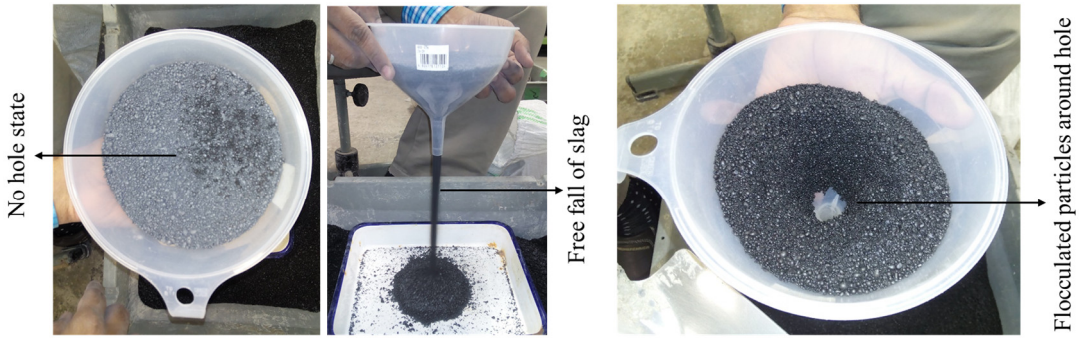

Figure 2-5 Technique to measure saturation level of spherical shaped EAF slag

Figure 2-5 shows a laboratory measurement technique of saturation level of spherical shaped EAF slag particles. As depicted in figure 2-5(a), if slag particles are completely dry, they are free to fall through a funnel without creating any flocks or hole inside the funnel on top of the exit route. The situation is different when the spherical slag particles are mixed with little amount of water. In this stage, the slag particles flocculate and can only fall through the exit part of the funnel if the funnel is tapped. In addition, a circular hole will be visible on top of the exit route of the funnel. This situation ensures adequate saturation of spherical shaped EAF slag. After reaching this condition, moisture content should be measured and design mix water should be adjusted. Saturated slag

particles should be covered until casting to minimize the loss of water due to quick evaporation.

2.6 Summary and conclusions

Physical properties along with chemical composition of spherical and angular shaped EAF slag fine aggregates were presented in this chapter. In addition, physical properties of natural sand and gravel as utilized in this study were introduced. The difference in shape of EAF slag particles were analyzed both qualitatively and quantitatively. Following major conclusions can be drawn based on the material properties presented in this chapter.

- The chemical composition of EAF slag suggests that the best possible utilization choice of such material in concrete is as replacement of aggregate, although BF slag can be used for both cement and aggregate replacement.
- The presence of larger sized particles in spherical shaped EAF slag is more than that of angular slag and natural sand.
- Both spherical and angular shaped EAF slag particles exhibit much higher density and lower water absorption than natural sand to be replaced.
- Higher sphericity (0.92) confirms the particle shape of spherical slag. In addition, the relationship between sphericity and mix water content indicates the possibility of higher reduction of mix water during casting if spherical shaped EAF slag is utilized.
- A laboratory based saturation measurement technique for spherical shaped EAF slag aggregate was introduced.

Design of concrete along with fresh concrete behavior will be discussed in the following chapter based on the material properties as discussed in this chapter.

3 Fresh behavior of EAF slag fine aggregate concrete

3.1 Introduction

This study investigates the applicability of a newly developed spherical shaped EAF slag fine aggregate in concrete as replacement of natural sand at different slag replacement ratio and water to cement ratio. In this context, all important properties (such as fresh behavior, physical, mechanical and durability) of normal and EAF slag concrete were investigated at ambient and extreme condition under different experimental programs. This chapter includes the selection criteria of different experimental parameters. In addition, a trial based method of obtaining minimum water content for spherical and angular shaped EAF slag concrete is presented this chapter. Designed mix proportions based on the material properties as discussed in chapter 2 are included for different water to cement ratio and slag replacement ratio. Finally, fresh concrete properties evaluated at the time of casting are included along with particle settlement behavior of EAF slag concrete.

3.2 Experimental parameters with selection criteria

It has been already pointed out in chapter 1, Figure 1-7 that this study primarily considered two different sets of experimental parameters to investigate the fundamental and durability properties of concrete produced by spherical shaped EAF slag fine aggregates. The considered experimental parameters include water to cement ratio (W/C),

slump and air content of 0.4, 5cm and 5% (series 1 and 2 of Figure 1-7) and 0.6, 12cm and 5% (series 3 in Figure 1-7) respectively. The reason for choosing the latter set was to investigate the utilization possibility of the newly developed spherical shaped EAF slag fine aggregates in normal concrete as replacement of natural sand. In contrary, the former set was chosen to investigate the utilization possibility of the material in concrete pavement due to following reasons.

It is fact that, concrete used in pavement are of special type having high flexural strength to distribute the wheel load in wider base/sub base. At the same time such concrete requires lower slump to increase the wearing resistance and facilitate the use of slipform construction and negate the effect of segregation caused by bleeding (FHWA, HIF-07-004). The expected merits of utilizing spherical shaped EAF slag in concrete as discussed in section 1.4 indicate that these materials possess high density (Table 2-3) and at the same time requires less water for concreting. These features indicate that the chance of obtaining high flexural strength with spherical shaped EAF slag concrete at low slump is more and therefore justifies the utilization of spherical shaped EAF slag fine aggregates in concrete pavement replacing natural aggregates. Based on the above justification, a low slump of 5cm ± 1.5cm and a relatively high modulus of rupture (ASTM C293-02) of 4.5MPa was targeted. To achieve the targeted flexural strength, a low W/C of 0.4 was considered.

The target for air content of all experimental series was considered as 5% ± 1.0% based on the suggestion of JSCE proportioning manual and guidelines (No. 1, 2004) for concrete structures by using electric arc furnace oxidizing slag aggregates that an air content to be set in between 5%-6% if EAF slag fine aggregates are used in concrete in combination with normal coarse aggregate of maximum size of 20mm.

3.3 Design of concrete

3.3.1 Evaluation of minimum water content for spherical shaped EAF slag concrete

Benefit of utilization of spherical shaped particles (section 1.4) in concrete is that they reduce the mix water requirement in comparison to angular or rounded shaped particles of rough texture when the target slump and air content is same. It has already

been discussed in section 3.2 that the target of this study is to utilize spherical shaped EAF slag in concrete at two different W/C, slump and air content of 0.4, 5cm, 5% and 0.6, 12cm and 5% respectively. In this context, several trial tests were conducted to obtain the minimum water content for normal as well as spherical and angular shaped EAF slag concrete.

Prior to trial tests, coarse aggregates were prepared in ample quantity by soaking them in water for 24 hours and drying them at saturated surface dry condition after cleaning so that the variation in the results of trail tests due to the variation of moisture content of coarse aggregates can be avoided. Moisture content of sand and EAF slag was measured before the respective trial tests. Initially, W/C, slump and air content case of 0.4, 5cm and 5% was considered and a trial mix proportion for normal and spherical shaped EAF slag concrete having slag ratio of 1.0 was prepared on absolute volume basis by the method described in JSCE guidelines for concrete (No. 16, 2007).

Initial assumption for water content of normal and spherical shaped EAF slag concrete of slag ratio 1.0 was made as 165 kg/m^3 and 140 kg/m^3 respectively. The former assumption was made within the prescribed range of 155-175 kg/m^3 as per Table C4.5.1 of JSCE guidelines (No. 16, 2007) for normal concrete produced by coarse aggregates of maximum size of 20mm while the latter assumption of water content for spherical slag concrete was made 15% lower than normal concrete based on the previously established approximation from sphericity as described in section 2.4.2. After each trial casting, slump and air content of freshly cast concrete were measured and the water content was adjusted accordingly based on the criteria provided in Table C4.5.3 of JSCE guidelines for concrete (No.16, 2007). Trial casting and subsequent testing for slump and air content were continued until the slump and air content were obtained within the target range of 5 ± 1.5cm and 5% ± 1.5% respectively.

Once the minimum water content of normal and spherical shaped EAF slag concrete of slag ratio 1.0 was obtained, trial mix proportions for other slag replacement ratio (i.e. 0.3 and 0.5) cases were computed by changing FM of sand and assuming a linear decrease in water requirement from no slag to 100% spherical slag case. Thereafter, several trial casting and subsequent testing were conducted to confirm the minimum water content for other slag ratio cases. The minimum water content obtained for the W/C and slump of 0.4 and 5cm case were further modified by using Table C4.5.3 of JSCE

guidelines for concrete (No.16, 2007) to obtain minimum water content for the case of W/C and slump of 0.6 and 12cm. Similar approach as described above was applied for angular shaped EAF slag concrete. This is to note that prior to actual casting trial tests were conducted to confirm the accuracy of prediction for the latter two cases. Figure 3-1 shows the flow of obtaining minimum water content for slag concrete.

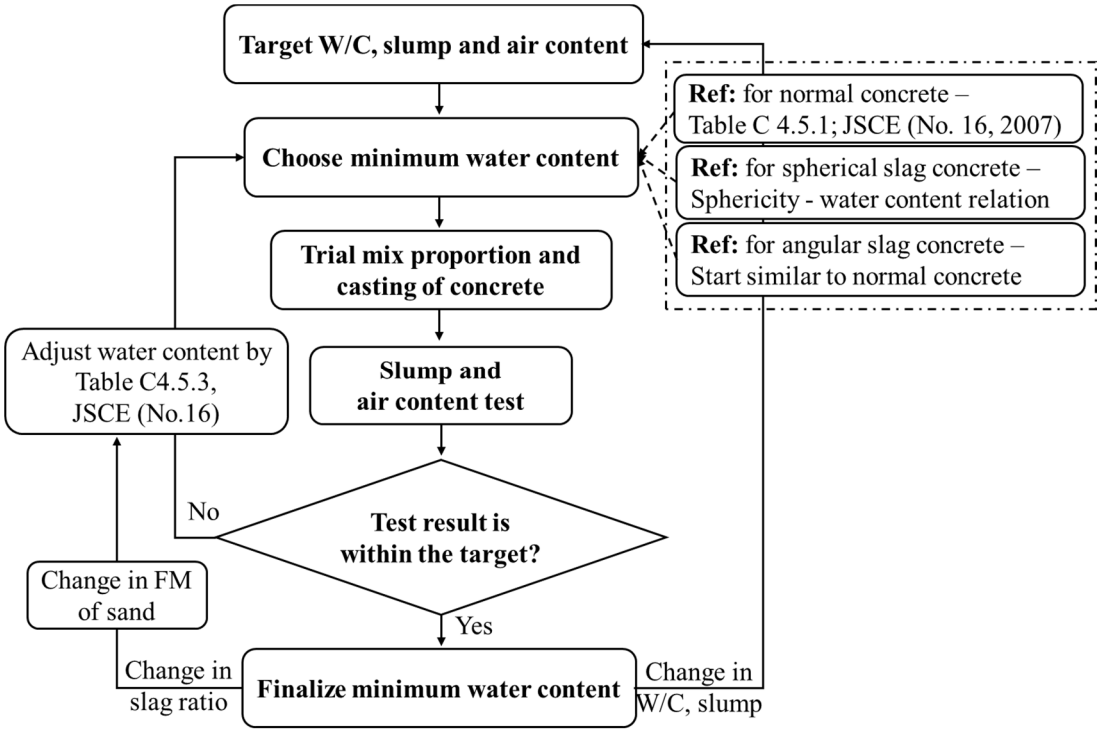

Figure 3-1 Evaluation of minimum water content

3.3.2 Mix proportions of concrete

Based on the obtained minimum water content for each type of concrete, mix proportions were computed, duly verified during casting for fresh concrete properties and used for casting of all types of specimen. Table 3-1 presents the mix proportions for normal, spherical and angular shaped EAF slag concrete for all experimental series as noted in Figure 1-7.

Table 3-1 Mix proportions of concrete (Roy et al., 2018)

Series	Slag Ratio	Slag Type	W/C	Target Slump (cm)	Target Air Content (%)	Water (kg/m^3)	Cement (kg/m^3)	Gravel (kg/m^3)	Sand (kg/m^3)	Slag (kg/m^3)	AE Admixture (kg/m^3)
1	0.0	No slag	0.4	5	5	150	376	1070	685	0	3.76
	0.3	Spherical	0.4	5	5	145	362	1077	493	298	3.62
	0.5					140	351	1089	356	503	3.51
	0.7					134	335	1107	217	715	3.35
	1.0					126	314	1135	0	1039	3.14
2	0.3	Angular	0.4	5	5	153	383	1083	461	298	3.83
	0.5					155	388	1082	326	492	3.88
	0.7					156	390	1079	195	687	3.90
	1.0					158	396	1066	0	983	3.96
2A	0.3	Angular	0.4	5	5	145	362	1077	493	319	3.62
	0.5					140	351	1089	356	537	3.51
	1.0					126	314	1135	0	1110	3.14
3	0.0	No slag	0.6	12	5	170	283	1070	700	0.0	2.83
	0.3	Spherical				169	282	1076	492	298	2.82
	0.5					167	279	1059	346	489	2.79
	1.0					160	267	1065	0.0	983	2.67

3.3.3 Reduction of water content due to particle shape

Table 3-1 confirms the previous assumption that concrete produced by spherical shaped EAF slag fine aggregates require much lesser water in comparison to normal and angular shaped EAF slag fine aggregates irrespective of W/C to attain same slump and air content. This indicates a similar amount of reduction in cement content since water to cement ratio (W/C) for a particular experimental series is constant. It has been discussed in section 2.4.2 that spherical shaped particles have higher sphericity along with lower maximum void content in comparison to angular shaped particles which demands for much lower water during concreting.

Based on the mix proportions as listed in Table 3-1, a relationship between change in mix water content with slag ratio for both spherical and angular shaped EAF slag concrete for W/C, slump and air content of 0.4, 5cm and 5% is shown in Figure 3-2. The relationship shows a linear decrease and increase in water content for spherical and angular shaped EAF slag concrete with the increase in slag ratio respectively. Based on Figure 3-2, two simple equations (Eq. 3.1 and 3.2) are proposed for spherical and angular

shaped EAF slag fine aggregate concrete for quick estimation of water content for any slag replacement ratio. Although water content of slag concrete is dependent on several factors such as gradation, type, water absorption, density of slag particles however, those expressions will be useful for the estimation of initial water content for a particular slag ratio which of course requires trial tests for validation based on targeted experimental parameters such as slump, air content etc.

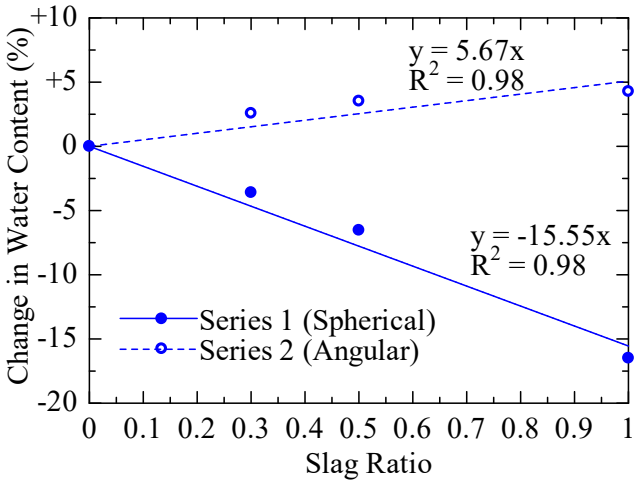

Figure 3-2 Change in water content with slag ratio

For spherical slag concrete, $$W_{C,S} = W_{C,NC} \times (1 - 0.1555 \times SR) \quad (3.1)$$

For angular slag concrete, $$W_{C,A} = W_{C,NC} (1 + 0.0567 \times SR) \quad (3.2)$$

Where, $W_{C,NC}$ = Mix water content of normal concrete, $W_{C,S}$ = Mix water content of spherical slag concrete, $W_{C,A}$ = Mix water content of angular slag concrete, SR = slag replacement ratio

Reduction of cement content for concreting has significant environmental impact. It has been estimated that, one ton of CO_2 is released in the atmosphere for the production of each ton of cement and cement industry alone is responsible for the generation of 7% CO_2 worldwide (Das et al., 2016). This indicates that utilization of byproduct material such as spherical shaped EAF slag in concrete is an economic and environment friendly choice that will promote to achieve SDG goal target 12 and 13 for respective industries as discussed in chapter 1.

3.4 Fresh concrete behavior

3.4.1 Slump and air content

Table 3-2 summarizes the results related to slump, air content and density of freshly mixed concrete for experimental series 1, 2 and 3 respectively. It has been discussed in section 3.2 that a low slump of 5cm and a high air content of 5% was targeted for series 1 and 2 to investigate the applicability of spherical and angular shaped EAF slag fine aggregate in concrete pavement. The results related to fresh concrete behavior as listed in Table 3-2 clearly show that the slump of all concrete under series 1 and 2 are closer to the target value of 5cm±1.5cm irrespective of the type of slag with a maximum deviation of 1.4cm for spherical shaped EAF slag concrete having slag ratio of 1.0. Similarly, values of air content for those concrete are closer to the target value of 5%±1.5% with a deviation of 0.9% for the angular shaped EAF slag concrete having slag ratio of 0.5 and 1.0 and 1.0% for the slag ratio of 0.7.

Table 3-2 Behavior of freshly mixed concrete (Roy et al., 2018)

Series	Slag type	W/C	Slag ratio	Target slump (cm)	Measured slump (cm)	Target air content (%)	Measured air content (%)	Fresh density (kg/m^3)
1	Spherical	0.4	0.0	5±1.5	4.7	5±1.5	4.8	2416
			0.3		4.0		4.6	2500
			0.5		5.8		5.0	2566
			0.7		4.1		4.9	2632
			1.0		3.6		5.0	2738
2	Angular	0.4	0.3	5±1.5	4.3	5±1.5	4.6	2501
			0.5		4.7		4.1	2578
			0.7		4.3		4.0	2652
			1.0		4.7		4.1	2743
3	Spherical	0.6	0.0	12±2	12.0	5±1.5	4.4	2334
			0.3		12.2		5.5	2405
			0.5		13.7		4.8	2469
			1.0		12.1		6.2	2659

Since, a lower slump and good air permeability was required due to the target of applying the slag materials in concrete pavement, the lower slump of spherical shaped EAF slag concrete (series 1) with slag ratio of 1.0 and lower air content of angular shaped EAF slag concrete (series 2) of slag ratio 0.5, 0.7 and 1.0 was considered acceptable

although it was marginal to the target boundaries. However, air content for the former case and slump for the latter case were found closer to the target values of 5% and 5cm respectively.

Similar to series 1 and 2 both slump and air content of concrete produced for series 3 showed closer values to the target range irrespective of slag ratio. It can be noted that series 3 was designed with high W/C, slump and air content of 0.6, 12cm and 5% respectively with an aim to utilize EAF slag fine aggregates in normal concrete. Thus, results related to fresh concrete behaviors of all experimental series confirmed the accuracy of mix proportion for the intended purpose.

3.4.2 Influence of particle shape on slump and air content of EAF slag concrete

The influence of shape of EAF slag on slump and air content of concrete can be discussed in light of mix water content. It has been already discussed in section 3.3.3 that spherical shaped EAF slag concrete requires less water and cement with the increase in slag ratio to attain similar slump and air content as of normal concrete under same W/C. This finding is similar to the observations of Dewar and Anderson (1992) and Shilstone (1999) that cubical or spherical particles require less paste and less water for workability.

For the slag ratio of 1.0, for series 1, a 16% (Figure 3-2) reduction in water and cement amount is observed in comparison to normal concrete due to the utilization of spherical shaped EAF slag as fine aggregates. In contrary, for series 2, an increase in water and cement content is recorded with the increase in slag ratio and this amount is 5.3% (Figure 3-2) in comparison to normal concrete when the slag ratio is 1.0. The phenomena is related to the void content in concrete as discussed in section 2.4.2. Since spherical particles have lower void ratio than angular particles as observed and shown in Table 2-5, concrete produced by spherical shaped EAF slag have lower demand for water compared to that produced by angular shaped EAF slag.

In order to validate the above result, three additional concrete batches (marked as series 2A in Table 3-1) were cast by using angular shaped EAF slag fine aggregates for the slag ratio of 0.3, 0.5 and 1.0 using the same mix proportions to that of spherical shaped EAF slag concrete as shown in Table 3-1. The purpose was to investigate the influence of slag shape on the water content and fresh concrete behaviors. For concrete cast under

series 2A, fresh concrete behaviors such as slump, air content, fresh concrete density and bleeding behavior were checked. A comparison of slump and air content with slag ratio of such concrete is depicted in Figure 3-3 and 3-4 respectively.

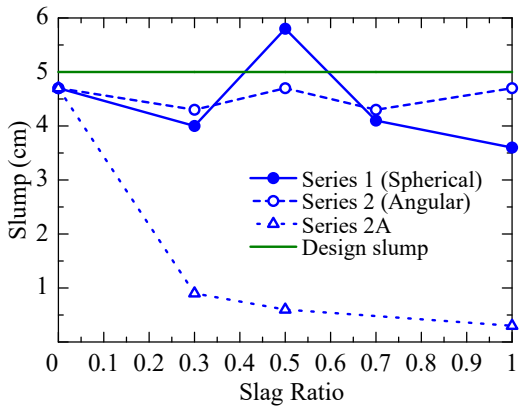

Figure 3-3 Comparison of slump with slag ratio (Roy et al., 2018)

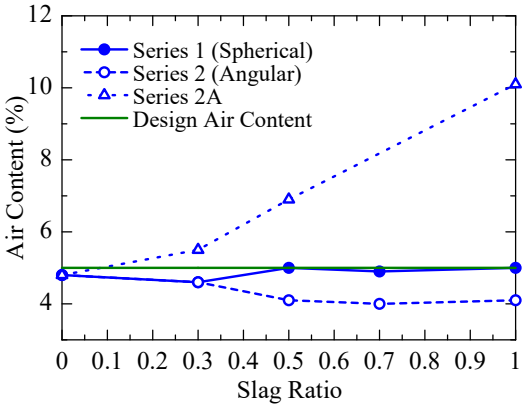

Figure 3-4 Comparison of air content with slag ratio (Roy et al., 2018)

It can be seen from Figure 3-3 that for the low water content as of spherical shaped EAF slag concrete, angular shaped EAF slag concrete shows a very low slump with the increase in slag ratio. In addition, the slump values were found to be decreasing with the increase in slag ratio which is reasonable due to the fact that for spherical shaped EAF slag concrete water amount reduces with the increase in slag ratio and the reduction in water amount for angular shaped EAF slag concrete causes the decrease in slump.

In contrary, air content of angular shaped EAF slag concrete was found to be increasing with the increase in slag ratio which is justified since reduction in water content enables more void spaces in the cast concrete of same volume. This is also true as per

JSCE guidelines for concrete (No. 16) Table C4.5.3 that for every 3% decrease in water content from a reference value, air content increases by 1% from the reference value. These results support the earlier assumption that spherical shaped EAF slag concrete requires less water and cement to attain similar slump as of angular shaped EAF slag and normal concrete when the W/C is same.

3.4.3 Fresh concrete density

Density of freshly mixed concrete was measured by the method as described in JIS A1116 [ASTM C 138 (2017)]. Fresh concrete density results of concrete under series 1, 2, 2A and 3 are shown in Table 3-2. In addition, experimentally obtained results of fresh concrete density was found closer to that computed from mix proportions, which confirms the accuracy of mixing and concreting. It is clear from Table 3-2 that, density of freshly mixed concrete increases linearly with the increase in slag ratio irrespective of the type of slag and water to cement ratio. This phenomena is obvious due to the incorporation of high density slag particles in concrete. Figure 3-5 depicts the change in fresh concrete density with the increase in slag ratio for different experimental series. It can be seen from Figure 3-5 that the increase in fresh concrete density of spherical shaped EAF slag concrete of different water to cement ratio (0.4 and 0.6) is similar, however angular shaped EAF slag concrete (series 2) shows slightly higher increase in fresh concrete density than the former two cases. This might be attributed to the slightly higher particle density of angular slag (3.85) than spherical slag (3.60) as shown in Table 2-3.

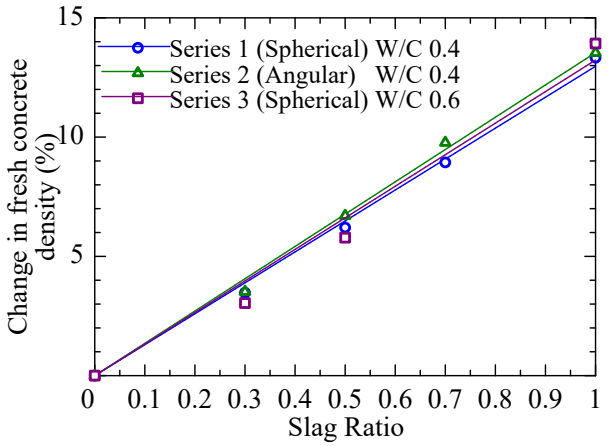

Figure 3-5 Change in fresh concrete density with slag ratio

3.4.4 Bleeding of concrete

Generally, rounded or spherical particles having higher density impart more bleeding in concrete. In addition, bleeding of concrete changes with the change in water to cement ratio. In this context, bleeding behavior of all concrete under series 1, 2 and 3 was evaluated soon after casting. For each series, under each slag replacement ratio, a minimum of two tests for bleeding were conducted and the average results were considered. The scatter of test results were found below 10%. Results related to the bleeding of concrete for series 1, 2 and 3 with time are depicted in Figures 3-6, 3-7 and 3-8 respectively. The notation 'N', 'S' and 'A' in those figures indicates normal, spherical and angular shaped EAF slag fine aggregate concrete at different slag replacement ratio as shown to the right of each notation. Rate of bleeding with slag ratio is also shown in Figure 3-9. Here, rate of bleeding indicates the bleeding of concrete in comparison to the mixing water used for concreting and it is computed by Eq. 3.3 as per ASTM C232 (2014).

$$\text{Rate of bleeding (\%)} = \frac{D}{C} \times 100 \tag{3.3}$$

$$C = \frac{w}{W} \times S \tag{3.4}$$

Where, D = mass of the bleeding water (gm), C = mass of the water in the test specimen (gm), w = net mixing water (kg), W = total mass of the batch (kg), S = mass of the sample (gm).

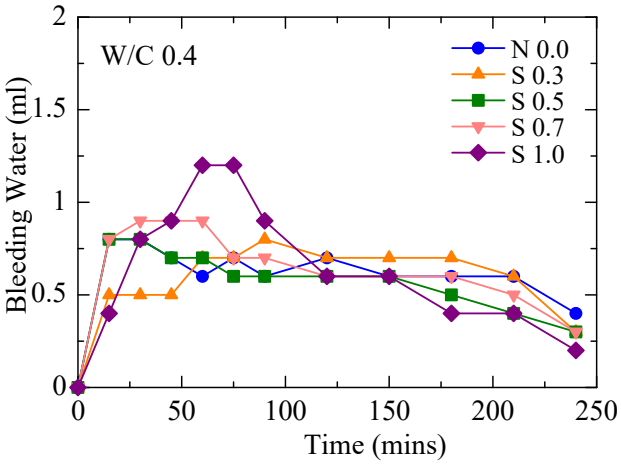

Figure 3-6 Bleeding of concrete with time for series 1 (Roy et al., 2018)

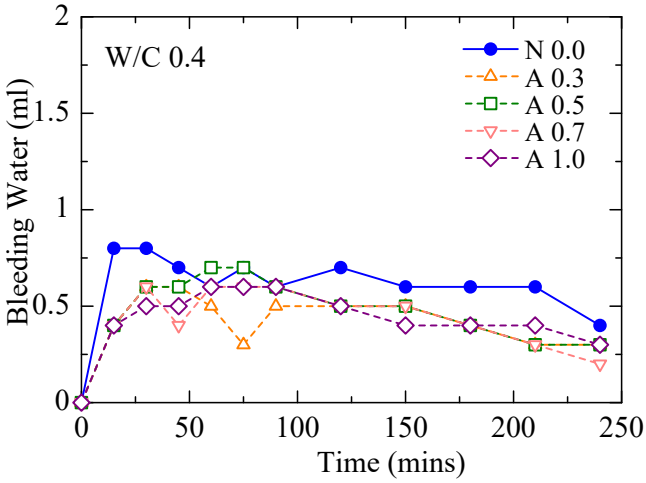

Figure 3-7 Bleeding of concrete with time for series 2 (Roy et al., 2018)

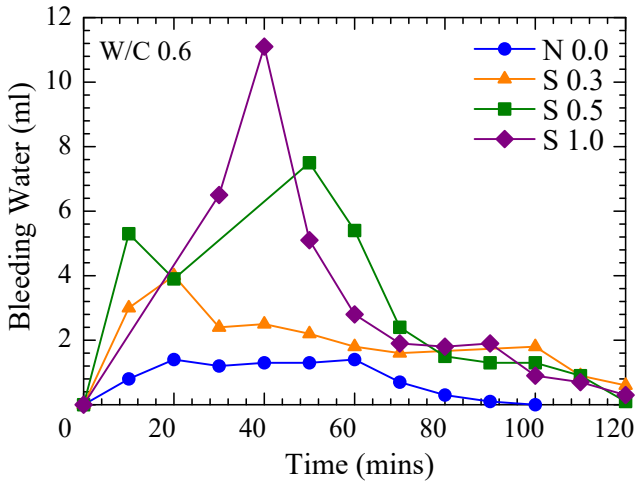

Figure 3-8 Bleeding of concrete with time for series 3 (Roy et al., 2018)

All the figures related to bleeding of concrete (Figure 3-6, 3-7 and 3-8) show an initial increasing slope for all types of concrete which indicates quick initial bleeding for all slag types irrespective of W/C ratio that gradually becomes constant with the progression of time. In case of spherical shaped EAF slag concrete of W/C of 0.4 (series 1, Figure 3-6), increase in bleeding with the increase in slag ratio is observed, which is highest for the slag ratio of 1.0. However, similar bleeding as of normal concrete is observed for the slag replacement ratio of 0.3. Maximum bleeding for the slag ratio of 0.5, 0.7 and 1.0 is observed at 20, 50 and 70 mins respectively.

Exactly similar behavior but higher in values of bleeding water is recorded for spherical shaped EAF slag concrete cast with W/C of 0.6 (series 3, Figure 3-8). For series 3, maximum bleeding for the slag replacement ratio of 0.5 and 1.0 is observed at 50 and 40 mins respectively. Interesting point is that apart from higher bleeding of concrete of series 3 (W/C 0.6) in comparison to series 1 and 2 (W/C 0.4), it was found to be finished within a comparatively shorter period of time (approximately 2hrs.) which might be due to the lower tightness of the mix because of lesser cement content.

In case of angular shaped EAF slag concrete (series 2, Figure 3-7), similar bleeding trend as of normal concrete is observed. However, the values are found to be much lesser than normal and spherical shaped EAF slag concrete (series 1 and 3, Figures 3-6 and 3-8). Interestingly, the bleeding of angular slag concrete (series 2, Figure 3-7) having slag ratio of 0.5 exhibits highest bleeding among the angular slag concretes followed by 0.7, 1.0 and 0.3 slag ratio cases.

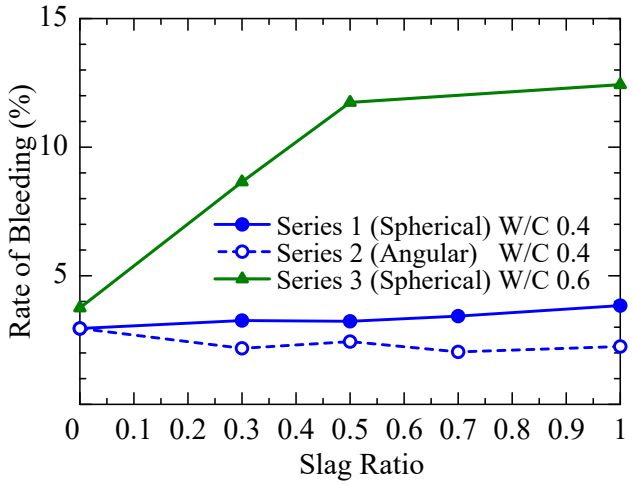

Figure 3-9 Bleeding rate with slag ratio (Roy et al., 2018)

The rate of bleeding as depicted in Figure 3-9 clearly shows the influence of shape of slag particles along with W/C. For spherical shaped EAF slag concrete produced at W/C of 0.4 (series 1), an increase in rate of bleeding is observed with the increase in slag ratio. Up to a slag replacement ratio of 0.5, the tendency is constant to slightly increasing in comparison to normal concrete. However, for the slag ratio of 1.0, 30% higher bleeding rate is observed in comparison to normal concrete. In contrary, for angular slag concrete (series 2) rate of bleeding is found to be lower than normal concrete although changes in

bleeding rate with the increase in slag ratio is almost constant. When the water to cement ratio is very high such as 0.6, spherical shaped EAF slag concrete (series 3) exhibit much higher bleeding in comparison to that of W/C of 0.4. The rate of bleeding increases with the increase in slag ratio and becomes steady from slag ratio of 0.5 and 1.0. For the slag ratio of 1.0 bleeding rate is found to be 3.3 times higher than that of normal concrete.

It is evident from the experimental results that spherical shaped EAF slag concrete especially with higher slag ratio such as 1.0 exhibits higher bleeding in comparison to normal concrete. In contrary, the bleeding of angular slag concrete is found similar to slightly decreasing than normal concrete. These behaviors might be attributed to the particle shape, gradation and water absorption of respective concrete. Galloway (1994) observed that if the fine aggregates are too coarse, they produce bleeding, segregation and harshness, but if they are too fine, the demand for water increases. Hudson (1999) and Kalcheff (1977) showed that mixtures with high amount of fines can significantly reduce bleeding and segregation.

In the present study, because of spherical shape and having lesser amount of finer particles in the mix, spherical shaped EAF slag concrete showed higher bleeding in comparison to normal and angular shaped EAF slag concrete. In addition, the water absorption capacity of spherical slag particles as reported in Table 2-3 are much lower than natural sand and angular slag, which might have triggered the bleeding of concrete.

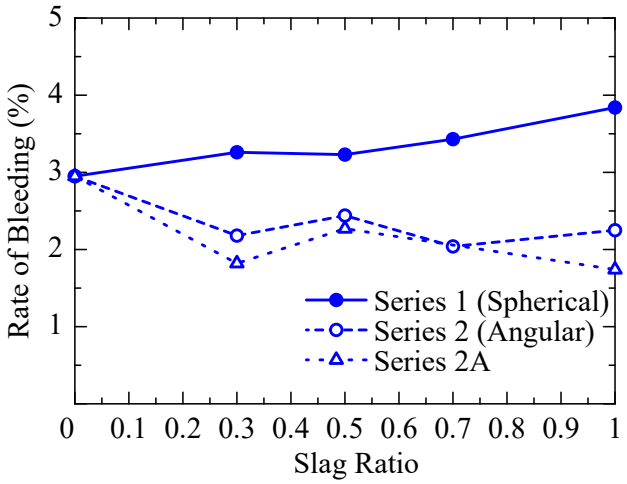

Figure 3-10 Comparison of bleeding rate with slag ratio (Roy et al., 2018)

The rate of bleeding of angular shaped EAF slag concrete having same mix proportion as of spherical shaped EAF slag concrete is shown in Figure 3-10. The new curve of series 2A shows similar trend as of previous curve of series 2, only with the reduction of rate of bleeding with slag ratio which is reasonable due to the fact that the water content is reduced for the current case and so does the bleeding.

3.5 Observation of particle settlement by density distribution

3.5.1 200mm long specimen

Due to high particle density and subsequent bleeding in association with the increase in spherical slag in concrete, possibility of slag settlement in the specimen requires to be investigated as high bleeding along with high slag density might lead to decrease in concrete strength and durability because of segregation and settlement of solid particles in reference to Poon et al. (2001).

In order to investigate the particle settlement in the specimen, cylinder specimens of Ø100x200mm sizes under series 1, 2 and 3 were sliced at a thickness of 50mm horizontally along its length at four distinct parts as shown in Figure 3-11 and 3-12. The thickness of concrete pavement is usually 200~300 mm. Based on this information with an objective of applying EAF slag in concrete pavement, particle settlement of 200mm specimens were tested. The sliced parts were oven dried at a temperature of 105°C for 24 hours.

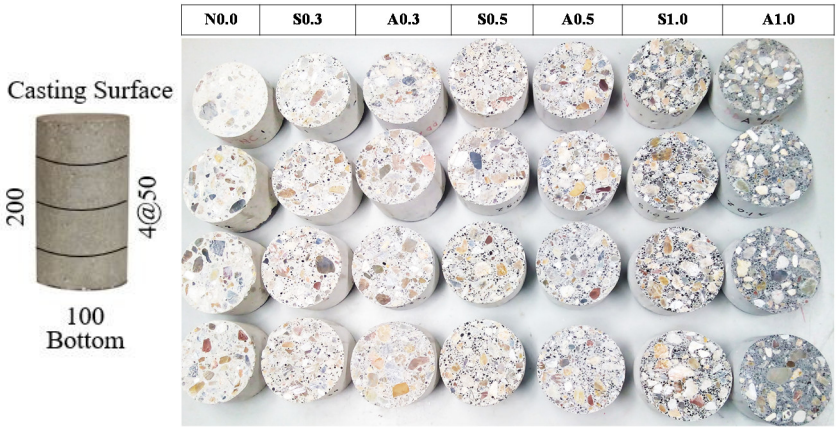

Figure 3-11 Sliced specimen surface of series 1 and 2 (Roy et al., 2018)

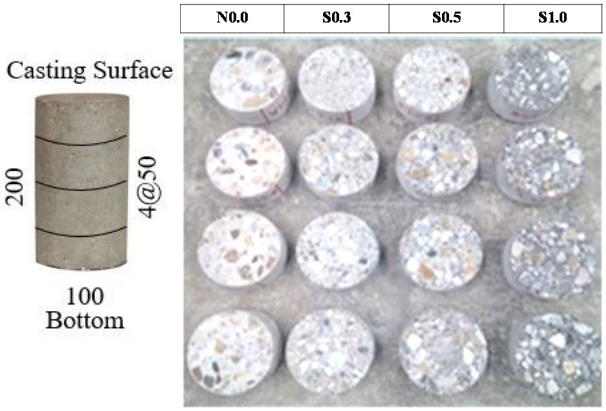

Figure 3-12 Sliced specimen surface of series 3 (Roy et al., 2018)

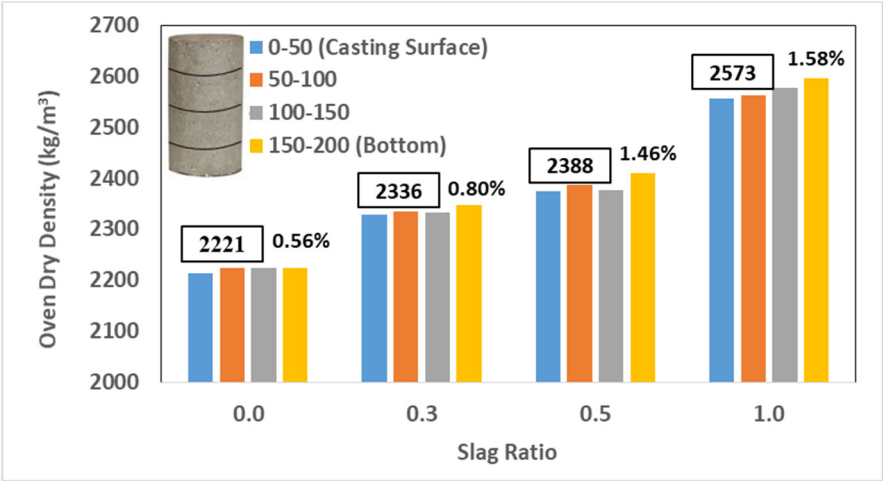

Figure 3-13 Density distribution of series 1 (Roy et al., 2018)

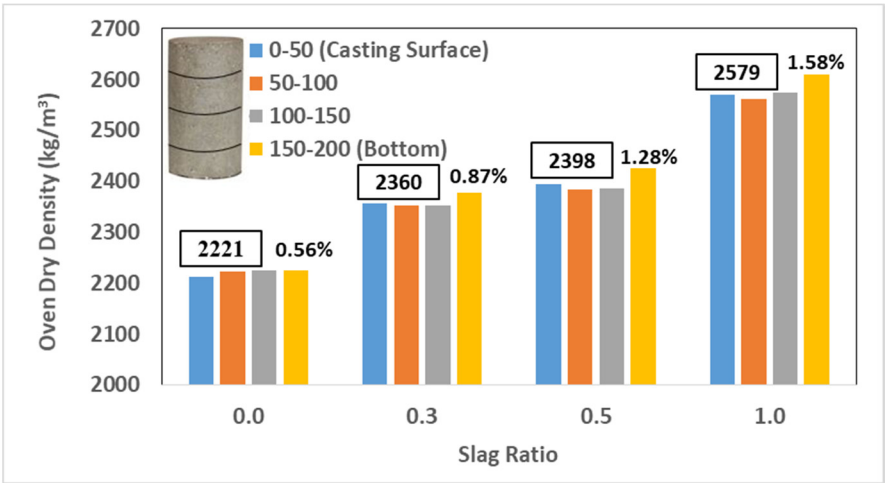

Figure 3-14 Density distribution of series 2 (Roy et al., 2018)

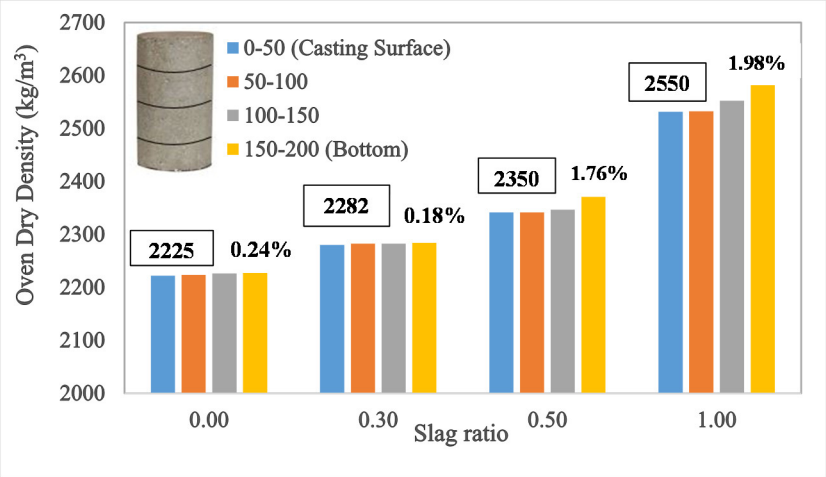

Figure 3-15 Density distribution of series 3 (Roy et al., 2018)

Dimension and weight of each of the sliced part was measured and average density of two representative specimens under each slag ratio case was computed in absolute drying condition. The density distribution results of series 1, 2 and 3 are shown in Figures 3-13, 3-14, 3-15 respectively. For each case, the average density is also provided in those figures. It can be seen from Figures 3-13 to 3-15 that hardened concrete density increases with the increment of slag ratio similar to fresh concrete density. The differences of density from top and bottom of the specimen for spherical shaped EAF slag concrete of W/C of 0.4 (series 1) in case of slag ratio 0.0, 0.3, 0.5 and 1.0 are 0.56, 0.80, 1.46 and 1.58% respectively. Whereas, for angular shaped EAF slag concrete of W/C 0.4 (series 2), these differences are 0.56, 0.87, 1.28 and 1.58% respectively. For series 3 (spherical shaped EAF slag concrete with W/C 0.6), these differences are computed as 0.28, 0.18, 1.76 and 1.98% respectively. This indicates that although the bleeding of spherical shaped EAF slag concrete at higher W/C of 0.6 is very high, subsequent particle settlement in concrete is very low to negligible.

All the experimental results of density distribution clearly indicate a very low particle settlement from concrete mix although high particle density in association with comparatively higher bleeding is observed especially in case of spherical shaped EAF slag concrete when the slag ratio and W/C is high. Angular shaped EAF slag concrete shows similar particle settlement as of spherical slag concrete. For both the cases, segregation amount is negligible. Therefore, the effect of change in shape of slag as well

as change in W/C on the particle settlement is not significant. The result is consistent as the influence of high particle density on settlement mostly comes from the coarse aggregates rather than fine aggregates. Therefore, the above results broaden the scope of utilization of spherical shaped EAF slag fine aggregate in concrete.

3.5.2 500mm long specimen

It has been already discussed in the previous section that the particle settlement of spherical shaped EAF slag fine aggregate concrete tested in regular sized cylinder (Ø100x200mm) is negligible although particle density and associated bleeding is high. To confirm the wider applicability of spherical shaped EAF slag fine aggregates, particle settlement was again investigated in mortar specimen cast using larger sized cylinders of Ø100x500mm sizes. JSCE guidelines for concrete (No.16, 2010) recommend that the maximum thickness of a single layer casting during construction should be 400~500mm. Therefore, the results of 500mm long specimen is applicable for conventional construction. Mortar was chosen to investigate the sole influence of spherical shaped EAF slag on particle settlement by omitting the effect of coarse aggregates. Specimens were cast by replacing natural sand with spherical shaped EAF slag at a volume replacement ratio of 0.0, 0.1, 0.2 and 0.5. W/C of 0.6 and slump greater than 20cm was targeted based on the previous experimental result (section 3.4.4) that spherical slag concrete shows higher bleeding at higher W/C and slump. Table 3-3 shows the mix proportion for mortar along with slump test results which shows that the obtained slump for all slag ratio cases are very high (>20cm).

Table 3-3 Mix proportions of mortar for density distribution test

Slag Ratio	Slag Type	W/C	Water (kg/m^3)	Cement (kg/m^3)	Sand (kg/m^3)	Slag (kg/m^3)	AE Admixture (kg/m^3)	Target Slump (cm)	Measured Slump (cm)
0.0	No slag	0.6	158	263	661	0	2.63	> 20	22.2
0.1	Spherical		156	260	601	94	2.60		21.7
0.2			154	256	541	191	2.56		21.7
0.5			147	246	350	494	2.46		21.3

Based on the mix proportions as shown in Table 3-3, larger sized (length = 500mm) mortar specimens were cast. All cast specimens were cured under water for 7 days and each of the cured specimen was sliced in five equal parts at an interval of 100mm. The sliced parts were oven dried and the oven dry density of each of the part was measured. Figure 3-16 depicts the sliced specimen while Figure 3-17 presents the results related to density distribution respectively.

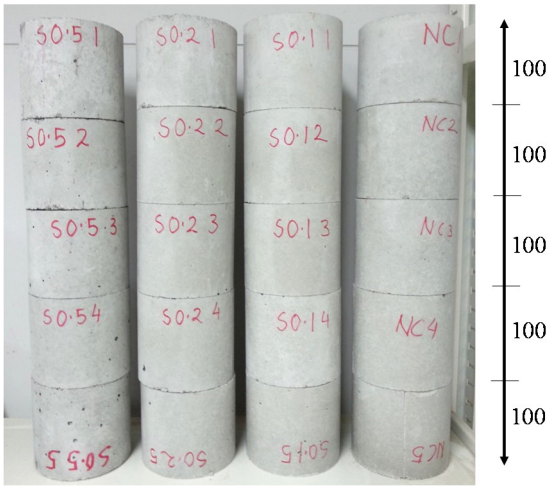

Figure 3-16 Sliced mortar specimen for density distribution test

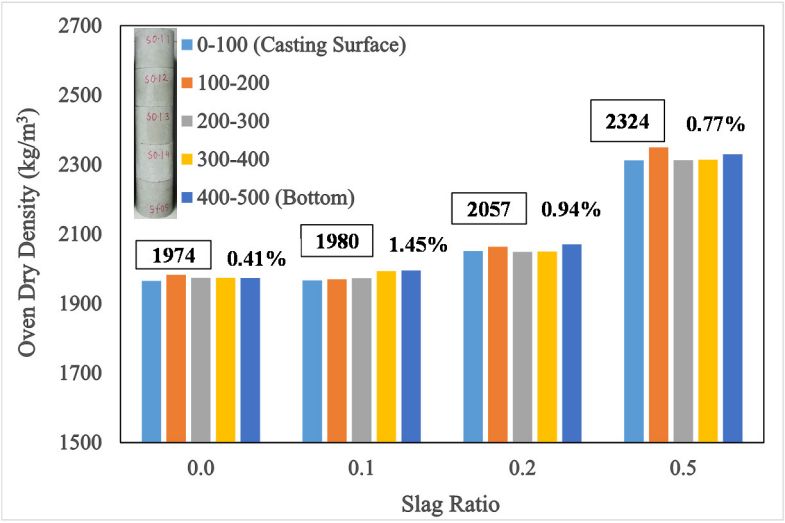

Figure 3-17 Density distribution of long mortar specimen

It is evident from figure 3-17 that, even at higher W/C along with higher slump, settlement of spherical shaped EAF slag particles are very low to negligible. The differences of density from top and bottom of the specimen in case of slag ratio of 0.0, 0.1, 0.2 and 0.5 are 0.41, 1.45, 0.94 and 0.77% respectively. This result indicates that the spherical shaped EAF slag is a promising alternative of natural sand in concrete provided that other concrete properties such as mechanical, thermal, high temperature influence etc. are satisfactory.

3.6 Summary and conclusions

This chapter included the fresh concrete properties of concrete cast using both spherical and angular shaped EAF slag aggregate. Prior to that, all experimental parameters were introduced and the reasons for choosing them were described. A trial based evaluation method of minimum water content for spherical shaped EAF slag concrete was proposed and mix proportions of concrete for all experimental series were included. Finally, results of fresh concrete behavior such as slump, air content, bleeding, fresh concrete density, particle settlement were introduced and discussed. Based on the study as presented in this chapter, following major conclusions can be drawn.

- The reason for choosing two different types of water to cement ratio (W/C) of 0.4 and 0.6 along with low (5cm) and high slump (12cm) was clarified due to the purpose of utilization of spherical shaped EAF slag fine aggregates in concrete pavement and normal concrete respectively.
- Despite of the characteristic feature of high density, spherical shaped EAF slag concrete requires less water and cement compared to normal and angular shaped EAF slag concrete which is economical, environment friendly and sustainable if utilized in concrete.
- Fresh concrete density for both spherical and angular shaped EAF slag concrete increases linearly with the increment of slag ratio. Influence of W/C is negligible and concrete produced by angular shaped EAF slag shows slightly higher fresh concrete density due to higher individual particle density.

- Spherical shaped EAF slag concrete imparts higher bleeding at higher water to cement ratio (W/C 0.6) and slag replacement ratio. At lower W/C of 0.4, up to a slag replacement ratio of 0.5, bleeding behavior of spherical slag concrete is similar to normal concrete. However, angular shaped EAF slag concrete shows lower bleeding than normal concrete for all slag replacement ratio.
- Although higher bleeding is observed with the increase in slag ratio and W/C for spherical shaped EAF slag concrete, a very low slag settlement was observed even at longer sized specimen of 500mm which broadens the scope of its wider utilization.

In a nutshell, spherical shaped EAF slag concrete demonstrates its strong applicability in concrete due to improved fresh behavior with reduced water and cement content. The effect of higher bleeding especially at higher slag ratio should not affect the mechanical and durability properties since the particle settlement is negligible. In the next chapter, mechanical and durability properties of EAF slag concrete will be investigated for different experimental parameters as introduced in this chapter.

4 Applicability of spherical shaped EAF slag fine aggregates in concrete – Mechanical and durability properties

4.1 Introduction

Study on the fresh behavior of concrete as reported in chapter 3 revealed that concrete produced by spherical shaped EAF slag fine aggregates requires less water and cement in comparison to normal and angular shaped EAF slag concrete. Due to the requirement of less water and cement, possibilities of obtaining improved durability properties of concrete by utilizing spherical shaped EAF slag fine aggregate is high. On the other hand, lower particle settlement corresponding to higher bleeding of spherical shaped EAF slag concrete at higher W/C, slump and slag replacement ratio indicates the prospect of obtaining improved mechanical properties of such concrete. To validate the above possibilities, this chapter will focus on the mechanical and durability properties of concrete produced by both spherical and angular shaped EAF slag fine aggregates at different W/C, slump and slag replacement ratio.

4.2 Brief overview of experiment

4.2.1 Experimental series and specimen notation

In order to investigate the mechanical and durability properties of concrete, three different series of specimens were prepared by utilizing spherical and angular shaped EAF slag fine aggregates in concrete by replacing natural sand at a volume replacement

ratio of 0.0, 0.3, 0.5 and 1.0 for two different target W/C, slump and air content. Concrete produced under series 1 and 2 were of spherical and angular shaped EAF slag fine aggregates respectively at W/C, slump and air content of 0.4, 5cm and 5% whereas, that of series 3 was produced by spherical shaped EAF slag fine aggregates at the W/C, slump and air content of 0.6, 12cm, 5%. As explained in section 3.2, target for series 1 and 2 is to investigate the behavior of spherical and angular shaped EAF slag fine aggregates in concrete pavement while for series 3 target is to investigate the performance of spherical shaped EAF slag fine aggregates in normal concrete. Table 4-1 summarizes the details of test series and specimen notation which will be used in all the plots of this study. Same mix proportions as reported in Table 3-1 was used for concreting.

Table 4-1 Experimental series and specimen notation

Series[1]	Slag Ratio	Slag Type	W/C[1] and Slump	Air Entrainment	Notation[1]
1 (Spherical)	0.0	No slag	W/C 0.4 Slump 5cm	Air Entrained	N 0.0
	0.3	Spherical			S 0.3
	0.5				S 0.5
	1.0				S 1.0
2 (Angular)	0.3	Angular	W/C 0.4 Slump 5cm	Air Entrained	A 0.3
	0.5				A 0.5
	1.0				A 1.0
3 (Spherical)	0.0	No slag	W/C 0.6 Slump 12cm	Air Entrained	N 0.0
	0.3	Spherical			S 0.3
	0.5				S 0.5
	1.0				S 1.0

4.2.2 Details of specimen, conducted tests and curing condition

Mechanical properties of concrete such as elastic modulus, compressive strength, compressive fracture energy, flexural strength, tensile strength and tensile fracture energy and durability properties such as drying shrinkage, water absorption and air permeability were examined. Cylinders of Φ100x200mm were used for conducting compressive and split tensile test whereas prisms of 100x100x400mm were used for bending and, shrinkage test. Specimens having size of 300x300x100mm were used for air permeability test. For all the test except shrinkage and air permeability a minimum of 3 specimens

were used. A summary of the conducted experiments, specimen numbers, type, size and curing age is listed in Table 4-2.

Table 4-2 Details of specimen used for Mechanical and durability properties

Series	W/C	Name of test	Specimen type & size	Curing age (days)	Specimen per batch	Total specimen
1	0.4	Compression	Cylinder Ø100x200	3	3	12
2	0.4			3	3	09
1	0.4			7	3	12
2	0.4			7	3	09
3	0.6			7	3	12
1	0.4			28	3	12
2	0.4			28	3	09
3	0.6			28	3	12
1	0.4	Split tensile	Cylinder Ø100x200	3	3	12
2	0.4			3	3	09
1	0.4			7	3	12
2	0.4			7	3	09
3	0.6			7	3	12
1	0.4			28	3	12
2	0.4			28	3	09
3	0.6			28	3	12
1	0.4	Flexural	Prism 100x100x400	3	3	12
2	0.4			3	3	09
1	0.4			7	3	12
2	0.4			7	3	09
3	0.6			7	3	12
1	0.4			28	3	12
2	0.4			28	3	09
3	0.6			28	3	12
1	0.4	Shrinkage	Prism 100x100x400	7	2	08
2	0.4			7	2	06
3	0.6			3	2	08
1	0.4	Water absorption	Prism 100x100x200	3	3	12
2	0.4			3	3	09
3	0.6			3	3	12
1	0.4			7	3	12
2	0.4			7	3	09
3	0.6			7	3	12
1	0.4			28	3	12
2	0.4			28	3	09
3	0.6			28	3	12
1	0.4	Air permeability	Prism 300x300x100	28	2	08
2	0.4			28	2	06

4.3 Mechanical properties

4.3.1 Compressive stress-strain relationship

Compressive stress was computed from the load data while corresponding strain was obtained from two vertically glued strain gauges (gauge length = 60mm) on opposite surface of each of the specimen during uniaxial compression test. Both load and strain gauge readings were recorded by data logger during compression test. Prior to the test 4 nos. of load varying displacement transducers (LVDT) were placed around four sides of the specimen to measure the specimen displacement. Double folded Teflon sheets with grease having a thickness of 0.05mm each were used in between the specimen and load plate to minimize the friction effect. Figure 4-1 shows the compression test protocol. For each series under each slag ratio, a minimum of 3 representative cylinder specimens (Ø100x200mm) were used and average results were considered.

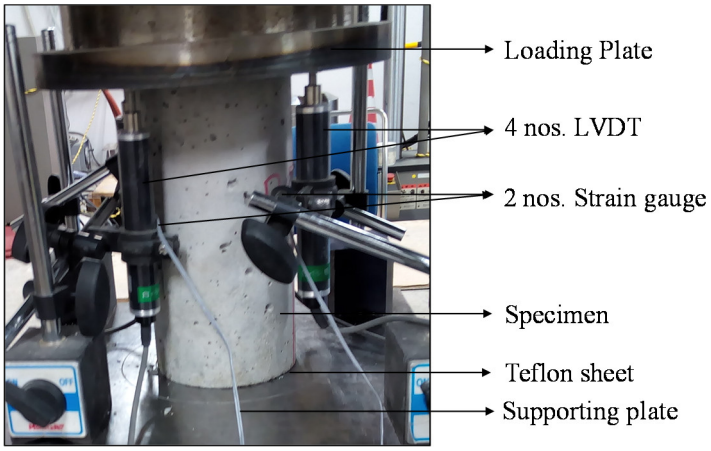

Figure 4-1 Compression test protocol

Figure 4-2 and 4-3 represents the compressive stress-strain relationship of concretes of series 1, 2 and 3 respectively after a curing age of 28 days. It is clear from Figure 4-2 and 4-3 that at low W/C of 0.4, both spherical and angular shaped EAF slag concrete (Figure 4-2, series 1 and 2) show improved peak load than normal concrete although strain at peak load and ultimate strain at failure are similar to normal concrete. In contrary, for the W/C of 0.6 (series 3, Figure 4-3) normal concrete exhibits higher peak load and corresponding higher peak strain in comparison to spherical shaped EAF slag concrete.

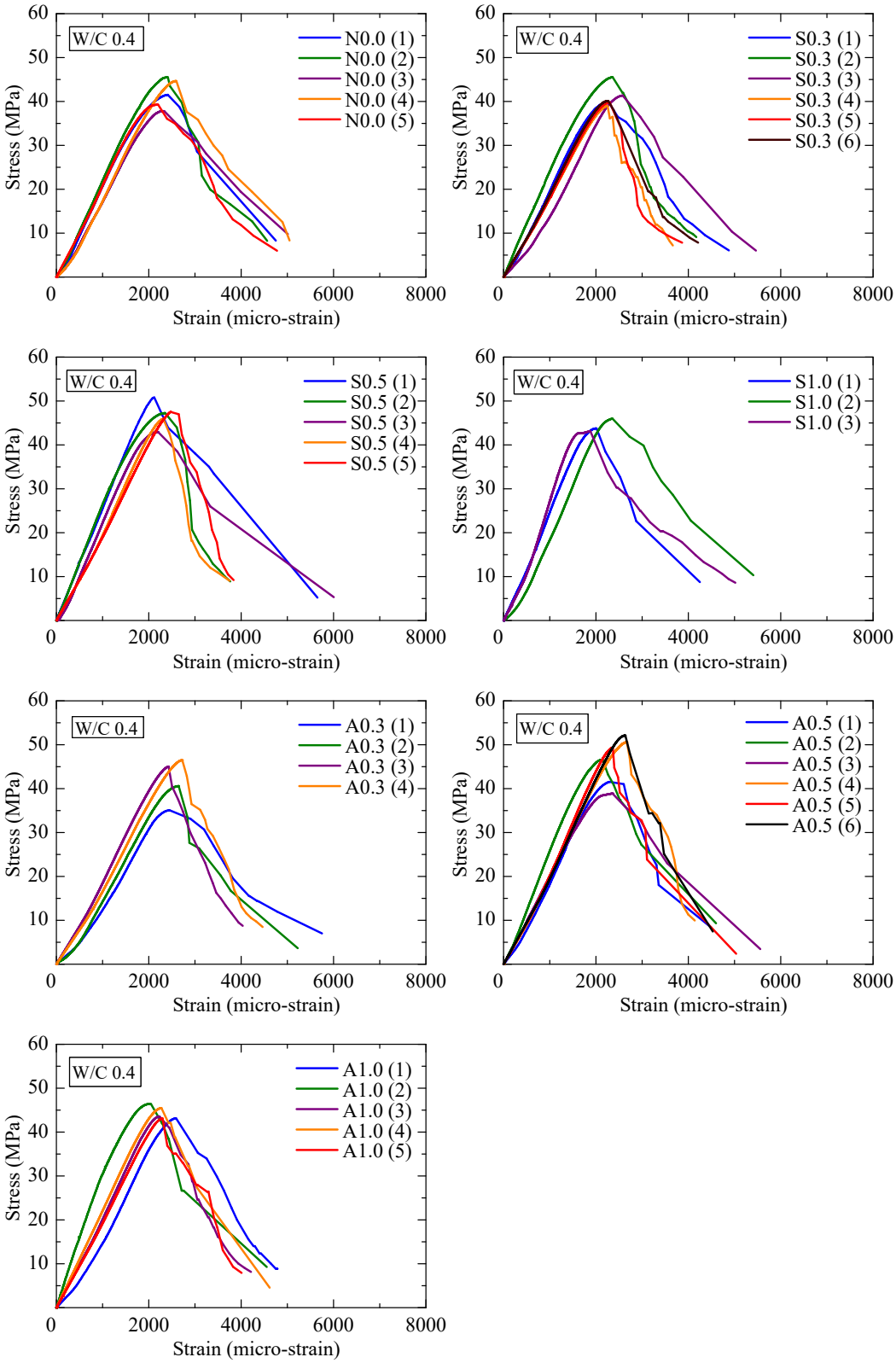

Figure 4-2 Compressive stress-strain relationship of concrete under series 1 and 2 (curing age = 28 days)

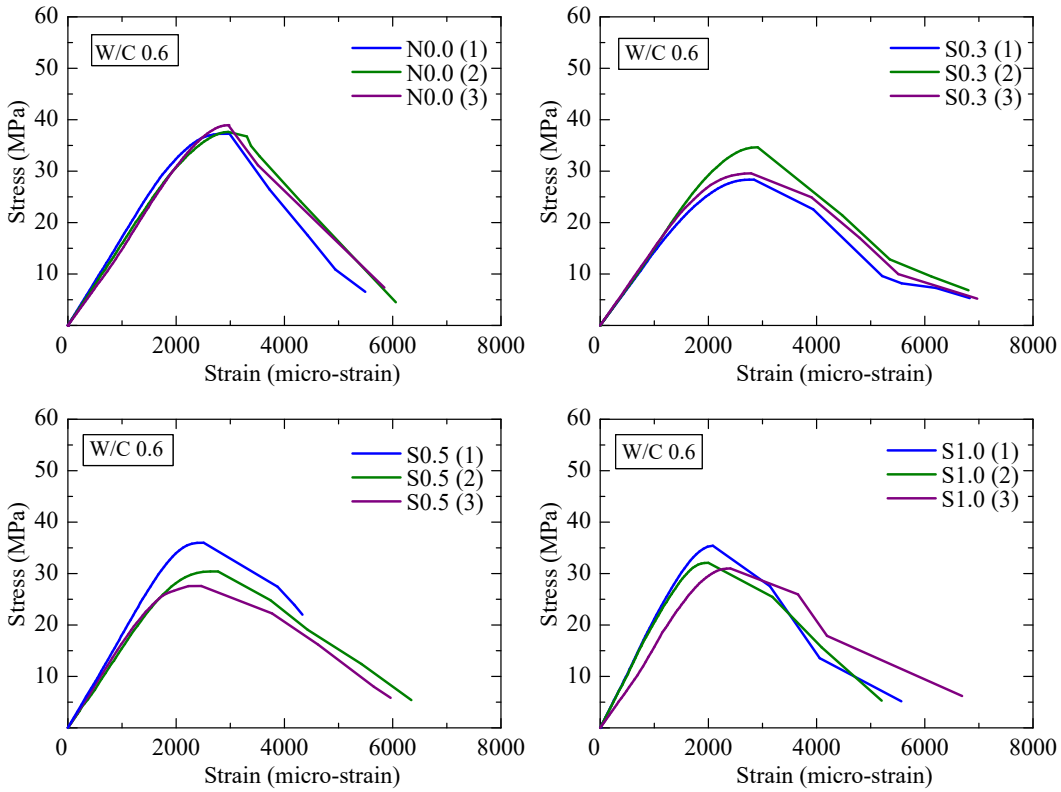

Figure 4-3 Compressive stress-strain relationship of concrete under series 3 (curing age = 28days)

4.3.2 Compressive strength and elastic modulus

Three representative cylindrical type (Φ100x200mm) concrete specimens cast under each slag replacement ratio of series 1 and 2 were tested for uniaxial compression after a curing age of 3, 7 and 28 days. For series 3, tests were conducted after a curing age of 7 and 28 days only. Figure 4-4 and 4-5 depict the compressive strength and elastic modulus of concrete of series 1, 2 and 3 after a curing age of 3, 7 and 28 days respectively. Elastic modulus was computed from the strain gauge reading by determining the slope of the compressive stress-strain curve between points of longitudinal strain of 50 micro strain and strain corresponding to one third of the peak compressive stress.

The increase in compressive strength of both spherical and angular shaped EAF slag concrete of series 1 and 2 (low W/C of 0.4) with the increment of slag ratio irrespective curing age is evident from Figure 4-4. However, for the W/C of 0.6 (series 3), a decrease in compressive strength in comparison to normal concrete is observed for

spherical shaped EAF slag concrete irrespective of curing age. Interestingly, from the slag ratio of 0.3 until 1.0, a slight increase in compressive strength is observed for series 3. As shown in Figure 4-4 for the curing age of 3 days, angular shaped EAF slag concrete (series 2) exhibits lesser compressive strength compared to spherical slag concrete (series 1). However, this situation improves with curing age and after the curing age of 28 days, the difference in compressive strength between spherical and angular shaped EAF slag concrete is not significant considering all the slag ratio of 0.3, 0.5 and 1.0. This indicates that for the W/C of 0.4, concrete produced by spherical shaped EAF slag gains higher strength within a shorter curing period than that produced by angular shaped EAF slag. At the curing age of 28 days, for the W/C of 0.4, compressive strength of both spherical and angular shaped EAF slag concrete having slag ratio of 0.3 is similar to normal concrete which increases to a maximum value when the slag ratio is 0.5 and slightly decreases when all sand is replaced by EAF slag.

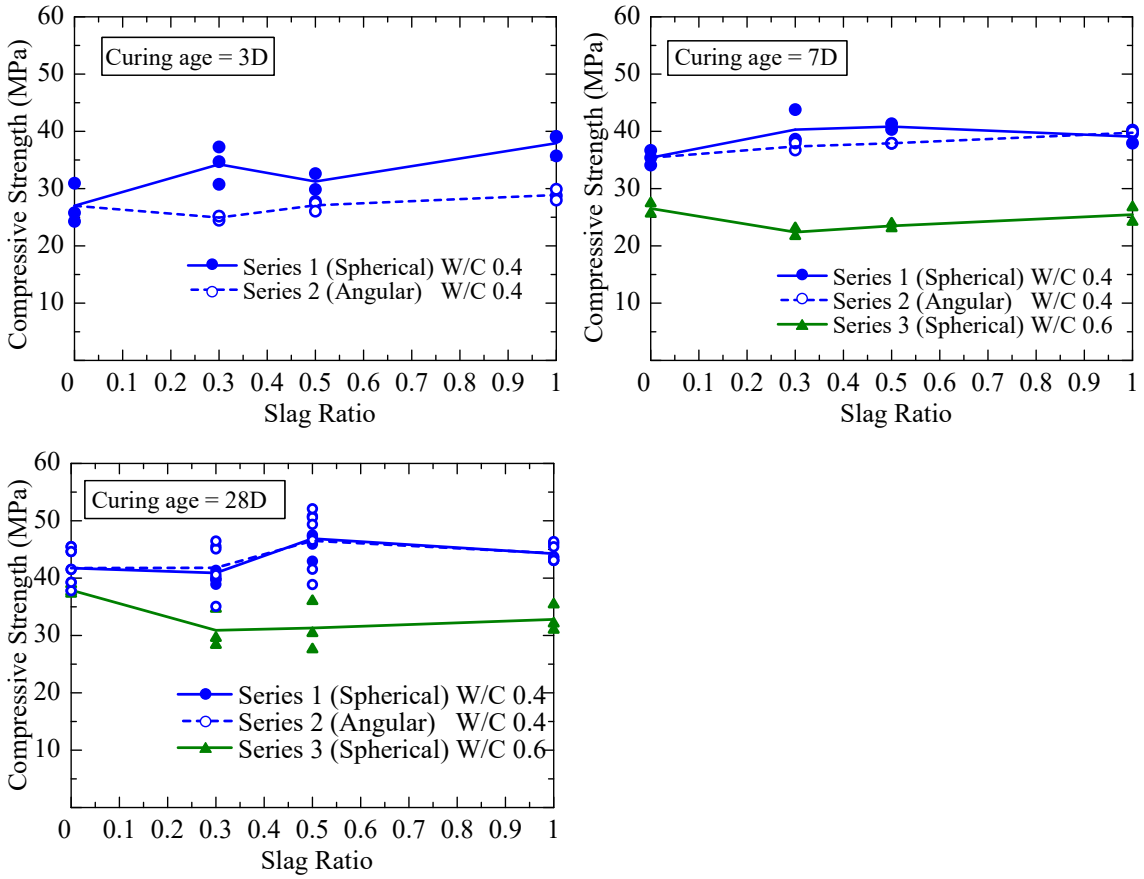

Figure 4-4 Compressive strength of concrete under series 1, 2 and 3

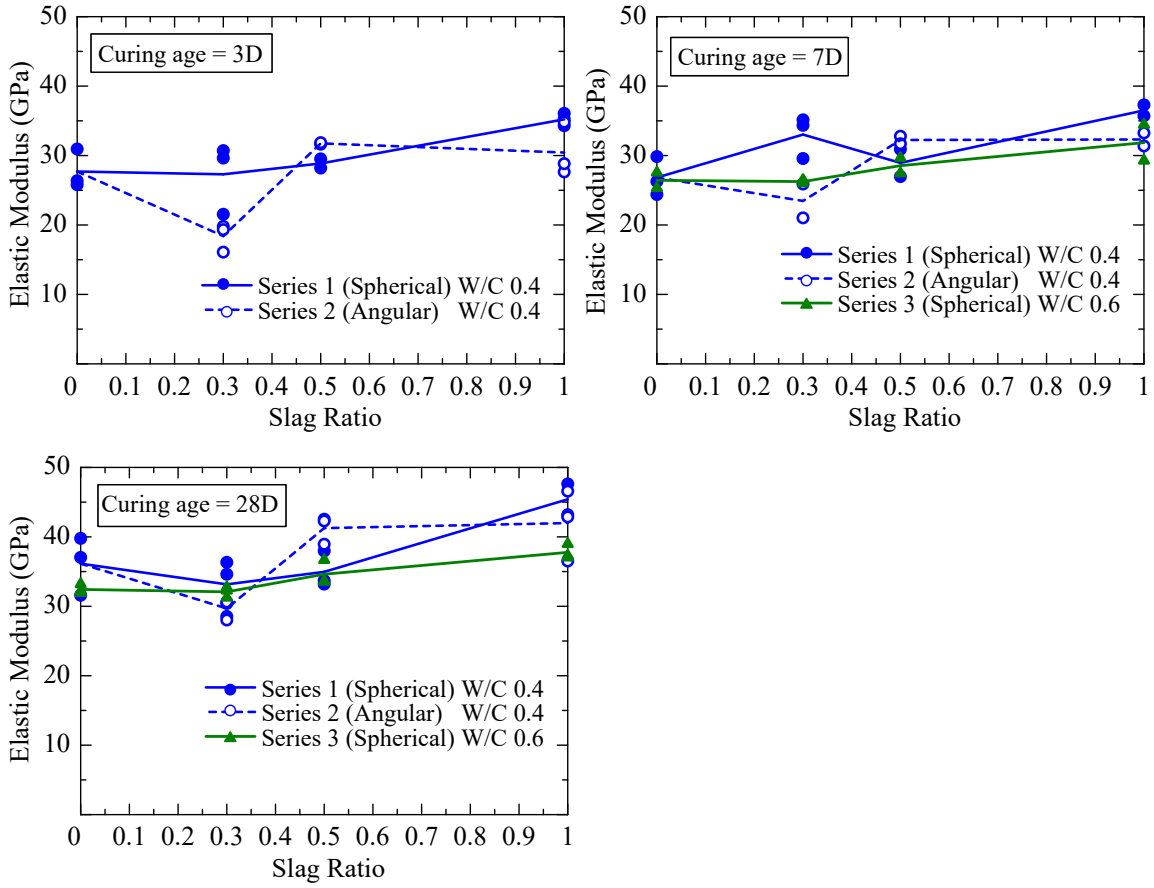

Figure 4-5 Elastic modulus of concrete of series 1, 2 and 3

It can be clearly seen from Figure 4-5 that irrespective of W/C and curing age, both spherical and angular shaped EAF slag concrete show improved elastic modulus than normal concrete and elastic modulus is found to be increasing with the increase in slag replacement ratio. The influence of curing age on the elastic modulus of concrete produced by spherical (series 1) and angular (series 2) shaped EAF slag is not so prominent like compressive strength at shorter curing period such as 3 days and the difference in elastic modulus in between concrete produced by two different shapes of EAF slag is not significant.

4.3.3 Compressive fracture energy

It has been identified by several researchers (Nakamura and Higai (2001), Lertsrisakulrat et al., 2001) that compressive fracture energy is independent of specimen geometry and it can be described as a function of concrete compressive strength. Zaitsev

and Whittmann (1981) indicate that the fracture process in concrete can be altered depending upon the strength of the paste. Nakamura et al. (2018) confirmed that size of coarse aggregate and existing crack width influences the compressive fracture energy of concrete. All these studies indicate that the utilization of spherical shaped EAF slag fine aggregate in concrete might have influence on the compressive fracture energy of concrete as it imparts to higher compressive strength depending on the W/C, slag type and slag replacement ratio as discussed in section 4.3.2. Therefore, a study in this regard is important. This study investigates the compressive fracture behavior of concrete produced by both spherical and angular shaped EAF slag fine aggregates at different W/C (0.4 and 0.6), slag type and slag replacement ratio after a curing age of 28 days.

In order to measure the compressive fracture energy, 4 load varying displacement transducers (LVDT) were placed in between loading plate and supporting plate around four sides of the specimen. The compression load was kept less than 0.5 kN/s during the loading cycle so that the sudden failure of specimen could be avoided. After peak load, continuous loading and unloading cycle was applied to each of the specimen. For each of the cycle, loading was maintained until the specimen reached peak load while unloading was controlled until the specimen reached 10% of peak load.

Deformation of each of the specimen was computed as the average of the displacement readings obtained from four different displacement transducers. For each of the specimen strain was computed as the ratio of average displacement of specimen and specimen length. Ultimate displacement was defined in the stress-displacement diagram corresponding to 20% of peak load.

Compressive fracture energy as defined by Nakamura and Higai (2001) is nothing but the area of absorbed plastic energy under the stress-displacement curve due to uniaxial compression loading as shown in Figure 4-6. Using this definition, compressive fracture energy was computed from the area under stress-displacement curve by deducting the area of first cycle of loading until peak load to ensure that only region of plastic energy is taken care of. Compressive fracture energy of all concrete under series 1, 2 and 3 were computed by using the stress-strain relationship as shown in Figure 4-2 and 4-3 by the method as discussed earlier in reference to Nakamura and Higai (2001).

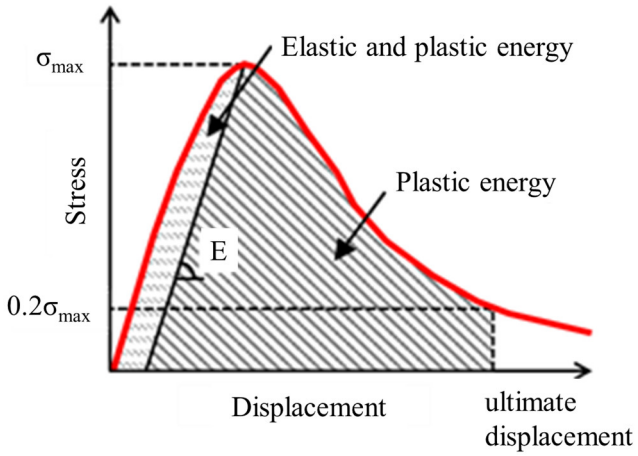

Figure 4-6 Definition of compressive fracture energy (after Nakamura et al. 2018)

Figure 4-7 shows the compressive fracture energy and slag ratio relationship. It is clear from the figure that compressive fracture energy increases with the increment of slag ratio for series 1 and 2 (low W/C of 0.4) similar to compressive strength as discussed in section 4.3.2. The difference in fracture behavior between spherical and angular shaped EAF slag concrete is not significant. In contrary, for the W/C of 0.6, compressive fracture energy of spherical shaped EAF slag concrete decreases with the increase in slag ratio which is also similar to the tendency of compressive strength as discussed earlier (section 4.3.2).

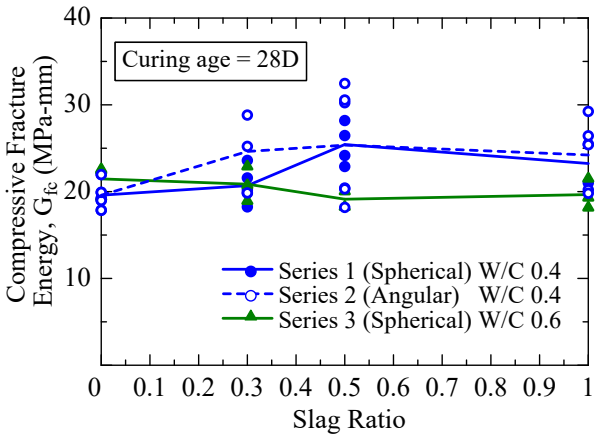

Figure 4-7 Compressive fracture energy of concrete under series 1, 2 and 3

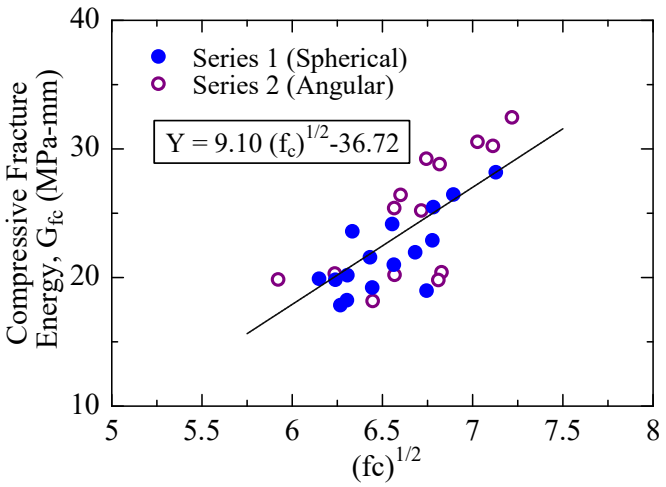

Figure 4-8 Compressive fracture energy of concrete with compressive strength

Nakamura and Higai (2001) proposed a model for predicting compressive fracture energy of normal concrete based on the respective compressive strength. They identified that the compressive fracture energy of normal concrete is related to the square root of corresponding compressive strength. Based on their model, compressive fracture energy of normal as well as spherical and angular shaped EAF slag fine aggregate concrete is plotted against square root of respective compressive strength in Figure 4-8. The relationship shows a linear behavior similar to that obtained by Nakamura and Higai (2001). This result again established the fact that compressive fracture energy is solely dependent on compressive strength of respective concrete. In addition, the effect of shape of EAF slag fine aggregates might be attributed to the increment of mortar strength which in turns helped in the improvement of compressive strength and corresponding compressive fracture energy.

4.3.4 Analysis of elastic modulus, compressive strength of slag concrete by digital image co-relation method (DICM)

It has been already discussed in the previous sections (4.3.2 and 4.3.3) that both spherical and angular shaped EAF slag concrete exhibit improved elastic modulus, compressive strength and compressive fracture energy in comparison to normal concrete when the W/C is lower such as 0.4. Generally, improved compressive strength and elastic

modulus corresponds to the stronger ITZ and higher strength of cement matrix (Arribas et al., 2015). One of the methods of identifying the phenomena could be investigation of origination, propagation and extent of cracking during uniaxial compression testing.

To facilitate the observation of origination and propagation of cracking, three different types of concrete prisms (100x100x200mm) such as N0.0, S1.0 and A1.0 cured up to 28 days were tested under uniaxial compression by digital image co-relation method (DICM). In this method, images of the desired side of the specimen were taken during compression loading at an equal time interval and then obtained images were co-related with load level by comparing the similarity of load recording and image taking time data. Finally, the photos were analyzed for crack development and propagation.

In order to obtain a view of the specimen surface, all three specimens were cut in the longitudinal direction and a viewing surface of 100x200mm and loading surface of 100x80mm was obtained. Speckle patterns were created on the specimen surface by using two color (red, black) sprays. Similar to other compression tests, four load varying displacement transducers (LVDT) were placed around four sides of the specimen to measure the specimen displacement. The loading was maintained at a speed of less than 0.5 kN/s to avoid brittle failure and the load and displacement data were recorded by data logger. Strain was computed by dividing the average transducer displacement by specimen length. During compression loading, images of the front side of the specimen were taken by normal DSLR camera at an interval of every 10 sec. The experiment was conducted in a light-insulated environment to confirm the accuracy and clarity of images. Figure 4-9 shows the detail experimental protocol. Obtained test images were analyzed by digital image correlation method (DICM) using the freeware called gom-correlate.

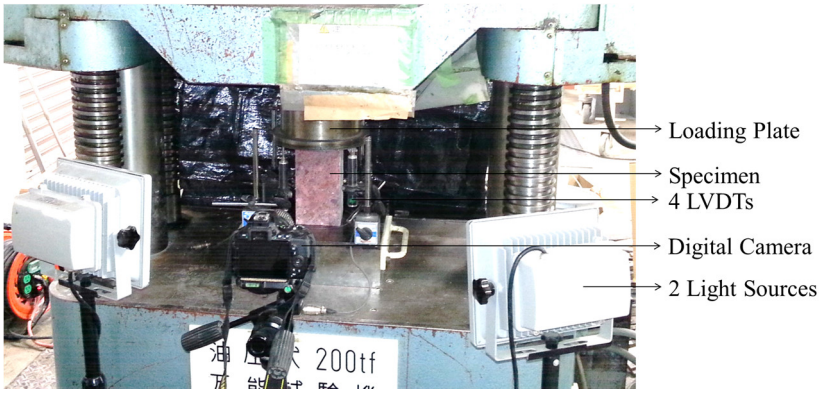

Figure 4-9 Digital Image Co-relation (DIC) experimental protocol

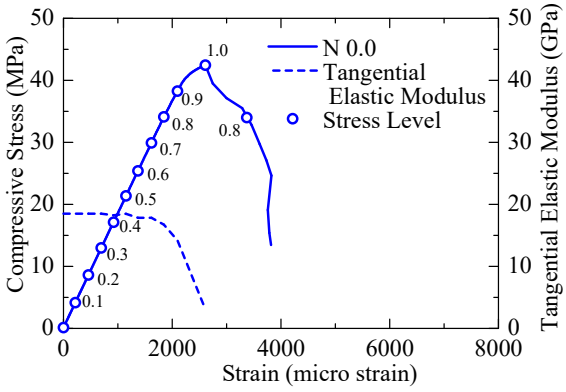

(a) Normal Concrete – N0.0

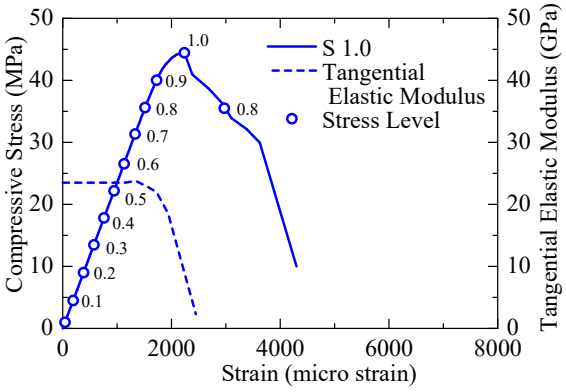

(b) Spherical Slag Concrete - S1.0

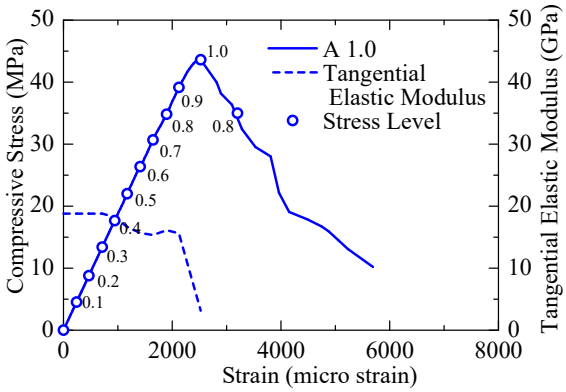

(c) Angular Slag Concrete - A1.0

Figure 4-10 Compressive stress-strain relationship of specimens used for image analysis

Figure 4-10 depicts the compressive stress-strain relationship including post peak behavior of N 0.0, S 1.0 and A 1.0 specimen. For each case, stress levels are also marked in those figures. Here, stress level refers to the ratio of stress of a particular strain to the peak stress. Instantaneous tangential elastic modulus, which is the ratio of change in stress and strain of two adjacent points of the stress-strain relationship were computed for each stress level and is plotted for each case of Figure 4-10.

The results as shown in Figure 4-10 indicates that the peak compressive stress of both spherical (44.45 MPa) and angular (43.62 MPa) shaped EAF slag concrete are higher than normal concrete (42.45 MPa). The tangential elastic modulus of spherical and angular shaped EAF slag concrete were computed as 23.50 GPa and 18.80 GPa which is higher than that of normal concrete (18.50 GPa). Strain values at peak compressive stress for all three cases are similar. These results confirm the previously described mechanical properties in section 4.3.1 and 4.3.2.

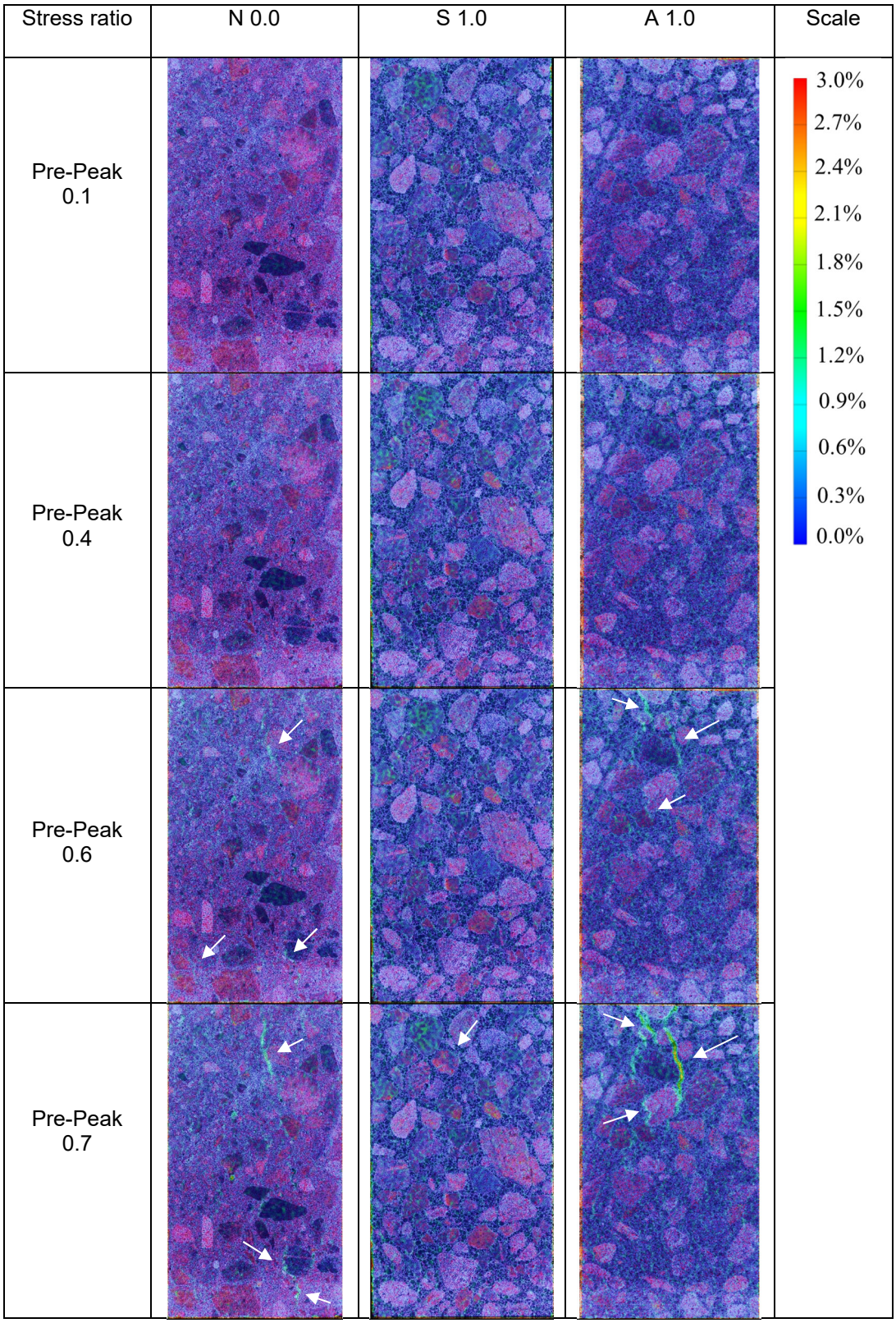

Figure 4-11 Maximum principal strain under uniaxial compression

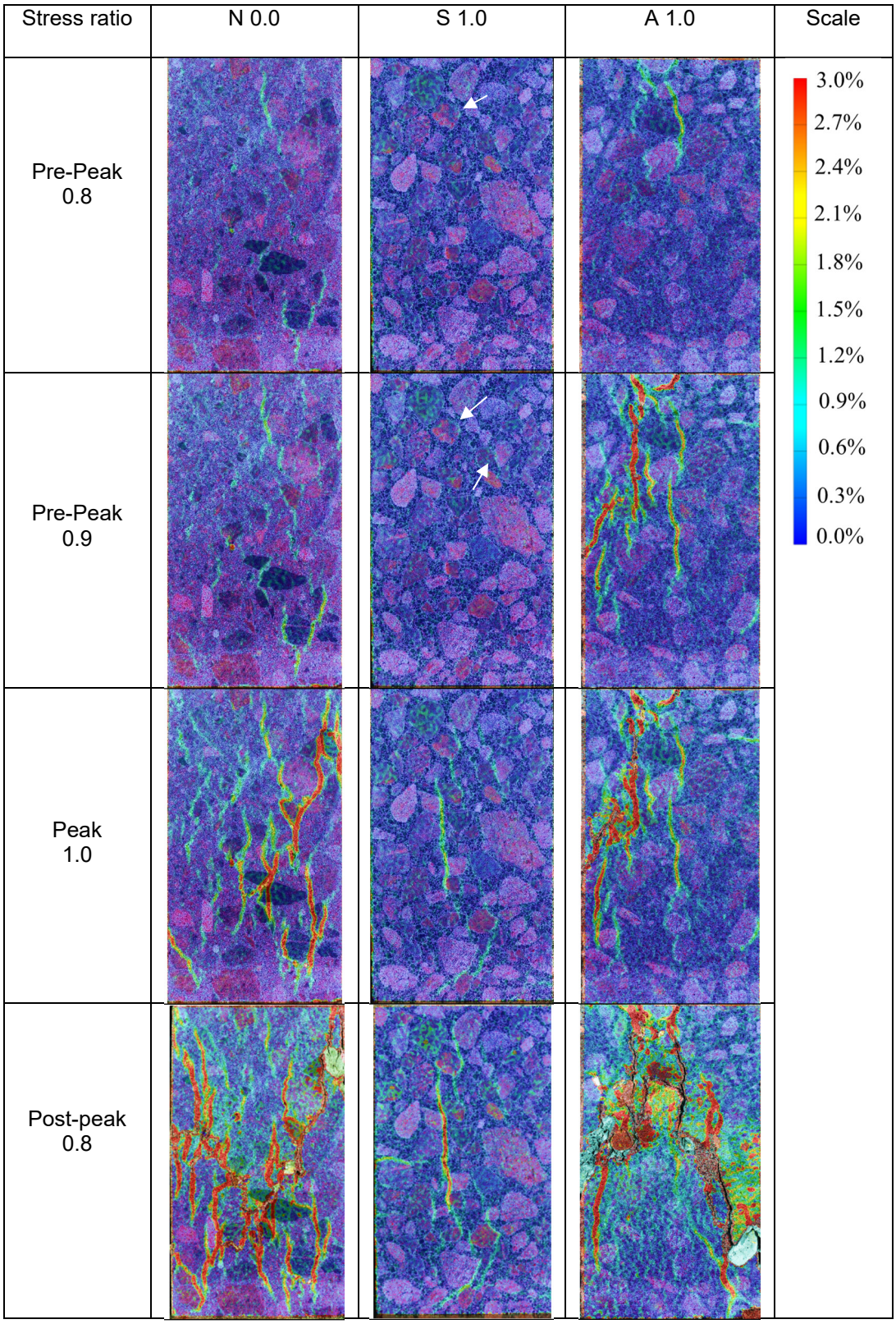

Figure 4-12 Maximum principal strain under uniaxial compression

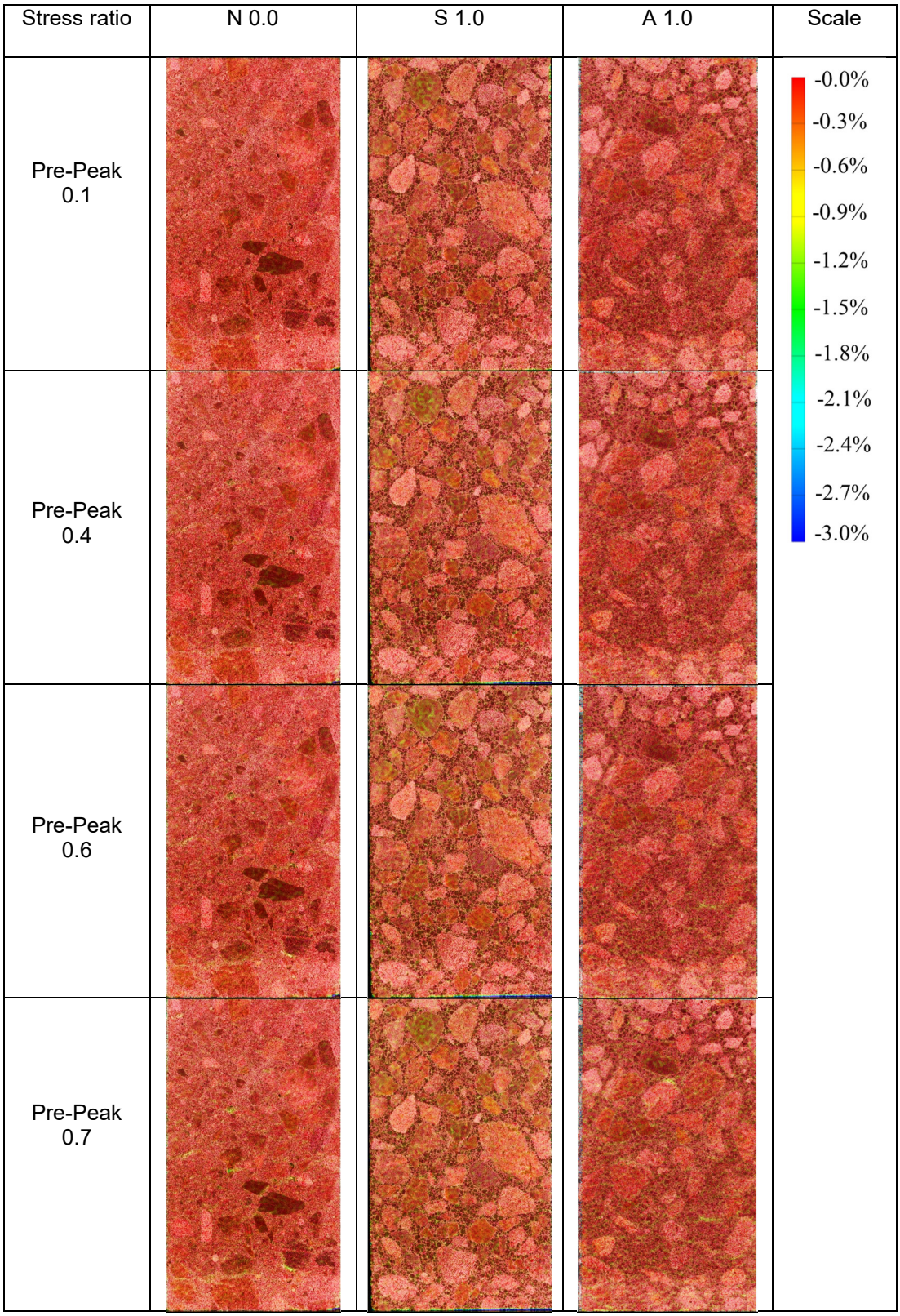

Figure 4-13 Minimum principal strain under uniaxial compression

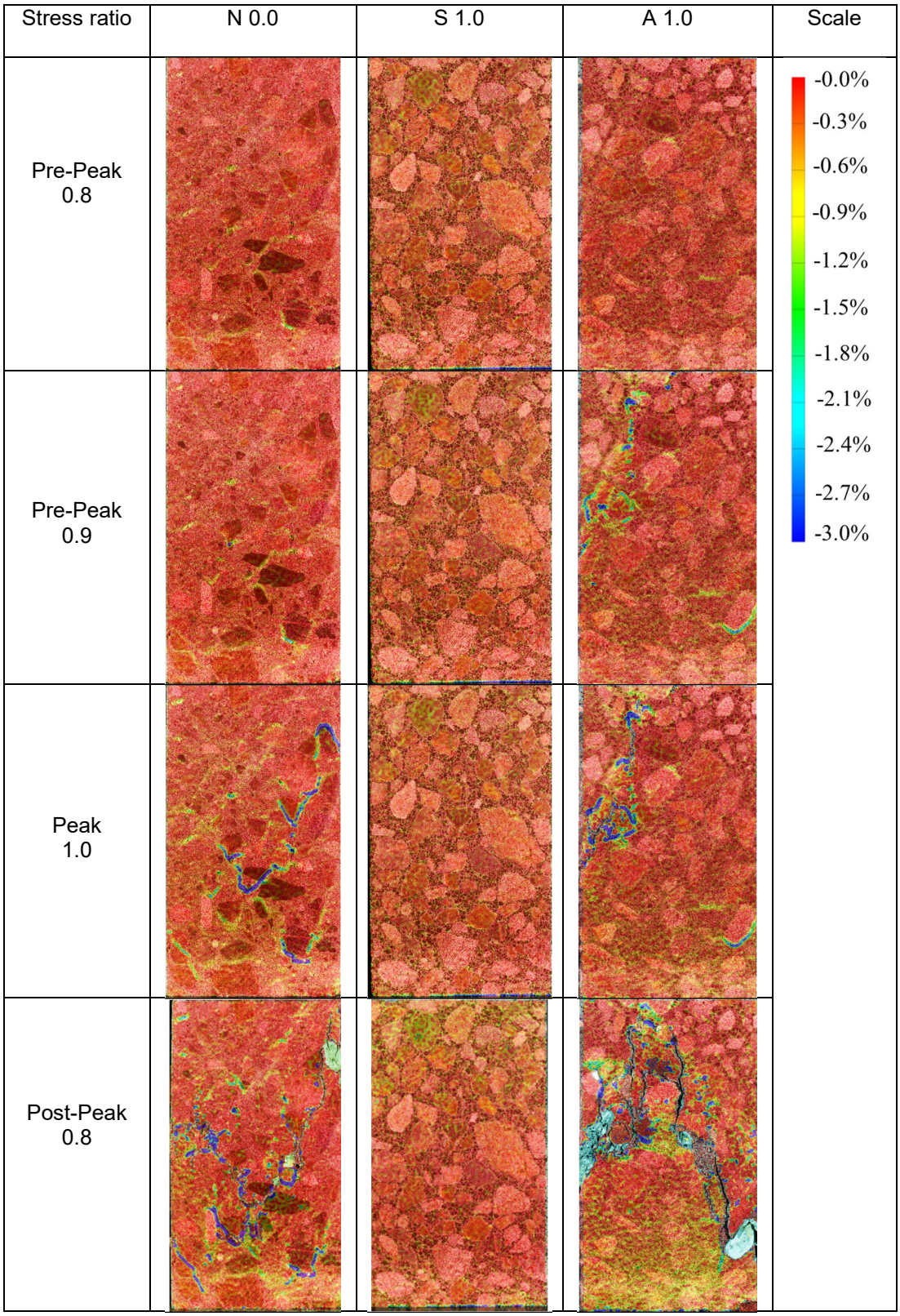

Figure 4-14 Minimum principal strain under uniaxial compression

Image analysis results of N 0.0, S 1.0 and A 1.0 specimen are depicted in Figure 4-11, 4-12 and 4-13, 4-14 in terms of maximum and minimum principal strain respectively. For each case, results are shown for the stress level of 0.1, 0.4, 0.6, 0.7, 0.8, 0.9 and 1.0 in the pre-peak region and 0.8 in the post-peak region. The scale for maximum and minimum principal strain was chosen as 0 to 3% and -3 to 0% respectively.

As discussed earlier (section 3.4.2) compressive strength and elastic modulus of concrete is strongly dependent on the balance of strength of mortar matrix and coarse aggregates and bond between them. Due to dissimilar strength and subsequent weaker bond, cracks in concrete often originate in the interface of coarse aggregate and mortar matrix under uniaxial compression load (National Research Laboratory, KAIST). Due to cracking, bond failure occurs and tensile strain develops in the concrete specimen which can be identified by observing the maximum principal strain. This phenomena causes the reduction of elastic modulus and compressive strength of concrete.

From the above discussion, it is clear that concrete in which crack originates at relatively lower stress level tends to have weaker mortar matrix and subsequent weaker bond between coarse aggregates and mortar matrix, which eventually provided lower compressive strength and elastic modulus. This can be proved from Figure 4-11 and 4-12 considering the maximum principal strain. It can be observed from these figures that for normal as well as angular shaped EAF slag concrete having slag ratio of 1.0 first visible cracks can be seen in between the coarse aggregates and mortar matrix when the stress level is within 0.4-0.6, whereas, for the case of spherical shaped EAF slag concrete having slag ratio of 1.0, visible crack initiates in between the stress level of 0.7 to 0.8. This can be confirmed from the stress-strain relationship as shown in Figure 4-10 that the tangential elastic modulus of both normal and angular shaped EAF slag concrete of slag ratio of 1.0 remains same as of initial loading condition up to a stress level of 0.4 and then drops from the initial value with the increase in stress level. For spherical shaped EAF slag concrete this happens when the stress level is more than 0.8. This result confirms that the origination of visible cracks for S 1.0 specimen occurs at higher stress level than N 0.0 and A 1.0 specimen. Since the origination, cracks were found to be propagated gradually in case of N 0.0 and A1.0 specimen and could be seen in highest numbers with maximum crack width at peak stress. In contrary, for S 1.0 specimen crack propagation is sudden from the stress level of 0.9 and number of cracks were very few along with

lesser crack width in comparison to the former two cases. The post peak behavior at the stress level of 0.8 shows increased number of cracks and crack widths for S 1.0 specimen than the pre-peak case although that of N 0.0 and A 1.0 cases are much higher.

Regarding the minimum principle strain as shown in Figure 4-13 and 4-14, both N 0.0 and A 1.0 specimens show some horizontal type compression closing cracks at the stress level of 0.9 to 1.0 in the pre-peak region and 0.8 in the post-peak region. This corresponds to the maximum principal strain as shown in Figure 4-11 and 4-12 at the same stress level since positions of the compression closing cracks are similar to that of earlier observed cracks. This indicates that due to the breakage of bonds between coarse aggregate and mortar matrix, cracks propagated at the bottom of coarse aggregates which were getting closed due to compression loading.

In a nutshell, origination of visible cracks at higher stress level along with less number of cracks and comparatively lower crack width confirmed that the strength of mortar matrix of spherical shaped EAF slag concrete of slag ratio 1.0 is higher than that of normal and angular shaped EAF slag concrete of slag ratio 1.0. As a result, such concrete manifests improved elastic modulus and compressive strength. The stronger mortar matrix produced by spherical shaped EAF slag fine aggregates might be due to the improved particle adhesion which is again discussed in section 4.3.6.

4.3.5 Bending stress-crack width relationship

Bending stress and crack width relationship of both spherical and angular shaped EAF slag concrete under series 1, 2 (W/C 0.4) and 3 (W/C 0.6) are depicted in Figure 4-15 and 4-16 including post peak behavior after a curing age of 28 days. Bending stress was computed from load data obtained from the three point loading test as per ASTM C 293 (2002) while crack width was recorded from the clip gauge reading which was positioned in the pre-crack zone of the prism specimen subjected to bending. It is evident that for lower W/C of 0.4, both spherical (series 1) and angular (series 2) shaped EAF slag concrete exhibit higher bending stress than normal concrete although initial stiffness and crack width at peak bending stress of all types of concrete are similar. In contrary, concrete produced by spherical shaped EAF slag fine aggregates at higher W/C of 0.6 shows opposite behavior as normal concrete manifests highest bending stress.

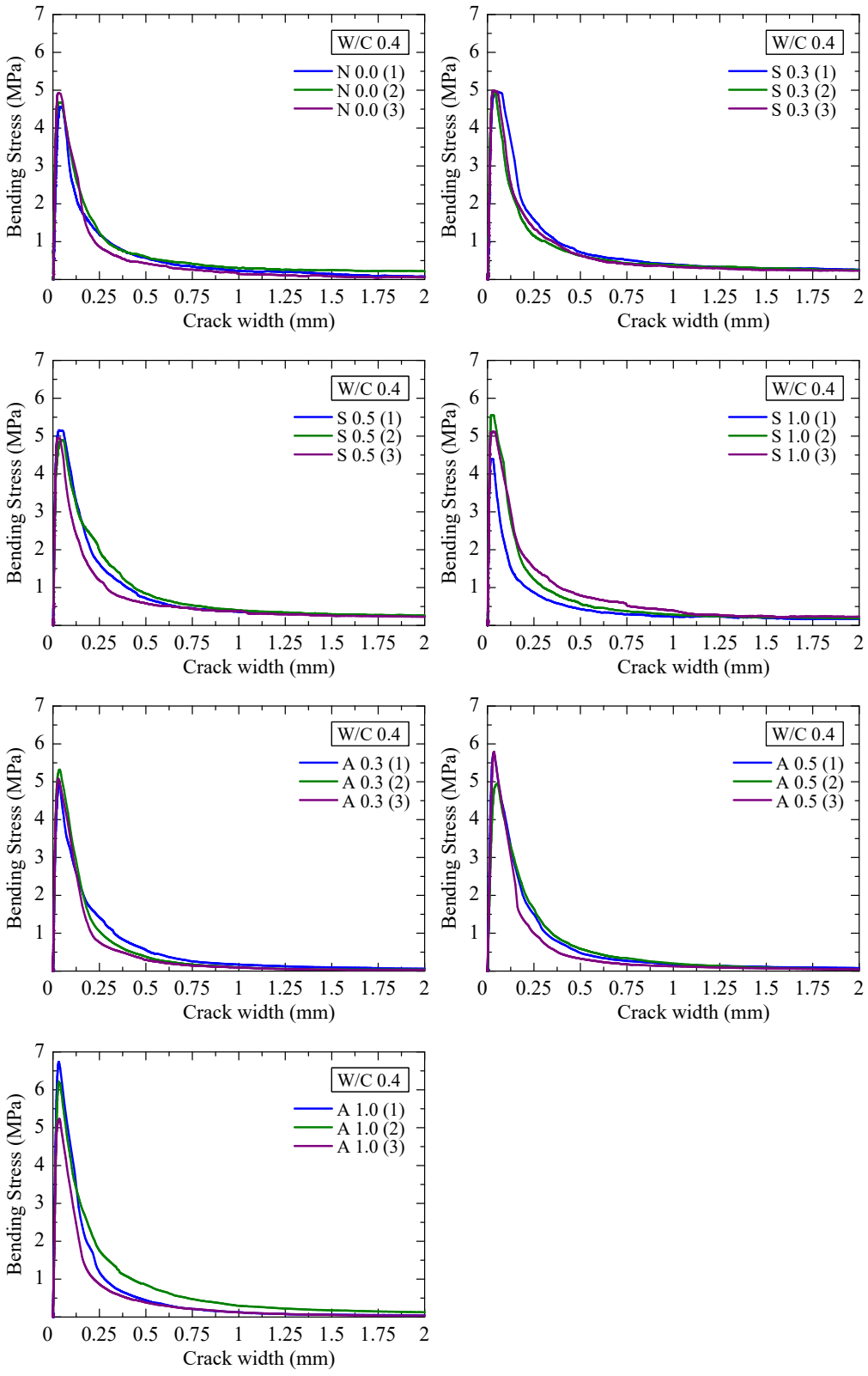

Figure 4-15 Bending stress-crack width relationship of concrete under series 1 and 2 (curing age = 28 days)

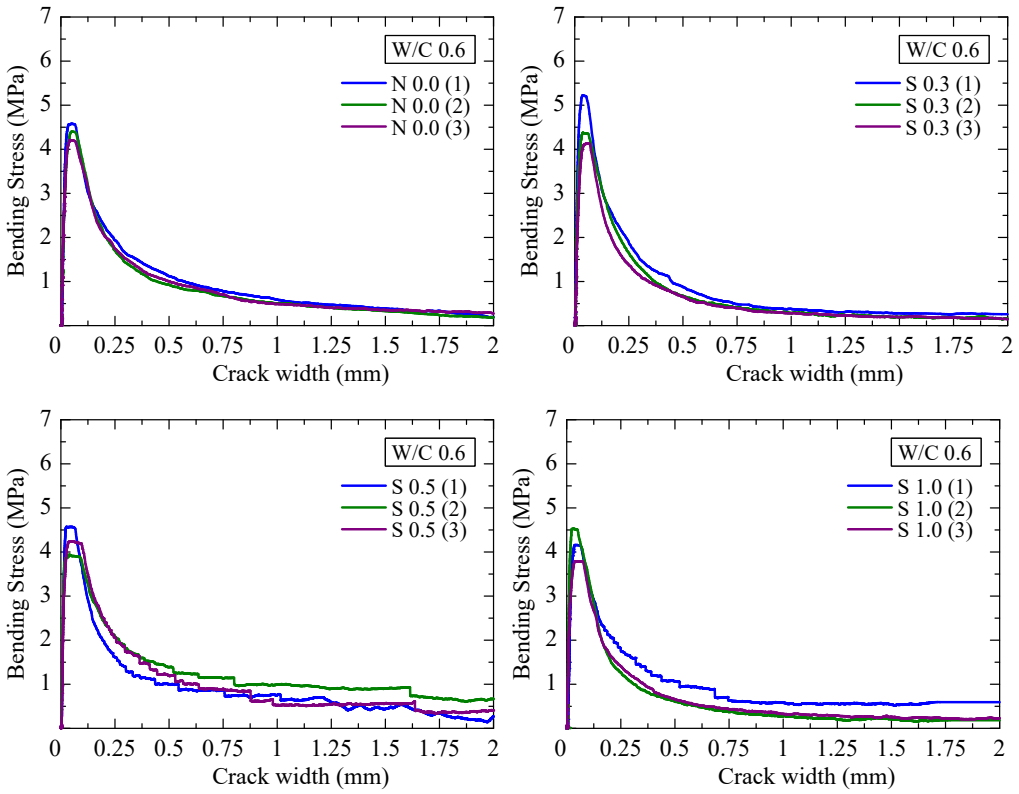

Figure 4-16 Bending stress-crack width relationship of concrete under series 3 (curing age = 28 days)

It can be seen from Figure 4-15 that for same bending stress, post peak portion of the bending stress-crack width curve of spherical shaped EAF slag concrete of slag ratio 0.3 and 0.5 are more flat and exhibit higher crack width than all other concrete of series 1 and 2. Similar tendency is evident for the slag replacement ratio of 0.5 under series 3 as shown in Figure 4-16. In comparison to lower (series 1, 2 Figure 4-15) and higher (series 3, Figure 4-16) W/C, higher crack width for the latter case is observed when the specimens are subjected to same bending stress.

4.3.6 Bending and tensile strength

The results of bending (which is also termed as modulus of rupture according to ASTM C 293 (2002)) and split tensile strength of concrete under series 1, 2 and 3 are plotted against slag ratio for the curing age of 3, 7 and 28 days in Figure 4-18 and 4-19

respectively. Detail experimental condition is shown in Figure 4-17. For each slag ratio under each series and curing age, 3 representative specimens were tested and average results were considered.

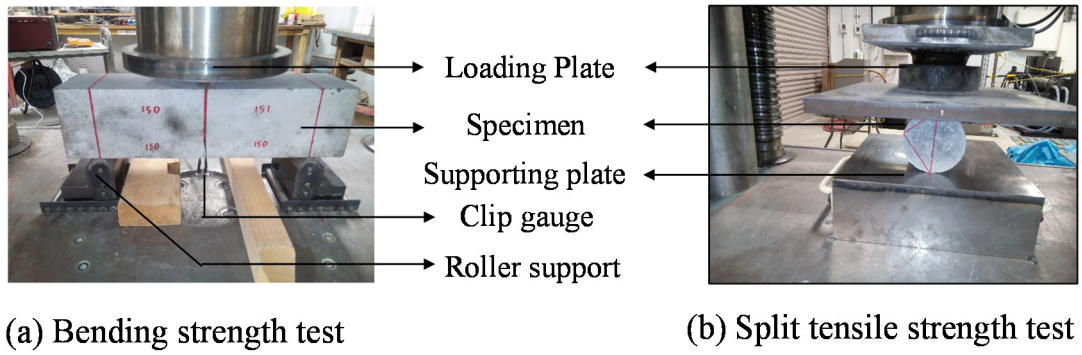

Figure 4-17 Bending and tensile strength test condition

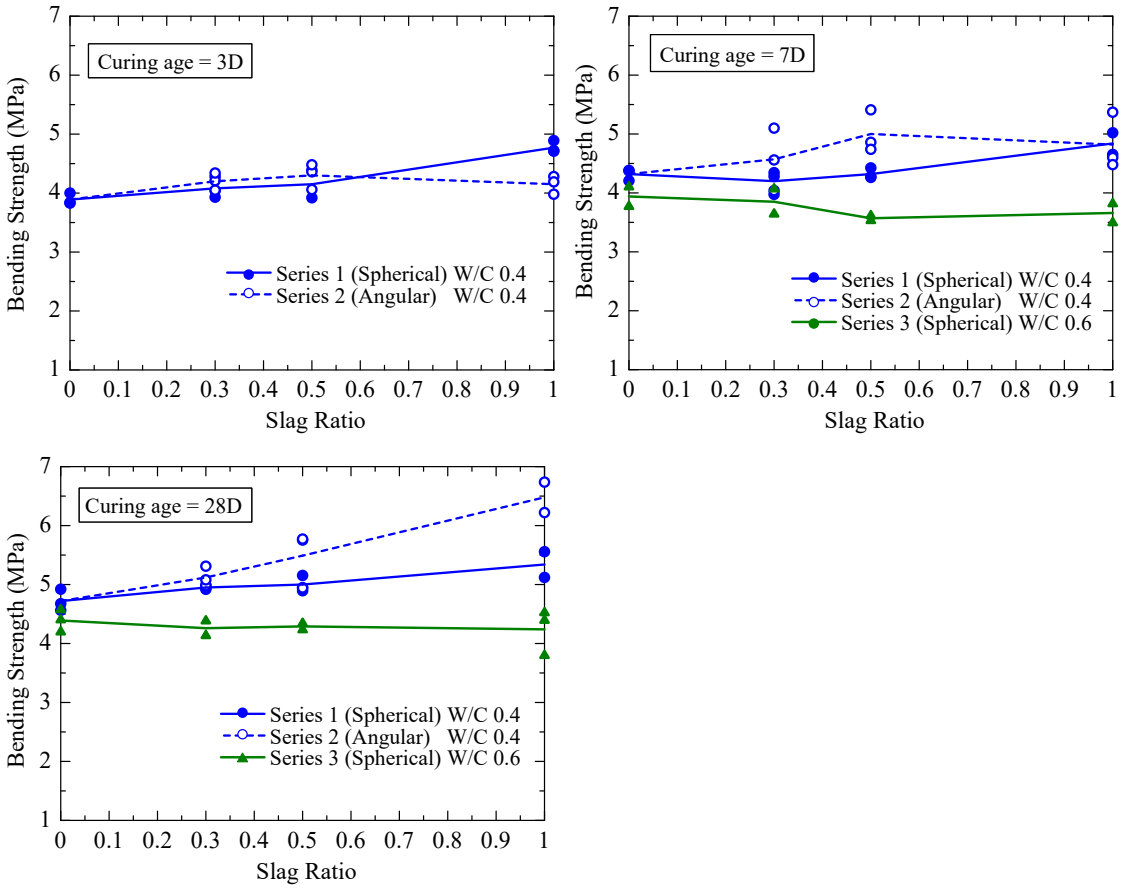

Figure 4-18 Flexural strength of concrete under series 1, 2 and 3

It can be seen from Figure 4-18 that after the curing age of 28 days, normal as well as spherical and angular shaped EAF slag concrete of series 1 and 2 exhibit higher bending strength than 4.5 MPa which was targeted (section 3.2) to achieve the purpose of utilizing the newly developed slag aggregates in concrete pavement. As depicted in Figure 4-18 irrespective of curing age, an increase in bending strength with the increment of slag ratio is observed for concrete produced at low W/C of 0.4 under series 1 and 2. However, angular shaped slag concrete (series 2) shows the highest bending strength for the slag ratio of 1.0. The increase in bending strength of concrete produced by angular (series 2) and spherical (series 1) shaped EAF slag in comparison to normal concrete for the slag ratio of 1.0 is 37.3% and 13.1% respectively when the curing age is 28 days. In contrary, bending strength of concrete produced by spherical shaped EAF slag fine aggregate at high W/C of 0.6 (series 3) is found to be similar to slightly decreasing with the increase in slag ratio when the curing age is 28 and 7 days respectively. This result clearly manifests that EAF slag can be utilized in concrete at lower W/C of 0.4 and thus suitable for pavement concrete in so far as flexural behaviors of such concretes are concerned.

Similar increasing trend like bending strength is evident from Figure 4-19 for the case of tensile strength of concrete of series 1 and 2 considering all curing age. However, for the curing age of 28 days both spherical (series 1) and angular (series 2) shaped EAF slag concrete produced at W/C of 0.4 shows a steady increment up to a slag replacement ratio of 0.5 which becomes constant when the slag ratio is 1.0. For all the curing age, angular shaped EAF slag concrete (series 2) exhibits slightly higher tensile strength in comparison to spherical shaped EAF slag concrete (series 1). When the W/C is higher such as 0.6, tensile strength of spherical shaped EAF slag concrete is similar to slightly decreasing with the increase in slag ratio.

In so far as the mechanical properties of EAF slag concrete are concerned, angular shaped EAF slag concrete (series 2) of lower W/C of 0.4 showed higher bending and tensile strength and similar compressive strength and elastic modulus than spherical slag concrete. This result resembles to the findings of Kaplan (1959) that, angular fine particles in concrete mix tend to increase the compressive and flexural strength. The mechanism can be discussed with the concept that angular particles might have better bond and

interlocking between the particles and cement matrix, thus increases strength, particularly flexural strength.

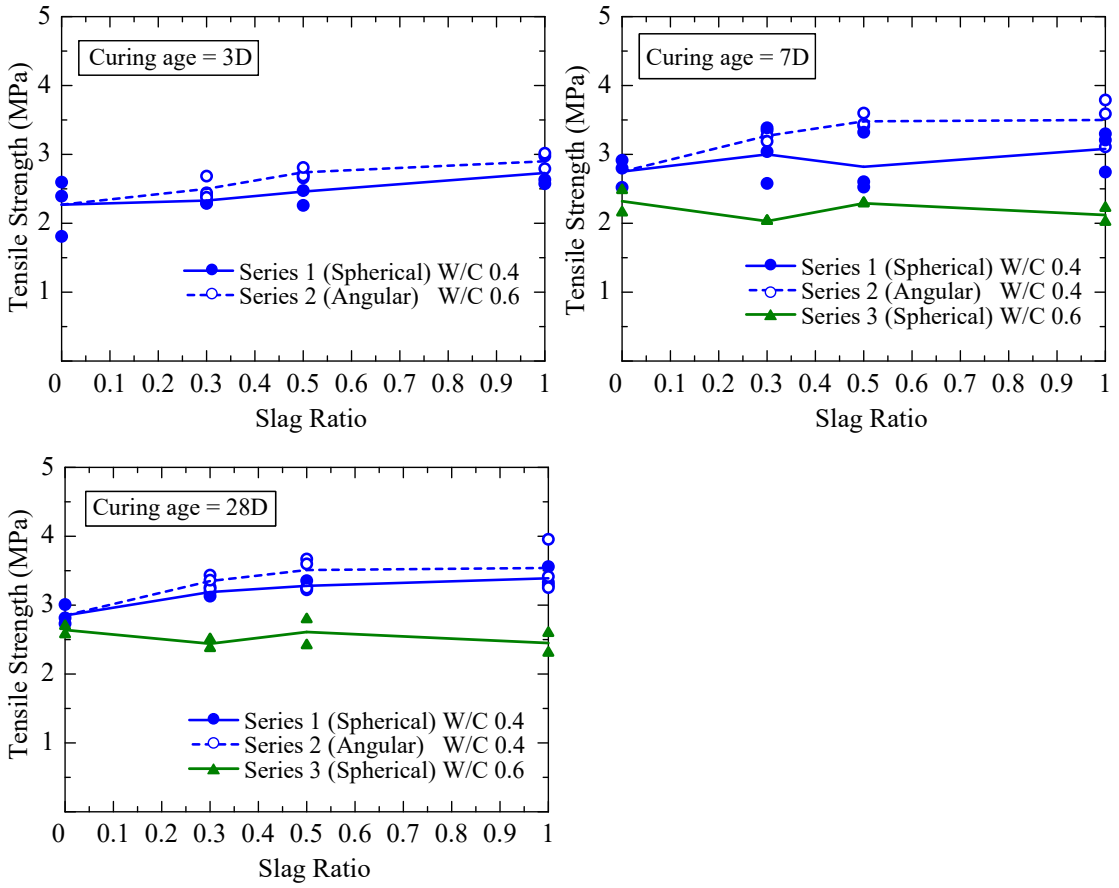

Figure 4-19 Tensile strength of concrete under series 1, 2 and 3

Overall, slag concrete (either spherical or angular) of lower W/C of 0.4 showed improved mechanical behavior than normal concrete although that of higher W/C of 0.6 showed similar to slightly decreasing mechanical behavior. This result can be comprehended by the balance of strength of cement matrix, and adhesion between slag aggregate and cement paste as discussed in section 4.3.4 related to image analysis. At lower W/C of 0.4, spherical shaped EAF slag aggregate might form little but stronger ITZ which in turns increases the bond and particle adhesion and thus pertains positive effect on the mechanical properties of slag concrete in reference to Arribas et al. (2015). When the W/C increases to 0.6, due to the presence of more water and less cement, particle adhesion as well as ITZ of slag concrete might get weaker which triggers the reduction

of mechanical properties in comparison to normal concrete of W/C of 0.6 and slag concrete of W/C of 0.4.

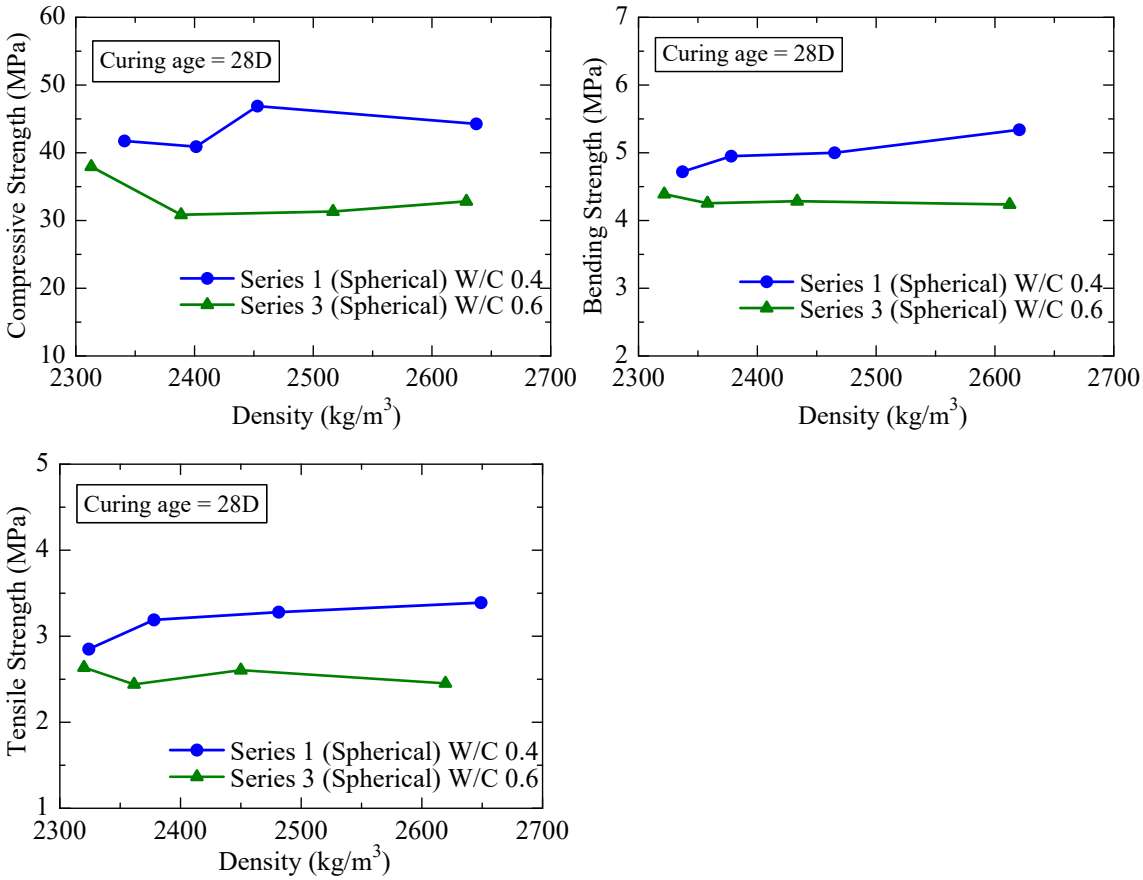

Figure 4-20 Relationship between concrete strength and hardened density

In order to justify this assumption all mechanical properties of concrete produced by spherical shaped EAF slag concrete of W/C 0.4 (series 1) and W/C 0.6 (series 3) are plotted against hardened concrete density after a curing age of 28 days in Figure 4-20. It is fact that due to high particle density, hardened concrete density of spherical shaped EAF slag concrete increases with the increase in slag ratio. It can be clearly seen from Figure 4-20 that all mechanical properties of concrete produced by spherical shaped EAF slag aggregates at W/C of 0.4 (series 1) increase with the increment of concrete density while that of W/C of 0.6 show a decreasing trend. Generally, mechanical properties of concrete increases with the increment of concrete density (Vidha, 2015, Iffat, 2015). The opposite tendency of slag concrete of W/C of 0.6 clearly indicates the fact that although

density of such concrete are higher, strength of cement matrix might be lower due to lower particle adhesion between slag aggregate and cement paste. This behavior justifies the previous assumption regarding the reduction tendency of mechanical properties of slag concrete with the change in W/C.

4.3.7 Tensile fracture energy

The effect of shape of EAF slag on the mechanical properties of concrete can be further discussed in light of tensile fracture energy and ductility. Figure 4-22 depicts the relationship between tensile fracture energy and slag ratio after a curing age of 28 days for all concrete of series 1 and 2. Tensile fracture energy, G_{ft} (MPa-mm) was computed by the method as described in JCI-S-001-2003 using a three point loading test as depicted in Figure 4-21. In this method, tensile fracture energy was calculated by Eq. 4.1 using the load displacement curve obtained from the experimental results.

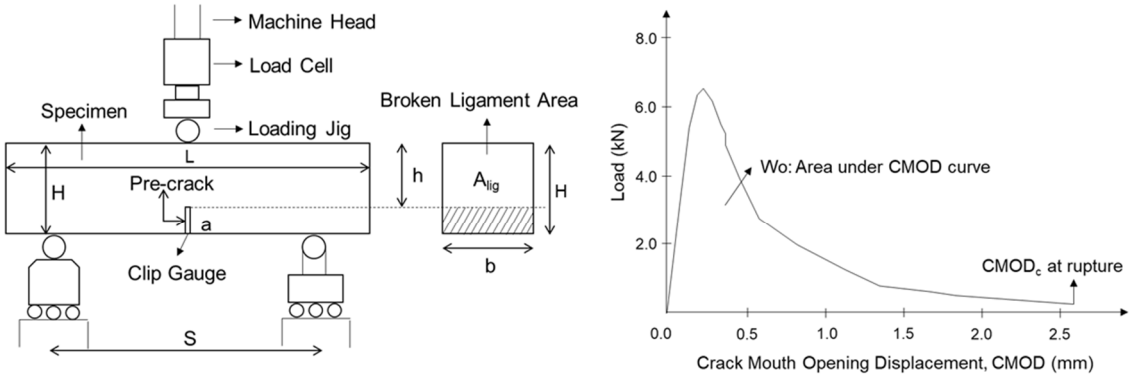

Figure 4-21 Tensile fracture energy calculation protocol (Roy et al., 2018)

$$G_{ft} = \frac{0.75W_0 + W_1}{A_{lig}} \tag{4.1}$$

$$W_1 = 0.75\left(\frac{S}{L}m_1 + 2m_2\right)g.CMOD_c \tag{4.2}$$

Where, G_{ft} = Tensile fracture energy (N/mm), W_0 = Area under the CMOD curve up to rupture of the specimen (N-mm), W_1 = Work done by dead weight of specimen and

loading jig (N-mm), A_{lig} = area of broken ligament (b x h) (mm^2), m_1 = Mass of specimen (kg), S = Loading span (mm), L = Specimen length (mm), m_2 = Mass of loading jig (kg), g = gravitational acceleration (9.807 m/s^2), $CMOD_c$ = Crack mouth opening displacement at the time of rupture (mm).

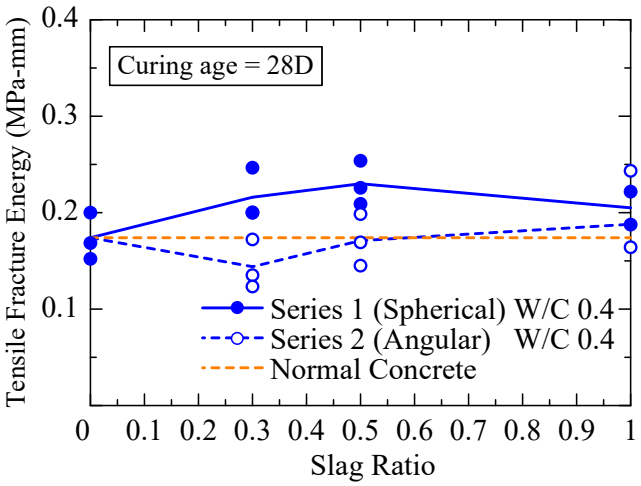

Figure 4-22 Tensile fracture energy

It can be seen from Figure 4-22 that, tensile fracture energy of angular shaped EAF slag concrete (series 2) is similar to slightly increasing with the increase in slag ratio although the values are much lower than that of spherical shaped EAF slag concrete (series 1). For spherical shaped EAF slag concrete (series 1), tensile fracture energy increases up to a slag replacement ratio of 0.5 and then decreases when the slag ratio is 1.0. However, irrespective of the slag replacement ratio, all the values of tensile fracture energy of spherical shaped EAF slag concrete are higher than normal concrete. Generally, concrete of higher tensile fracture energy imparts lower brittleness. Based on this assumption, it is apparent that concrete produced by spherical shaped EAF slag aggregate might attribute to higher ductility.

4.3.8 Ductility of spherical shaped EAF slag concrete

It is fact that tensile fracture energy alone cannot demonstrate the ductile/brittle behavior of concrete. Hillerborg et al. (1976) introduced the concept of characteristic

length (L_{ch}) as defined by Eq. 4.3 to be an indicator of ductility/brittleness of concrete. The higher the characteristic length, the higher the ductility.

$$L_{ch} = \frac{E_c G_{ft}}{f_t^2} \tag{4.3}$$

Where, L_{ch} = Characteristic length (mm), E_c = Elastic Modulus of concrete (MPa), G_{ft} = Tensile fracture energy of concrete (N/mm) and f_t = Tensile strength of concrete (MPa)

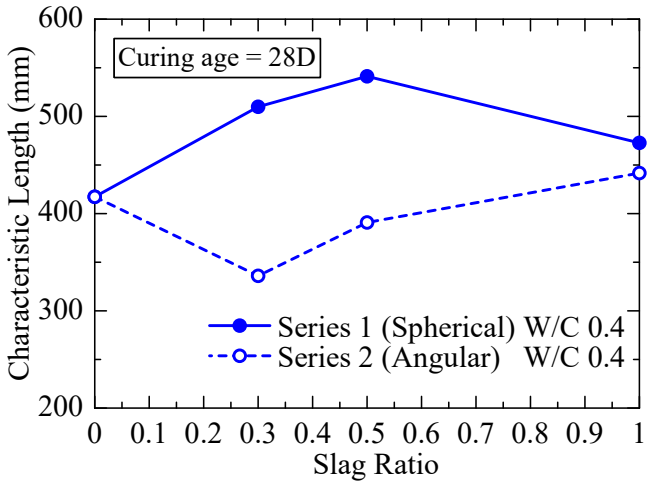

Figure 4-23 Characteristic length with slag ratio

Figure 4-23 presents the average characteristic length of concrete made of spherical (series 1) and angular (series 2) shaped EAF slag fine aggregate at different slag replacement ratio. The characteristic length of normal strength concrete was measured as 417 mm which is within the standard range of 200-500mm for normal concrete as suggested by Karihaloo (1995). It is clear from Figure 4-23 that inclusion of spherical shaped EAF slag in concrete increases the ductile behavior of concrete especially up to a slag ratio of 0.5 and remains similar to normal concrete even if all sand is replaced by spherical slag. However, angular shaped EAF slag concrete shows lower ductility in comparison to spherical shaped EAF slag concrete although for the slag replacement ratio of 1.0, ductility of angular shaped EAF slag concrete is closer to normal and spherical shaped EAF slag concrete.

The mechanism behind this result lies in the balance between tensile fracture energy, elastic modulus and tensile strength as shown in Eq. 4.3. The elastic modulus of spherical and angular shaped EAF slag concrete as shown in Figure 4-5 is almost similar. Although tensile strength of angular shaped EAF slag concrete is higher than spherical shaped EAF slag concrete (Figure 4-19), tensile fracture energy of angular shaped EAF slag concrete is lower (Figure 4-22). This tendency might happen due to lower aggregate volume in case of angular shaped EAF slag concrete compared to spherical shaped EAF slag concrete as shown in the mix proportion in Table 3-1. Because of lower tensile fracture energy and higher tensile strength, characteristic length (Eq. 4.3) of angular shaped EAF slag concrete was found to be lower in comparison to spherical shaped EAF slag concrete. As a result, although angular shaped EAF slag concrete showed higher flexural and tensile strength (Figure 4-18 and 4-19) compared to normal and spherical shaped EAF slag concrete, tensile fracture energy is observed opposite to those behavior and so does the ductility.

The above result might be attributed to the difference in mix proportions. Cifuentes et al. (2018) in their study on the effect of concrete mix proportion parameters on concrete fracture energy concluded that, concrete having higher paste to solid (p/s) ratio exhibits lesser tensile fracture energy than that of lower p/s. Here, p/s indicates the ratio of volume of cement and water to that of sand, slag and gravel. In this study, the volumetric p/s ratio as computed from Table 3-1 for spherical and angular shaped EAF slag concrete having slag ratio 0.3, 0.5, 1.0 are 0.377, 0.361, 0.311 and 0.407, 0.414, 0.427 respectively. The value of p/s for normal concrete is 0.396. Since, angular shaped EAF slag concrete requires more water and cement compared to normal and spherical shaped EAF slag concrete, the p/s ratio is higher. Therefore, the result as shown in Figure 4-22 and 4-23 that the tensile fracture energy and ductility of spherical shaped EAF slag concrete is higher than normal and angular shaped EAF slag concrete is justified.

Hence, all mechanical behaviors of EAF slag concrete are found to be higher than normal concrete at lower W/C of 0.4 even if all sands are replaced by EAF slag. Although angular shaped EAF slag concrete shows improved strength compared to normal and spherical shaped EAF slag concrete, ductility of such concrete were found to be lesser than that of spherical shaped EAF slag concrete. Therefore, higher elastic modulus,

strength and improved ductility than normal concrete, specifies spherical shaped EAF slag as the best possible alternative of natural sand in concrete of lower W/C.

4.4 Durability properties

4.4.1 Shrinkage

Two representative prism specimens of 100x100x400mm sizes were used for each slag ratio under each series. Subsequent to casting, all specimens of series 1 and 2 were cured under water for 7 days while that of series 3 were cured for 3 days. Soon after curing, all the specimens were removed from water and stored in the curing room at a temperature and humidity of 20°C ± 5°C and 65% ± 5% respectively for drying and drying shrinkage of each of the specimen under each series was measured. To facilitate the measurement, on each side of the specimen two contact chips were attached at the center part at a spacing of 300mm. For all the specimen, initial length (L_i) was measured at all four sides prior to drying and subsequently measurement of length was taken at different drying age. Length change was computed by deducting the length of specimen at a certain drying age from the initial length (L_i) at no drying condition. Shrinkage strain at particular drying age was calculated by dividing the change in length with the initial length (L_i) of specimen. The experiment was conducted up to a drying age of 91 days. Figure 4-24 shows the specimen preparation for the measurement of length change.

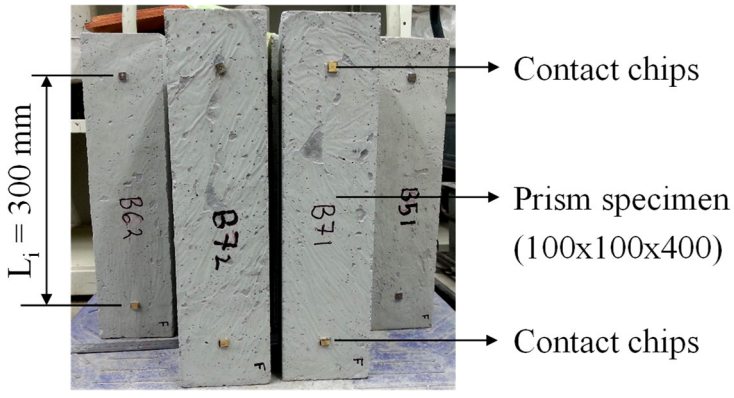

Figure 4-24 Specimen condition for measurement of length change

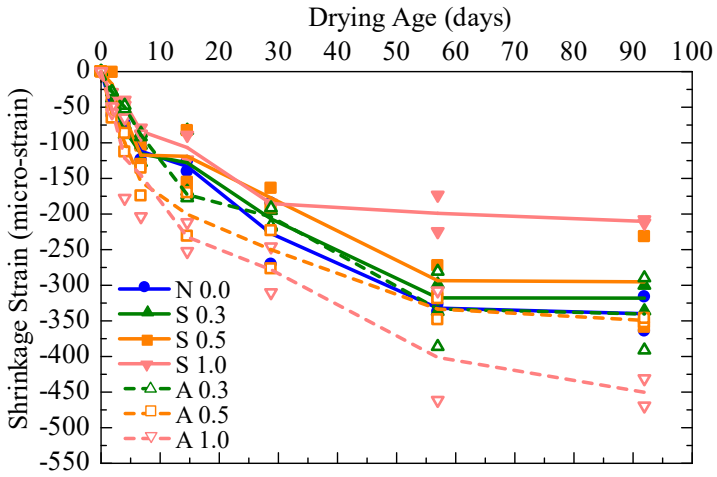

Figure 4-25 Shrinkage of concrete of series 1 and 2

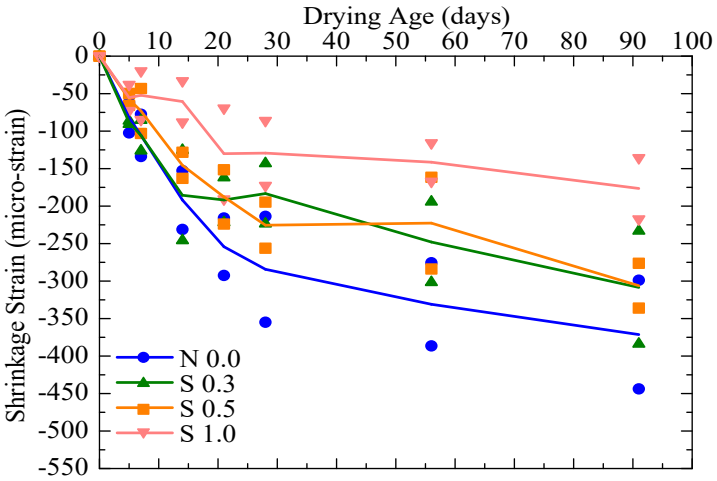

Figure 4-26 Shrinkage of concrete of series 3

Figure 4-25 and 4-26 depict the experimental results related to the shrinkage of concrete of series 1, 2 and 3 respectively. Figure 4-25 illustrates a clearly distinguishing shrinkage behavior for spherical (series 1) and angular (series 2) shaped EAF slag concrete when the W/C is 0.4. Shrinkage strain of spherical shaped EAF slag concrete of all slag ratio cases is found lesser than that of normal and angular shaped slag concrete. The lowest shrinkage strain is observed for the spherical shaped EAF slag concrete having a slag ratio of 1.0. In comparison to normal concrete, after the drying age of 91 days, 6.5% and 13.2% reduction in shrinkage strain is observed for the spherical shaped EAF

slag concrete having slag replacement ratio of 0.3 and 0.5 respectively. This value is 38% when the slag replacement ratio is 1.0. The above experimental results show that the shrinkage of spherical shaped EAF slag concrete decreases with the increase in slag ratio and is almost half than that of angular shaped EAF slag concrete when the slag ratio is 1.0 and W/C is 0.4. However, for angular shaped EAF slag concrete, the shrinkage strain is closer to normal concrete up to a slag replacement ratio of 0.5 and higher when the slag ratio is 1.0.

Exactly similar shrinkage behavior (Figure 4-26) as of W/C of 0.4 is obtained for concrete produced under series 3 where the W/C is 0.6. In comparison to normal concrete, for the drying age of 91 days, approximately, 17% lesser shrinkage strain was recorded for spherical shaped EAF slag fine aggregate concrete having slag ratio of 0.3 and 0.5. For the slag replacement ratio of 1.0, the reduction was computed as 52%.

Generally, drying shrinkage of concrete is related to many factors such as water and cement content, specimen size and surface area, relative humidity, temperature etc. (Neville, 2010). Since, all other factors like specimen size, relative humidity, and temperature were constant for all the specimens under this study, therefore, it can be judged that the decrease in shrinkage might be primarily due to the decrease in water and cement content. Based on this assumption, drying shrinkage of concrete of series 1 and 2 was calculated by JSCE prediction equation (JSCE guidelines for concrete No. 15, 2010) as provided in Eq. 4.3. The reason for choosing JSCE equation for prediction of shrinkage strain is that the equation considers the effect of change in water content in the mix proportion and most importantly, it was found to be closely predicting the shrinkage strain of normal concrete.

$$\text{Shrinkage strain, } \varepsilon'_{sh} = -50 + 78\left[1 - e^{\left(\frac{RH}{100}\right)}\right] + 38 log_e W - 5[log_e\left(\frac{V}{S * 10}\right)]^2 \qquad (4.4)$$

Where, RH = Relative humidity (%), W = Unit water content (kg/m^3), V = Volume (mm^3), S = Surface (mm^2)

JSCE predicted shrinkage strain for spherical (series 1) and angular (series 2) shaped EAF slag concrete at different slag replacement ratio along with their experimental results at the drying age of 91 days are shown in Figure 4-27. It can be seen from the figure that JSCE equation predicts the drying shrinkage of normal concrete closely to the experimental value with a deviation of 5%. In case of spherical shaped EAF slag concrete, JSCE model always over predicts the experimental results although predicted shrinkage strain decreases with the increase in slag ratio due to the change in water content. For angular shaped EAF slag concrete, JSCE equation over predicts up to a slag ratio is 0.5 and then it under predicts the experimental shrinkage strain. The deviation in experimental and predicted shrinkage strain clearly indicates that the shrinkage of slag concrete may not be due to the change in water and cement content only.

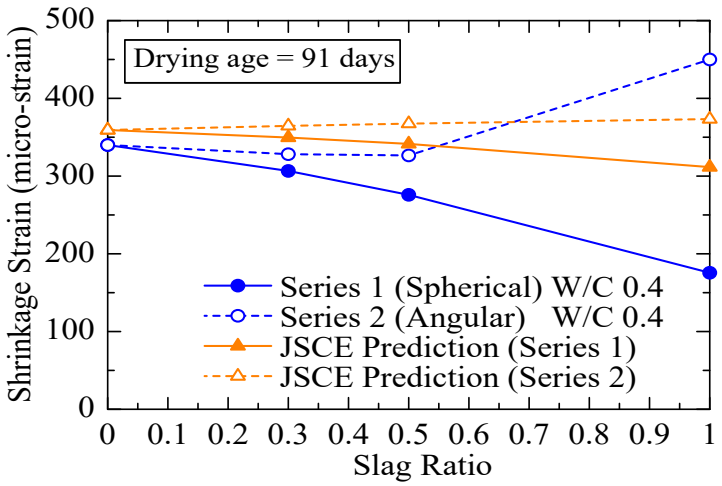

Figure 4-27 Experimental and JSCE predicted shrinkage strain

The experimental results of shrinkage can be further discussed with the findings of researchers like Shilstone (1990), Washa (1998), Forster (1994) and Ahmed (1989). According to Shilstone (1990), spherical or cubical particles produce higher strengths and lower shrinkage than flaky and elongated particles. Washa (1998) observed that aggregates with lower absorption tend to reduce shrinkage. Forster (1994) and Ahmed (1989) pointed out that presence of more fine contents in aggregate mix increases shrinkage. In the current study, spherical slag aggregates had lower water absorption than that of normal sand and angular slag. In addition, angular slag had more fine contents

than spherical slag. Therefore, the shrinkage behavior of spherical slag concrete might be attributed to the particle shape, lower water and cement requirement, lower water absorption and stronger particle adhesion in resisting shrinkage.

In order to investigate the sole influence of spherical shaped EAF slag fine aggregates on the shrinkage reduction ability of concrete, mortar specimen of 100x100x400mm sizes were cast by replacing natural sand with spherical shaped EAF slag at a volume ratio of 0.0, 0.1, 0.2 and 0.5 and W/C of 0.6. Mix proportions are shown in Table 4-3. The specimens were cured under water for 3 days and the length change of each of them were measured by the similar method as discussed earlier up to a drying age of 95 days. For each case two representative specimens were used and average results were considered. Figure 4-28 shows the experimental results of the shrinkage test of mortar specimen.

Table 4-3 Mix proportions of mortar for shrinkage test

Slag Ratio	Slag Type	W/C	Water (kg/m^3)	Cement (kg/m^3)	Sand (kg/m^3)	Slag (kg/m^3)	AE Admixture (kg/m^3)
0.0	No slag	0.6	158	263	661	0	2.63
0.1	Spherical		156	260	601	94	2.60
0.2			154	256	541	191	2.56
0.5			147	246	350	494	2.46

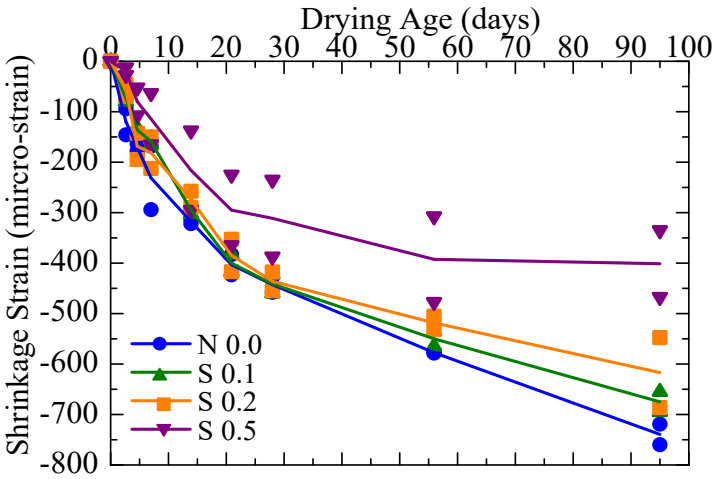

Figure 4-28 Shrinkage of mortar specimen

It can be reconfirmed from Figure 4-28 that spherical shaped EAF slag aggregates help in reducing the shrinkage strain of mortar/concrete when the slag replacement ratio is higher. Up to a slag replacement ratio of 0.2 for the drying age of 95 days, a 16.57% reduction in shrinkage strain was computed for spherical shaped EAF slag mortar in comparison to normal mortar which was 45.74% when the slag replacement ratio is 0.5.

In concrete structures especially of foundations at grade and pavements, joints are usually provided to account for cracking due to stresses caused by drying shrinkage and applied load (ACI 325.12R-02, 2012). Oehler (1963) reported that putting joints in concrete are useful in managing cracks, however, the first sign of distress occur near joints. Therefore, number of joints in concrete members should be minimum. Now, the result that the drying shrinkage of spherical shaped EAF slag concrete is much lower than that of normal and angular shaped EAF slag concrete seems to be advantageous as it can play a significant role in reducing number of joints in concrete members if they are cast by spherical shaped EAF slag fine aggregates.

4.4.2 Water absorption

It has been already discussed that EAF slag is composed of different metal oxides. As a result in order to avoid the possible detrimental environmental impact it is necessary to investigate the susceptibility of such concrete against leaching prior to their utilization in concrete pavement. Therefore, water absorption test was conducted for all the specimens under series 1 and 2 of low W/C of 0.4 after a curing age of 3, 7 and 28 days by the method as described in JSCE–K571 (2005). The experiment was conducted on the 100x100x200mm specimen by installing a pipet on the surface completely sealed against water. Initially, the pipet was filled by water and the change in water quantity was recorded after 7 days which is the water absorption by concrete. In order to reduce the effect of evaporation, temperature and other environmental factors, the top of the pipet were sealed by plastic wrap and the experiment was conducted in the curing room under controlled temperature and humidity. Figure 4-29 depicts the water absorption test condition while experimental results are plotted in Figure 4-30 with all respective data points.

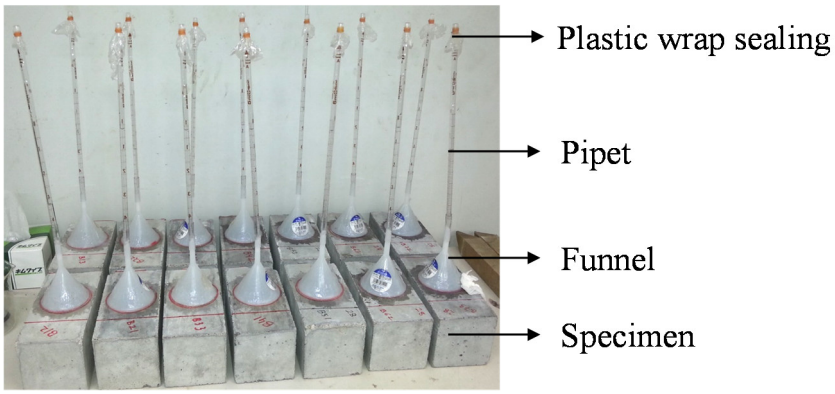

Figure 4-29 Water absorption test condition

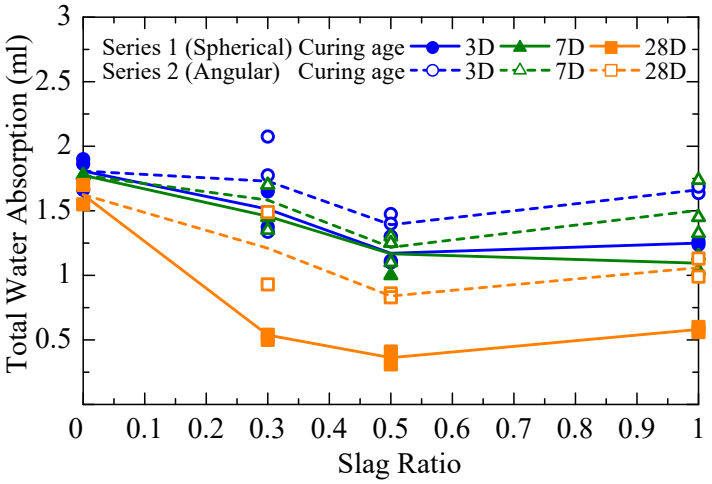

Figure 4-30 Water absorption with slag ratio

It can be observed from Figure 4-30 that slag concrete shows lower water absorption in comparison to normal concrete irrespective of curing age and slag replacement ratio. The result that the water absorption of slag concrete decreases with the increase in curing age is reasonable as concrete becomes denser with curing and subsequently, water penetration capacity decreases. In case of angular shaped EAF slag concrete, the lowest water absorption was observed for the slag ratio of 0.5 at the curing age of 3, 7 and 28 days. However, for the slag ratio of 0.3 and 1.0, water absorption is almost similar to that of normal concrete irrespective of curing age. Spherical shaped EAF slag concrete exhibits similar trend as of angular shaped EAF slag concrete although water absorption for the slag ratio of 0.3 and 0.5 are much lower than normal concrete.

For the curing age of 28 days, spherical shaped EAF slag concrete experiences half the water absorption as of angular shaped EAF slag concrete when the slag ratio is 1.0 and this behavior is found to be constant for all other slag ratio cases of 0.3 and 0.5.

In the present study, hardened concrete density of both spherical and angular shaped EAF slag concrete of all W/C increases with the increase in slag ratio (Figure 3-13 and 3-14). In addition, water absorption capacity of spherical and angular shaped EAF slag aggregates as shown in Table 2-3 are smaller than natural sand. Primarily, water absorption of concrete increases due to the relative water absorption capacity of different type of aggregates. Therefore, the result that the water absorption of spherical and angular shaped EAF slag concrete are lesser than normal concrete is justified. Regarding different types of concrete, results show that water absorption of angular shaped EAF slag concrete (series 2) is higher than that of spherical shaped EAF slag concrete (series 1). Since, the main difference of the two types of slag remains in the shape there is possibility that during mixing, angular shaped EAF slag concrete might involve more air surrounding the slag. As a result, the possibility of having more interconnected pores in the angular shaped EAF slag concrete is high even though air content of the two types of slag concrete is similar. The porosity results of both types of EAF slag concrete as reported in Figure 5-10 confirms this assumption.

Thus, it can be said that the water absorption of concrete is related to the difference between natural sand and slag aggregates in terms of absorption of aggregates and the amount of interconnected pores. Due to the balance of both the effects, water absorption of both types of slag concrete at the slag ratio of 1.0 is slightly higher than that of slag ratio 0.3 and 0.5.

Zhang and Zong (2014) described the water absorption of concrete as an indicator of durability properties which provides information regarding the resistance against the intrusion of detrimental materials. The experimental results that the spherical shaped EAF slag concrete exhibits much lower water absorption compared to angular slag and normal concrete seem to be beneficial against intrusion possibility of chloride and sulfate ions. Moreover, because of lower water absorption capacity, chances of leaching and penetration through the spherical shaped EAF slag concrete is expected to be low.

4.4.3 Air permeability

Similar to water absorption, air permeability is another important durability indicator of concrete. In this study, coefficient of air permeability of concrete produced at low W/C of 0.4 by using both spherical (series 1) and angular (series 2) shaped EAF slag was measured by torrent method (1992) after a curing age of 28 days. Two representative specimens of 300x300x100mm sizes were used for each of the slag ratio cases under each series. For each specimen, air permeability was measured in five different locations as shown in Figure 4-31 and the average air permeability coefficient (k_T) was recorded. The distance of the edge of the specimen to that of the air permeability measuring cone was kept 50mm which is higher than that of minimum recommended distance of 20mm by Torrent method (1992). All the experimental data points along with the average line is shown in Figure 4-32. The experimental results did not show big scatter and the results are useful to differentiate the air permeability behavior of different type of EAF slag concrete.

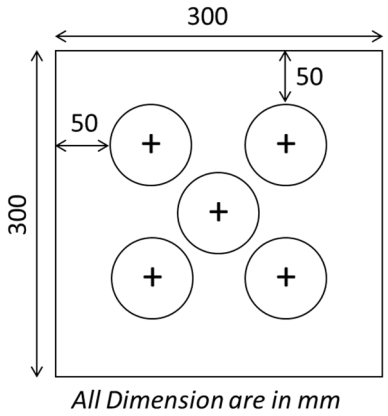

Figure 4-31 Measurement location of air permeability

Overall, the results as shown in Figure 4-32 indicate low air permeability irrespective of the type of slag. However, angular shaped EAF slag concrete shows higher air permeability than normal and spherical shaped EAF slag concrete. Spherical shaped EAF slag concrete for the slag replacement ratio of 0.5 and 1.0 shows lower air permeability than that of normal and angular shaped EAF slag concrete although that of slag ratio of 0.3 is similar to normal concrete. The air permeability indicators as developed

and suggested by Torrent (1992) after extensive experimental works are also shown in Figure 4-32. According to these indicators, the lesser the air permeability, the more durable the concrete is. It is evident from Figure 4-32 that, spherical shaped EAF slag concrete especially with higher slag ratio cases of 0.5 and 1.0 lies in the 'good' range than normal and slag ratio 0.3 case which lies in the borderline of 'good' and 'medium' range. In contrary, angular shaped EAF slag concrete shows higher air permeability than normal and spherical shaped EAF slag concrete and lies in the 'medium' range. Therefore, the effect of shape of EAF slag fine aggregates on the air permeability of concrete is confirmed. The above experimental results might be attributed to the higher porosity of normal and angular shaped EAF slag concrete due the presence of more interconnected pores as discussed in the previous section (4.4.3) related to water absorption.

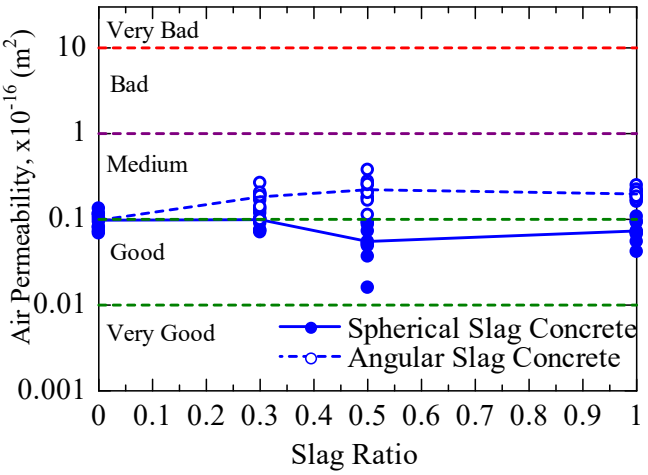

Figure 4-32 Air permeability with slag ratio

In so far as the durability properties of slag concrete are concerned, spherical shaped EAF slag concrete shows lower shrinkage, water absorption and air permeability compared to normal and angular shaped EAF slag concrete. These behaviors confirm the signature property spherical shaped EAF slag concrete of high density along with lower porosity and justify their environmental sustainability if utilized in concrete pavement.

4.5 Summary and conclusions

In conjunction with the study related to fresh concrete behavior as reported in chapter 3, this study investigated the applicability of spherical shaped EAF slag in concrete in terms of mechanical and durability properties at two different W/C and slump of 0.4, 5cm and 0.6, 12cm respectively. Based on this comparative experimental research, following conclusions can be summarized.

- In so far as the mechanical properties of concrete is concerned, replacement of sand by spherical shaped EAF slag in concrete is advantageous as it increases the compressive strength, elastic modulus, bending and tensile strength of concrete in comparison to normal concrete when the W/C and slump is lower such as 0.4 and 5cm. At higher W/C of 0.6 and slump of 12cm, spherical shaped EAF slag concrete shows a decreasing trend with the increase in slag ratio.
- The improved compressive strength and elastic modulus of spherical shaped EAF slag concrete at lower W/C and slump has been identified by digital image co-relation method as stronger particle adhesion in resisting crack origination and propagation under uniaxial compression loading. Spherical shaped EAF slag concrete exhibits lesser number of cracks than other types of concrete at same stress level and origination of initial crack happens at relatively higher stress level.
- Although angular shaped EAF slag concrete provides higher bending and tensile strength in comparison to spherical shaped EAF slag concrete, comparatively lower ductility of such concrete indicates that spherical shaped EAF slag concrete is suitable for concrete pavement considering all aspects of mechanical behavior.
- Spherical shaped EAF slag concrete exhibits half of shrinkage than angular shaped EAF slag concrete when all sand in concrete is replaced by it. In comparison to normal concrete spherical shaped EAF slag concrete shows much lower shrinkage irrespective of W/C and slump. In addition, lesser water absorption and lower air permeability of such concrete turns out spherical shaped EAF slag fine aggregates to be a promising, economic and durable alternative of natural sand in concrete.

The results as discussed in this chapter confirmed that spherical shaped EAF slag is advantageous for concreting at lower W/C and slump and thus useful for concrete pavement considering the fresh behavior, strength, durability, sustainability and economy of construction. In the next chapter, investigation of some other characteristic features of concrete pavement such as thermal properties and freezing and thawing resistance will be addressed to confirm their wider applicability.

5 Material stability of spherical shaped EAF slag concrete during thermal change

5.1 Introduction

Study on the fundamental and durability properties of concrete as reported in chapter 3 and 4 confirmed that spherical shaped EAF slag fine aggregates are advantageous to be utilized in concrete as replacement of natural sand at lower water to cement ratio and slump of 0.4 and 5cm respectively. Therefore, the applicability of this material in concrete pavement is reasonable. In case of concrete pavement, changes in thermal properties such as thermal expansion, thermal conductivity, thermal diffusivity, specific heat etc. have significant impact on the mechanical and durability properties since the distress in concrete pavement such as faulting, joint openings, blow ups, spalling, breaking of corners, crack development and propagation etc. are directly or indirectly related to the thermal properties of concrete (Huang, 2004, Jeong et al., 2012, Xu et al., 2000 and Juknevicius et al., 2006). Moreover, in cases when the thermal property of EAF slag concrete is different from normal concrete, the traditional design approach for deformation behavior due to thermal stress might not be applied directly. Apart from thermal properties, measurement of freezing and thawing resistance is equally important for concrete pavement in the region where frost and defrost action is severe and common. It is fact that a high temperature difference such as freezing and thawing condition affects the thermal properties of concrete pavement significantly resulting in series of potential closely spaced, crescent-shaped cracks near joint/corner as termed as durability cracking or D-Cracking (Gokce et al., 2004, Larosche, 2009). In this context, to confirm the wider

utilization of spherical shaped EAF slag in concrete pavement, this study aims to investigate the material stability and thermal properties including freezing and thawing resistance during thermal change of concrete pavement produced by spherical shaped EAF slag fine aggregate and compare the results with angular shaped EAF slag concrete to clarify the mechanism and effect of slag shape on thermal properties of such concrete.

5.2 Experimental outline

5.2.1 Experimental series and specimen notation

Three different experimental series were undertaken to investigate the thermal behavior of concrete produced by spherical and angular shaped EAF slag fine aggregates by replacing natural sand. Table 5-1 summarizes the experimental series along with specimen notation which will be used for all the plots of this study.

Table 5-1 Experimental series and specimen notation (Roy et al., 2019)

Series	Slag Ratio	Slag Type	Air Entrainment	Notation	Tests Conducted
1 (Spherical)	0.0	No slag	Air Entrained	N 0.0 AE	Both thermal properties and freezing and thawing resistance
	0.3	Spherical		S 0.3 AE	
	0.5	Spherical		S 0.5 AE	
	1.0	Spherical		S 1.0 AE	
2 (Angular)	0.3	Angular		A 0.3 AE	
	0.5	Angular		A 0.5 AE	
	1.0	Angular		A 1.0 AE	
2B	0.0	No slag	Low Air Entrained	N 0.0 LAE	Only freezing and thawing resistance
	1.0	Spherical		S 1.0 LAE	
	1.0	Angular		A 1.0 LAE	

Concrete under series 1 and 2 were produced by considering sufficient air entrainment and the specimens thus produced were tested for all thermal properties and freezing and thawing resistance. In contrary, concrete under series 2B were produced for low air entrainment to investigate the influence of air content on freezing and thawing resistance of concrete. For series 1 and 2, four different types of concrete were produced by replacing natural sand with spherical and angular shaped EAF slag fine aggregate at a volume replacement ratio of 0.0, 0.3, 0.5 and 1.0. For series 2B, three different types of

concrete were produced by using only sand and spherical and angular shaped EAF slag at a volume ratio of 1.0 respectively.

5.2.2 Experimental parameters, mix proportions, conducted tests and specimen details

Due to the purpose of utilizing the EAF slag fine aggregates in concrete pavement, a low W/C and slump of 0.4 and 5cm was considered (detail reasoning for choosing these parameters are discussed in chapter 3, section 3-2). Target for air content for air entraining concrete as marked as series 1 and 2 in Table 5-1 was considered 5% ± 1% according to the JSCE proportioning manual and guidelines (No.1, 2004) for concrete structures by using EAF slag aggregates. In order to investigate the effect of low air content on freezing and thawing resistance of concrete, air content for series 2B was targeted as 2%.

Table 5-2 Mix proportions of concrete (Roy et al., 2019)

Series	Slag Ratio	Slag Type	W/C	Target Slump (cm)	Target Air Content (%)	Water (kg/m^3)	Cement (kg/m^3)	Gravel (kg/m^3)	Sand (kg/m^3)	Slag (kg/m^3)	AE Admixture (kg/m^3)
1	0.0	No slag	0.4	5	5	150	376	1070	685	0	3.76
	0.3	Spherical	0.4	5	5	145	362	1077	493	298	3.62
	0.5					140	351	1089	356	503	3.51
	0.7					134	335	1107	217	715	3.35
	1.0					126	314	1135	0	1039	3.14
2	0.3	Angular	0.4	5	5	153	383	1083	461	298	3.83
	0.5					155	388	1082	326	492	3.88
	0.7					156	390	1079	195	687	3.90
	1.0					158	396	1066	0	983	3.96
2B	0.0	No slag	0.4	5	2	150	376	1070	685	0	0.0
	1.0	Spherical				126	314	1135	0	1089	0.0
	1.0	Angular				158	396	1066	0	983	0.0

Based on the above experimental parameters, mix proportions were designed and duly verified by trial tests for slump and air content which is listed in Table 5-2. Fresh concrete behaviors are tabulated in Table 5-3. It is fact that the mix proportions and fresh concrete behaviors of series 1 and 2 are identical to that reported in Table 3-1 and 3-2 respectively. In preparation of concrete under series 2B, similar mix proportion as of series 1 and 2 were used without using the air entraining admixtures. Due to the

consideration of very low air content for series 2B and subsequently because of using no air entraining admixtures, a very low slump in comparison to series 1 and 2 was obtained for series 2B irrespective of slag type. In addition, the values of air content were closer to the target value of 2% with a maximum variation of ±0.6%.

Table 5-3 Behavior of freshly mixed concrete (Roy et al. 2019)

Series	Slag type	W/C	Slag ratio	Target slump (cm)	Measured slump (cm)	Target air content (%)	Measured air content (%)	Fresh density (kg/m^3)
1	Spherical	0.4	0.0	5±1.5	4.7	5±1.5	4.8	2416
			0.3		4.0		4.6	2500
			0.5		5.8		5.0	2566
			0.7		4.1		4.9	2632
			1.0		3.6		5.0	2738
2	Angular	0.4	0.3	5±1.5	4.3	5±1.5	4.6	2501
			0.5		4.7		4.1	2578
			0.7		4.3		4.0	2652
			1.0		4.7		4.1	2743
2B	No slag	0.4	0.0	-	0.9	2	1.6	2399
	Spherical		1.0		0.8		2.3	2727
	Angular		1.0		1.3		1.4	2730

In this study, thermal properties like thermal expansion, thermal conductivity, thermal diffusivity, specific heat and freezing and thawing resistance of concrete were examined. Cylinders of Φ100x200mm sizes were used for thermal conductivity, thermal diffusivity and specific heat tests whereas, prisms of 100x100x400mm were used for thermal expansion and freezing and thawing resistance test. For each test, three representative specimens from each batch were used after the underwater curing of specimens for 28 days. A summary of conducted experiments, specimen numbers, type, size and curing age is listed in Table 5-4.

Table 5-4 Details of specimen for thermal properties and freezing and thawing resistance (Roy et al., 2019)

Series	W/C	Name of test	Specimen type & size	Curing age (days)	Specimen per batch	Total specimen
1	0.4	Thermal conductivity	Cylinder Ø100x200	28	3	12
2	0.4					09
1	0.4	Thermal diffusivity	Cylinder Ø100x200	28	3	12
2	0.4					09
1	0.4	Specific heat	Cylinder Ø100 X 200	28	3	12
2	0.4					09
1	0.4	Thermal expansion	Prism 100x100x400	28	3	12
2	0.4					09
1	0.4	Freezing and thawing	Prism 100x100x400	28	3	12
2	0.4					09
2B	0.4					09

5.3 Thermal properties

5.3.1 Thermal expansion

In order to evaluate the linear expansion of concrete produced by both spherical and angular shaped EAF slag under elevated temperature, prism specimens of series 1 and 2 having 100x100x400mm sizes were tested after a curing age of 28 days. Detail experimental protocol is shown in Figure 5-1. In order to measure the linear thermal expansion of concrete, mold gauge was installed inside each of the concrete specimen. This mold gauge is a special device which has the gauge length of 60 mm and can measure both the strain and temperature of the specimen. The mold gauge was positioned at the center of the specimen by using tying string as shown in Figure 5-1 (b).

It is fact that, humidity and moisture content play an important role for linear thermal expansion of concrete (Jeong et al., 2012). For this reason, all the specimens were kept submerged in water bath during the experiment to minimize the effect of differential moisture content as shown in Figure 5-1 (c). Prior to test, all the specimens were kept under water having a controlled temperature of 20±2°C for 24 hours. During test, water temperature was increased uniformly in the water container from 20°C to 60°C in about 2 hours. The specimens were kept at the highest temperature for at least 1 hour for thermal

stability. Readings of water temperature, strain and temperature at the center of each of the specimens were taken at an interval of every 1 min by using data logger.

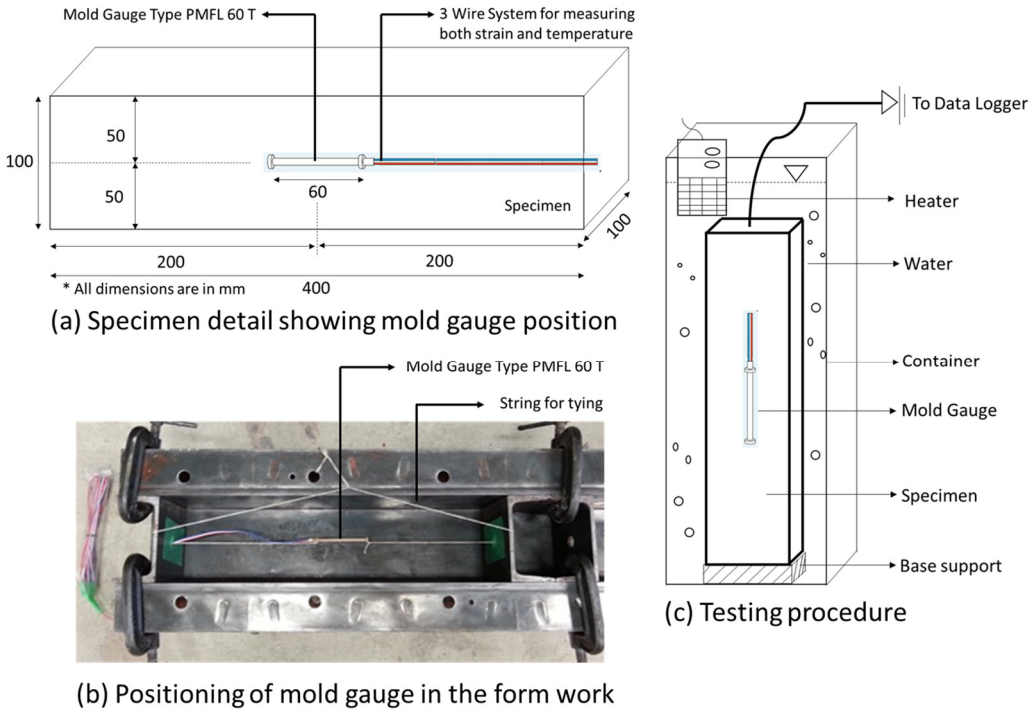

Figure 5-1 Thermal expansion measurement protocol (Roy et al., 2019)

The experimental results of thermal expansion of concrete are depicted in Figure 5-2. It can be seen from the figure that thermal strain increases linearly with the increase in heating temperature for normal as well as EAF slag aggregate concrete. Coefficient of thermal expansion (CTE) of all concrete of series 1 and 2 were computed by using Eq. 5.1 based on the results as shown in Figure 5-2.

$$Coefficient\ of\ thermal\ expansion, CTE = \frac{\Delta\varepsilon}{\Delta T} \qquad (5.1)$$

Where, $\Delta T = T_2 - T_1$, T_1 = Initial temperature, T_2 = Final temperature, $\Delta\varepsilon = \varepsilon_2 - \varepsilon_1$, ε_1 and ε_2 = Thermal strain (micro-strain) at temperature T_1 and T_2 respectively.

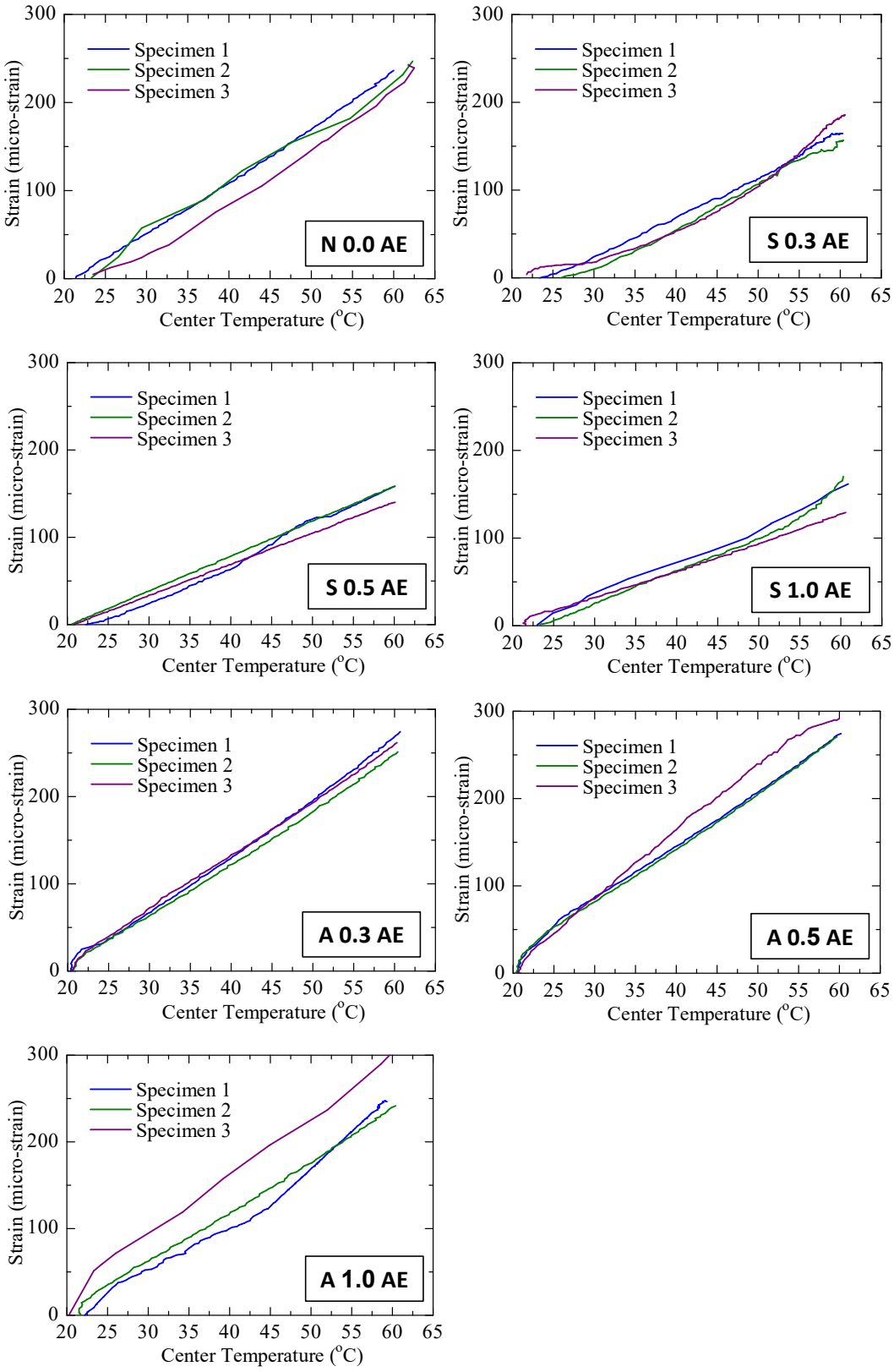

Figure 5-2 Thermal strain due to thermal expansion (Roy et al., 2019)

Coefficient of thermal expansion (CTE) for normal, spherical and angular shaped EAF slag concrete with the increase in slag ratio is plotted in Figure 5-3 with all respective experimental points. Although the value of CTE for normal concrete is found to be in the lower side, however, according to Neville, 2010, CTE can widely range from 6.1 to 12.2 μ-strain/°C depending on the type of coarse aggregates utilized in concrete. Since the target of current study is to identify the influence of EAF slag fine aggregate on CTE, similar type of coarse aggregates as of normal concrete was utilized for slag concrete to negate the effect of coarse aggregates. It is evident from Figure 5-3 that the CTE values of spherical shaped EAF slag concrete decrease with the increase in slag ratio and becomes constant after the slag replacement ratio of 0.5 whereas, that of angular shaped EAF slag concrete remains constant to slightly increasing with the increment of slag ratio.

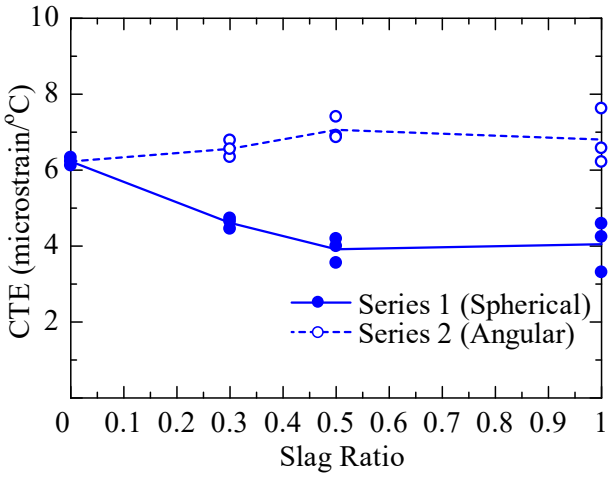

Figure 5-3 Coefficient of thermal expansion with slag ratio (Roy et al., 2019)

5.3.2 Specific heat

The specific heat of normal and EAF slag concrete was measured by the principal of calorimetry. In this test, three representative cylindrical specimens from each slag ratio under each series having 100mm x 200 sizes were heated until the temperature at the center of the specimens reaches 60˚C. Prior to heating, mass of each the specimens were recorded. The preheated specimens were then placed inside the calorimeter having water of known mass and temperature. Temperature reading obtained from the thermocouple wires placed at the center of the specimen and in calorimeter water were recorded by data

logger at an interval of every 20 s until the temperature of both the specimen and calorimeter water approaches similarity. A schematic diagram of the test condition is provided in Figure 5-4.

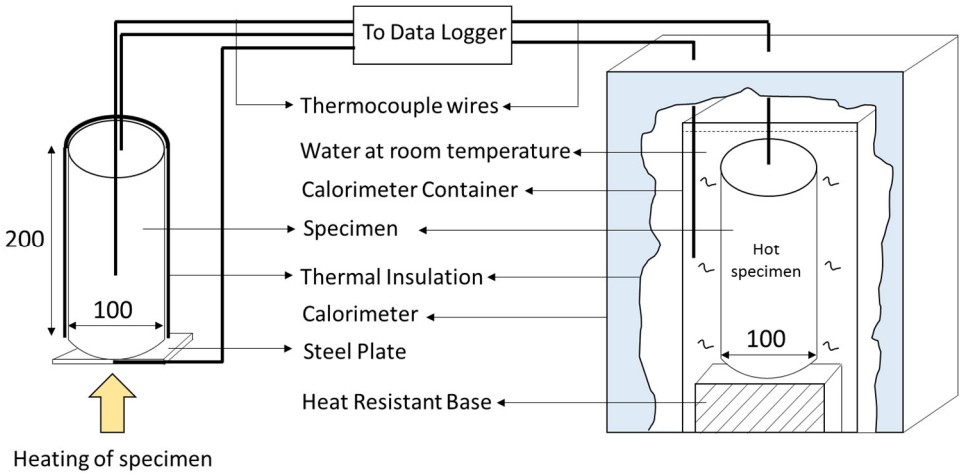

Figure 5-4 Test condition of specific heat of concrete (Roy et al., 2019)

Based on the above experimental setup, specific heat of concrete was computed by the following equation.

$$Specific\ heat, S_c = \frac{m_w S_w (T_m - T_w)}{m_s (T_s - T_m)} \tag{5.2}$$

Where, m_w = Mass of water (kg), S_w = Specific heat of water (4.186 kJ/kg-K), T_w = Initial temperature of calorimeter water (˚C), m_s = Mass of specimen (kg), T_s = Initial temperature at center of specimen (˚C), T_m = Final temperature of the mix (specimen and calorimeter water) (˚C).

Specific heat of all seven types of concrete produced under series 1 and 2 was computed by using Eq. 5-2. Experimental results are depicted in Fig. 5-5. The value of specific heat for normal strength concrete was found as 0.76 kJ/kg-K which is within the standard range of 0.75 to 0.96 kJ/kg-K depending on the type of concrete (Engineering toolbox, 2003). It can be seen from Figure 5-5 that the specific heat of both spherical and angular shaped EAF slag concrete is lesser than normal concrete especially after the slag ratio of 0.3. Until slag ratio of 0.3 specific heat is similar to normal concrete while at slag

ratio of 0.5, specific heat is much lesser than that of slag ratio of 0.3. However, a slightly higher specific heat is observed from slag ratio 0.5 to 1.0. In addition, both spherical and angular shaped EAF slag concrete show similar behavior for same slag ratio and there is nothing different to choose from the two types.

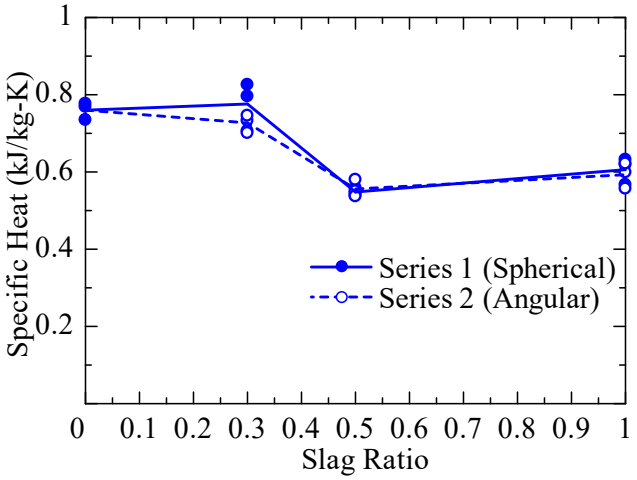

Figure 5-5 Specific heat with slag ratio (Roy et al., 2019)

5.3.3 Thermal diffusivity

All different types of concrete specimens cast by spherical and angular shaped EAF slag fine aggregates were tested for thermal diffusivity after a curing age of 28 days. For each slag ratio case, three representative cylinder specimens having 100mm x 200mm sizes were used. In this test, all the specimens were heated uniformly by keeping them completely submerged in water. Temperatures at the center of each of the specimens were recorded by the thermocouple wire installed at the center of each of the specimen during casting. In addition, water temperature was measured by the external thermocouples placed in water. A schematic diagram of the test procedure is shown in Fig. 5-6. During the heating phase, water was heated until the center temperature of each of the specimen reaches 75°C. The specimens were then placed in the cold-water bath where the temperature was continuously maintained around 20°C ± 1°C by supplying cold water through inlet and removing the relatively hot water through the outlet at constant speed. Temperature reading at the center of the specimen and outside water was recorded by data logger at an interval of every 1 min. The specimens were kept in the cold-water bath until

the temperature difference between the center of the specimen and outside water reaches 4°C.

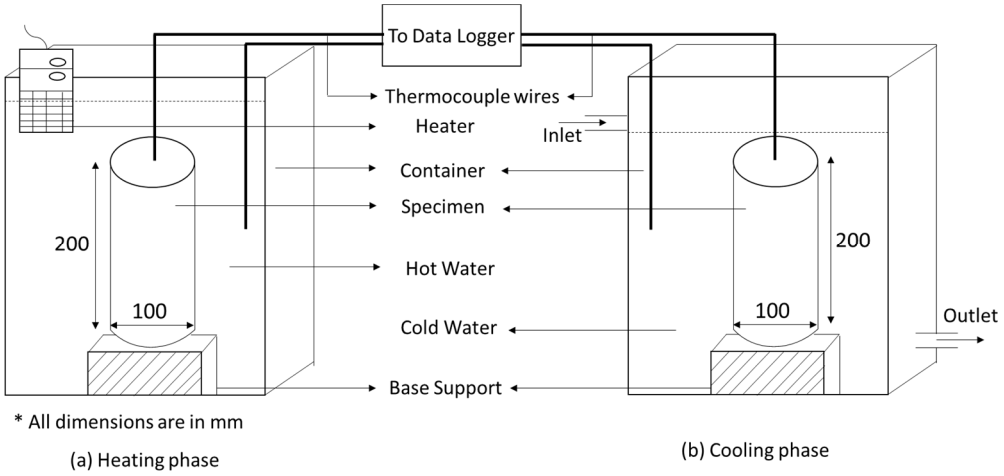

Figure 5-6 Thermal diffusivity test procedure (Roy, et al., 2019)

Based on the experimental setup and procedure as discussed above, thermal diffusivity (m^2/hr.) of concrete was computed by using the equations (5.3-5.5) as suggested in CRD-C 36-73 Method.

$$Thermal\ diffusivity, \alpha = \frac{M}{t_2 - t_1} \tag{5.3}$$

$$For\ prism\ specimen, M = \frac{60 \ln \frac{T_1}{T_2}}{\pi^2 (\frac{1}{a^2} + \frac{1}{b^2} + \frac{1}{c^2})} \tag{5.4}$$

$$For\ cylindrical\ specimen, M = \frac{60 \ln \frac{T_1}{T_2}}{(\frac{5.783}{r^2} + \frac{\pi^2}{l^2})} \tag{5.5}$$

Where, M = specimen size and shape factor; t_1 and t_2 = Time (mins) at which center of the specimen reaches any specified temperature difference; T_1 and T_2 =

Temperature differences (˚C) at time t_1 and t_2; a, b, c = Sides of prism (m), r and l = Radius and length of cylinder (m).

A semi logarithmic temperature difference vs. time curve is plotted (Figure 5-7) for each of the specimen and thermal diffusivity of concrete is calculated by using Eq. 5.3 and 5.5 for any two arbitrary temperature difference (T_1 and T_2) and corresponding time (t_1 and t_2).

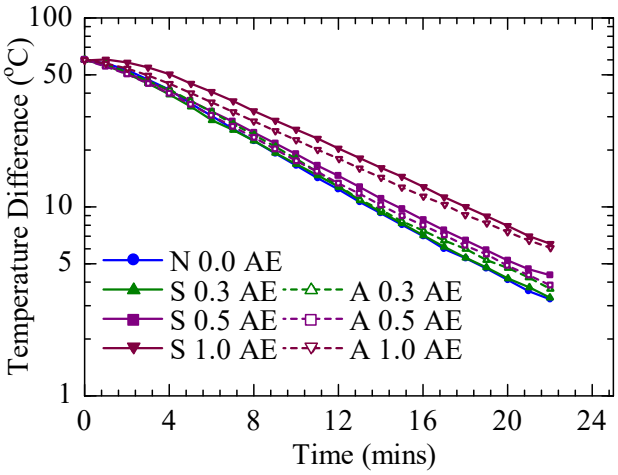

Figure 5-7 Thermal difference with time (Roy et al., 2019)

Figure 5-7 shows the average temperature difference vs. time plot for spherical and angular shaped EAF slag concrete. Ideally, specimen that require more time to reach the same temperature difference has lower thermal diffusivity than that require less time. Based on this concept, from Figure 5-7 qualitatively it can be confirmed that the thermal diffusivity of spherical shaped EAF slag concrete is lower than that of normal concrete irrespective of slag ratio. The result of thermal diffusivity with slag ratio is plotted in Figure 5-8 which quantitatively demonstrates the above finding. Clearly, thermal diffusivity decreases linearly with the increase in slag ratio for both spherical and angular shaped EAF slag concrete. This reduction is 25% when natural sand is completely replaced by spherical or angular shaped EAF slag fine aggregate in concrete. The value of diffusivity of normal strength concrete is found as 0.986 mm^2/s which is well within the standard range of 0.55 to 1.55 mm^2/s as reported by Neville, 2010 for different types of concrete.

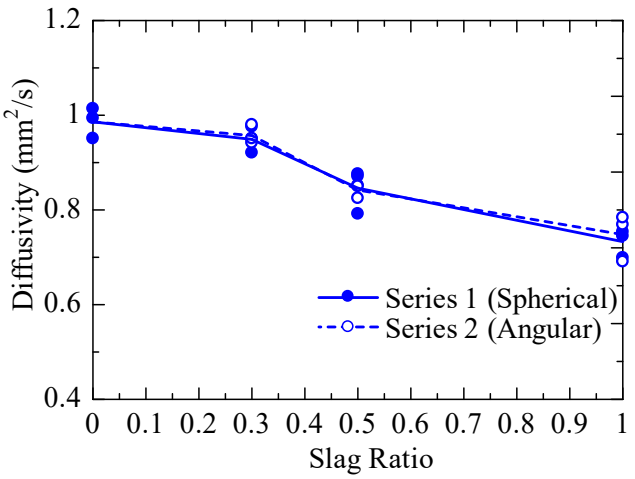

Figure 5-8 Thermal diffusivity with slag ratio (Roy, et al., 2019)

5.3.4 Thermal conductivity

Thermal conductivity of all types of concrete under series 1 and 2 was computed by the simple and popular relationship used in ACI 122R-02, 2014 between thermal conductivity with density, specific heat and diffusivity as shown in Eq. 5.6.

$$Thermal\ conductivity, k = \rho S_c \alpha \quad (5.6)$$

Where, ρ = Density (kg/m^3), S_c = Specific heat (kJ/kg-K) and α = Thermal diffusivity (m^3/s).

The thermal conductivity of series 1 and 2 is shown in Table 5-5. The relationship between thermal conductivity and slag ratio is depicted in Figure 5-9. Thermal conductivity for normal concrete is found as 1.749 W/m-K which lies within the standard range of 1.4 to 3.6 W/m-K (Neville, 2010).

Similar to thermal diffusivity and specific heat, thermal conductivity of slag concrete is found to be decreasing with the increase in slag ratio irrespective of the shape of EAF slag as utilized in concrete in this study. The value of thermal conductivity for the slag ratio of 0.3 is found to be similar to normal concrete although that of slag ratio of 0.5 and 1.0 is found to be lesser than normal concrete and almost constant.

Table 5-5 Density, specific heat, diffusivity and thermal conductivity (Roy et al., 2019)

Series	Notation	Specimen ID	Density (kg/m^3)	Specific heat, S_c (kJ/kg-K)	Diffusivity, α (mm^2/s)	Conductivity, k (W/m-K)
1	N 0.0 AE	1	2337	0.74	1.01	1.74
		2	2325	0.77	0.95	1.70
		3	2338	0.78	0.99	1.81
	S 0.3 AE	1	2412	0.80	0.92	1.77
		2	2398	0.83	0.98	1.93
		3	2407	0.71	0.95	1.61
	S 0.5 AE	1	2433	0.54	0.88	1.15
		2	2455	0.56	0.87	1.19
		3	2454	0.55	0.79	1.06
	S 1.0 AE	1	2621	0.57	0.70	1.04
		2	2617	0.62	0.75	1.22
		3	2625	0.63	0.74	1.24
2	A 0.3 AE	1	2481	0.73	0.98	1.75
		2	2443	0.75	0.94	1.72
		3	2401	0.70	0.95	1.63
	A 0.5 AE	1	2497	0.55	0.85	1.17
		2	2493	0.54	0.85	1.14
		3	2487	0.58	0.83	1.19
	A 1.0 AE	1	2604	0.56	0.77	1.12
		2	2604	0.60	0.78	1.22
		3	2629	0.62	0.69	1.13

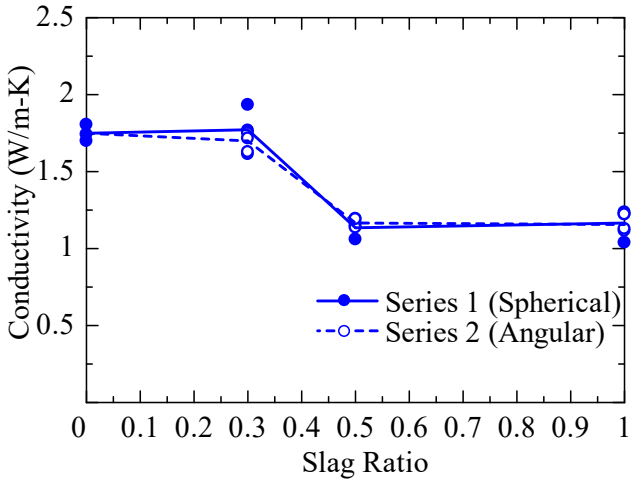

Figure 5-9 Thermal conductivity with slag ratio (Roy et al., 2019)

5.3.5 Influence of fine aggregate type and shape on thermal properties of concrete

Linear thermal expansion of concrete is dependent on several factors (Neville, 2010) such as chemical composition and fineness of cement, dissimilar thermal expansion of hydrated cement paste and coarse aggregate, moisture condition and porosity of concrete. The experimental results of the current study might be influenced by the latter two cases since cement of similar fineness and chemical composition was utilized for all different types of concrete. Similarly, the type of coarse aggregate was same for all types of concrete under discussion. Therefore, the main factor remains in the change of thermal behavior of hydrated cement paste.

With the inclusion of different types of slag in concrete at different slag replacement ratio, the properties and behavior of hydrated cement paste changes which might influence the thermal expansion of cement paste. It is evident from the previous study (chapter 4, section 4.4.1) that, concrete produced by using spherical shaped EAF slag fine aggregates exhibits much lesser drying shrinkage compared to normal and angular shaped EAF slag concrete. It was discussed that the phenomena might originate due to the stronger particle resistance of spherical slag during drying shrinkage of concrete. This tendency clearly indicates that, cement paste having spherical shaped EAF slag fine aggregate might have higher resistance against expansion or contraction of paste

with the increase in slag ratio resulting in lower thermal expansion or contraction of such concrete.

Stronger particle resistance in cement paste is associated with the pore structure and porosity of concrete. The lower the porosity, the narrower is the ITZ width resulting in stronger particle resistance in cement paste (An et al., 2017). It is fact that concrete having higher porosity tends to have higher amount of capillary pore resulting in higher apparent thermal expansion during heating because of higher capillary vapor pressure over saturation pressure (Neville, 2010, Powers, 1946). Based on the above studies, it can be assumed that the porosity of spherical shaped EAF slag concrete might be lower than normal and angular shaped EAF slag concrete.

In order to validate the above assumption, porosity of all cast concrete specimen was evaluated by JIS 1634:1988 method. In order to facilitate the test, sample of 100x100x50 mm sizes was cut from each of the prism specimen of 100x100x400 mm sizes which was used for thermal expansion test under each slag ratio case. The samples were oven dried at 105°C for 24 hours and oven dry weight of each of them were recorded. The samples were then put into a vacuum desiccator by completely submerging in water for 24 hours to ensure saturated condition and the weight of each of them at saturated surface dry condition and in water was taken. Porosity was computed by using Eq. 5.7.

$$Porosity, P_b(\%) = \frac{W_3 - W_1}{W_3 - W_2} x100 \tag{5.7}$$

Where, W_1 = Oven dry weight of sample (kg), W_2 = Weight of saturated sample in water (kg), W_3 = Weight of saturated surface dry sample (kg).

The test results of porosity are plotted in Figure 5-10 for different slag replacement ratio. It is clear that the porosity of spherical shaped EAF slag concrete is decreasing linearly with the increase in slag ratio while that of angular shaped EAF slag concrete is nearly constant to slightly increasing than normal concrete. This result justifies the previous assumption and thereafter the mechanism of decrease in CTE with the increase in slag ratio for spherical shaped EAF slag concrete is clarified. An et al. (2017) utilized rounded natural sand and angular manufactured sand to study the effect of aggregate

mineralogy and concrete microstructure on thermal expansion and strength of concrete. They identified that higher thermal expansion is often the result of higher porosity due to wider ITZ. Based on this finding, it can be said that the formation of ITZ by spherical shaped EAF slag fine aggregate might be smaller with the increase in slag ratio in comparison to normal and angular shaped EAF slag concrete resulting in lower porosity.

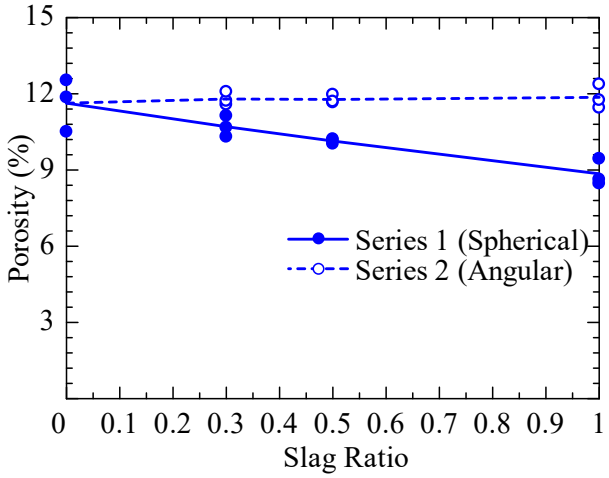

Figure 5-10 Porosity with slag ratio (Roy et al., 2019)

Lower CTE is often desirable in concrete pavement as lower CTE allows for high temperature gradient resulting in more resistance to thermal cracking (Gajda, 2007). Therefore, the result as shown in Figure 5-3 that the thermal expansion of spherical shaped EAF slag concrete is lower than that of normal and angular shaped EAF slag concrete is advantageous in managing thermal cracks. In addition, because of less thermal expansion along with lower drying shrinkage (Roy et al., 2018) of spherical shaped EAF slag concrete, lesser number of expansion/contraction joints will be required in concrete pavement which is beneficial from the durability point of view (Oehler, 1963).

Specific heat of concrete is dependent on its constituent's materials and moisture content (Neville, 2010). Mehta and Monteiro (2013) indicate that specific heat of concrete is affected by the mineralogical characteristics of aggregate. Fernandez et al. (2015) conducted a study on the thermo-physical properties of two different types of EAF slag aggregate produced by rapid and slow cooling and observed that at lower temperature (below 250°C) the values of specific heat of different type of slag was similar due to their

similar chemical compositions. In this study other than spherical and angular shaped EAF slag fine aggregates, type of all concrete constituents are similar. In addition, the changes in the type of slag remains only in their shape since the chemical compositions are same as reported in chapter 2 (section 2.2). Therefore, the result (as shown in Figure 5-5) that the spherical and angular shaped EAF slag concrete of same slag ratio show similar specific heat is justified due to their similar mineralogical compositions. Again, for the same reason normal concrete show higher specific heat than slag concrete.

The variation in the result of specific heat with the increase in slag ratio can again be discussed in light of balance between moisture content and density of concrete at different slag replacement ratio. A relationship between specific heat and slag density is depicted in Figure 5-11. Generally, specific heat of concrete increases with the increase in moisture content (Neville, 2010) and decrease in concrete density (Schutter and Taerwe, 1995). The mix water content (Table 5-2) and water absorption capacity (Figure 4-30) of normal concrete is higher than spherical and angular shaped EAF slag concrete indicates the presence of higher moisture content in normal concrete. At the same time density of normal concrete is lower than slag concrete. Therefore, higher specific heat is obtained for normal concrete. When the slag ratio is 0.5, density of slag concrete increases along with the decrease in mix water content and water absorption due to which the specific heat of slag concrete decreases. The slight increase in specific heat from slag ratio 0.5 to 1.0 might be due to the resultant of increase and decrease in specific heat caused by increase in moisture content and density respectively. In comparison to spherical shaped EAF slag concrete, despite of same mineralogical composition, angular shaped EAF slag concrete has slightly higher density and moisture content. The combined effect of which might result in similar specific heat of spherical and angular shaped EAF slag concrete.

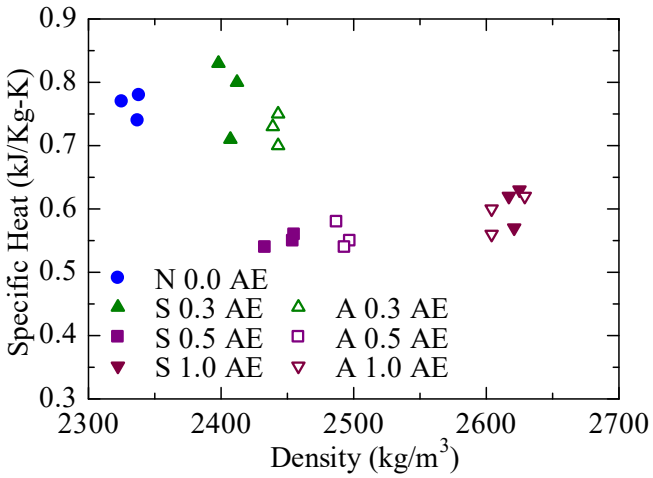

Figure 5-11 Specific heat with concrete density (Roy et al. 2019)

The result as shown in Figure 5-8 that the diffusivity of spherical and angular shaped EAF slag concrete is similar for same slag replacement ratio can be discussed with the same principle of mineralogical composition of EAF slag as discussed in the previous point related to specific heat. However, the behavior that slag concrete shows lower thermal diffusivity in comparison to normal concrete can be discussed in light of the findings of Tokuda and Shoya (1972) that the diffusivity of concrete can be expressed in terms of the diffusivities and volume fractions of the constituent material.

In this study, only natural sand is replaced by spherical and angular shaped EAF slag fine aggregate at different volume fractions keeping other concrete constituents constant. Therefore, it can be assumed that the thermal diffusivity of slag concrete is dependent on the relative thermal diffusivity and volume fraction of sand and slag in cast concrete. Thermal diffusivity of saturated fine and coarse sand ranges between 0.83 to 1.20 mm^2/s respectively (Hamdhan and Clarke, 2010) whereas that of EAF slag is around 0.4 mm^2/s (Mills, 2011). Although the above values of thermal diffusivity of sand and slag are related to several factors such as temperature, heat flow and other experimental condition, the above information provides an idea that the thermal diffusivity of sand is higher than slag. As a result, the assumption that thermal diffusivity of concrete decreases linearly with the increase in slag ratio due to the relative thermal diffusivity of sand and slag and their volume fraction in concrete is justified.

Similar to thermal diffusivity and specific heat, thermal conductivity of slag concrete as shown in Figure 5-9 is found to be decreasing with the increase in slag ratio irrespective of the type of EAF slag utilized in concrete. The value of thermal conductivity for the slag ratio of 0.3 was found to be similar to normal concrete although that of slag ratio 0.5 and 1.0 was found to be lesser than normal concrete and almost constant. Laughlin (2012) observed similar result in the study on mechanical and thermal properties of concrete cast using copper slag. The study concluded that utilization of materials formed at higher temperature tends to provide lower thermal conductivity in concrete. Generally, the formation of slag happens in the combustion zone of iron production having temperature more than 1300°C (Yang et al., 2014). In contrary, natural sand is available at normal temperature. Therefore, based on the information of Laughlin (2012), it can be said that concrete produced by EAF slag fine aggregate should manifest lower thermal conductivity than that of concrete produced by natural sand.

Thermal conductivity of sand (2-4 W/m-K) is much higher than EAF slag (0.85-1.2 W/m-K) (Engineering toolbox, 2003, Barra et al., 2016). Therefore, similar analogy of Tokudu and Shoya (1972) for thermal diffusivity is applicable to thermal conductivity and the decrease in thermal conductivity with the increase in slag ratio is hereby justified. The behavior of thermal conductivity as shown in Figure 5-9 resembles the behavior of specific heat as shown in Figure 5-5 and clearly depicts the influence of balance of decreasing moisture content and increasing concrete density with slag ratio as discussed in the section related to specific heat.

In a nutshell, the above experimental results indicate a decrease in all thermal properties such as thermal expansion, thermal conductivity, thermal diffusivity and specific heat of spherical shaped EAF slag concrete in comparison to normal concrete. Lower thermal conductivity coupled with lower thermal expansion is desirable for concrete generally exposed to highly local rise in temperature, such as pavement used for vertical take-off of aircraft (Neville, 2010). In addition, lower thermal conductivity helps in reducing temperature rise of embedded steel in concrete in case of fire. In order to prepare concrete that can provide both lower thermal expansion and conductivity, lightweight aggregates are commonly used although their performance in resisting drying shrinkage of concrete is not satisfactory. The experimental result that concrete cast with spherical shaped EAF slag fine aggregate exhibits both lower thermal expansion and

conductivity along with lower drying shrinkage (Roy et al., 2018) opens up a new horizon in solving many structural problems.

5.4 Freezing and thawing resistance

5.4.1 Test procedure

In this section, freezing and thawing resistance of EAF slag concrete is examined to confirm the wider utilization possibility of EAF slag fine aggregates in concrete pavement. In order to examine the freezing and thawing resistance of EAF slag fine aggregate concrete, all cast specimens (Series 1, 2 and 2B as shown in Table 5-1) were put inside the freezing thawing chamber as per the arrangement shown in Figure 5-12 after a curing age of 28 days. The specimens were immersed in water in separate containers while the chamber was filled with brine solution which do not get frozen at lower temperature and thus can quickly control the container temperature.

Prior to the placement in the freezing thawing chamber, flexural frequency, size and weight of each of the specimens were recorded. The specimens were tested according to the freezing and thawing protocol as shown in Figure 5-13 based on JIS A 1148 (2010). Each freezing and thawing cycle was operated for 4 hours with a change in maximum and minimum temperature from +20°C to -20°C respectively. The change from freeze to thaw cycle and thaw to freeze cycle was done within 45mins while the specimens were retained in maximum and minimum temperature for 60mins and 30mins respectively. All the specimens were tested up to 300 freezing and thawing cycles.

At every 35 freezing thawing (FT) cycle, the specimens were brought out of the freezing thawing chamber and flexural frequency and mass of all the specimens were measured. For each specimen, the measurement of flexural frequency was taken on each side of the specimen by the device as shown in Figure 5-14 and an average value of all the four sides was reported. Based on the measured flexural frequency, relative dynamic modulus of elasticity (RDME) was measured by using Eq. 5.8 as described in ASTM C666/C (2015). After 300 freezing thawing cycle, a durability factor was also computed by Eq. 5.9 as per ASTM C666/C (2015) standard.

$$Relative\ dynamic\ modulus\ of\ elasticity, P_c(\%) = \frac{n_c^2}{n^2} \quad (5.8)$$

$$Durability\ factor, DF = \frac{P \times N}{M} \quad (5.9)$$

Where, c = No. of cycles, n_c = Flexural frequency after c cycles of freezing thawing test, n = Flexural frequency before freezing thawing test, P = Relative dynamic modulus of elasticity at the end of the test, N = No. of cycle completed by the specimen, M = No. of cycle intended for the experiment (300 for current study).

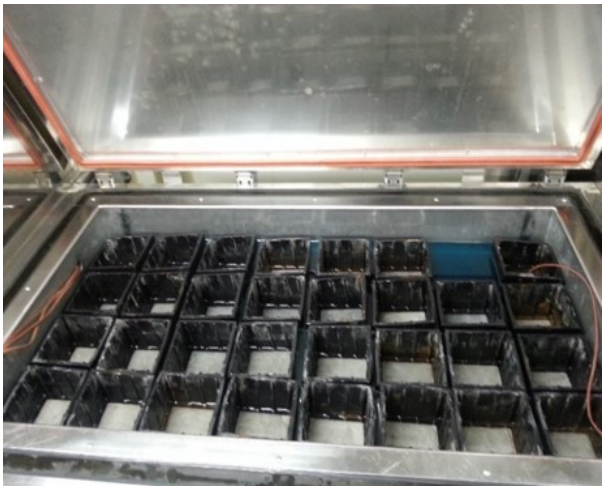

Figure 5-12 Specimen arrangement in freezing thawing chamber (Roy et al., 2019)

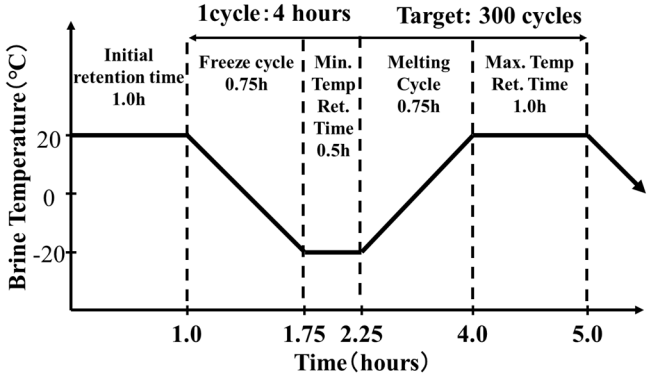

Figure 5-13 Freezing and thawing experimental protocol (Roy et al., 2019)

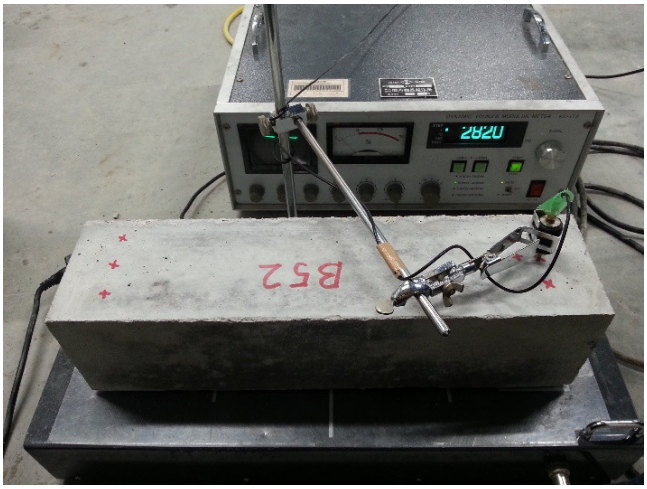

Figure 5-14 Measurement of flexural frequency (Roy et al., 2019)

5.4.2 Results of freezing and thawing test

The experimental results related to the freezing and thawing test are shown in Figure 5-15 and 5-16 for series 1, 2 and 2B respectively. It is evident from Figure 5-15 that both air entraining spherical and angular shaped EAF slag concrete show high freezing thawing resistance compared to normal concrete up to 200 freezing thawing cycles and RDME for all slag ratio cases with spherical and angular shaped EAF slag are more than 90%. In this region, the highest resistance is shown by the angular shaped EAF slag concrete having slag ratio 1.0, although the other results of spherical and angular shaped EAF slag concrete in this region are closer.

After 200 FT cycles, spherical shaped EAF slag concrete especially of slag ratio 1.0 starts deteriorating its resistance against freezing and thawing and this tendency is found to be continued up to 300 FT cycles. However, other slag ratio cases show higher freezing and thawing resistance up to 250 FT cycles and then starts to deteriorate. After 300 freezing thawing cycles, RDME of normal concrete is measured as 80% while that for spherical shaped EAF slag concrete with different slag ratio cases were within 60-65%. However, angular shaped EAF slag concrete with slag ratio 0.5 and 1.0 was found to have RDME values closer to 81 and 94% respectively.

The RDME of low air entrained concrete as shown in Figure 5-16 decreases rapidly with the increase in freezing thawing cycle. For all the low air entrained concrete

case, experiment was suspended before 300 FT cycles as the specimens degraded in such a manner that measurement of RDME was not possible. Low air entrained normal concrete shows poor resistance against freezing and thawing and degrades at only 135 cycles followed by spherical and angular shaped EAF slag low air entrained concrete having slag ratio of 1.0.

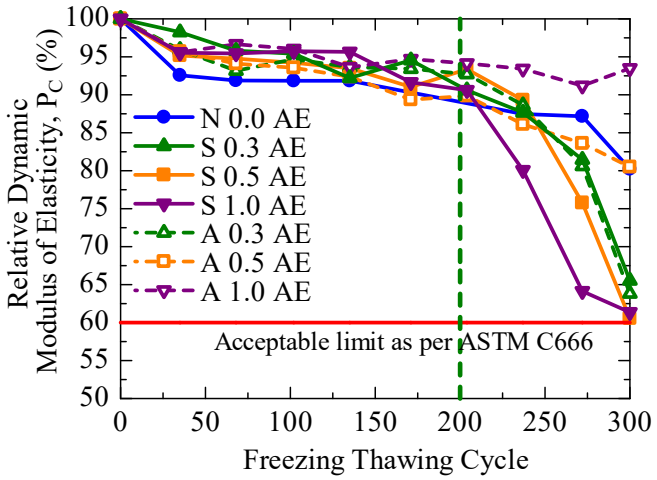

Figure 5-15 RDME of series 1 and 2 (AE concrete) (Roy et al., 2019)

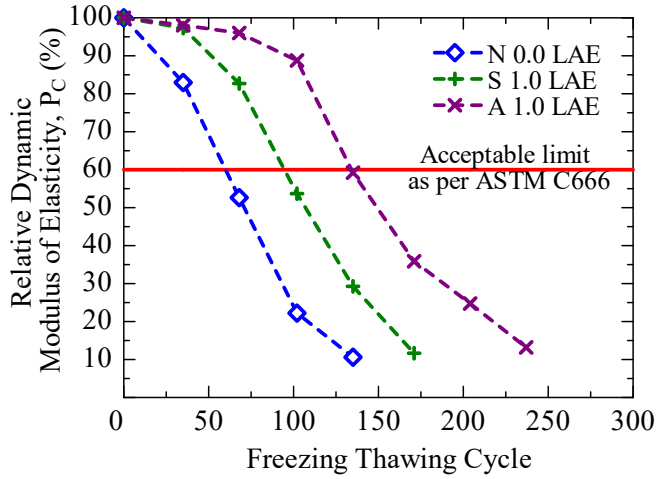

Figure 5-16 RDME of series 2B (low AE concrete) (Roy et al., 2019)

The durability factors (DF) for spherical and angular shaped EAF slag concrete with high and low air entrainment are shown in Figure 5-17. In fact, the index of good (DF≥ 80) and bad durability (DF ≤ 20) as used by Cordon et al. (1963) are also taken as

reference in this study. Figure 5-17 clearly indicates that angular slag with higher slag replacement ratio, especially greater than 0.5, pertains good durability. On the other hand, angular shaped EAF slag concrete having slag ratio of 0.3 and spherical shaped EAF slag concrete of all slag ratio cases show moderate durability. Low air entrained (~2%) concretes show bad durability irrespective of the type of slag and the durability factors were calculated in the range of 5-7% only. This result again establishes the fact that the dominating factor in case of freezing and thawing resistance of concrete lies in its air entrainment property.

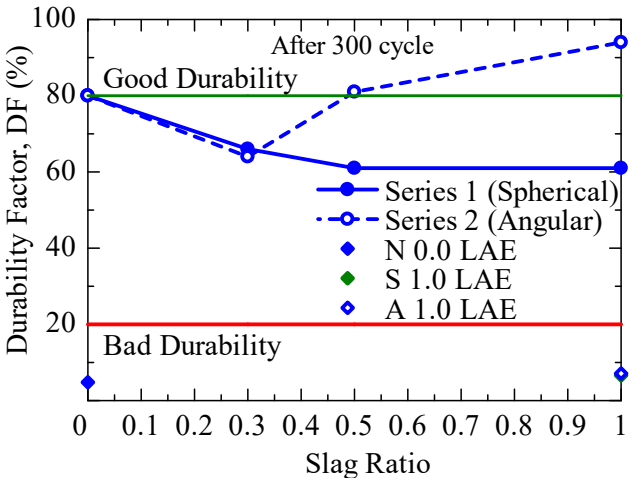

Figure 5-17 Durability factor with slag ratio (Roy et al., 2019)

5.4.3 Influence of type and shape of fine aggregate on freezing and thawing resistance of concrete

In summary of the results of freezing and thawing resistance of slag concrete it is confirmed that although spherical shaped EAF slag air entraining (AE) concrete shows good performance up to 200 freezing thawing cycles, however, from 200 cycles until the end of the experiment the values are much lesser in comparison to angular shaped EAF slag concrete. Since, air content of concrete plays a dominant role in resisting freezing and thawing action it is apparent from these results that the entrapped air content inside the specimen might have reduced after casting although it was within the target range (5%) at the time of casting. The materials might have a relatively poor air retention capacity in concrete due to their shape which triggered the degradation of freezing and

thawing resistance after 200 cycles. Based on this assumption, attempts were taken to investigate the air retention capacity of normal, spherical and angular shaped EAF slag concrete. In this test, air contents of normal concrete, spherical (slag ratio = 1.0) and angular (slag ratio = 1.0) shaped EAF slag concrete were measured immediately after casting. Subsequent readings of air contents were taken after each interval of rigorous concrete mixing. Figure 5-18 depicts the normalized air content of concrete with time. For each case, normalization is done by dividing all respective air contents by the initial air content of that batch.

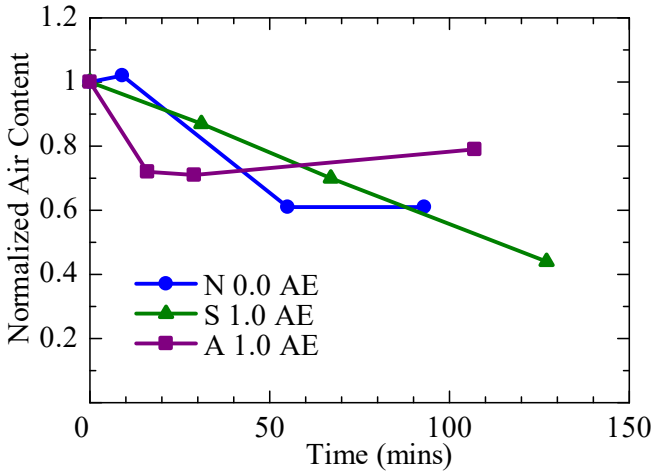

Figure 5-18 Normalized air content with time (Roy et al., 2019)

It can be seen from Figure 5-18 that, for normal and angular shaped EAF slag concrete, normalized air content reduces with time and becomes constant and no changes can be observed even after rigorous mixing. However, for spherical shaped EAF slag concrete the air content decreases linearly with time. This result clearly indicates the sensitivity of spherical shaped EAF slag against its air retention capacity in concrete. In addition, the result of porosity of spherical shaped EAF slag concrete as shown in Figure 5-10 also justifies the above finding as decrease in porosity is related to less number of interconnected pores in concrete because of lower air retention capacity of spherical shaped EAF slag concrete. Therefore, the assumption that the freezing and thawing resistance of spherical shaped EAF slag concrete gets reduced because of poor air retention capacity is justified. The problem of lower freezing and thawing resistance of

spherical shaped EAF slag concrete can be improved by increasing either the design air content without compromising the mechanical properties and/or, finer contents in the spherical slag mix.

In addition to these results, mass loss of the concrete subjected to freezing and thawing was computed by deducting the mass of each specimen after 300cycles from the initial mass. Figure 5-19 shows the mass loss of normal, spherical and angular shaped EAF slag concrete. As can be seen from Figure 5-19 that mass loss of angular shaped EAF slag air entraining concrete for all slag ratio and spherical shaped EAF slag concrete up to a slag ratio of 0.5 is found similar to normal concrete. However, for the slag ratio of 1.0, spherical shaped EAF slag concrete shows higher mass loss due to higher disintegration of specimen because of lower freezing and thawing resistance of such concrete.

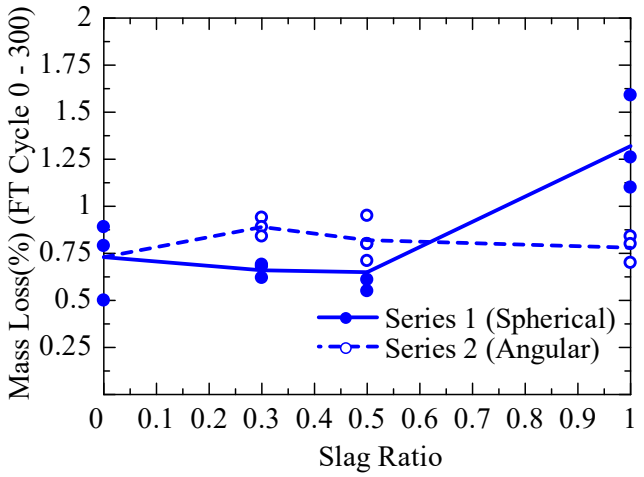

Figure 5-19 Mass loss due to freezing and thawing action (Roy et al., 2019)

5.5 Summary and conclusions

In this chapter, material stability and thermal properties including freezing and thawing resistance during thermal change of spherical and angular shaped EAF slag fine aggregate concrete were investigated for low W/C ratio and slump of 0.4 and 5cm respectively. Based on the experimental results, following conclusions can be drawn.

- Spherical shaped EAF slag fine aggregate concrete shows lower thermal expansion with the increase in slag ratio although that of angular shaped EAF slag concrete is similar to normal strength concrete. For the slag ratio of 1.0, the reduction of thermal expansion is 35% in comparison to normal concrete.
- Both spherical and angular shaped EAF slag concrete exhibits lower thermal conductivity, diffusivity and specific heat with the increase in slag ratio due to several factors such as density, moisture content and, relative mineralogical composition of slag and sand. For the slag ratio of 1.0 both type of concrete shows 33%, 25% and 20% reduction in thermal conductivity, diffusivity and specific heat respectively than normal concrete.
- Both spherical and angular shaped EAF slag concrete having air entrainment shows higher freezing and thawing resistance than normal concrete up to 200 freezing thawing cycles irrespective of slag ratio. After 200 cycles, the freezing and thawing resistance of angular shaped EAF slag concrete is found higher than that of normal and spherical shaped EAF slag concrete when the slag ratio is 0.5 or more. The mechanism of lower freezing and thawing resistance of spherical shaped EAF slag concrete was identified as lower air retention capacity of such concrete.
- Porosity of concrete produced by spherical shaped EAF slag fine aggregate decreases linearly with the increase in slag ratio, whereas, that of angular shaped EAF slag concrete is similar to slightly increasing than normal concrete. The reduction is 24% for the slag ratio of 1.0 in comparison to normal concrete. This result explains the behavior of spherical shaped EAF slag concrete in terms of lower water absorption, thermal expansion and freezing thawing resistance due to lower number of interconnected pores.

In conjunction with the results related to fresh, physical, mechanical and durability properties of slag concrete as described in chapter 3 and 4, current experimental study confirms that spherical shaped EAF slag fine aggregate is a promising alternative of natural sand in concrete of low W/C of 0.4 due to improved thermal behavior along with durability and construction economy. Lower drying shrinkage, lower thermal expansion in combination with lower thermal conductivity of spherical shaped EAF slag concrete opens up a new prospect for utilization of this material in cases where

susceptibility of fire is high. In the next chapter, effect of high temperature on the physical and mechanical properties of spherical shaped EAF slag fine aggregate concrete will be investigated for their wider applicability.

6 High temperature influence on concrete produced by spherical shaped EAF slag fine aggregates

6.1 Introduction

It has been discussed in chapter 4 and 5 that concrete produced by spherical shaped EAF slag fine aggregate at lower W/C pertains improved mechanical, durability and material stability during thermal change. Generally, concrete having higher mechanical properties coupled with lower thermal expansion and thermal conductivity is desirable for several reasons. Firstly, thermal cracking due to higher temperature gradient caused by fire (either natural or accidental) can be reduced and counter measured by using concrete of lower thermal expansion (Gajda, 2007). Secondly, in cases where local rise in temperature is very high such as pavement used for the vertical take-off of aircrafts (Neville, 2010), concrete having both lower thermal expansion and thermal conductivity imparts more resistance to thermal cracking by allowing higher temperature gradient (Gajda, 2007). Thirdly, lower thermal conductivity helps in reducing temperature rise in embedded steel when concrete is subjected to fire (Neville, 2010).

In order to ensure both lower thermal expansion and thermal conductivity, lightweight aggregates are generally used although their behavior in resisting drying shrinkage of concrete is not satisfactory (Hamad, 2014, Sherin and Jain, 2018). The problem of higher drying shrinkage can be counter measured by using limestone aggregates (Inoue et al., 2010, Maruyama et al., 2016) although mechanical properties of concrete produced by lime stone aggregates at high temperature exposure is not

satisfactory (Neville, 2010, Tufail et al., 2017, Kodur, 2014, Hager, 2013, Schneider, 1988, Hager et al., 2015).

It has been already reported that at lower W/C and slump, concrete produced by spherical shaped EAF slag fine aggregate exhibits improved mechanical properties along with lower drying shrinkage (chapter 4) as well as both lower thermal expansion and thermal conductivity (chapter 5). These features indicate that spherical shaped EAF slag fine aggregate can be a viable choice for concrete susceptible to high temperature exposure. In this context, this chapter investigates the influence of high temperature on the physical and mechanical properties of concrete produced by spherical shaped EAF slag fine aggregates and compare the results with angular shaped EAF slag concrete to understand the reduction mechanism.

6.2 Experimental outline

6.2.1 Experimental series, specimen notation and test condition

In this study, two different experimental series were undertaken to investigate the influence of high temperature on the physical and mechanical properties of concrete produced by spherical and angular shaped EAF slag fine aggregates. A summary of the experimental series along with specimen notation is listed in Table 6-1 which will be used in all the plots used in this chapter.

Table 6-1 Experimental series and specimen notation

Series	Slag Ratio	Slag Type	Heating Temp., T (°C)	Concrete Notation	Temp. Notation	Tests Conducted
1 (Spherical)	0.0	No slag	Room Temp. (RT) 200°C 500°C 800°C 1000°C	NC	NC-T	Compressive and flexural strength test of specimens subjected to high temperature
	0.3	Spherical		S 0.3	S 0.3-T	
	0.5	Spherical		S 0.5	S 0.5-T	
	1.0	Spherical		S 1.0	S 1.0-T	
2 (Angular)	0.3	Angular		A 0.3	A 0.3-T	
	0.5	Angular		A 0.5	A 0.5-T	
	1.0	Angular		A 1.0	A 1.0-T	

The experimental series 1 and 2 as shown in Table 5-1 are similar to that reported in chapter 3, 4, 5 and same mix proportions as shown in Table 3-1 were used for producing all the specimens of current study. It was confirmed from the studies as reported in chapter 3, 4 and 5 that spherical shaped EAF slag concrete exhibits improved mechanical and thermal properties than normal concrete when the W/C and slump is lower and hence suitable for concrete pavement. Now, in order to investigate the high temperature influence on the same concrete as reported earlier, similar water to cement (W/C) ratio of 0.4 and slump of 5.0cm ± 1.5cm was considered for the current study. Target for air content was also same as before as 5.0% ± 1.0%. However, it is fact that W/C does not influence the loss of physical and mechanical properties of concrete due to high temperature exposure (Arioz, 2007 and Hertz, 2005). Therefore, current study and experimental results are applicable for normal, spherical and angular shaped EAF slag fine aggregate concrete irrespective of W/C. As shown in Table 5-1, under series 1 and 2, a total of seven different types of concrete was produced by replacing natural sand with spherical and angular shaped EAF slag fine aggregates at a volume replacement ratio of 0.0, 0.3, 0.5 and 1.0 respectively.

6.2.2 Test overview and specimen details

All the specimens cast under series 1 and 2 (Table 6-1) were tested for physical properties such as mass loss, length change and mechanical properties such as compressive strength, flexural strength and tensile fracture energy after being heated at different temperature protocol starting from room temperature (RT) to 1000°C. Cylinders of Φ100x200mm sizes were used for the evaluation of length change and compressive strength; whereas, prisms of 100x100x400mm sizes were used for the case of flexural strength and tensile fracture energy. Mass loss was investigated by using both cylinder and prism specimens. For each slag ratio under each series, three representative specimens were used for each temperature state. All the cast specimens were cured under water for 28 days. Table 6-2 summarizes the conducted experiments, heating temperature, specimen type, size and numbers as considered in this study.

Table 6-2 Specimen details and test condition

Series	W/C	Name of test	Specimen type & size	Curing age (days)	Specimen per batch x test temp. type (5)	Total specimen
1	0.4	Length change	Cylinder Ø100x200	28	15	60
2	0.4					45
1	0.4	Compressive strength	Cylinder Ø100x200	28	15	60
2	0.4					45
1	0.4	Flexural strength	Prism 100x100x400	28	15	60
2	0.4					45
1	0.4	Mass loss	Cylinder & prism	28	30	120
2	0.4					90

6.3 Details of temperature protocol and heating condition

As reported in Table 6-2, all cast specimens were tested after being heated at different temperature state ranging from room temperature (RT) to 1000°C. The room temperature specimens are sound case and tested soon after removing from curing water whereas, other specimens were heated in the electric furnace for the designated temperature and tested 24 hours after being cooled down to room temperature. Prior to heating in the electric furnace, all specimens were preheated in the ordinary oven at a temperature of 105 ± 5°C for 24 hours to minimize the risk of explosive spalling due to high initial water content of concrete.

Figure 6-1 depicts the heating process while Figure 6-2 and Table 6-3 show the temperature-time relationship which was followed during the heating process. It is clear from Figure 6-2 that the heating condition comprises of three phases. In the first phase, a steady heating rate of 4°C/min was maintained until the specimens reach the target temperature. This consideration is in line with many reported studies (Khoury, 2000, Pan et al., 2018, Sun et al., 2019, Saha et al., 2019, Saha et al., 2018, Vickers et al., 2016, Liang et al., 2019] where a comparatively lower heating rate (≤ 5°C/min) was considered to minimize the thermal stress and damage of specimen caused by temperature difference between surface and core of the specimen. Secondly, a thermostatic or constant heat condition was kept for a minimum of 1 hour to ensure temperature equilibrium inside and outside the specimen. Finally, cooling of the specimens were carried out at a rate of

3°C/min until the specimens reach room temperature. Since, faster cooling accelerates the cracking and deterioration of concrete (Hager, 2013), a relatively lower cooling rate than heating was considered. It can also be noted from Table 6-3 that for all the specimens heated at 1000°C, a longer thermostatic condition of 2 hours was maintained. This is due to the higher target temperature and to confirm that the specimens can reach temperature equilibrium within this period. However, the temperature protocol was similar for all different types of concrete. As discussed earlier, tests for physical properties and mechanical properties were carried out 24 hours after cooling the specimens to room temperature.

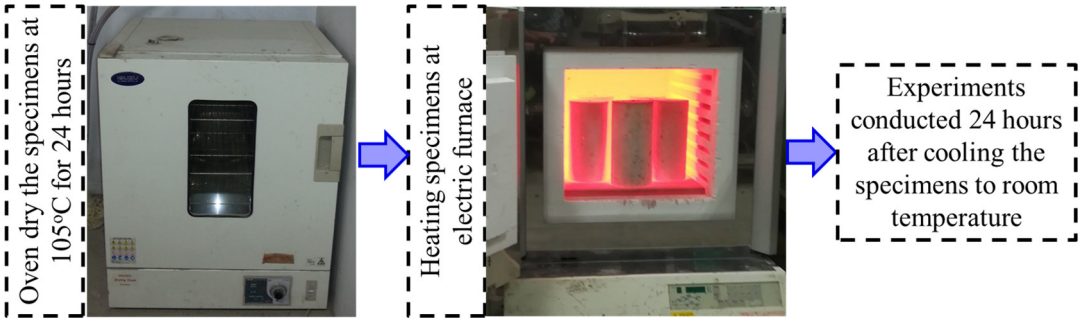

Figure 6-1 Heating process

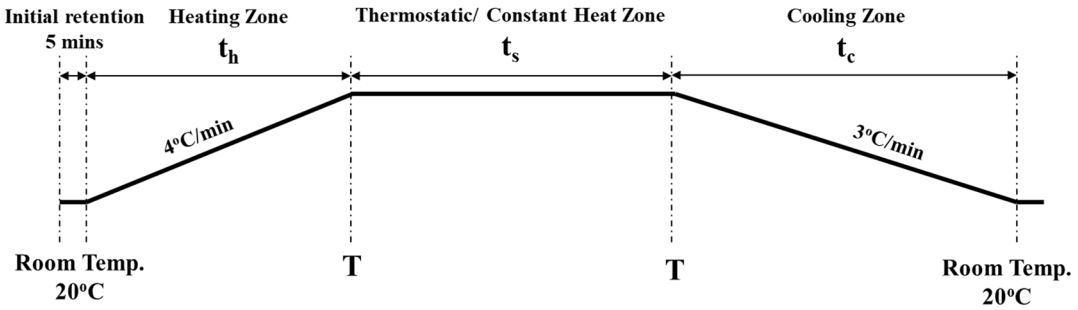

Figure 6-2 Temperature time relationship

Table 6-3 Temperature time parameters

T (°C)	t_h (mins)	t_s (mins)	t_c (mins)
200	45	60	60
500	120	60	160
800	195	60	260
1000	245	120	327

6.4 Physical properties

6.4.1 Visual observation of heated specimen

External views of the specimens (100x200mm) subjected to high temperature are depicted in Figure 6-3. For ease of understanding, observed surface cracks were marked by blue lines on the specimen. It is evident that surface cracks increase in both numbers and crack width with the increment of heating temperature irrespective of the type of concrete. However, patterns and extent of cracking show a clear difference between normal and EAF slag concrete. Until the temperature exposure of 200°C, no visible cracks were seen in any of the specimens whereas, fine cracks were observed in all types of specimen when the temperature exposure is 500°C. At this temperature state, maximum crack width (W_m) was measured as 0.05mm. At 500°C, fewer but longer cracks were seen for normal concrete whereas, for the case of spherical shaped EAF slag concrete many very small localized cracks were observed. For the case of angular shaped EAF slag concrete having slag ratio of 0.5 and 1.0, many smaller mesh like interconnected cracks were seen at this temperature.

When the heating temperature reaches 800°C, normal concrete shows similar tendency as of 500˚C with fewer but longer interconnected mesh like cracks. In contrary, both spherical and angular shaped EAF slag concrete shows many smaller mesh like cracks. Maximum crack width (Wm) was measured as 0.3mm for all types of concrete except for the case of spherical shaped EAF slag concrete having slag ratio of 1.0 (0.4mm). At the temperature exposure of 1000°C, crack patterns for normal concrete is similar to the former temperature case although crack width increases. However, for spherical and angular shaped EAF slag concrete more intense mesh like surface cracks were observed than normal concrete. Highest maximum crack width (Wm) was observed for S1.0 specimen (0.6mm) followed by NC (0.5mm) and A1.0 specimen (0.5mm). For other slag ratio cases, maximum crack width was measured as 0.4mm. Interestingly, no change in maximum crack width from the heating temperature of 800°C to 1000°C was observed for S0.5 specimen.

Therefore, it can be concluded that although the values of maximum crack width of slag concrete are closer to normal concrete, slag concrete exhibits more cracks and

higher damage in comparison to normal concrete when the heating temperature is very high.

Specimen ID	Room Temperature	200°C	500°C	800°C	1000°C
NC			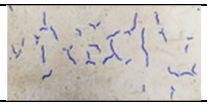	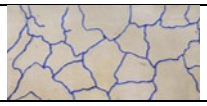	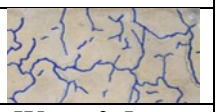
			W_m = 0.05	W_m = 0.3 mm	W_m = 0.5 mm
S 0.3			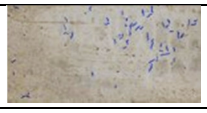	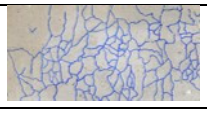	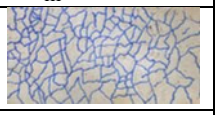
			W_m = 0.05	W_m = 0.3 mm	W_m = 0.4 mm
S 0.5		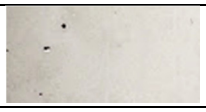	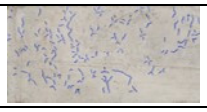	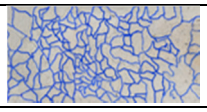	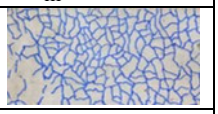
			W_m = 0.05	W_m = 0.3 mm	W_m = 0.3 mm
S 1.0			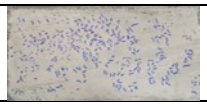	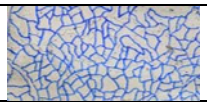	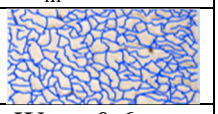
			W_m = 0.05	W_m = 0.4 mm	W_m = 0.6 mm
A 0.3	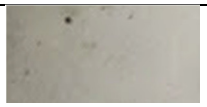	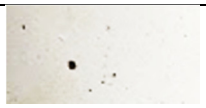	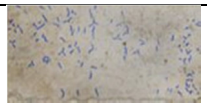	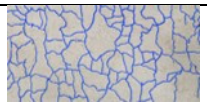	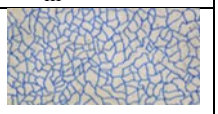
			W_m = 0.05	W_m = 0.3 mm	W_m = 0.4 mm
A 0.5				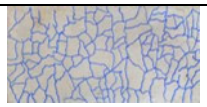	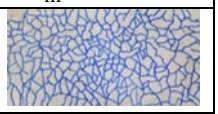
			W_m = 0.05	W_m = 0.3 mm	W_m = 0.4 mm
A 1.0			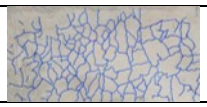	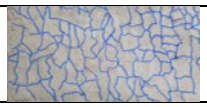	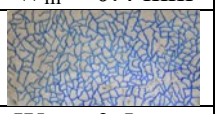
			W_m = 0.05	W_m = 0.3 mm	W_m = 0.5 mm

W_m = Maximum crack width (mm) measured by crack scale

Figure 6-3 Specimen condition at different heating temperature

The observed surface cracks especially for the case of EAF slag concrete at higher temperature resemble the shape of spider web and are similar to plastic shrinkage cracks. Generally, this type of cracks originate due to the evaporation of moisture from concrete as a result of quick drying. However, it is apparent that the influence of evaporation of free water is less in this study since all the specimens were preheated at 105°C for 24

hours at drying oven before they were subjected to high temperature exposure. The dominating factor might be the relative bond strength of mortar matrix and coarse aggregate. Generally, during the heating regime of 400°C-500°C, decomposition of $Ca(OH)_2$ happens, which removes the chemically bound water from the cement paste (Hager, 2013, Fernandes et al., 2017) and causes intense shrinkage of the paste. In contrary, coarse aggregates undergo thermal expansion at the same temperature. The differential thermal contraction of cement paste and expansion of coarse aggregate lead to cracking of concrete (Fernandes et al., 2017).

Now, the improved mechanical properties of EAF slag concrete at ambient temperature as discussed in chapter 4 indicate the fact that the bond strength of mortar matrix and coarse aggregate of slag concrete is higher than normal concrete. Higher bond strength might be associated with stronger particle resistance of slag. Thus, provides more resistance to shrinkage of cement paste during temperature rise and causes more surface cracks. The slightly different behavior of very fine localized crack for the case of spherical shaped EAF slag concrete at the heating temperature of 500°C might be due to their higher shrinkage resisting ability which improved the bond strength even further. Consequently, with the increase in heating temperature from 500°C to 1000°C, similar tendency continues and slag concrete shows more physical deterioration than normal concrete irrespective of slag type and slag ratio.

6.4.2 Mass loss

Influence of heating on the change in mass of concrete was investigated for all types of concrete under series 1 and 2 of Table 2. Mass loss was computed by using Eq. 6.1 which is nothing but the reduction of weight of specimen after being heated at designated temperature from the initial weight taken at SSD (saturated surface dry) condition.

$$Mass\ Loss, \Delta m\ (\%) = \frac{W_{SSD} - W_T}{W_{SSD}} \times 100 \qquad (6.1)$$

Where, W_{SSD} = Weight of specimen at saturated surface dry (SSD) condition and, W_T = Weight of specimen after being heated at designated temperature, T (20°C, 200°C, 500°C, 800°C, 1000°C).

The results of mass loss for normal, spherical and angular shaped EAF slag concrete at different slag replacement ratio are plotted against heating temperature in Figure 6-4. It can be seen from Figure 6-4 that normal concrete exhibits higher mass loss than spherical and angular shaped EAF slag concrete. At lower slag replacement ratio of 0.3, mass loss of angular shaped EAF slag concrete is similar to normal concrete, however, mass loss of concrete produced by spherical shaped EAF slag is much lesser and decreases with the increase in slag ratio.

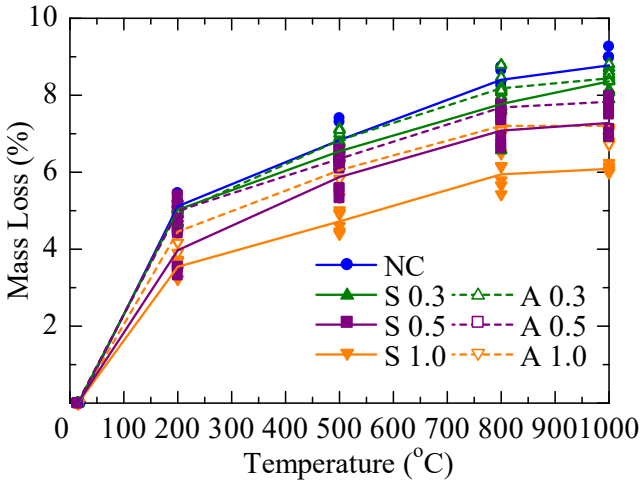

Figure 6-4 Mass loss with heating temperature

As shown in Figure 6-4, mass loss-temperature curves show initial steep slope up to a heating temperature of 200°C and the corresponding mass loss values at 200°C for all the concrete except spherical shaped slag concrete of slag ratio 0.5 and 1.0 are closer. This behavior clearly indicates the mass retention capacity of spherical shaped EAF slag concrete at higher temperature. The tendency is more distinct when the heating temperature is more than 200°C. The slope of the mass loss-temperature curves at the heating temperature of 200°C-800°C becomes flat and shows distinct differences between normal/angular and spherical shaped EAF slag concrete. At 800°C to 1000°C, those curves approach to more flat keeping similar difference in mass loss among different types of concrete as noted in the 500°C to 800°C heating range.

The above experimental results clearly indicate that physicochemical changes happen in concrete during heating. It has been discussed in several studies (Karahan, 2017, Ma et al., 2018, Hager, 2013, Saha et al., 2019, Ma et al., 2015, William et al., 2009) that

initial mass loss in concrete is rapid and happens due to the loss of both physically and chemically bound water. Here, physically bound water refers to the free water which is evaporable and not influenced by the Van der Waals attraction forces (Fernandes et al., 2017) and chemically bound water refers to those which are bounded by chemical reactions (such as C-S-H gel, CH etc.) and are not evaporable under normal circumstances (Zhang and Scherer, 2011).

At 20°C-200°C, along with the evaporation of physically bound water, dehydration of ettringite, decomposition of C-S-H gel happens in cement paste which releases more water and causes mass loss (Hager, 2013, Zhang and Scherer, 2011, Tantawy, 2017, Zhang, 2011). When the heating temperature ranges between 400°C-500°C, mass loss occurs mainly due to the decomposition of Portlandite (CH) (Hager, 2013). At the heating temperature of 800°C-1000°C, calcium carbonate decomposes and releases CO_2 which further causes mass loss (Hager). Based on this information it is clear that the slope of mass loss temperature curve is steeper at the lower heating temperature (200°C) due to the loss of both physically and chemically bound water. At higher heating temperature the slope becomes flat since mass loss happens only due to the chemical changes. Lee et al. (2008) reported similar findings that the slope of the mass loss-temperature curve becomes flat when the heating temperature is more than 200°C, which is similar to the findings of current study.

It is evident from Table 3-1 that spherical shaped EAF slag concrete requires less water and cement than normal and angular shaped EAF slag concrete. Due to the less water requirement along with lower water absorption of spherical shaped EAF slag concrete (Roy et al., 2018), amount of water in such concrete is lesser. In addition, due to the lesser cement content, formation of hydration products such as C-S-H, CH etc. in case of spherical shaped EAF slag concrete is expected to be lower. As a result, less amount of hydration product will be available for decomposition for the case of spherical shaped EAF slag concrete than normal concrete at higher temperature and lower will be the mass loss.

In order to verify this assumption, mass loss of series 1 and 2 is plotted in Figure 6-5 against volume of cement paste. Here, volume of cement paste indicates the sum of the volume of water and cement for each specimen under each slag ratio. For spherical shaped EAF slag concrete, clearly mass loss decreases linearly with the decrease in

volume of cement paste irrespective of the heating temperature. In contrary, mass loss of angular shaped EAF slag concrete is found to be decreasing for all heating temperature even though the volume of cement paste is slightly increasing with the increment of slag ratio. This behavior might be attributed to the combined influence of amount of cement paste and aggregates (sand and gravel) along with stronger mass loss retention ability of angular slag. It is fact that, decomposition of cement paste due to heating is the dominant factor for mass loss. However, for angular shaped EAF slag concrete, the increment of volume of cement paste is very small and such concrete possess lower sand and higher gravel content than normal concrete. Therefore, the influence of all these factors decreases the mass loss of angular shaped EAF slag concrete.

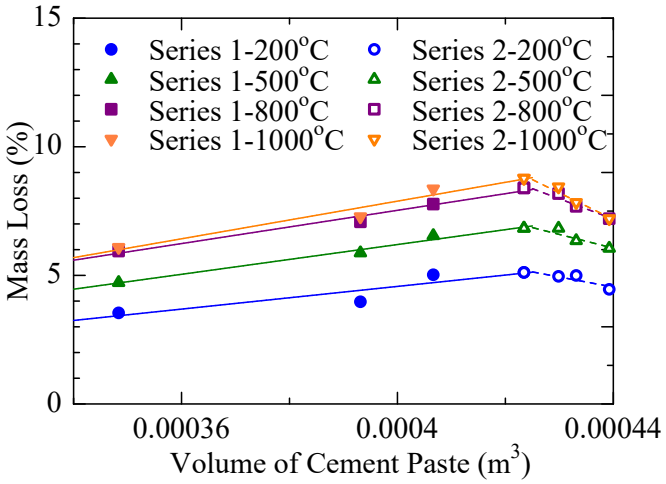

Figure 6-5 Mass loss with volume of cement paste

6.4.3 Length change

Concrete shrinks when it undergoes drying at ambient temperature and humidity. Numerous studies have been reported and models have been proposed on the drying shrinkage of concrete at normal temperature and humidity. Studies on the length change of concrete due to high temperature heating is equally important. In this study, concretes produced under series 1 and 2 (Table 6-1) were tested for length change after being heated at designated temperature (200°C, 500°C, 800°C and 1000°C). Figure 6-6 shows the experimental setup in which the length of the specimens were measured before and after heating. Length of the heated specimens were measured only after cooling them down to

room temperature. Length change was computed by using Eq. 6.2 and the results are plotted against heating temperature in Figure 6-7.

$$Length\ Change, \Delta L\ (\%) = \frac{L_T - L_i}{L_i} \times 100 \qquad (6.2)$$

where, L_i = Initial length of specimen before heating (mm) and, L_T = Length of specimen after heating at designated temperature, T (200°C, 500°C, 800°C, 1000°C) and cooled down to room temperature.

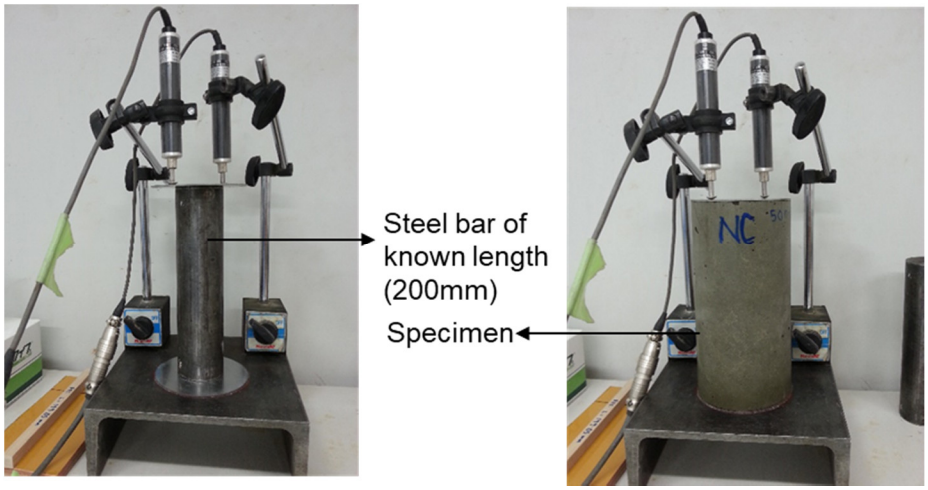

Figure 6-6 Measurement setup for length change

The experimental results show an initial shrinkage of specimens up to a heating temperature of 500°C for all types of concrete except that of spherical shaped EAF slag concrete of slag ratio 1.0. The values of shrinkage of different types of concrete at this temperature level are closer. When the heating temperature is 800°C, all concrete specimens exhibit expansion. Both spherical and angular shaped EAF slag concrete specimens show higher expansion than normal concrete. Specimens prepared by spherical shaped EAF slag concrete having slag ratio of 1.0 show lowest initial shrinkage up to a heating temperature of 200°C and starts to expand from 200°C to 1000°C.

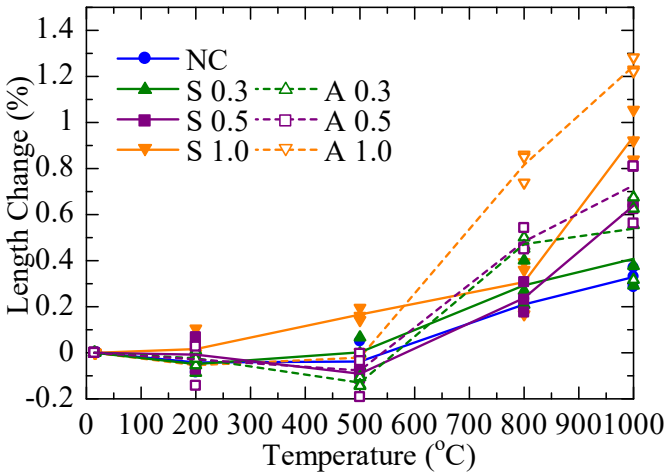

Figure 6-7 Length change with heating temperature

The shrinkage of concrete up to a heating temperature of 500°C might be due to the evaporation of free water and decomposition of C-S-H and CH as discussed in the previous section 6.4.2 related to mass loss. The improved shrinkage behavior of spherical shaped EAF slag concrete having slag ratio of 1.0 up to a heating temperature of 200°C might be attributed to the lower water requirement and stronger particle resistance of spherical slag against shrinkage similar to the case as discussed in chapter 4 for the shrinkage of such concrete at ambient temperature. The expansion behavior of concrete at higher temperature (>500°C) might depend on the extent of cracking.

It has been discussed by Ma et al. (2015) that at higher temperature, concrete starts to cracking due to the imbalance of decomposition of hydration products, shrinkage of cement matrix and expansion of coarse aggregates. Based on this reference, it is apparent that the dissimilar rate of shrinkage of cement paste and decomposition of hydration products at higher temperature (>500°C) causes more cracks in slag concrete which in turns increases the length of specimen. Visual inspection of specimen surface (section 6.4.1) already confirms more cracks in EAF slag concrete specimen than normal concrete during the heating exposure of 800°C-1000°C. Therefore, the result (as shown in Figure 6-7) that slag concrete shows higher expansion than normal concrete is reasonable.

6.5 Mechanical properties

Mechanical properties such as elastic modulus, compressive strength, flexural strength and tensile fracture energy of normal, spherical and angular shaped EAF slag concrete were investigated after keeping the specimens at different designated temperature exposure. Under each temperature category, 3 representative specimens were used from each slag ratio group and the change in mechanical properties with the change in slag ratio is discussed in detail in following subsections. In addition, residual strength (either compressive or bending) and Elastic Modulus were calculated by Eq. 6.3 and 6.4 respectively based on the results of room temperature specimen.

$$Residual\ Strength = \frac{Strength\ (compressive\ or\ bending)\ at\ temperature,\ T}{Strength\ (compressive\ or\ bending)\ at\ room\ temperature} \times 100 \quad (6.3)$$

$$Residual\ Elastic\ Modulus = \frac{Elastic\ Modulus\ at\ temperature,\ T}{Elastic\ Modulus\ at\ room\ temperature} \times 100 \quad (6.4)$$

Where, T = Heating temperature (200°C, 500°C, 800°C, 1000°C).

6.5.1 Compressive stress-strain relationship

Compressive stress-strain relationship including post peak behavior for all concrete under series 1 and 2 subjected to high temperature exposure is shown in Figure 6-8. Here, stress has been computed from the load data obtained by data logger and strain has been computed from the average displacement of 4 nos. of Load Varying Displacement Transducer (LVDT) placed around four sides of the specimen. Experimental results as depicted in Figure 6-8 do not show big scatter and the variation of highest and lowest strength under each particular slag replacement ratio and temperature case is less than 10%.

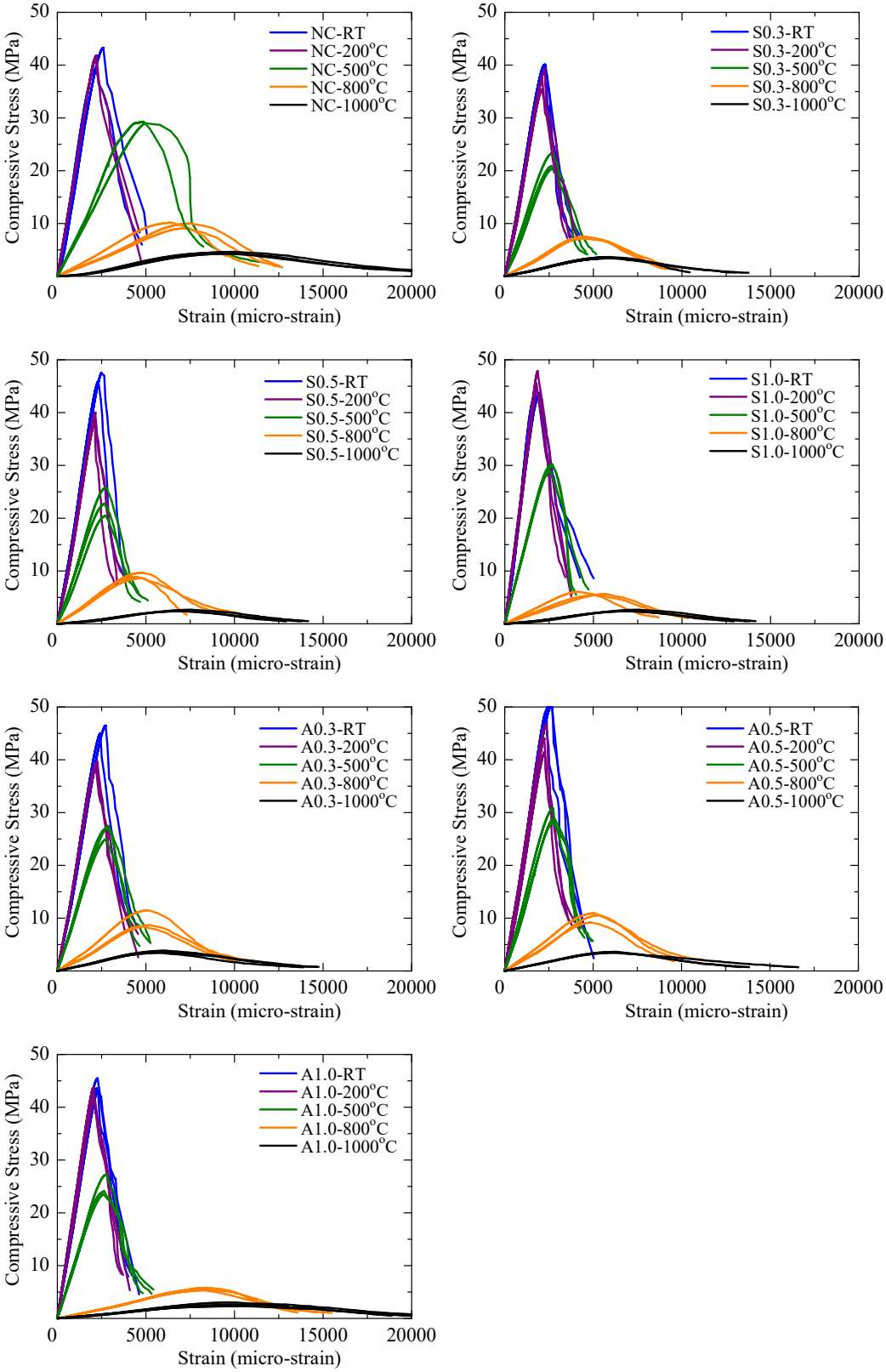

Figure 6-8 Compressive stress-strain relationship

Decrease in strength and stiffness along with the increase in peak strain is observed with the increase in heating temperature (especially when the heating exposure is more than 200°C) irrespective of slag type and slag replacement ratio. This is obvious due to the formation and extent of cracking in concrete specimen which increases with the increase in heating exposure. Up to a heating temperature of 200°C, stiffness and peak strain do not change significantly from that of room temperature case. This indicates that the elastic modulus of all types of concrete is somewhat constant to room temperature case up to a heating temperature of 200°C. The post peak part of the stress-strain curve of normal concrete at 200°C is comparatively flat than that of EAF slag concrete.

When the heating exposure is 500°C, distinct difference in stress-strain relationship between normal and EAF slag concrete can be observed since normal concrete shows higher reduction in stiffness along with higher peak strain in comparison to both spherical and angular shaped EAF slag concrete. At this temperature exposure, the post peak part of the stress-strain curve of EAF slag concrete is similar to that of 200°C case and the failure strain is also similar to that of the former heating exposure. However, normal concrete exhibits more flat post peak behavior with the increase in failure strain. At the heating exposure of 800°C and 1000°C both spherical and angular shaped EAF slag concrete manifests slight increase in peak strain than 500°C case although that of normal concrete is gradually larger. Moreover, the failure strain of normal concrete is much bigger than that of spherical and angular shaped EAF slag concrete.

6.5.2 Elastic modulus

Table 6-4 shows the average elastic modulus of normal, spherical and angular shaped EAF slag concrete subjected to different heating exposure. Elastic modulus was computed by determining the slope of the compressive stress-strain curve between points of longitudinal strain of 50 micro strain and strain corresponding to one third of the peak compressive stress. Residual elastic modulus as computed by Eq. 6.4 is plotted in Figure 6-9 against heating temperature.

Table 6-4 Elastic Modulus of concrete subjected to high temperature heating

Temperature (°C)	Average Elastic Modulus (GPa)						
		Spherical shaped EAF slag concrete			Angular shaped EAF slag concrete		
	NC	S 0.3	S 0.5	S 1.0	A0.3	A0.5	A1.0
16.6	20.5	17.7	17.8	23.4	17.7	19.5	20.4
200	19.2	16.5	17.0	24.8	17.4	18.3	20.9
500	6.9	9.0	8.8	13.1	10.3	10.8	10.4
800	1.5	1.7	2.1	1.4	1.9	2.1	0.7
1000	0.5	0.7	0.7	0.3	0.7	0.7	0.3

As shown in Table 6-4, elastic modulus of spherical shaped EAF slag concrete at room temperature is similar to normal concrete up to a slag replacement ratio of 0.5 and shows an increment when the slag ratio is 1.0. In case of angular shaped EAF slag concrete the behavior is similar to normal concrete. When the exposure temperature is 200°C, the behavior is similar to that of room temperature case which is already discussed in the previous section. At the heating temperature of 500°C, a reduction in elastic modulus from 200°C case is observed for all types concrete and the tendency of slag concrete is improved than normal concrete. When the heating temperature is very high such as 800°C and more, the values of elastic modulus for all types of concrete are very low and approaches to zero when the heating temperature is 1000°C.

In terms of residual elastic modulus as shown in Figure 6-9, up to a heating temperature of 200°C, both spherical and angular shaped EAF slag concrete shows improved performance than normal concrete. The reduction in elastic modulus for those cases due to heating is negligible in comparison to room temperature specimen. In addition, both spherical and angular shaped EAF slag concrete having slag ratio of 1.0 shows slightly improved elastic modulus than that of room temperature case. At 500°C, EAF slag concrete of all type exhibits higher residual elastic modulus than normal concrete and the remaining elastic modulus for those cases lies closer to the range of 55%±5%. Whereas, remaining elastic modulus of normal concrete at this temperature level is observed as 33%. Both spherical and angular shaped EAF slag concrete show

similar behavior at 500°C. At higher heating temperature such as 800°C and 1000°C, the remaining elastic modulus is found to be very low and in the range of 10% and 3% respectively. The experimental result of residual elastic modulus of normal concrete shows matching similarity to that of Euro code model (EN 1992-1-2) (2004) prediction. However, residual elastic modulus of slag concrete is much higher than the EN 1992-1-2 predicted elastic modulus.

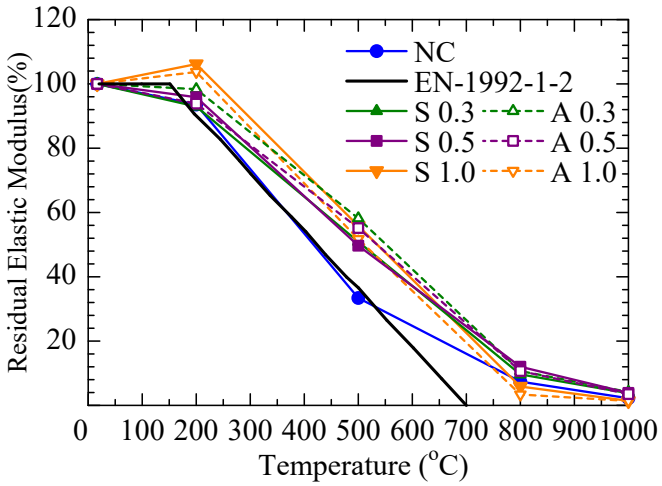

Figure 6-9 Residual elastic modulus with heating temperature

6.5.3 Compressive strength

Results related to the compressive strength of all concrete subjected to high temperature heating is listed in Table 6-5. Residual compressive strength is also computed by Eq. 6.3 based on the compressive strength of room temperature specimen. Figure 6-10 shows the residual compressive strength-heating temperature relationship.

It is evident from Table 6-5 that concrete produced by both spherical and angular shaped EAF slag indicate improved compressive strength at room temperature which is comparable to the previously reported findings (chapter 4). Up to a heating temperature of 200°C, slightly increasing tendency with the increase in slag ratio is observed for both spherical and angular shaped EAF slag concrete. In addition, no significant change in compressive strength in comparison to the room temperature case is observed at this temperature state. When the heating temperature is 500°C, all concrete shows lower compressive strength than 200°C heating case and tendency of EAF slag concrete is

similar to normal concrete. At 800°C, a larger reduction in compressive strength in comparison to 500°C case is observed and both spherical and angular shaped EAF slag concrete having slag ratio of 1.0 manifests slightly decreasing strength than those of other slag ratio cases. The compressive strength of all types of concrete heated at 1000°C were found to be similar and the values were recorded to be as small as less than 5MPa.

Table 6-5 Compressive strength of concrete subjected to high temperature heating

Temperature (°C)	Average compressive strength (MPa)						
		Spherical shaped EAF slag concrete			Angular shaped EAF slag concrete		
	NC	S 0.3	S 0.5	S 1.0	A0.3	A0.5	A1.0
16.6	41.3	39.6	44.6	44.1	44.9	48.9	44.3
200	41.6	37.3	39.1	45.9	39.2	44.0	42.4
500	27.7	22.2	23.0	29.6	26.5	29.2	24.9
800	9.7	7.3	9.1	5.7	9.5	10.2	5.5
1000	4.4	3.5	3.4	2.5	3.6	3.5	2.7

The residual compressive strength as shown in Figure 6-10 indicates similar decreasing behavior with the increase in heating temperature irrespective of slag type and slag ratio. At 200°C, spherical shaped EAF slag concrete having slag ratio of 1.0 and normal concrete shows improved tendency than room temperature case although a slightly decreasing behavior was observed for all other slag type and slag ratio cases. The residual strength of the former two cases at this temperature level is evaluated as 104%. When the heating temperature is 500°C, similar tendency as of 200°C case was observed. At this temperature state, residual compressive strength of spherical shaped EAF slag concrete having slag ratio of 1.0 and normal concrete was recorded as 67%. Other slag type and slag ratio cases show lower residual compressive strength in the range of 55±5%. Although the variation in between former and latter case is higher (12%), however, the variation among the other slag type and slag ratio cases are negligible. At higher temperature exposure of 800°C and 1000°C, superior performance of normal concrete over slag concrete was observed. The remaining strength of normal concrete at these temperature states is observed as 24% and 10% respectively whereas that of slag concrete is found as 15±5% and 6% respectively.

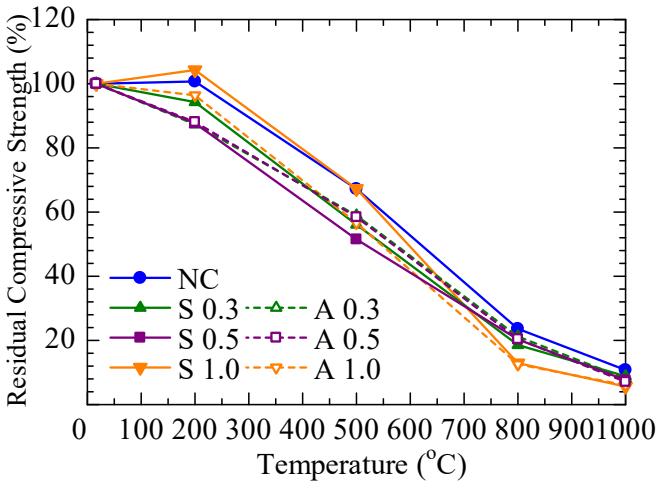

Figure 6-10 Residual compressive strength with heating temperature

Experimentally obtained residual compressive strength results for normal, spherical and angular shaped EAF slag concrete are compared with Eurocode 2: EN 1992-1-2- (2004), ACI 216.1-07 (2007) and ASCE Manual (1992) provided prediction models and the results are shown in Figure 6-11. It is evident from Figure 6-11 that ASCE model over predicts while ACI 216.1-07 model for both siliceous and carbonate aggregate concrete under predicts the experimental results of residual compressive strength of all types of concrete subjected to high temperature exposure. The experimental result of normal concrete as shown in Figure 6-11(a) lies in between the Euro Code 2 (EN-1992-1-2-Siliceous) prediction models for siliceous and carbonate aggregate concrete. However, the trend is comparable to EN-1992-1-2-Siliceous model prediction. Similar to normal concrete experimental results of both spherical and angular shaped EAF slag concrete (Figure 6-11(b) and Figure 6-11(c)) show matching similarity to the same prediction model.

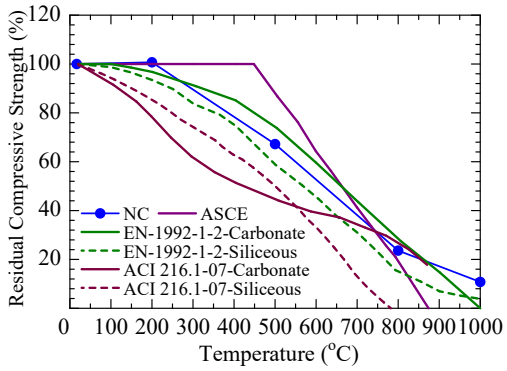

(a) Normal concrete

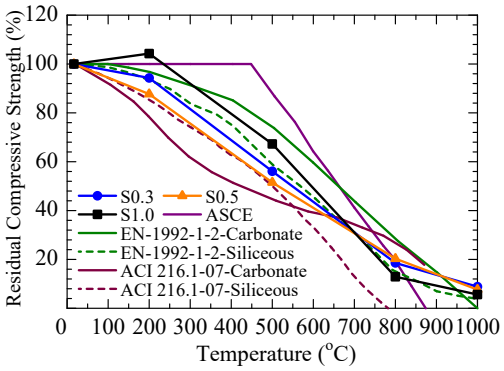

(b) Spherical shaped EAF slag concrete

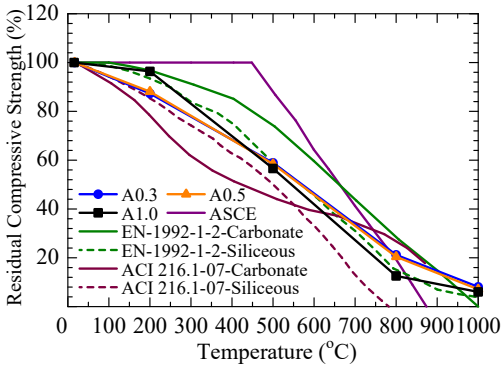

(c) Angular shaped EAF slag concrete

Figure 6-11 Experimental and predicted residual compressive strength

6.5.4 Compressive fracture energy

Compressive fracture energy (G_{fc}) of all concrete under series 1 and 2 subjected to high temperature exposure is computed from the stress-strain relationship (Figure 6-8) including post peak behavior by the method introduced by Nakamura and Hiagai (2001) as described in chapter 4 (section 4.3.3). Average compressive fracture energy (G_{fc}) for each slag ratio and heating temperature case is listed in Table 6-6. Based on the tabulated results, residual compressive fracture energy (G_{fc}) of slag concrete is computed by Eq. 6.5 and plotted in Figure 6-12 against slag ratio.

$$Residual\ Compressive\ Fracture\ Energy\ (\%) = \frac{Compressive\ fracture\ energy\ \ at\ temperature,\ T}{compressive\ fracture\ energy\ at\ room\ temperature} \quad (6.5)$$

Where, T = Heating temperature (200°C, 500°C, 800°C, 1000°C).

Table 6-6 Compressive fracture energy of concrete subjected to high temperature

Temperature (°C)	Average compressive fracture energy (MPa-mm)						
		Spherical shaped EAF slag concrete			Angular shaped EAF slag concrete		
	NC	S 0.3	S 0.5	S 1.0	A0.3	A0.5	A1.0
16.6	17.6	21.2	24.0	19.8	27.0	29.9	27.3
200	29.1	20.3	19.0	22.0	23.1	22.8	23.6
500	25.5	15.8	15.9	16.3	19.5	20.5	18.8
800	11.7	11.0	12.3	8.0	14.9	15.3	12.1
1000	9.4	6.7	6.4	4.7	8.2	8.0	8.5

It can be seen from Table 6-6 that at ambient temperature, compressive fracture energy (G_{fc}) of both spherical and angular shaped EAF slag concrete are higher than normal concrete which reconfirms the findings as reported in chapter 4 (section 4.3.3). When the heating temperature is 200°C, compressive fracture energy (G_{fc}) of normal and spherical shaped EAF slag concrete having slag ratio of 1.0 shows an increment from the room temperature case although all other slag ratio cases manifest decrease in fracture energy. This can be discussed from the compressive strength results and corresponding stress-strain relationship as shown in Table 6-5 and Figure 6-8 respectively. It is evident from Table 6-5 that when the heating temperature is 200°C, compressive strength decreases for all slag ratio cases except normal and spherical shaped EAF slag concrete of slag ratio 1.0. In addition, post peak regions of the stress-strain curve (Figure 6-8) are similar for all types of concrete. As a result comparatively higher compressive strength and similar post peak behavior attributes to higher compressive fracture energy (G_{fc}) for normal and spherical shaped EAF slag concrete of slag ratio 1.0.

When the heating temperature increases to 500°C, compressive fracture energy (G_{fc}) decreases for all types of concrete than that of former temperature case (200°C). However, normal concrete still exhibits higher compressive fracture energy (G_{fc}) than the room temperature case which can be correlated to the more flat post peak region of stress strain curve in comparison to the degree of reduction of compressive strength (Table 6-5)

as shown in Figure 6-8. At very high heating exposure such as 800°C and 1000°C, all types of concrete exhibit lower compressive fracture energy (G_{fc}) than the former heating temperature, of which spherical shaped EAF slag concrete shows the lowest followed by angular shaped EAF slag and normal concrete.

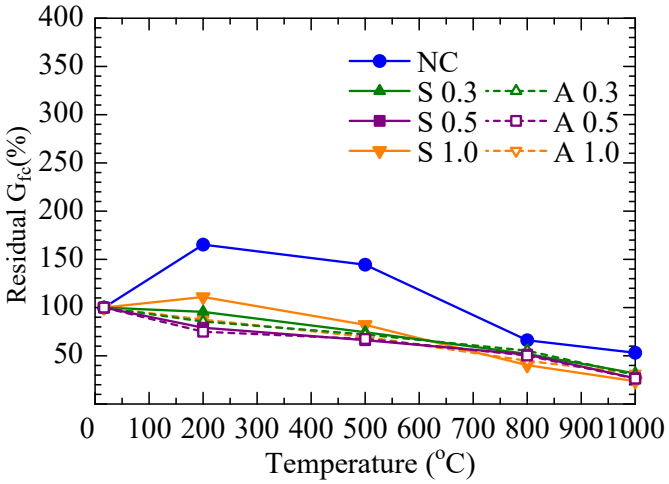

Figure 6-12 Residual compressive fracture energy with heating temperature

In terms of residual compressive fracture energy as shown in Figure 6-12, normal concrete exhibits superior performance than all other slag type irrespective of the heating temperature. Up to a heating temperature of 500°C, a higher residual compressive fracture energy of normal concrete is observed and the values are 165% and 145% for 200°C and 500°C respectively. When the heating temperature reaches 800°C and 1000°C, a reduction in residual compressive fracture energy is observed although the values are higher than both spherical and angular shaped EAF slag concrete. With the increase in heating temperature residual compressive fracture energy of EAF slag concrete decreases linearly irrespective of slag type and slag replacement ratio which is also clear from the stress-strain relationship (Figure 6-8) that with the gradual decrease in compressive strength, post peak regions remain straight in comparison to normal concrete.

In order to predict the compressive fracture energy (G_{fc}) of both spherical and angular shaped EAF slag concrete subjected to high temperature heating, attempt was taken to develop a relationship between compressive fracture energy (G_{fc}) and heating temperature (T). To formulate the relationship, obtained results of compressive fracture energy were normalized by square root of respective compressive strength in reference to

Nakamura and Higai (2001) as discussed in detail in chapter 4 (section 4.3.3). Furthermore, to identify the influence of heating, obtained normalized compressive fracture energy results of heated specimen were again normalized by that of room temperature specimen. The relationship is shown in Eq. 6.6. Figure 6-13 shows the relationship between η and heating temperature (T).

$$\eta = \frac{(\frac{G_{fc}}{\sqrt{f_c}})_T}{(\frac{G_{fc}}{\sqrt{f_c}})_{RT}} \tag{6.6}$$

Where, $(\frac{G_{fc}}{\sqrt{f_c}})_T$ is the normalized compressive fracture energy at different heating temperature, T (200°C, 500°C, 800°C, 1000°C) and $(\frac{G_{fc}}{\sqrt{f_c}})_{RT}$ is the normalized compressive fracture energy at room temperature (RT).

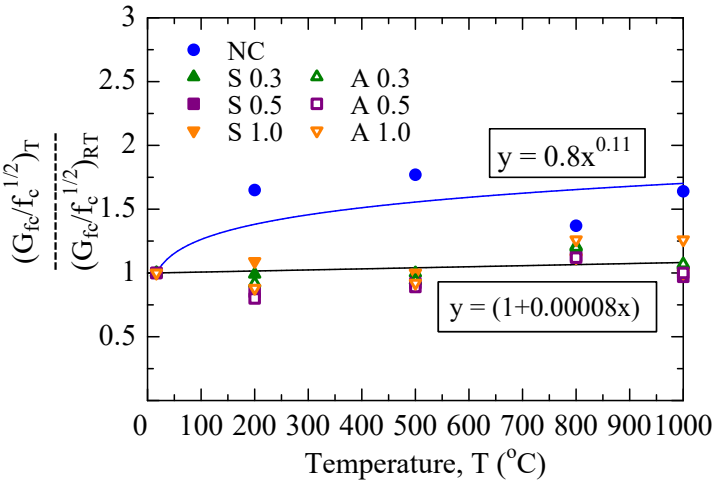

Figure 6-13 Relationship between η and heating temperature (T)

A clear distinguishing behavior of compressive fracture energy of normal and both spherical and angular shaped EAF slag fine aggregate concrete subjected to high temperature heating is evident from Figure 6-13. Normalized compressive fracture energy (η) of normal concrete increases in the form of power function with the increase in heating temperature (T) while that of both spherical and angular shaped EAF slag fine aggregate

concrete shows a linear trend. Difference in normalized compressive fracture energy due to the change in shape of EAF slag is not significant. Eq. 6.7 and 6.8 represents two simple experimentally obtained expression for normalized compressive fracture energy of normal and both spherical and angular shaped EAF slag fine aggregate concrete respectively which can be used for the prediction of compressive fracture energy of heated concrete produced by normal as well as both spherical and angular shaped EAF slag fine aggregates.

For Normal Concrete, $$\eta = 0.8T^{0.11} \quad (6.7)$$

For EAF slag Concrete, $$\eta = (1 + 0.00008T) \quad (6.8)$$

Where, T is the heating temperature (200°C, 500°C, 800°C, 1000°C).

6.5.5 Discussion on influence of particle shape on elastic modulus, compressive strength and compressive fracture energy of concrete

It is fact that the reduction in elastic modulus of concrete happens due to the decomposition of hydrated cement products and breakage of bonds because of excessive thermal stress caused by high temperature heating (Kodur, 2014). In so far as the reduction in compressive strength is concerned, several studies (Kodur, 2014, Khaliq and Kodur, 2012, Poon et al., 2001, Chen et al., 2004) figured out that concrete incorporating slag exhibits superior strength at ambient temperature due to the formation of denser microstructure although this denser microstructure turns out to be adverse when the same concrete is subjected to fire. The governing reason is that concrete having denser microstructure is highly impermeable and under high temperature it allows very little moisture to escape resulting in build-up of pore pressure and rapid development of micro cracks leading to faster deterioration of strength.

Apart from denser microstructure, bond behavior of concrete and transformation of cement paste due to heating as discussed in the sections related to visual inspection (section 6.4.1) and mass loss (section 6.4.2) play important role in the degradation of strength and elastic modulus of concrete. It has been already discussed that slag particles

form improved bond between cement matrix and coarse aggregate which impart stronger resistance during heating and causes more cracks. Moreover, spherical shaped EAF slag particles show higher resistance to drying shrinkage (Roy et al., 2018) and causes many micro cracks (as shown in Figure 6.3) when the specimens are heated at higher temperature (>500°C). In a nutshell, the degradation mechanism of strength and elastic modulus of slag concrete due to high temperature heating is attributed to the origination and extent of cracking because of the shrinkage and transformation of cement paste.

In order to investigate the origination and crack propagation in the deteriorated concrete specimen due to heating during compression loading, prism (100x100x200mm) specimens of normal concrete (NC), spherical and angular shaped EAF slag concrete of slag ratio 1.0 (S 1.0, A1.0 respectively) were tested for uniaxial compression by following the test procedure as described in section 4.3.4 to enable the analysis by digital image co-relation method (DICM). From each group one specimen was tested after being heated at a temperature of 500°C by following the same heating protocol used in this study (Figure 1 and 2 and Table 6-3) for other experiments.

Compressive stress-strain relationships for S1.0-RT, S1.0-500 and NC-500 specimens are depicted in Figure 6-14 along with corresponding stress level. Here, stress level corresponds to the ratio of stress at a particular strain to the peak stress. For each case, instantaneous tangential elastic modulus, which is nothing but the ratio of change in stress and strain of two adjacent points of the stress-strain curve has also been shown. Figure 6-15, 6-16 and 6-17, 6-18 depict the image analysis results in terms of maximum and minimum principal strain for S 1.0-500 and NC-500 cases at 0.1, 0.2, 0.3, 0.5, 0.7, 0.8, 1.0 stress level in the pre-peak region and 0.8 in the post-peak region corresponding to the stress levels as marked in the individual stress-strain curve in Figure 6-14. To compare the image analysis results of the damaged specimen, image analysis result of spherical shaped EAF slag concrete having slag ratio of 1.0 tested at room temperature condition (S1.0-RT) is also included in Figure 6-15 to 6-18 along with image analysis results of other cases. The scale for maximum and minimum principal strain has been taken as 0 to 3% and -3 to 0% for the former and later case respectively.

Figure 6-14 reconfirms the earlier described mechanical properties such as reduction in strength and stiffness and increase in peak strain of spherical shaped EAF slag and normal concrete subjected to high temperature. This figure will be used in

conjunction with Figure 6-15, 6-16 and 6-17, 6-18 to further discuss the cracking behavior of such concrete under uniaxial compression loading.

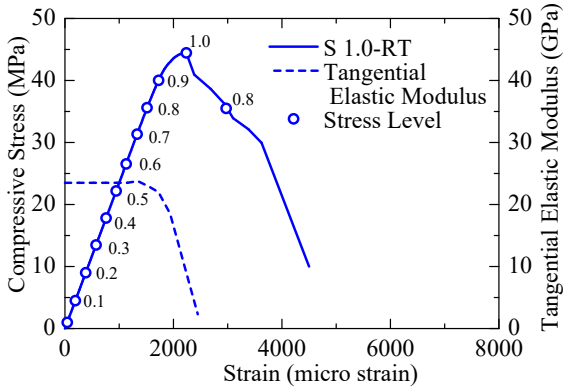

(a) S 1.0 –Room Temperature

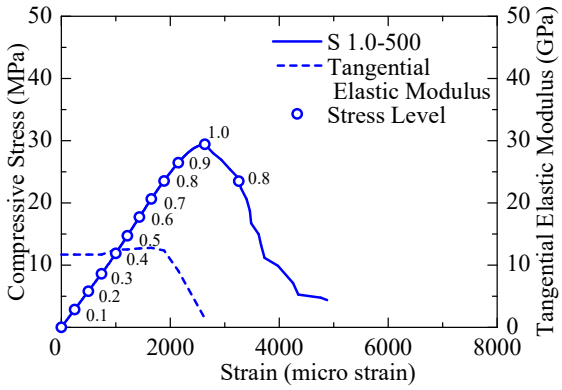

(b) S 1.0 - 500°C

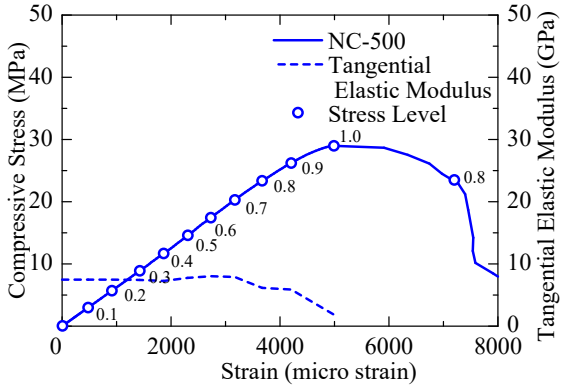

(c) Normal Concrete – 500°C

Figure 6-14 Compressive stress-strain relationship of specimens used for image analysis

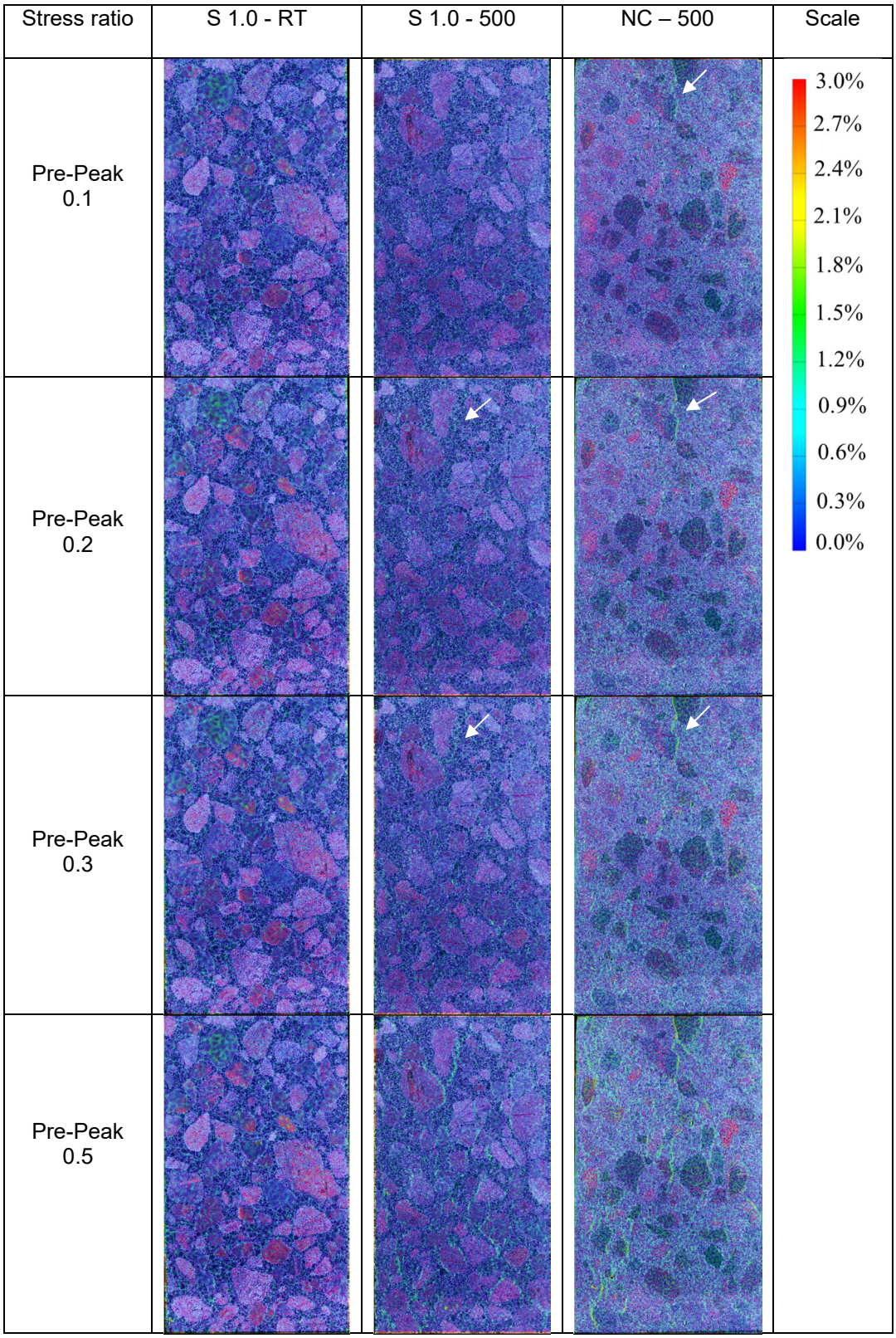

Figure 6-15 Maximum principal strain under uniaxial compression

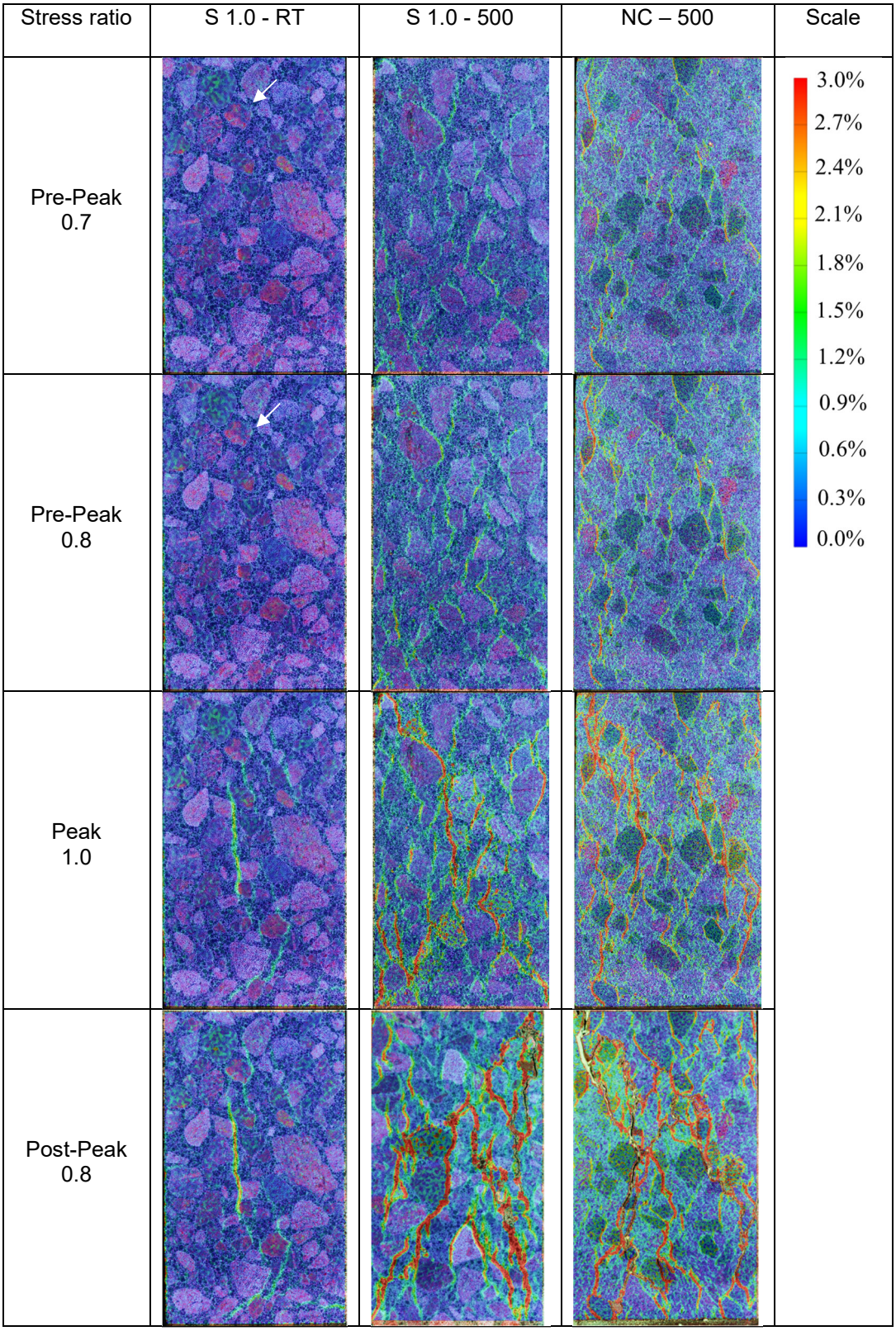

Figure 6-16 Maximum principal strain under uniaxial compression

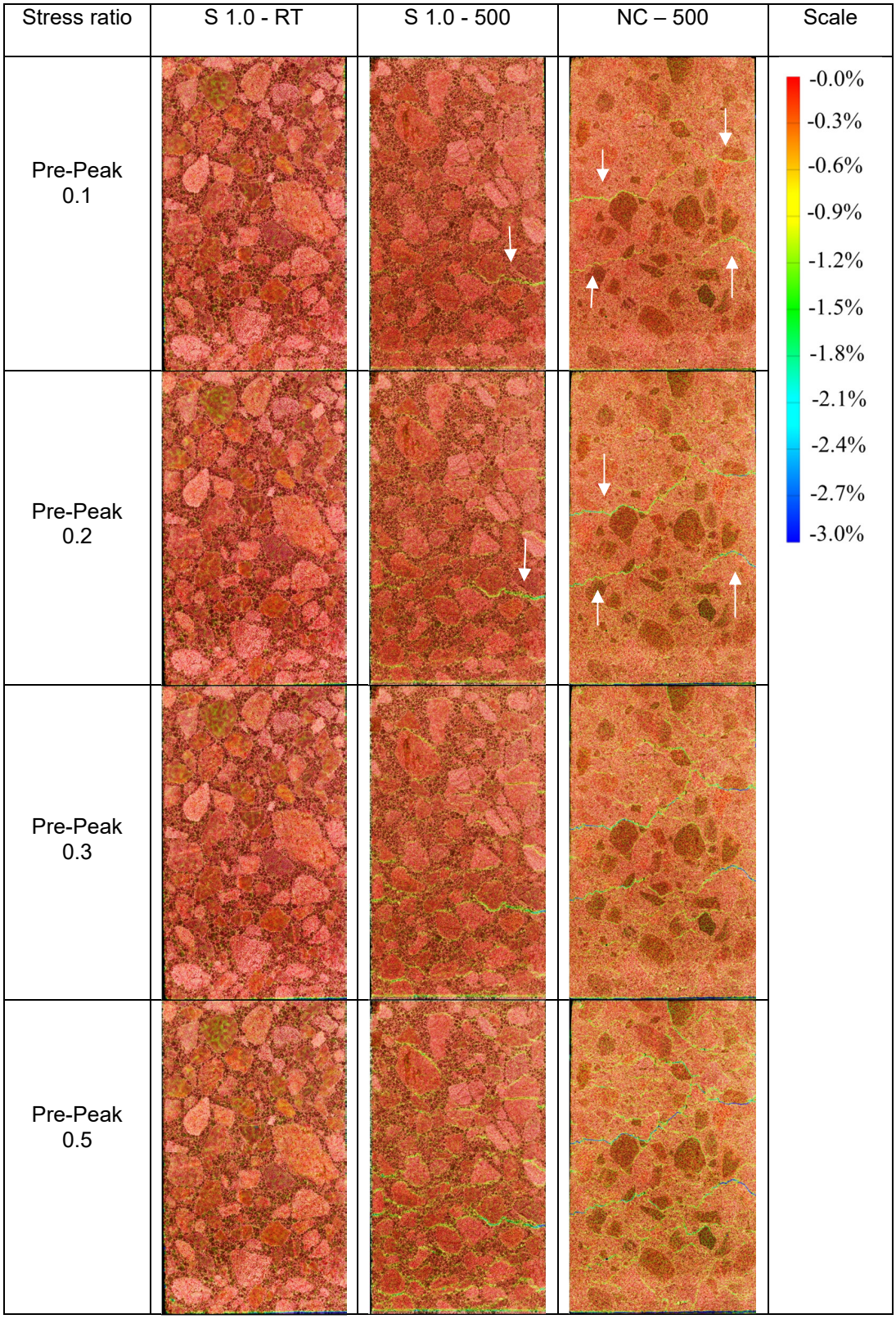

Figure 6-17 Minimum principal strain under uniaxial compression

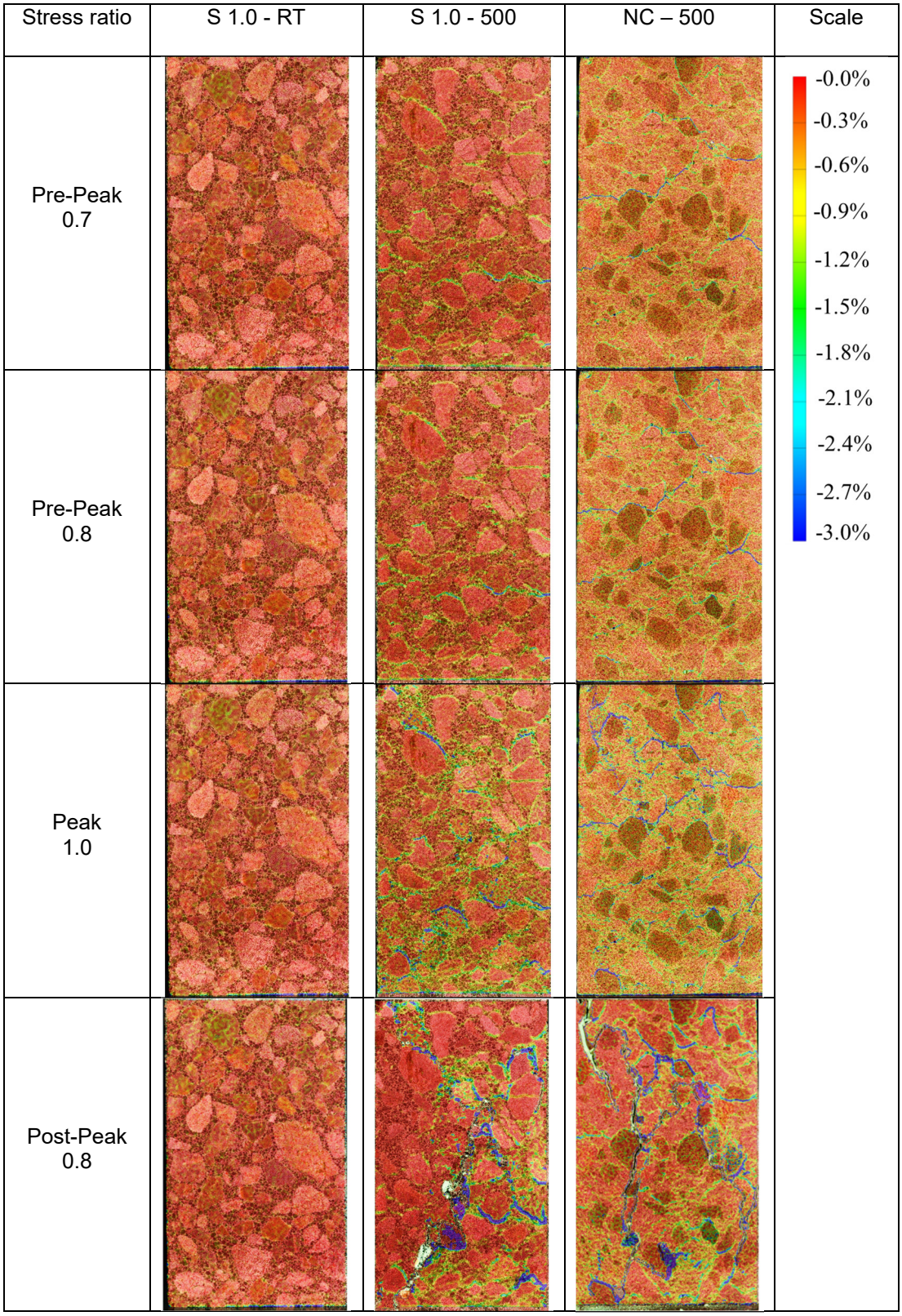

Figure 6-18 Minimum principal strain under uniaxial compression

Change in elastic modulus and compressive strength is related to the damage or cracking of concrete due to loading which can be monitored by assessing the maximum principal strain. It has been observed from the series of image analysis results that, for S1.0-RT specimen first visualized crack can be seen in between the stress level of (0.7-0.9) at the boundary of coarse aggregate and mortar matrix which is by the way the weakest part to be affected due to compression loading according to the weakest link theory (National Research Laboratory, KAIST). This is also evident from Figure 6-16 at the stress level of 0.8. Figure 6-14(a) supports the above finding that up to a stress level of 0.8, instantaneous tangential elastic modulus is similar to that of initial loading condition and decreases from the stress level of 0.8 onwards. At the stress level of 1.0, tangential elastic modulus quickly drops down which indicates the propagation of existing cracks and at the same time origination of new cracks. This behavior is confirmed from Figure 6-15 and 6-16 for S1.0-RT specimen. The higher compressive strength and corresponding lower peak strain of such concrete might be attributed to the origination of cracks at comparatively higher stress level and at the same time formation of lesser number of new cracks. At the post peak region (Stress level = 0.8), although existing crack widths increases however origination of new cracks are very few. This tendency indicates the chance of sudden failure of the specimen at comparatively lower failure strain which is identical to the finding as shown in the post peak behavior of the stress-strain curve in Figure 6-14(a).

Although the cracking behavior of concrete is attributed to the maximum principal strain at ambient condition (room temperature, normal loading) interestingly, the same behavior of concrete subjected to high temperature heating is related to the minimum principal strain. At the minimum principal strain, horizontal type closing cracks can be seen in between coarse aggregates and mortar matrix indicating the pre-damage of the specimen due to heating. This can be proved from the minimum principal strain (Figure 6-17 and 6-18) results of S 1.0-RT, S 1.0-500 and NC-500 specimens. It is evident from Figure 6-17 that the specimen tested at room temperature (S1.0-RT) does not show any crack although those tested after being heated at 500°C (S1.0-500 and NC-500) show closing cracks. This indicates that, cracks that originated because of heating are closing up due to compression loading. Of the two types of concrete, NC-500 specimen shows more closing cracks at the same stress level of 0.1 followed by S 1.0-500 specimen. This

result is similar to the visual inspection result (section 6.4.1) that normal concrete shows large number of cracks at 500°C and S1.0-500 specimen shows only very small and localized cracks. This behavior clearly describes the reduction mechanism of elastic modulus due to high temperature heating. Because of having larger number of closing cracks at the same stress level (Figure 6-17, stress level 0.3), normal concrete exhibits lower elastic modulus than spherical shaped EAF slag concrete having slag ratio of 1.0. For the same reason because of having no closing cracks or pre damage, S 1.0-RT specimen manifests much higher elastic modulus.

In so far as the maximum principal strain is concerned, visualized cracks are observed at the stress level of 0.0-0.1 and 0.1-0.3 for NC-500 and S 1.0-500 specimen respectively. The cracking behavior of the two types of concrete is similar which results in relatively similar compressive strength. Up to a stress level of 0.5, crack widths does not increase significantly although some new cracks are formed. This tendency clarifies the influence of compression closing cracks as discussed earlier by the results (Figure 6-17 and 6-18) of minimum principal strain. When the stress level reaches 0.7, many new cracks can be observed for both types of concrete which might be due to the fact that the cracks originated due to high temperature heating are completely closed due to compression loading up to a stress level of 0.7 and triggers the initiation of new cracks. The tangential elastic modulus as shown in Figure 6-14 (b) and Figure 6-14(c) supports this assumption as it starts to decrease from the stress level of 0.7 and drops until stress level of 1.0. The lower compressive strength and corresponding higher peak strain of S 1.0-500 and NC-500 specimen in comparison to S 1.0-RT specimen might be attributed to the pre-damage of specimen due to heating and early origination of cracks at very lower stress level as discussed before.

In comparison to S 1.0- 500 specimen, NC-500 specimen shows higher peak strain which can be discussed in light of Figure 6-14(b) and Figure 6-14(c). The tangential elastic modulus of S1.0-500 specimen decreases rapidly while that of NC-500 decreases gradually from the stress level of 0.7 to 1.0. This indicates sudden increase in crack width and number of cracks for S 1.0-500 specimen while for NC-500 specimen the increase is gradual and reaches more peak strain which is evident according to Figure 6-15 and 6-16. For the same reason, the post peak part of NC-500 specimen as depicted in Figure 6-14(c) is more flat in comparison to S 1.0-500 specimen (Figure 6-14(b)).

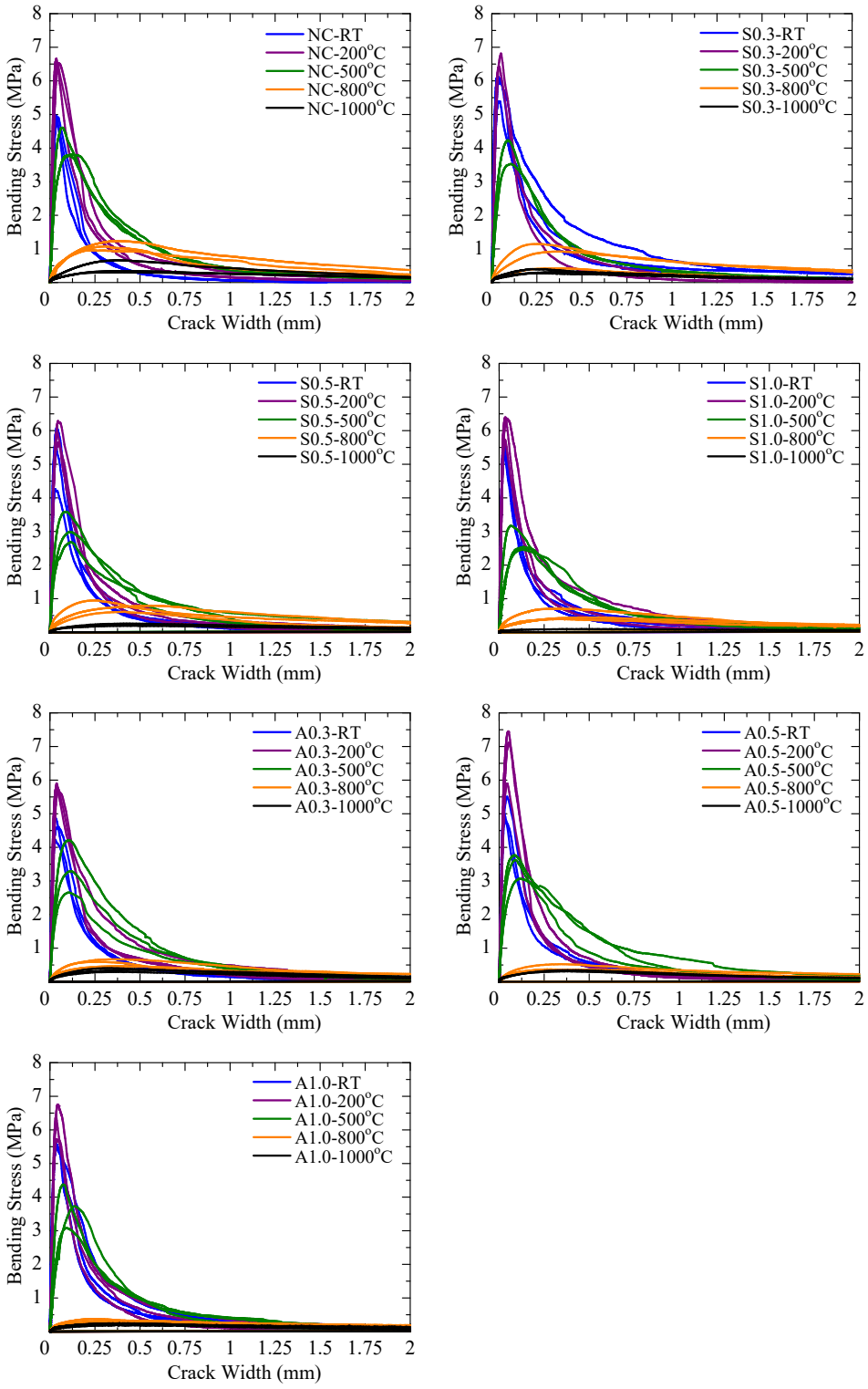

Figure 6-19 Bending stress-crack width relationship

6.5.6 Bending stress-crack width relationship

Figure 6-19 shows the bending stress-crack width relationship for different types of concrete subjected to high temperature exposure. Here, bending stress is measured by the three point bending test as described in ASTM C293 (2002). It is evident from Figure 6-19 that at a temperature exposure of 200°C, all types of concrete exhibit higher bending stress than the room temperature case. The tendency is more pronounced for the case of angular shaped EAF slag concrete having slag ratio of 0.5. The change in stiffness and crack width at peak bending stress does not show significant difference from that of room temperature specimen irrespective of slag type and slag ratio. At this temperature exposure, for the same bending stress, post peak behavior of all types of concrete is slightly improved and flat than the room temperature case.

When the heating temperature is 500°C, decrease in bending stress along with change in stiffness is observed for all types of concrete irrespective of slag type and slag replacement ratio. In addition, crack opening is found to be much higher under same bending stress in comparison to room temperature and 200°C heated specimen. At the temperature exposure of 800°C and 1000°C, initial stiffness of all types of concrete decreased significantly with lower flexural strength in association with larger crack opening.

6.5.7 Flexural strength

Flexural strength of different types of concrete produced by both spherical and angular shaped EAF slag fine aggregates was evaluated by three point bending test at room temperature and after heating the specimens at 200°C, 500°C, 800°C and 1000°C. Table 6-7 and Figure 6-20 includes the flexural strength results and residual flexural strength-heating temperature relationship respectively.

Initially, at room temperature, both spherical and angular shaped EAF slag concrete shows improved flexural strength than normal concrete which resembles to the earlier discussed findings (chapter 4). When the heating temperature is 200°C, tendency of flexural strength of spherical shaped EAF slag concrete is observed similar to normal concrete although that of angular shaped EAF slag concrete is found to be slightly higher especially for the slag replacement ratio of 0.5. At this temperature exposure, all slag ratio

cases show higher flexural strength than the room temperature case. When the heating exposure is 500°C, flexural strength of spherical shaped EAF slag concrete is decreasing with the increase in slag ratio although that of angular shaped EAF slag concrete is closer to normal concrete. The values of flexural strength at this temperature state for different types of concrete are lower than 200°C and room temperature case. At 800°C both spherical and angular shaped EAF slag concrete show lower flexural strength than normal concrete with higher reduction of flexural strength from the former temperature cases. When the heating temperature is very high such as 1000°C, all types of concrete indicate similar flexural strength and the values are found to be approaching to zero.

Table 6-7 Flexural strength of concrete subjected to high temperature heating

Temperature (°C)	Average Flexural Strength (MPa)						
		Spherical shaped EAF slag concrete			Angular shaped EAF slag concrete		
	NC	S 0.3	S 0.5	S 1.0	A0.3	A0.5	A1.0
16.3	4.91	5.30	5.85	5.51	4.57	5.10	5.50
200	6.56	5.99	5.96	6.16	5.79	6.82	6.28
500	4.07	3.29	3.08	2.72	3.38	3.48	3.72
800	1.09	0.88	0.78	0.51	0.58	0.42	0.34
1000	0.44	0.29	0.22	0.17	0.35	0.38	0.23

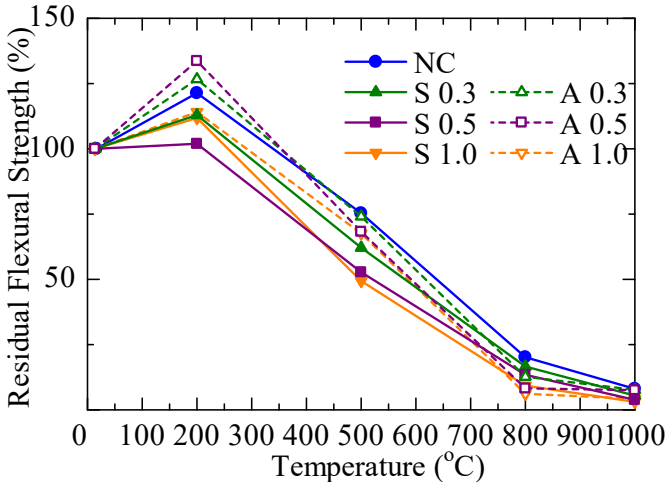

Figure 6-20 Residual flexural strength with heating temperature

In so far as the residual flexural strength of concrete is concerned, at 200°C all types of concrete manifests higher values in comparison to their respective room temperature specimen. Angular shaped EAF slag concrete especially of slag ratio of 0.3 and 0.5 shows improved behavior than normal and spherical shaped EAF slag concrete at this temperature. When the heating temperature is 500°C, the residual flexural strength of normal and all three types of angular shaped EAF slag concrete are closer and ranges within 72±3%. However, spherical shaped EAF slag concrete retains much lower of initial strength at this temperature exposure and the values are in the range of 55±7%. When the heating temperature is 800°C, clearly normal concrete possesses higher flexural strength retention ability than slag concrete and the corresponding value is 20%, which is approximately half for the case of slag concrete. At the temperature exposure of 1000°C, residual flexural strength of all types of concrete falls less than 10%.

6.5.8 Tensile fracture energy

Results related to the tensile fracture energy of all concrete under series 1 and 2 of Table 6-1 subjected to high temperature heating are listed in Table 6-8. Tensile fracture energy, G_{ft} (MPa-mm) was computed by the method as described in JCI-S-001-2003 using a three point bending test as reported in chapter 4. Residual tensile fracture energy is computed by Eq. 6.9.

$$Residual\ Tensile\ Fracture\ Energy\ (\%) = \frac{Tensile\ fracture\ energy\ at\ temperature,\ T}{Tensile\ fracture\ energy\ at\ room\ temperature} \quad (6.9)$$

Where, T = Heating temperature (200°C, 500°C, 800°C, 1000°C).

As shown in Table 6-8, both spherical and angular shaped EAF slag concrete exhibit improved tensile fracture energy than normal concrete at ambient condition. With the increase in heating exposure the tendency becomes similar to slightly decreasing than normal concrete. At a heating temperature of 800°C, tensile fracture energy of angular shaped EAF slag concrete is found to be clearly decreasing with the increase in slag ratio. Interesting to note that, the value of tensile fracture energy increases with the increase in heating temperature irrespective of the slag type and slag replacement ratio and remains

similar to the room temperature concrete even if the specimens are heated at a temperature of 1000°C.

Table 6-8 Tensile fracture energy of concrete subjected to high temperature heating

Temperature (°C)	Average Tensile Fracture Energy (MPa-mm)						
		Spherical shaped EAF slag concrete			Angular shaped EAF slag concrete		
	NC	S 0.3	S 0.5	S 1.0	A0.3	A0.5	A1.0
16.3	0.121	0.186	0.140	0.166	0.134	0.138	0.194
200	0.219	0.180	0.222	0.184	0.227	0.208	0.177
500	0.261	0.210	0.235	0.201	0.237	0.255	0.224
800	0.226	0.198	0.168	0.187	0.151	0.123	0.123
1000	0.155	0.099	0.108	0.115	0.123	0.138	0.109

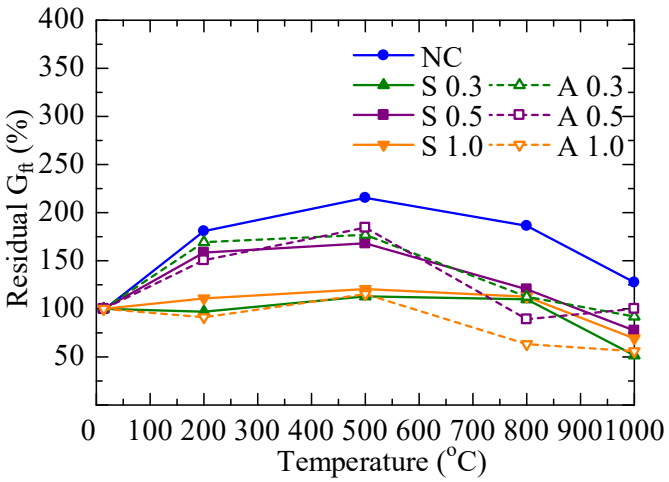

Figure 6-21 Residual tensile fracture energy with heating temperature

Residual tensile fracture energy as computed by Eq. 6.9 is plotted in Figure 6-21 against heating temperature. It is evident from the figure that the residual tensile fracture energy of normal concrete increases similar to a parabolic function with the increment of heating temperature. The tendency is similar to the compressive fracture energy of normal concrete as discussed in section 6.5.4. Highest residual tensile fracture energy of normal concrete is obtained at the heating temperature of 500°C, which reduces similar to the rate of increment when the heating temperature is 800°C and 1000°C respectively. At

1000°C the residual tensile fracture energy is measured 27% higher than concrete tested at room temperature. Angular shaped EAF slag concrete of slag ratio 0.3 and 0.5 and spherical shaped EAF slag concrete of slag ratio 0.5 exhibit similar tendency as of normal concrete although lower in values. Other concretes neither show increment nor decrease in tensile fracture energy with the increase in heating temperature. The above result comes up with an interesting finding that the residual tensile fracture energy of concrete increases with the increase in heating temperature which might be due to presence of micro cracks in the specimen formed during heating.

6.5.9 Discussion of flexural strength and tensile fracture energy

The reduction mechanism of flexural strength and tensile fracture energy of EAF slag concrete in comparison to normal concrete due to high temperature heating might be discussed in light of particle fragility characteristics. To understand the mechanism, bending failure surface of concrete casted using spherical shaped EAF slag was investigated. Figure 6-22 shows the bending surface of S 0.3 specimen tested at room temperature and after the temperature exposure of 500°C. It is apparent from the figure that the brittleness of slag particles have increased due to heating, which triggers the earlier reduction of tensile fracture energy and corresponding flexural failure of spherical shaped EAF slag concrete specimen than normal concrete specimen.

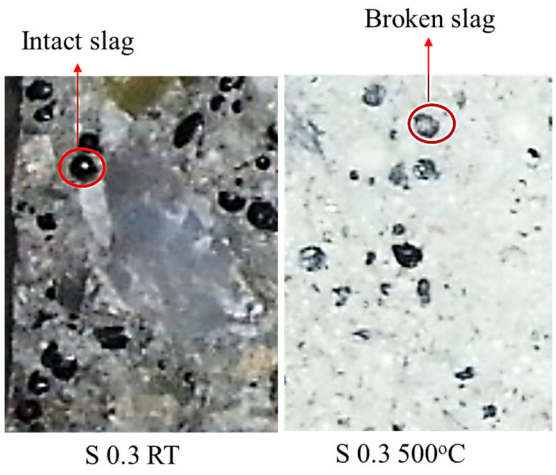

Figure 6-22 Bending failure surface of S 0.3 at RT and 500°C

In order to validate the above assumption, natural sand (NS), spherical (SS) and angular (AS) shaped EAF slag particles retained in three sieve sizes (S = 1.2mm, 0.6mm and 0.3mm sieve) were tested for impact at both room temperature (RT) and after being heated at 500°C and 800°C. All the heated materials were tested for impact after being cooled down to room temperature. Prior to impact test, each type of materials were sieved in the respective sieve (S) and the retained materials were placed in the container of 150mm diameter up to a height of 20 mm. Weight (W_i) of the materials stored in the container was recorded. For impact test, a hammer weighing 6 kg was dropped on to the stored materials 15 times from a free fall height of 300 mm. The materials were re-sieved after impact and weight (W_f) of the materials retained in the same sieve was recorded. Weight of the particles being broken due to impact is computed by deducting the final weight (W_f) from the initial weight (W_i). Table 6-9 shows the heating and impact factor for individual sieve size and heating temperature which is calculated by Eq. 6.10.

$$Heating\ and\ Impact\ Factor = \frac{weight\ of\ heated\ broken\ particles\ after\ impact}{weight\ of\ non\ heated\ broken\ paticles\ \ after\ impact} \times 100 \qquad (6.10)$$

Table 6-9 Heating and impact factor

Heating and Impact factor for particles retained in 1.2 mm sieve			
Temperature (°C)	Sand	Spherical Slag	Angular Slag
18	1.00	1.00	1.00
500	1.10	1.65	1.16
800	1.18	2.27	1.58
Heating and Impact factor for particles retained in 0.6 mm sieve			
Temperature (°C)	Sand	Spherical Slag	Angular Slag
18	1.00	1.00	1.00
500	1.15	1.76	1.15
800	1.45	1.84	1.79
Heating and Impact factor for particles retained in 0.3 mm sieve			
Temperature (°C)	Sand	Spherical Slag	Angular Slag
18	1.00	1.00	1.00
500	1.31	1.83	1.37
800	1.60	1.87	1.57

It can be seen from Table 6-9 that, for natural sand (NS), the influence of heating is more pronounced when the particle size is smaller such as 0.6 and 0.3mm, whereas, for

spherical slag (SS), the influence of heating is more intense and the rate of breaking of particles are more than normal sand (NS) or angular slag (AS). Important to note that, larger sized particles are more in spherical slag mix (Table 1) and such particles have been found to be more susceptible to heating and impact. In case of angular slag (AS), the effect of heating and impact is lesser than spherical slag and found to be more on the smaller sized particles only.

Above experimental result clarifies the fact that most of the spherical slag particles become fragile due to heating. Because of spherical shape, slag particles can be broken in only one direction under impact load due to fragility, while angular slag can be broken in several directions because of the shape. However, the weaker parts in the angular slag particles are comparatively lesser since they have already been eliminated during the production stage because of crushing of large slag lumps. This behavior triggers the quick reduction of flexural strength and tensile fracture energy of spherical shaped EAF slag concrete in comparison to angular shaped EAF slag concrete.

6.6 Summary and conclusions

In this chapter, high temperature response of spherical and angular shaped EAF slag fine aggregate concrete was investigated for the W/C and slump of 0.4 and 5cm respectively. Based on the experimental results, following conclusions can be drawn.

- Spherical shaped EAF slag concrete exhibits lower mass loss than normal and angular shaped EAF slag concrete.
- With the increase in heating temperature, both spherical and angular shaped EAF slag concrete show many smaller, interconnected surface cracks although normal concrete shows comparatively fewer and wider interconnected surface cracks. Higher length change (expansion) of slag concrete specimens at higher temperature (>500°C) confirms the presence of more internal cracks in slag concrete than normal concrete.
- Both spherical and angular shaped EAF slag concrete manifests improved elastic modulus and similar to slightly increasing compressive strength up to a heating temperature of 500°C. When the heating temperature is more, normal concrete performs better.

- The pre-damage of concrete due to heating was observed as horizontal type closing cracks during uniaxial compression by digital image co-relation (DIC) method. The reduction of elastic modulus and compressive strength of both normal and EAF slag fine aggregate concrete subjected to high temperature exposure was identified as the extent of compression closing cracks.
- Flexural strength of normal and angular shaped EAF slag concrete was found better than spherical shaped EAF slag concrete. The mechanism behind the behavior was identified as the fragility of spherical slag particles due to heating.
- Tensile fracture energy of normal concrete as well as slag concrete was found to be increasing with the increase in heating temperature although residual tensile fracture energy of normal concrete was found to be better followed by angular and spherical shaped EAF slag concrete.

In a nutshell, apart from lower mass loss, spherical shaped EAF slag concrete was found to exhibit improved elastic modulus and similar to slightly improved compressive strength in comparison to normal and angular shaped EAF slag concrete up to a heating temperature of 500°C. The finding of this study will improve the knowledge base for wider utilization of this material.

7 Water proofing performance of spherical shaped EAF slag concrete

7.1 Introduction

Apart from superior mechanical properties, spherical shaped EAF slag concrete showed improved durability properties such as lower drying shrinkage, water absorption and air permeability as reported in chapter 4. In addition, spherical shaped EAF slag concrete requires less mix water (chapter 3), entails lower porosity and pertains enhanced material stability (chapter 5) during thermal change in comparison to normal concrete. All these results indicate the higher application possibility of spherical shaped EAF slag in concrete. However, to improve the knowledge base and explore the wider applicability it is important to investigate the performance of such material in concrete at various experimental conditions such as static and dynamic repetitive loading.

It is fact that many structural concrete members i.e., pavement concrete, bridge deck, pier, wind turbine etc. subjected to repetitive loading exhibit failure at much lower stress level than that of ultimate compressive strength of corresponding concrete. Moreover, studies on the combined effect of fatigue and water is important because the deterioration of deck slab is strongly influenced by water and demand of construction of wind turbine on the sea is increasing. The deterioration of concrete due to fatigue happens because of the rapid propagation of micro cracks that initiate at the boundary of coarse aggregates and cementitious matrix. The effect is much pronounced when the same concrete is submerged in water due to several reasons such as porosity and pore structure, lower surface energy, accelerated crack propagation due to pumping action under cyclic

loading etc. As mentioned before, spherical shaped EAF slag concrete demonstrates much lower water absorption (section 4.4.2) along with lower porosity (Figure 5-10) than normal concrete. As a result, possibility of obtaining superior static and fatigue behavior of such concrete under water is high. In this context, this study aims to investigate the water proofing performance of spherical shaped EAF slag concrete subjected to repetitive loading at static condition in both air and water and different levels of dynamic fatigue loading under water.

7.2 Experimental outline

7.2.1 Test plan and specimen notation

To facilitate the purpose of investigating the water proofing performance of both normal and spherical shaped EAF slag concrete, two separate test plans were targeted. First target was to test the concrete specimen in dry and submerged condition under uniaxial static compression while second target was to test all concrete specimens for dynamic fatigue behavior at different stress levels by keeping them submerged in water.

For each of the test plans as mentioned above, three different types of concrete specimen were produced by replacing natural sand with spherical shaped EAF slag at a volume replacement ratio of 0.0, 0.3 and 0.5. The selection of those slag replacement ratios were made based on the experimental results of water absorption of such concrete as shown in Figure 4-30 that up to a slag replacement ratio of 0.5, for the curing age of 28 days spherical shaped EAF slag concrete manifests decrease in water absorption which slightly increases when the slag replacement ratio is 1.0. Table 7-1 shows the test plan and specimen notation which will be used for all the plots of this chapter.

Table 7-1 Test plan and specimen notation

Test Type	Slag Ratio	Slag Type	Test condition	Notation
Static Compression	0.0	No slag	Dry & Wet	N 0.0 S
	0.3	Spherical		S 0.3 S
	0.5	Spherical		S 0.5 S
Dynamic Fatigue	0.0	No slag	Wet	N 0.0 F
	0.3	Spherical		S 0.3 F
	0.5	Spherical		S 0.5 F

7.2.2 Specimen details, experimental parameters and mix proportions

For static compression test at dry and wet condition, three representative cylindrical specimens of Ø100x200mm sizes were used for each slag replacement ratio. However, for the case of dynamic fatigue test under water, a relatively smaller sized specimens (Ø60x120mm) than that of static condition were used because of the limitation of testing machine. However, it is apparent that the influence of different size of specimen on the fatigue behavior of concrete is negligible since dynamic tests were conducted based on the stress level of static compressive strength.

In order to cast the specimens as discussed above, a relatively higher water to cement ratio of 0.6 was considered to obtain concrete of comparatively lower compressive strength due to the limited loading capacity (maximum load = 100 kN) of the dynamic fatigue testing machine. For the same reason, smaller sized specimens were chosen as discussed above. Mix proportions as listed in Table 7-2 were used for the concreting of different types of specimens. Prior to testing, all specimens were cured under water for 28 days.

Table 7-2 Mix proportions of concrete

Slag Ratio	Slag Type	W/C	Water (kg/m^3)	Cement (kg/m^3)	Gravel (kg/m^3)	Sand (kg/m^3)	Slag (kg/m^3)	AE Admixture (kg/m^3)
0.0	No slag	0.6	156	261	1045	789	0	2.61
0.3	Spherical		151	252	1047	565	332	2.52
0.5			146	244	1057	407	559	2.44

7.2.3 Conducted tests and testing condition

Both static and fatigue tests under uniaxial compression loading were conducted by using the respective concrete specimens as discussed in the previous section after a curing age of 28 days. For the former case, tests were conducted in both drying and submerged condition while for the latter case specimens were tested only in submerged condition. Prior to any test in water, all respective specimens were kept submerged for at least 48 hours in water so that the specimens can reach uniform and complete saturation. Similarly, specimens to be tested in drying condition were kept in air for at least 3 hours

before testing to ensure equal drying of different types of concrete specimen produced by spherical shaped EAF slag fine aggregates at different slag replacement ratio.

The static compression test in air was conducted by the same method as discussed in chapter 4 (section 4.3.1). For the compression test in water, specimens (Ø 100x200mm) were kept inside a slightly larger (Ø150x180mm) cylindrical shaped container in submerged condition. Figure 7-1 shows the comparison of static compression test condition in air and in water. The compression loading was maintained at a speed of 0.5 kN/s and the readings of load and displacement data were recorded by data logger. Each of the specimens either in air or in water were tested for multiple loading unloading cycles prior to failure similar to the method as discussed in section 4.3.3 to quantify the compressive fracture behavior of normal as well as spherical shaped EAF slag fine aggregate concrete under water.

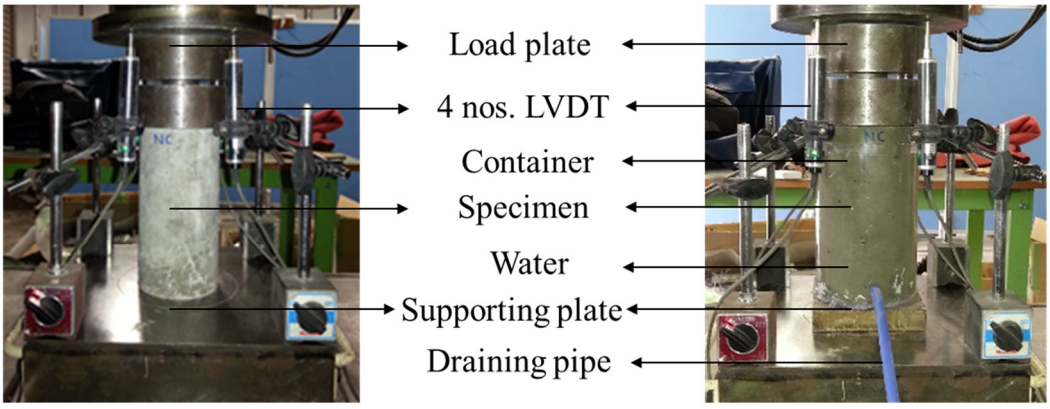

Figure 7-1 Comparison of static compression test condition

The fatigue test in compression was performed by using a relatively smaller sized specimen (Ø 60x120mm) than static test in hydraulically operated dynamic testing machine with a maximum load capacity of 100 kN. Similar to the static test condition in water, an artificial water pool was created around the supporting plate of fatigue testing machine to ensure that the specimens can be tested under water. Detail test conditions are depicted in Figure 7-2. In order to measure the displacement of the specimen, 02 nos. of load varying displacement transducers (LVDT) were placed in the diagonal direction of the supporting plate. Prior to test, diameter and length of each of the specimens were

measured. Strain was computed as the ratio of average transducer displacement and specimen length.

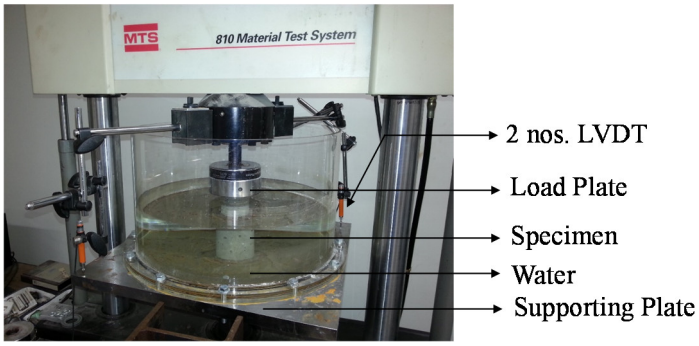

Figure 7-2 Dynamic fatigue test condition

During the fatigue test, three different maximum stress levels such as 60%, 70% and 80% were considered. For all those cases, minimum stress level was considered as 10%. Here, maximum and minimum stress levels correspond to the percentage of compressive strength of respective concrete at static dry condition. In actual design of concrete structures subjected to repetitive loading, fatigue strength of concrete is computed on the basis of concrete compressive strength at static dry condition. Based on this criteria, maximum and minimum stress levels were fixed in this study by considering the concrete compressive strength results of static dry condition. Maximum (S_{max}) and minimum (S_{min}) stress ratios are expressed by Eq. 7.1 and 7.2. For each specimen, under each slag replacement ratio fatigue test was discontinued until the failure of specimen or 2 million cycles whichever comes first.

$$S_{max} = \frac{\sigma_{max}}{f_c'} \tag{7.1}$$

$$S_{min} = \frac{\sigma_{min}}{f_c'} \tag{7.2}$$

Where, σ_{max} and σ_{min} are maximum and minimum stress of the specimen at submerged condition under fatigue test respectively and f_c' is the uniaxial compressive strength of concrete at static dry condition.

Fatigue load was applied to the specimen in the form of sine wave with constant amplitude as shown in Figure 7-3 (a). Prior to that, all the specimens were loaded to a mean (S_m) value of maximum and minimum stress level. Once the specimen reached the

mean stress ratio (S_m), fatigue loading was applied in an incremental fashion until the specimen reaches the target maximum and minimum stress level and loading was continued until failure of the specimen or 2 million fatigue cycle whichever happens first. During the test, both total and fatigue cycle at maximum stress were counted automatically. Here, Fatigue cycle measured from the initial incremental loading until failure of the specimen is termed as total fatigue cycle whereas, that measured only during the maximum stress level is termed as fatigue cycle at maximum stress which is shown in Figure 7-3(b). It is fact that frequency of fatigue loading influences the fatigue life of concrete when the stress level is very high such as 75% or more (Mederios et al., 2015, Sparks and Menzies, 1973). Kesler (1953) pointed out that up to 75% stress level, loading frequency within the range of 1-15 Hz has little effect on the fatigue life of concrete. In this study, a lower loading frequency of 5Hz was considered to minimize the loading instability due to different target stress levels ranging from 60% to 80%. This consideration is similar to the study of Farooq et al. (2017) where fatigue performance of blast furnace slag mortar was investigated at similar stress level ranging from 60% to 80%.

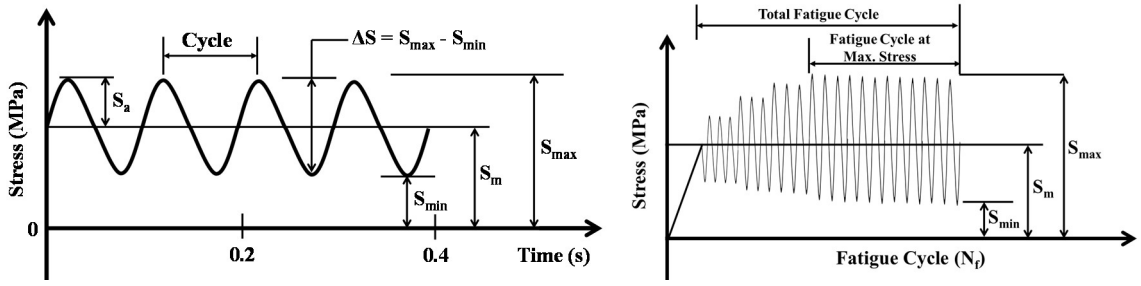

(a) Sinusoidal fatigue loading cycle (b) Definition of fatigue cycle

Figure 7-3 Fatigue load cycle and definition of fatigue cycle

7.3 Static compressive strength in air and in water

7.3.1 Stress-strain relationship

The stress-strain relationship including post peak behavior of all concrete produced by spherical shaped EAF slag fine aggregates at W/C of 0.6 after a curing age

of 28 days is provided in Figure 7-4. For each slag replacement ratio under each test condition (either dry or wet) a minimum of three representative specimens were used and average results were considered. For each condition, the results did not show big scatter. It can be clearly seen from figure 7-4 that irrespective of slag replacement ratio specimens tested in water show relatively lower stiffness, lower peak stress and relatively higher peak strain than those tested in air. In addition, post peak portion of the stress-strain relationship of such concrete are more flat. However, the differences of stiffness, peak stress and corresponding strain and failure strain between specimens tested in air and in water are more distinct for normal concrete. With the increase in slag ratio, these differences were reduced and stress-strain relationship of specimens tested at dry and submerged condition were found to be similar when the slag replacement ratio is 0.5.

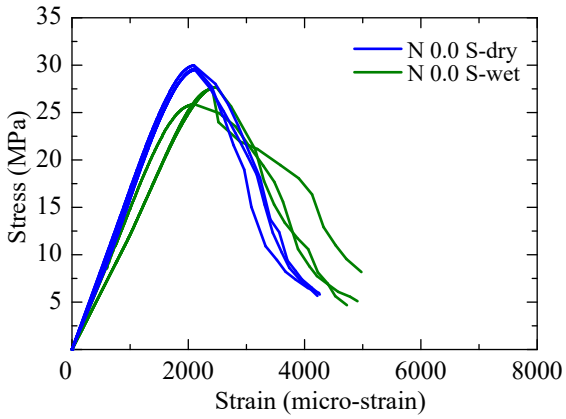

(a) N 0.0 S concrete

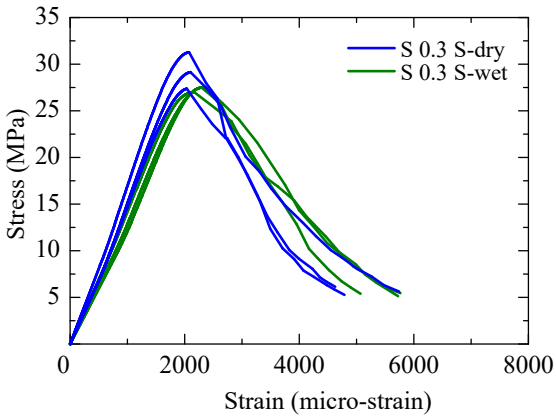

(b) S 0.3 S concrete

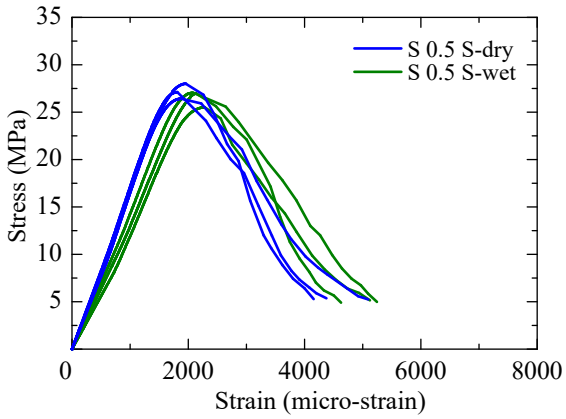

(c) S 0.5 S Concrete

Figure 7-4 Static compressive stress-strain relationship of concrete at dry and submerged condition (curing age 28 days)

7.3.2 Compressive strength, elastic modulus and compressive fracture energy

Experimental results related to the compressive strength, elastic modulus and compressive fracture energy of spherical shaped EAF slag concrete tested at dry and submerged condition are plotted in Figures 7-5 against slag ratio. Elastic modulus and compressive fracture energy were computed by the same method as described in chapter 4 section 4.3.2 and 4.3.4 respectively.

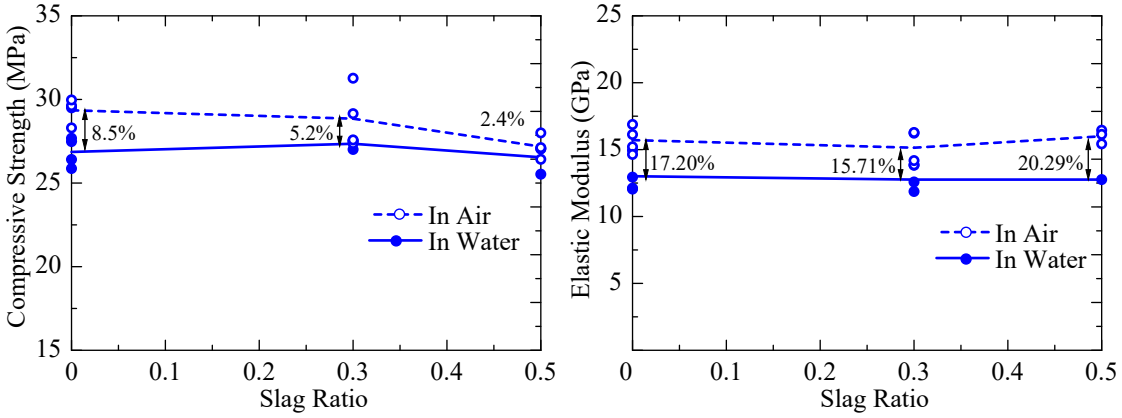

(a) Compressive strength

(b) Elastic Modulus

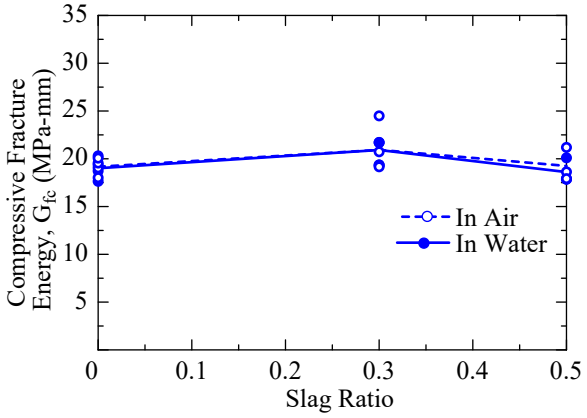

(c) Compressive fracture energy

Figure 7-5 Mechanical properties of concrete at static dry and submerged condition (curing age 28 days)

It is evident from Figure 7-5 that concrete tested at submerged condition show lower strength and elastic modulus than those tested in dry condition although results of compressive fracture energy for both the experimental conditions are equal. The results

of compressive strength, elastic modulus and compressive fracture energy of normal and spherical shaped EAF slag concrete in air are comparable to those reported in chapter 4. As depicted in figure 7-5 (a) for spherical shaped EAF slag concrete of slag ratio 0.5, influence of water during uniaxial compression test is minimum and the difference in compressive strength between the dry and wet test condition is only 2.4% which gradually increases with the decrease in slag replacement ratio. For normal concrete, water effect is more pronounced and higher variation (8.5%) of strength is observed. Figure 7-5 (b) clearly indicates that the presence of water during uniaxial compression test mostly affects the elastic modulus of concrete irrespective of slag replacement ratio. A constant variation of elastic modulus due to different test condition (dry or wet) is observed for all three types of concrete.

7.4 Fatigue compressive strength in water

Based on the test results of average static compressive strength at drying condition, target maximum stresses were computed for all three types of concrete due to different stress levels (60%, 70% and 80%) and the corresponding specimens were tested for fatigue under water by the method as described in section 7.2.3. All the experimental results are listed in Table 7-3. For each case, fatigue cycle at maximum stress are included in the parenthesis along with total fatigue cycles as defined in Figure 7-3 (b). It has been discussed in section 7.2.3 that at very high stress level, higher loading frequency can influence the damage of specimen, therefore total fatigue cycles were considered for plotting the S-N (stress ratio- fatigue cycle) curves. Figures 7-6 and 7-7 represent two different S-N curves where stress ratios were computed based on static dry and static wet condition respectively.

It can be seen from figure 7-6 that spherical shaped EAF slag concrete of slag ratio 0.5 exhibits higher fatigue life under water in comparison to normal concrete at same maximum stress ratio (S_{max}). The tendency is more pronounced at lower maximum stress ratio of 0.6. The behavior of spherical shaped EAF slag concrete at slag ratio of 0.3 is similar to that of normal concrete which is also clear from the slope of the S-N curve of corresponding concrete as shown in Figure 7-6. This result discloses an important finding

that spherical shaped EAF slag concrete of higher slag replacement ratio possesses improved water proofing capacity than that of normal concrete especially at lower stress level which was also observed during the static test in air and in water as shown in Figure 7-5 (a).

Table 7-3 Stress ratio and corresponding fatigue cycles

Specimen ID	Static dry f_c (MPa)	Static wet f_c (MPa)	Based on static dry		Based on static wet		Total Fatigue cycle (Fatigue cycle at maximum stress)
			S_{max}	S_{min}	S_{max}	S_{min}	
N 0.0 F-1	29.35	26.86	0.60	0.10	0.66	0.11	110855 (110563)
N 0.0 F-2			0.60	0.10	0.66	0.11	44611 (44272)
N 0.0 F-1			0.70	0.10	0.77	0.11	369 (147)
N 0.0 F-2			0.70	0.10	0.77	0.11	2038 (1788)
N 0.0 F-1			0.80	0.10	0.87	0.11	303 (162)
N 0.0 F-2			0.80	0.10	0.87	0.11	92 (7)
S 0.3 F-1	28.85	27.35	0.60	0.10	0.63	0.11	232817 (232546)
S 0.3 F-2			0.60	0.10	0.63	0.11	13312 (13000)
S 0.3 F-1			0.70	0.10	0.74	0.11	2601 (2288)
S 0.3 F-2			0.70	0.10	0.74	0.11	1770 (1506)
S 0.3 F-1			0.80	0.10	0.84	0.11	152 (16)
S 0.3 F-2			0.80	0.10	0.84	0.11	452 (356)
S 0.5 F-1	27.18	26.54	0.60	0.10	0.61	0.11	731772 (731505)
S 0.5 F-2			0.60	0.10	0.61	0.11	>2000000
S 0.5 F-1			0.70	0.10	0.72	0.11	2159 (1748)
S 0.5 F-2			0.70	0.10	0.72	0.11	780 (461)
S 0.5 F-1			0.80	0.10	0.81	0.11	273 (8)
S 0.5 F-2			0.80	0.10	0.81	0.11	294 (7)

Note: Figures in the parenthesis, includes fatigue cycles at maximum stress S_{max} only

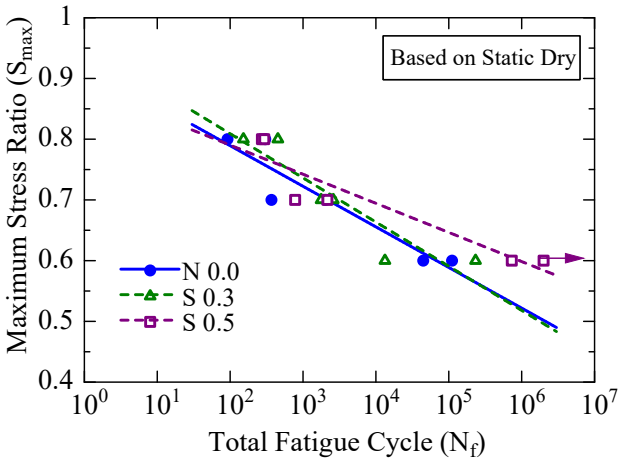

*Arrow indicates running out test

Figure 7-6 S-N curve based on static dry condition

Since the difference of static compressive strength of normal concrete in air and in water is much higher (8.5%) than that of spherical shaped EAF slag concrete of slag ratio 0.5 (2.4%), it is fact that normal concrete was subjected to higher stress ratio (0.66, 0.77 and 0.87) than spherical shaped EAF slag concrete of slag ratio 0.5 (0.61, 0.72 and 0.81) based on static compressive strength results in water. Therefore, lower fatigue life for the former case is quite obvious. The S-N curve as provided in Figure 7-7 illustrates similar fatigue life of normal as well as spherical shaped EAF slag concrete of different slag replacement ratio (0.3 and 0.5) when the maximum stress levels were considered based on the static compressive strength of respective concrete under water.

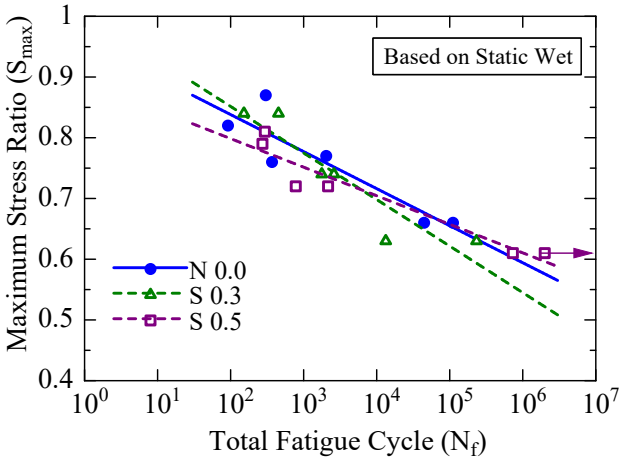

*Arrow indicates running out test

Figure 7-7 S-N curve based on static wet condition

Figure 7-8 depicts the axial strain-cycle ratio relationship of normal and spherical shaped EAF slag concrete at different stress level. Here, cycle ratio is defined as the ratio of a particular fatigue cycle to the total number of fatigue cycles that a specimen experienced until failure. For each slag ratio, maximum and minimum strain results were plotted against cycle ratio at 60%, 70% and 80% of static dry compressive strength in Figure 7-8 (a), (b) and (c) respectively. Values of maximum and minimum strain corresponds to maximum and minimum stress which were computed from the average displacement reading of two diagonally placed displacement transducers during fatigue loading.

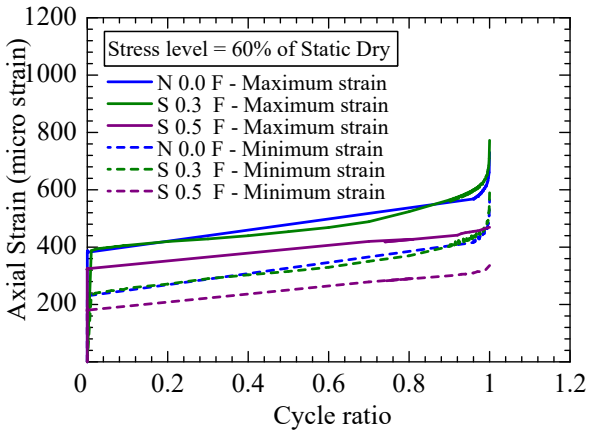

(a) Stress level = 60% of static dry

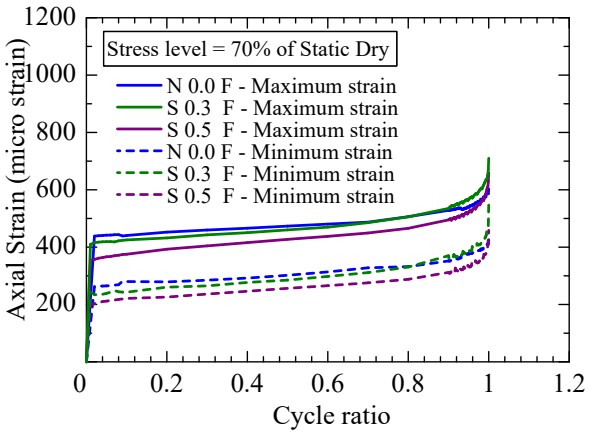

(b) Stress level = 70% of static dry

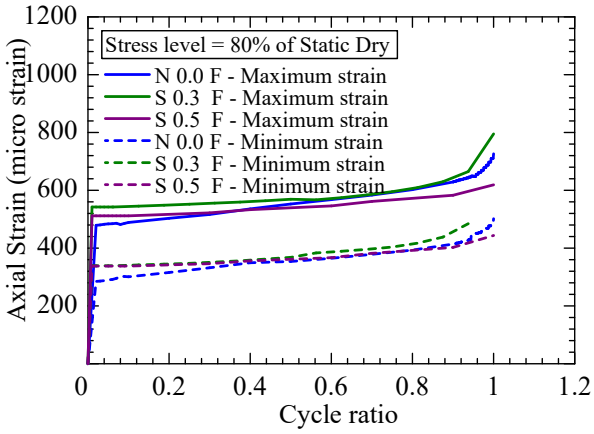

(c) Stress level = 80% of static dry

Figure 7-8 Axial strain and cycle ratio relationship

It can be clearly seen from Figure 7-8 that with the increase in stress level both maximum and minimum strain of all types of concrete increases and the difference in between maximum and minimum strain are similar irrespective of the stress level and slag replacement ratio. When the stress level is very high such as 80%, initial maximum and minimum strain values along with their increment with the increment of cycle ratio is similar for all three types of concrete which indicates similar sort of damage accumulation either in normal or spherical shaped EAF slag concrete. This is also evident from Table 7-3 that at the stress level of 80%, both normal and spherical shaped EAF slag concrete shows similar and very low fatigue life. With the decrease in stress level, clear difference in fatigue performance of slag concrete can be visualized. When the stress level is 60%, both normal and spherical shaped EAF slag concrete of slag ratio 0.3 show similar initial maximum and minimum strain along with similar increment of strain with cycle ratio although that of spherical shaped EAF slag of slag ratio 0.5 is much lower and the axial strain vs. cycle ratio curves for maximum and minimum strain becomes flat after a cycle ratio of 0.7. This result clearly indicates higher fatigue life due to lower damage accumulation and more water tightness of spherical shaped EAF slag concrete of higher slag replacement ratio of 0.5 at lower stress level of 60% which is also true as per Table 7-3.

7.5 Discussion of static and fatigue compression test results under water

It is fact that strength and elastic modulus of concrete is primarily dependent on the strength of mortar matrix and coarse aggregates and bond between them (Giaccio and Zebrino, 1998). Now, the strength of mortar matrix is dependent on the degree of particle interlocking, void and liquid content. Higher void and liquid content results in lower strength of mortar matrix and subsequent reduction of concrete compressive strength and elastic modulus.

When concrete specimens are subjected to uniaxial compression loading under submerged condition several changes happen inside them. Firstly, most of the void spaces inside concrete specimen become saturated and due to saturation adsorbed water layers

reduce the surface energy of hydration products because of surface tension of water (Farooq, et al., 2017). Secondly, due to the reduction of surface energy, particle interlocking gets reduced and causes the reduction of elastic modulus and compressive strength of concrete. It is clear from the above discussion that the more the reduction of surface energy, the more will be the reduction of strength and elastic modulus. Matsushita and Onoue (2006) indicate that the surface energy of concrete reduces significantly if larger amount of voids and liquid contents are present in concrete.

It has been discussed in chapter 5 (Figure 5-10) that the porosity of normal concrete is much higher than that of spherical shaped EAF slag concrete which indicates the presence of more void spaces in the former case. In addition, water absorption capacity of normal concrete is much higher than that of spherical shaped EAF slag concrete (chapter 4 section 4.4.2). Furthermore, water absorption capacity of sand particles are higher than spherical shaped EAF slag particles (chapter 2 Table 2-3). All these results confirm the presence of more void and liquid contents in case of normal concrete than spherical shaped EAF slag concrete. Therefore, the result that spherical shaped EAF slag concrete exhibits improved compressive strength than normal concrete in submerged condition during uniaxial compression test is justified.

Now, the behavior of concrete during repetitive loading under submerged condition might be discussed in light of pore water pressure at crack tip in conjunction with the factors as discussed above. When a concrete specimen is subjected to fatigue loading in air, micro crack originates and propagates and causes the failure of the specimen. In such situation, origination and propagation of micro cracks depend on the quality of ITZ. However, in water, under cyclic loading pumping action triggers the propagation of cracks due to the wedge effect of pore water pressure at crack tip. Due to the pumping effect, leaching of hydration product happens which causes the change in pore structure along with pore water pressure (Cheng et al., 2013). As a result, quick fatigue failure happens in water than in air and fatigue life of concrete in water is shortened. It is expected that concrete produced by spherical shaped EAF slag fine aggregate will experience lower pore water pressure due to lower porosity. In addition, stronger particle adhesion of such concrete (as discussed in chapter 4 section 4.3.6) might resist the wedge cracking effect during pumping action and ensures longer fatigue life than normal concrete especially at lower maximum stress ratio of 0.6.

7.6 Summary and conclusions

Fatigue performance of spherical shaped EAF slag concrete in submerged condition was investigated in this chapter. Prior to that, water proofing capacity of such concrete was tested in static condition. Based on the studies as reported in this chapter following conclusions can be drawn.

- The reduction of static compressive strength in water in comparison to that in air is much lower for spherical shaped EAF slag fine aggregate concrete of slag ratio 0.5 (2.4%) than that of normal concrete (8.5%). The reason behind this phenomena was identified as lower porosity and water absorption of such concrete.
- A higher reduction in elastic modulus but similar in values for all types of concrete was observed when they were tested in air and in water respectively. Interestingly, no significant influence of water was observed for the case of compressive fracture energy of all types of concrete.
- Spherical shaped EAF slag concrete of slag ratio 0.5 manifests higher fatigue life under same maximum stress ratio (S_{max}) in comparison to normal concrete when S_{max} was computed based on static dry condition. The behavior is more pronounced at lower S_{max} of 0.6 which was clarified from the axial strain-cycle ratio relationship. Axial strain results revealed that damage accumulation due to fatigue loading under water for spherical shaped EAF slag concrete of slag ratio 0.5 is slower than normal concrete. For the maximum stress ratio evaluated based on static wet condition, fatigue life of all types of concrete were found to be similar.

The above results confirmed that spherical shaped EAF slag concrete imparts superior water proofing performance which is promising for their wider applicability.

8 Conclusions and recommendations for future study

8.1 Conclusions

This study systematically investigated the applicability of a newly developed spherical shaped steel manufacturing by-product (EAF slag) as replacement of fine aggregates in concrete. First of all, physical properties of different types of fine aggregates such as natural sand, spherical and conventional angular shaped EAF slag were examined and compared to identify their possible scope of utilization. Based on the material level study and possible scope of utilization, experimental parameters (W/C, slump, air content, slag replacement ratio) were selected. Subsequently, methods for obtaining accurate mix proportions for particles of different shape were formulated and confirmed by trial tests. Fresh properties of concrete produced by both spherical and angular shaped EAF slag fine aggregates were examined. Finally, all important and relevant properties (mechanical, durability, thermal) of such concrete were tested under various experimental conditions (ambient, high temperature, fatigue under water etc.). Based on the studies as presented from chapters 2 to 7, following major conclusions can be drawn.

In chapter 2, the difference in shape of EAF slag particles were identified by laser scanning and the differences were quantified from sphericity calculation (0.92 for spherical and 0.74 for angular). Furthermore, lower maximum and minimum void ratios of spherical shaped EAF slag particles differentiated them from the conventional angular shaped EAF slag particles. It was evident from the test results that both types of slag particles possess higher particle density and lower water absorption in comparison to natural sand. Higher amount of larger sized particles were found in spherical slag mix

than angular slag due to their unique production technique where granulation was ensured by rapid air cooling rather than crushing. Studies on the chemical composition of both types of EAF slag particles revealed that these materials are suitable to be utilized in concrete as replacement of aggregates due to the presence of CaO, SiO_2 and FeO.

Depending on the material properties such as higher particle density and spherical shape, fresh concrete properties were investigated in chapter 3. Two different types of concrete were produced with W/C, slump and air content of 0.4, 5cm and 5% and 0.6, 12cm and 5% with an aim to investigate the utilization scope of spherical shaped EAF slag fine aggregates in concrete pavement and normal concrete respectively. It was revealed that at lower W/C and slump of 0.4 and 5cm, spherical shaped EAF slag concrete require 16% less mix water and cement during concreting when natural sand is completely replaced by them. In contrary, at this situation angular shaped EAF slag concrete require 5.6% more water and cement. In addition, fresh concrete density was found to be increasing with the increase in slag replacement ratio irrespective of slag type and W/C. The bleeding behavior of spherical shaped EAF slag concrete at higher W/C and slag replacement ratio was found to be much higher than normal and angular shaped EAF slag concrete although corresponding particle settlement due to segregation even with larger sized (500mm) specimen was found to be very low to negligible.

Studies on the mechanical properties of concrete as reported in chapter 4 confirmed that at lower W/C and slump of 0.4 and 5cm, spherical shaped EAF slag concrete imparts higher strength and elastic modulus than normal concrete. However, at higher W/C and slump of 0.6 and 12cm, normal concrete manifests improved mechanical properties. In comparison to spherical shaped EAF slag concrete, angular shaped EAF slag concrete showed improved flexural and tensile strength although ductility of such concrete was found to be lower which indicates that it is better to utilize the newly developed spherical shaped EAF slag particles for concreting considering all aspects of mechanical properties. The mechanism of improved strength and elastic modulus of spherical shaped EAF slag concrete was revealed from the image analysis results by digital image co-relation method (DICM) as improved particle adhesion of spherical shaped EAF slag concrete that prolongs the origination and resists the propagation of cracks. Regarding durability properties, spherical shaped EAF slag concrete showed much lower drying shrinkage, water absorption and air permeability in comparison to

normal and angular shaped EAF slag concrete. The reasons behind the improved durability properties were pointed out as lower water and cement requirement, lower water absorption of slag particles and stronger particle resistance. In a nutshell, improved mechanical and durability properties in conjunction with improved fresh behavior of spherical shaped EAF slag concrete at lower W/C demonstrates their strong applicability in concrete pavement.

In chapter 5, material stability of spherical shaped EAF slag concrete was investigated during thermal change (<100°C) and freezing-thawing action. The study revealed an interesting finding that spherical shaped EAF slag concrete shows much lower thermal expansion in comparison to normal and angular shaped EAF slag concrete. The reason behind the phenomena was clarified as stronger particle resistance against thermal expansion due to much lower porosity of such concrete. Apart from thermal expansion, both spherical and angular shaped EAF slag concrete exhibited much lower thermal diffusivity, specific heat and thermal conductivity than normal concrete. The dominating factors influencing such behaviors were identified as density, moisture content and, relative mineralogical composition of slag and sand. In so far as the freezing and thawing resistance of concrete is concerned, both air entrained spherical and angular shaped EAF slag concrete showed improved behavior up to 200 freezing-thawing cycles than normal concrete. After 200 freezing and thawing cycles, resistance of spherical shaped EAF slag concrete deteriorated although that of angular shaped EAF slag concrete were higher than normal concrete until 300 cycles. The deteriorating behavior of spherical shaped EAF slag concrete in resisting freezing-thawing action after 200 cycles was examined as lower air retention capacity of such concrete which can be improved by increasing the design air content or fine content in slag mix without compromising the mechanical properties. All the results related to thermal properties of concrete reconfirmed the utility of spherical shaped EAF slag in concrete.

It is fact that concrete of lower thermal expansion coupled with lower thermal conductivity imparts resistance in cases where susceptibility of fire is high. Based on this assumption, influences of high temperature on the physical and mechanical properties of concrete produced by both spherical and angular shaped EAF slag fine aggregates at W/C and slump of 0.4 and 5cm were investigated in chapter 6. The results showed that spherical shaped EAF slag concrete exhibits much lower mass loss than normal and

angular shaped EAF slag concrete. The influencing factor was pointed out as less degradation of hydration products because of lower volume of cement paste of spherical shaped EAF slag concrete in comparison to normal concrete. Due to stronger particle resistance, many very small localized surface cracks were observed for both spherical and angular shaped EAF slag concrete at higher temperature and higher slag replacement ratio. This behavior was confirmed from the higher length change of slag concrete. In so far as mechanical properties of slag concrete under high temperature exposure are concerned, spherical shaped EAF slag concrete manifested improved residual elastic modulus and similar to slightly improved residual compressive strength in comparison to normal and angular shaped EAF slag up to a heating temperature of 500°C. The pre-damage of concrete due to heating was observed as horizontal type closing cracks during uniaxial compression by digital image co-relation method (DICM). The extent of compression closing cracks due to heating was found to be dictating the reduction of elastic modulus and compressive strength of concrete subjected to heating. Residual flexural strength and tensile fracture energy of spherical shaped EAF slag concrete was found to be lower than that of normal and angular shaped EAF slag concrete due to the higher particle fragility of spherical shaped EAF slag during heating.

Finally, water proofing performance of spherical shaped EAF slag concrete was investigated by both static and fatigue compression test in chapter 7. The reduction of static compressive strength due to water was found to be much lower in case of spherical shaped EAF slag concrete of slag ratio of 0.5 than normal concrete. The mechanism was identified as lower water absorption and porosity of such concrete. The influence of water was observed to be higher for the reduction of elastic modulus of all types of concrete and the results were similar. However, no reduction of compressive fracture energy was noted for all types of concrete. Regarding dynamic fatigue life under water, spherical shaped EAF slag concrete of slag ratio of 0.5 exhibited improved performance due to slower damage accumulation than normal concrete at lower maximum stress ratio computed based on static dry condition.

All-together, spherical shaped EAF slag fine aggregates demonstrate their strong applicability in concrete of lower W/C and slump of 0.4 and 5cm as replacement of natural sand. Considering all the properties as discussed earlier, a slag replacement ratio of 0.5 might be considered as a beneficial choice. Nevertheless, utilization of this

otherwise waste industrial by-product in concrete will solve many structural problems as well as durability concerns and will not only enhance the sustainability and economy of construction but also ensure environmental safety.

8.2 Recommendations for future study

In order to enhance the wider applicability of spherical shaped EAF slag concrete, studies on the following topic will be of importance.

- Current study investigated the applicability of spherical shaped EAF slag fine aggregates in concrete without altering the material gradation to promote their economic utilization. At present, the presence of coarser particles in the slag mix is much higher. In future, studies can be conducted by adjusting the material gradation by finer particles in such a way that the change will not cause degradation of mechanical properties. This step might improve the air retention capacity of spherical shaped EAF slag concrete which subsequently should improve the freezing and thawing resistance of spherical shaped EAF slag concrete. Alternatively, tests can be conducted with same material gradation but higher air content such as 6% for the improvement of freezing and thawing resistance of such concrete.
- It was observed in this study that the mechanical properties of spherical shaped EAF slag concrete at higher W/C of 0.6 and slump of 12cm was lower than normal concrete although that of W/C of 0.4 and slump of 5cm showed improved behavior. Now, for extensive and wider use, it is necessary to obtain a bifurcation point in between the two W/C cases where mechanical properties of slag concrete are better than normal concrete. Therefore, studies on other W/C ratio cases such as 0.45, 0.50 and 0.55 might be carried out.
- This study made an assumption that ITZ in concrete produced by spherical shaped EAF slag might be smaller but stronger than that of normal and angular shaped EAF slag concrete. It is fact that the assumption was made based on the existing literatures of microstructure properties of slag concrete. However, for thorough understanding as well as validating the current experimental results, examination of

microstructure behavior of spherical and angular shaped EAF slag concrete is important and requires to be investigated in future.

- Current study suggested that spherical shaped EAF slag fine aggregates are promising alternatives of natural sand in concrete pavement and therefore all associated tests were conducted. It is fact that abrasion resistance is also an important test that dictates the durability of concrete pavement. In future, studies on abrasion resistance of concrete produced by spherical shaped EAF slag fine aggregates are required to be conducted prior to their application in concrete pavement.
- Due to high density, utility of spherical shaped EAF slag concrete is limited. To expand their utility, EAF slag materials can be tested in water retention dam structures. It is fact that in case of dam structures, due to water effect deterioration of concrete happens frequently and requires maintenance. Since, spherical shaped EAF slag concrete exhibits lower water absorption and at the same time imparts improved static compressive strength under water, their performance in dam structure might solve the existing problem, which requires to be investigated in future.

References

ACI 122-R-14-02 (2014), Guide to Thermal Properties of Concrete and Masonry Systems, American Concrete Institute, ACI/TMS Committee 122.

ACI-TMS Committee 216, Code requirements for determining fire resistance of concrete and masonry construction assemblies (ACI-TMS 216.1-07), Farmington Hills, MI, 2007.

ACPA Concrete Information (1992): Design and Construction of Joints for Concrete Streets, American Concrete Pavement Association.

Ahmed, E. and, El-Kourd, A. (1989): Properties of Concrete Incorporating Natural and Crushed Stone Very Fine Sand, Materials Journal, American Concrete Institute, vol. 86, No. 4, pp. 417-424.

Alizadeh, R., Chini, M., Ghods, P., Hoseini, M., Montazer, Sh., and, Shekarchi, M. (2003): Utilization of Electric Arc Furnace Slag as Aggregates in Concrete – Environmental Issue, 6th CANMET, ACI International Conference on Recent Advances in Concrete Technology, Bucharest, Romania, pp. 451-464.

An, J., Kim, S.S., Nam, B.H., and, Durham, S.A. (2017): Effect of Aggregate Mineralogy and Concrete Microstructure on Thermal Expansion and Strength Properties of the Normal Strength Concrete, Applied Sciences, 7, 1307.

Arioz, O. (2007): Effects of elevated temperatures on properties of concrete, Fire Safety Journal, vol. 42, pp. 516-522.

Arribas, I., Santamaría, A., Ruiz, E., Ortega-López, V., and, Manso, J. M. (2015): Electric arc furnace slag and its use in hydraulic concrete, Construction and Building Materials, vol. 90, May, pp. 68-79.

ASCE committee for Fire Protection, Structural Fire Protection: Manual of Practice, Manual and Report No. 78, American Society of Civil Engineers, Structural division, New York, NY, 1992.

ASTM C138 / C138M-17a, Standard Test Method for Density (Unit Weight), Yield, and Air Content (Gravimetric) of Concrete, ASTM International, West Conshohocken, PA, 2017.

ASTM C232 / C232M-14, Standard Test Method for Bleeding of Concrete, ASTM International, West Conshohocken, PA, 2014.

ASTM C293-02, Standard Test Method for Flexural Strength of Concrete (Using Simple Beam with Center-Point Loading), ASTM International, West Conshohocken, PA, 2002.

ASTM C666 / C666M-15, Standard Test Method for Resistance of Concrete to Rapid Freezing and Thawing, ASTM International, West Conshohocken, PA, 2015

ASTM D4253-14, Standard Test Methods for Maximum Index Density and Unit Weight of Soils Using a Vibratory Table, ASTM International, West Conshohocken, PA, 2014.

ASTM D4254-14, Standard Test Methods for Minimum Index Density and Unit Weight of Soils and Calculation of Relative Density, ASTM International, West Conshohocken, PA, 2014.

Barra, M., Aponte, D., Vazquez, E., Mendez, B., Miro, R., and, Valls, S. (2016): Experimental Study of the Effect of the Thermal Conductivity of EAF Slag Aggregates Used in Asphaltic Concrete of Wearing Courses on the Durability of Road Pavements, SCMT4, Las Vegas, August.

Belhadj, B., Bederina, M., Benguettache, K., and, Queneudec, M. (2014): Effect of type of sand on the fracture and mechanical properties of sand concrete, Advances in Concrete Construction, vol. 2, no. 1, March, pp. 13-27.

Caggiano, A., Schicchi, D.S., Etse, G., and, Ripania, M. (2018): Meso-scale Response of Concrete under High Temperature based on Coupled Thermo-Mechanical and Pore-Pressure Interface Modeling, Engineering Failure Analysis, vol. 85, pp. 167-188.

Cepuritis, R., Jacobsen, S., Pedersen, B., and, Mørtsell, E. (2016): Crushed sand in concrete – Effect of particle shape in different fractions and filler properties on rheology, Cement and Concrete Composites, vol. 71, April, pp. 26-41.

Chen, B., and Liu, J. (2004): Residual strength of hybrid-fiber-reinforced high strength concrete after exposure to high temperature, Cement and Concrete Research, vol. 34, no. 6, pp. 1065-1069.

Cheng, A., Chao, S.J., Lin, W.T. (2013): Effects of leaching behavior of calcium ions on compression and durability of cement-based materials with mineral admixtures, Materials, vol.6, pp. 1851-1872.

Cifuentes, H., Ríos, J.D., and, Gómez, E.J. (2018): Effect of mix design on the size-independent fracture energy of normal-and high-strength self-compacting concrete, MATERIALES DE CONSTRUCCION, vol. 68, Issue-329.

Cordon, W.A., and, Merrill, D. (1963): Requirements for Freezing and Thawing Durability properties for Concrete, Proceedings, ASTM vol. 63, pp. 1026–1036.

Coppola, L., Buoso, A., Coffetti, D., Kara, P., and, Lorenzi, S. (2016): Electric arc furnace granulated slag for sustainable concrete, Construction and Building Materials, vol. 123, July, pp. 115-119.

Cortes, D. D., Kim, H. –K., Palomino, A. M., and, Santamarina, J. C. (2008): Rheological and mechanical properties of mortars prepared with natural and manufactured sands, Cement and Concrete Research, vol. 38, March, pp. 1142-1147.

CRD-C 36-73, Method of Test for Thermal Diffusivity of Concrete, US Army Corps of Engineers.

Dash, M. K., Patro, S. K., and, Rath, A. K. (2016): Sustainable use of industrial-waste as partial replacement of fine aggregate for preparation of concrete – A review, International Journal of Sustainable Built Environment, vol. 5, April, pp. 484-516.

Dewar, J.D., and Anderson, R. (1992): Manual of Ready-Mixed Concrete, Blackie Academic and Professional, 2nd ed., London.

Engineering Toolbox (2003), Specific Heat of Solids/ [online].

Engineering Toolbox (2003), Thermal conductivity of common material and glasses/ [online].

EN 1992-1-2: Design of Concrete Structures. Part 1-2: General Rules – Structural Fire Design, Eurocode 2, European Committee for Standardization, Brussels, Belgium, 2004.

Faleschini, F., Brunelli, K., Zanini, M. A., Dabalà, M., and, Pellegrino, C. (2016): Electric Arc Furnace Slag as Coarse Recycled Aggregate for Concrete Production, Journal of Sustainable Metallurgy, vol. 2, issue 1, March, pp. 44-50.

Faleschini, F., Fernández-Ruíz, M. A., Zanini, M. A., Brunelli, K., Pellegrino, C., and, Hernández-Montes, E. (2015): High performance concrete with electric arc furnace slag as aggregate: Mechanical and durability properties, Construction and Building Materials, vol. 101, October, pp. 113-121.

Farooq, M.A., Sato, Y., Ayano, T., and, Niitani, K. (2017): Experimental and numerical investigation of static and fatigue behavior of mortar with blast furnace slag sand as

fine aggregates in air and water, Construction and Building Materials, vol. 143, pp. 429-443.

Fernandes, B, Gil, A.M., Bolina, F.L., and, Tutikian, B.F. (2017): Microstructure of concrete subjected to elevated temperatures: physico-chemical changes and analysis techniques, IBRACON Structures and Materials Journal, vol. 10, no. 4, August, pp. 838-863.

Fernandez, I. O., Calvet, N., Gil, A., Rodriguez-Aseguinolaza, J., Faik, A., and D'Aguanno, B. (2015): Thermophysical characterization of a by-product from the steel industry to be used as a sustainable and low-cost thermal energy storage material, Energy, vol. 89, pp. 601-609.

Forster, S.W. (1994): Soundness, Deleterious Substances, and Coatings, ASTM Special Technical Publication No. 169C, Philadelphia, pp. 411-420.

Galloway, J. E. Jr. (1994): Grading, Shape, and Surface Properties, ASTM Special Technical Publication No. 169C, Philadelphia, pp. 401-410.

Gajda, J. (2007), Mass Concrete for Buildings and Bridges, Skokie, III, Portland cement Association.

Giaccio, G. and, Zerbino, R. (1998): Failure mechanism of concrete-Combined effects of coarse aggregates and strength level, Advanced Cement Based Materials, vol. 7, pp. 41-48.

Gokce, A., Nagataki, S., Saeiki, T. and Hisada, M. (2004): Freezing and thawing resistance of air-entrained concrete incorporating recycled coarse aggregate: The role of air content in demolished concrete, Cement and Concrete Research, vol. 34, pp. 799-806.

Hager, I. (2013): Behaviour of Cement Concrete at High Temperature, Bulletin of the Polish Academy of Sciences, vol. 61, no. 1.

Hager, I., Tracz, T., Sliwinski, J., and, Krzemien, K. (2015): The Influence of Aggregate Type on the Physical and Mechanical Properties of High-Performance Concrete subjected to High Temperature, Fire and Materials, Wiley Online Library, August.

Hamad, A.J. (2014): Materials, Production, Properties and Application of Aerated Lightweight Concrete: Review, International Journal of Materials Science and Engineering, vol. 2, No. 2, December, pp. 152-157.

Hamdhan, I. N., and, Clarke, B. G. (2010): Determination of Thermal Conductivity of Coarse and Fine Sand Soils, Proceedings World Geothermal Congress, Bali, Indonesia.

Hertz, K.D. (2005): Concrete strength for fire safety design, Magazine of Concrete Research, vol. 57, no. 8, pp. 445-453.

Hillerborg, A., Modéer, M., and, Petersson, P.-E. (1976): Analysis of crack formation and crack growth in concrete by means of fracture mechanics and finite elements, Cement and Concrete Research, vol. 6, Issue-6, November, pp. 773-781.

Howlader, M.K., Rashid, M.H., Mallick, D., and, Haque, T. (2012): Effects of aggregate types on thermal properties of concrete, ARPN Journal of Engineering and Applied Science, July, pp. 900-907.

Huang, Y.H. (2004): Pavement analysis and design, 2nd edition, Prentice Hall, Pearson plc, Englewood Cliffs, New Jersey.

Hudson, B.P. (1999): Concrete workability with high fines content sands, Quarry, vol. 7, pp. 22-25.

Iffat, S. (2015): Relation between Density and Compressive Strength of Hardened Concrete, Concrete Research Letters, vol. 6(4), pp. 182-189.

Inoue, M., Aquino, C., Miura, H., and, Okamoto, T. (2010): Influence of limestone aggregate on strength and drying shrinkage of concrete, Journal of the Society of Materials Science, Japan, vol. 59, no. 10, October, pp. 769-774.

Integrated Materials and Construction Practices for Concrete Pavement: (2007): A State-of-the-Practice Manual, U.S. Department of Transportation, Federal Highway Administration, FHWA Publication No. HIF-07-004, 2nd Edition.

Jeong, J.-H., Zollinger, D.G., Lim, J.-S., and, Park, J.-Y. (2012): Age and Moisture Effects on Thermal Expansion of Concrete Pavement Slabs, Journal of Materials in Civil Engineering, ASCE, vol. 24, issue 1, pp. 8-15.

JCI-S-001-2003, (2003): Method of test for fracture energy of concrete by use of notched beam, Japan Concrete Institute Standard.

JIS A 1102, Method of test for sieve analysis of aggregates, Japanese Industrial Standards, 2014.

JIS A 1109, Methods of test for density and water absorption of fine aggregates, Japanese Industrial Standards, 2006.

JIS A 1148, Method of test for resistance of concrete to freezing and thawing, Japanese Industrial Standards, 2010.

JIS R 1634, Test methods for density and apparent porosity of fine ceramics, Japanese Industrial Standards, 1998.

JSCE Guideline for Concrete No. 1 (2004): Recommendations for Design and Construction of Concrete Structures using Electric Arc Furnace Oxidizing Slag Aggregate, Japan Society of Civil Engineers (JSCE).

JSCE Guideline for Concrete No. 15 (2010): Standard Specifications for Concrete Structures-2007, 'Design', Japan Society of Civil Engineers (JSCE).

JSCE Guideline for Concrete No. 16 (2010): Standard Specifications for Concrete Structures-2007 Materials and Construction, Japan Society of Civil Engineers (JSCE).

JSCE K-571, Test methods of surface penetrants for concrete structures, Japan Society of Civil Engineers, 2005

Juckes, L. (2011): Basics of slag production, Global slag.

Juknevicius, L., Marciukaitis, G., and Valivonis, J. (2006): Influence of technological factors on the state of stress and strain in three-layer reinforced concrete structures, Journal of Civil Engineering and Management, vol. 12, issue 3, pp. 195-204.

Kalcheff, I. (1977): Portland cement Concrete with Stone Sand, Special Engineering Report, National Crushed Stone Association.

Kaplan, M. F. (1959): Flexural and Compressive Strength of Concrete as Affected by the Properties of Coarse Aggregates, Proceedings, American Concrete Institute, Vol. 55, pp. 1193-1208.

Karahan, O. (2017): Transport Properties of High Volume Fly Ash or Slag Concrete exposed to High Temperature, Construction and Building Materials, vol. 152, pp. 898-906.

Karihaloo, B.L. (1995): Fracture Mechanics and Structural Concrete, Harlow: Longman.

Kesler, C.E. (1953): Effect of speed testing on flexural fatigue strength of plain concrete, Highway Research Board, vol. 32, pp. 251-258.

Khaliq, W. and Kodur, V. (2012): High Temperature Mechanical Properties of High Strength Fly ash Concrete with and without Fibers, ACI Materials Journal, vol. 109, no. 6, pp. 665-674.

Khoury, G. A. (2000): Effect of Fire on Concrete and Concrete Structures, Progress in Structural Engineering and Materials, vol. 2, pp. 429-447.

Kizilkanat, A.B., Yuzer, N., and, Kabay, N. (2013): Thermo-physical Properties of Concrete Exposed to High Temperature, Construction and Building Materials, vol. 45, August, pp. 157-161.

Kockal, N. (2016): Investigation about the effect of different fine aggregates on physical, mechanical and thermal properties of mortars, Construction and Building Materials, vol. 124, August, pp. 816-825.

Kodur, V. (2014): Properties of Concrete at Elevated Temperatures, ISRN Civil Engineering, vol. 2014, March, Article ID 468510.

Kodur, V.K.R., Cheng, F.P., Wang, T.C., and, Sultan, M.A. (2003) Effect of strength and fiber reinforcement on the fire resistance of high-strength concrete columns, Journal of Structural Engineering, vol. 129, issue-2, pp.253-259.

Krumbein, W. C., and, Sloss, L. L. (1951): Stratigraphy and sedimentation, W. H. Freeman and Company, San Francisco.

Lantsoght, E.O.L., Van der Veen, C., and, Boer, A.de. (2016): Proposal for the fatigue strength of concrete under cycles of compression, Construction and Building Materials, vol. 107, pp.138-156.

Larosche, C.J. (2009): Types and causes of cracking in concrete structures, Failure, Distress and Repair of Concrete Structures, Woodhead Publishing Limited, UK, pp. 57-83.

Lertsrisakulrat, T., Watanabe, K., Niwa, J. (2001): Experimental study on parameters in localization of concrete subjected to compression, Journal of Materials and Concrete Structures, JSCE 50, no. 669, pp. 309-321.

Laughlin, C. (2012): Mechanical and Thermal Properties of Copper Slag Concrete, Thesis submitted to Barrett, the Honors College, Arizona State University.

Lee, K. (2008): Evaluation of Concrete Behavior under High Temperature, PhD Thesis, Department of Civil Engineering, University of Colorado at Boulder.

Liang, X., Wu, C., Yang, Y., and, Li. Z. (2019): Experimental study on ultra-high performance concrete with high fire resistance under simultaneous effect of elevated temperature and impact loading, Cement and Concrete Composites, vol. 98, pp. 29-38.

Maruyama, I., Sasano, H. and, Lin, M. (2016): Impact of aggregate properties on the development of shrinkage-induced cracking under restraint conditions, Cement and Concrete Research, vol. 85, pp. 82-101.

Manso, J. M., Polanco, J. A., Losaňez, M., and, González, J. J. (2006): Durability properties of concrete made with EAF slag as aggregate, Cement & Concrete Composites, vol. 28, March, pp. 528-534.

Ma, Q., Guo, R., Zhao, Z., Lin, Z., and, He, K. (2015): Mechanical Properties of Concrete at High Temperature – A Review, Construction and Building Materials, vol. 93, pp. 371-383.

Ma, Q., Du, H., Zhou, X., He, K., Lin, Z., Yan, F., Huang, L., and, Guo, R: (2018): Performance of Copper Slag contained Mortars after Exposure to Elevated Temperatures, Construction and Building Materials, vol. 172, pp. 378-386.

Maslehuddin, M., Sharif, A. M., Shameem, A., Ibrahim, M., and, Barry, M. S. (2003): Comparison of properties of steel slag and crushed limestone aggregate concretes, Construction and Building Materials, vol. 17, August, pp. 105-112.

Matsushita, H., and Onoue, K. (2006): Influence of surface energy on compressive strength of concrete under static and dynamic loading, Journal of Advanced Concrete Technology, vol. 4, issue-3, pp. 409-421.

Mederios, A., Zhang, X., Ruiz, G., Yu, R.C., Velasco, M.S.L. (2015): Effect of loading frequency on the compressive fatigue behavior of plain and fiber reinforced concrete, International Journal of fatigue, vol. 70, pp. 342-350.

Mehta, P.K., and, Monteiro, J.M. Paulo. (2013): Concrete: Microstructure, Properties, and Materials, 4th edition, Mc Graw Hill Education.

Meyer, C. (2009): The greening of the concrete industry, Cement & Concrete Composites, vol. 31, January, pp. 601-605.

Mills, K. (2011): The estimation of slag properties, Short course presented as part of Southern African Pyrometsallurgy, March.

Monosi, S., Ruello, M. L., and, Sani, D. (2016): Electric arc furnace slag as natural aggregate replacement in concrete, Cement and Concrete Composites, vol. 66, December, pp. 66-72.

Nakamura, H., and, Higai, T. (2001): Compressive fracture energy and fracture zone length of concrete, modelling of inelastic behavior of RC structures under seismic loads, American Society of Civil Engineers, vol. 44, no. 627, pp. 471-487.

Nakamura, H., Nanri, T., Miura, T., and, Roy, S. (2018): Experimental investigation of compressive strength and compressive fracture energy of longitudinally cracked concrete, Cement and Concrete Composites, vol., 93, pp. 1-18

Neville, A. M., and, Brooks, J. J. (2010): Concrete Technology, Longman Scientific & Technical, England, Second Edition.

Nippon Steel Association (NSA), Types of Iron and Steel Slag, http://www.slg.jp/e/slag/kind.html.

Oehler, L.T. (1963): Joints in Portland Cement Concrete Pavement, The Fourth Annual Highway Conference , Michigan College of Mining and Technology, Houghton.

Onoue, K., Masateru, T., Masayasu, O., and, Bier, T.A. (2014): Fatigue characteristics of steel-making slag concrete under compression in submerged condition, Construction and Building Materials, vol. 70, pp. 231-242.

Onoue, K., and, Matsushita, H. (2012): Reduction mechanisms of fatigue strength of concrete under compression due to permeation of liquids, Construction and Building Materials, vol. 37, pp. 82-92.

Pan, Z., Tao, Z., Cao, Y.F., Wuhrer, R., and, Murphy, T. (2018): Compressive Strength and Microstructure of Alkali-activated Fly ash/ slag binders at High temperature, Cement and Concrete Composites, vol. 86, pp. 9-18.

Patel, J.P. (2008): Broader Use of Steel Slag Aggregates in Concrete, Cleveland State University.

Pellegrino, C., and, Gaddo, V. (2009): Mechanical and durability properties characteristics of concrete containing EAF slag as aggregate, Cement & Concrete Composites, vol. 31, May, pp. 663-671.

Polat, R., Yadollahi, M. M., Sagsoz, A. E., Arasan, S., The Correlation between Aggregate Shape and Compressive Strength of Concrete: Digital Image Processing Approach, International Journal of Structural and Civil Engineering Research, Vol. 2, No. 3, August 2013.

Poon, C.S., Anson, A.M., and, Wong, Y.I. (2001): Comparison of the strength and durability performance of normal and high-strength pozzolanic concretes at elevated temperature, Cement and Concrete Research, vol.31, no. 9, pp. 1291-1300.

Powers, T. C., and, Brownyard, T.L. (1946): Studies of the Physical Properties of Hardened Portland Cement Paste, American Concrete Institute, vol. 43, issue-9, pp. 469-504.

Prabhu, G. G., Hyun, J. H., and, Kim, Y. Y. (2014): Effects of foundry sand as a fine aggregate in concrete production, Construction and Building Materials, vol. 70, September, pp. 514-521.

Qasrawi, H. (2014): The use of steel slag aggregate to enhance the mechanical properties of recycled aggregate concrete and retain the environment, Construction and Building Materials, vol. 54, March, pp. 298-304.

Qasrawi, H., Shalabi, F., and, Asi, I. (2008): Use of low CaO unprocessed steel slag in concrete as fine aggregate, Construction and Building Materials, Vol. 23, July, pp. 1118-1125.

Quiroga, P. N., and, Fowler, D. W. (2003): The Effects of Aggregates Characteristics on the Performance of Portland Cement Concrete, International Centre for Aggregates Research (ICAR), The University of Texus at Austin, Research Report ICAR – 104-1F, December.

Rondi, L., Bregoli, G., Sorlini, S., Cominoli, L., Collivignarelli, C, and, Plizzari, G. (2016): Concrete with EAF steel slag as aggregate: A comprehensive technical and environmental characterization, Composites Part B: Engineering, vol. 90, April, pp. 195-202.

Roy, S., Miura, T., Nakamura, H., and, Yamamoto, Y. (2018): Investigation of fresh behaviors and mechanical properties of concrete produced by air granulated spherical shaped EAF slag fine aggregate, Transactions of the Japan Concrete Institute, vol. 40, issue 1, July, pp. 1947-1952.

Roy, S., Miura, T., Nakamura, H., and, Yamamoto, Y. (2018): Investigation on Applicability of Spherical Shaped EAF Slag Fine Aggregate in Pavement Concrete: Fundamental and Durability Properties, Construction and Building Materials, vol. 192, December, pp. 555-568.

Roy, S., Miura, T., Nakamura, H., and, Yamamoto, Y. (2019): Investigation on Material Stability of Spherical Shaped EAF Slag Fine Aggregate Concrete for Pavement during Thermal Change, Construction and Building Materials, vol. 215, pp. 862-874.

Saha, A.K., Sarker, P.K., and, Golovanevkhiy, V. (2019): Thermal Properties and Residual Strength after High Temperature Exposure of Cement Mortar using Ferronickel Slag Aggregate, Construction and Building Materials, vol. 199, pp. 601-612.

Saha, A.K., Sarker, P.K., and Majhi, S. (2018): Effect of Elevated Temperatures on Concrete Incorporating Ferronickel Slag as Fine Aggregate, Fire and Materials, vol. 43, pp. 8-21.

Santamaria, A., Orbe, A., San Jose, J.T., and, Gonzalez, J.J. (2018): A study on the durability of structural concrete incorporating electric steelmaking slags, Construction and Building Materials, vol. 161, pp. 94-111.

Schneider, U. (1988): Concrete at High Temperatures – A General Review, Fire Safety Journal, vol. 13, pp. 55-68.

Schutter, G., and, Taerwe, L. (1995): Specific Heat and Thermal Diffusivity of Hardening Concrete, Magazine of Concrete Research, vol. 47, no. 172, September, pp. 203-208.

Sekaran, A., Palaniswami, M. and, Balaraju, S. (2015): A Study on Suitability of EAF Oxidizing Slag in Concrete: An Eco-Friendly and Sustainable Replacement for Natural Coarse Aggregate, The Scientific World Journal, vol. 2015, Article ID 972567.

Sezer, G. I., and, Gülderen, M. (2015): Usage of steel slag in concrete as fine and/or coarse aggregate, Indian Journal of Engineering & Materials Sciences, vol. 22, June, pp. 339-344.

Shang, H.-S., and, Yi, T.-H. (2013): Freeze-Thaw Durability properties of Air-Entrained Concrete, The Scientific World Journal, vol. 2013, Article ID 650791.

Sherin, K., and, Jain, S. K. (2018): An Overview of Advantages and Disadvantages of Autoclaved Aerated Concrete, Proceedings of National Conference: Advanced Structures, Materials and Methodology in Civil Engineering, ASMMCE, November, pp. 35-39.

Shilstone, J. M. Sr. (1990): Concrete Mixture Optimization, Concrete International: Design and Construction, vol. 12, no. 6, June, pp. 33-39.

Shilstone, J. M. (1999): The Aggregate: The Most Important Value-Adding Component in Concrete, Proceedings, Seventh Annual International Center for Aggregates Research Symposium, Austin, Texas.

Shin, A.H-C., and, Kodide, U. (2012): Thermal conductivity of ternary mixtures for concrete pavement, Cement and Concrete Composites, vol. 34, pp. 575-582.

Sikora, P., Horszczaruk, E., Skoczylas, K., and, Rucinska, T. (2017): Thermal properties of cement mortars containing waste glass aggregate and nano silica, Procedia Engineering, vol. 196, pp. 159-166.

Sparks, P.R., and, Menzies, J.B. (1973): The effect of loading upon static and fatigue strength of concrete in compression, Magazine of Concrete Research, vol. 75, issue 83, pp. 73-80.

Sun, J., Feng, J., and, Chen, Z. (2019): Effect of Ferronickel Slag as Fine Aggregate on Properties of Concrete, Construction and Building Materials, vol. 206, pp. 201-209.

Tantawy, M.A. (2017): Effect of High Temperatures on the Microstructure of Cement Paste, Journal of Materials Science and Chemical Engineering, vol. 5, pp. 33-38.

Tokuda, H., and, Shoya, M. (1972): Thermal Diffusivity of Concrete as a Composite Material, Journal of the Society of Material Science, Japan, vol. 21, issue 230, pp. 1017-1023.

Torrent, R.J. (1992): A two-chamber vacuum cell for measuring the coefficient of permeability to air of the concrete cover on site, Materials and Structures, vol. 25, pp. 358-365.

Tufail, M., Shahzada, K., Gencturk, B., and, Wei. J. (2017): Effect of elevated temperature on mechanical properties of limestone, quartzite and granaite concrete,

International Journal of Concrete Structures and Materials, vol. 11, no. 1, March, pp. 17-28.

United States Environmental Protection Agency (EPA) (1970), https://www.epa.gov/.

Vickers, L., Pan, Z., Tao, Z., and, Riessen, A.V. (2016): In situ elevated temperature testing of fly ash based geopolymer composites, Materials, special issue-Advances in Geopolymers and Alkali-Activated Materials, 9(6), 445.

Vidha, K., Dhilipkumar, R. (2015): An Experimental Investigation on Strength Characteristic of High Density Concrete Incorporating Hematite, International Journal for Innovation Research in Science and Technology, Vol-2, Issue-7.

Washa, G.W. (1998): Concrete Construction Handbook, J. McGraw-Hill, 4th ed., New York.

William, K., Xi, Y., Lee, K., and, Kim. B. (2009): Thermal Response of Reinforced Concrete Structures in Nuclear Power Plants, Structural Engineering and Structural Mechanics Report -02, University of Colorado at Boulder.

World Business Council for Sustainable Development (WBCSD) (1990), https://www.wbcsd.org/.

World Steel in Figures, World Steel Association (WSA), https://www.worldsteel.org/.

www.gom-correlate.com

Xu, Y. and, Chung, D.D.L. (2000): Cement of high specific heat and high thermal conductivity, obtained by using silane and silica fume as admixtures, Cement and Concrete Research, vol. 30, pp. 1175-1178.

Yang, Y., Raipala, K., Holappa, L. (2014): Treatise on Process Metallurgy, vol. 3, pp. 2-88.

Zaitsev, Y.B.,and, Whittmann, F.H. (1981): Simulation of crack propagation and failure of concrete, Materials and Structures, vol. 14, no. 83, pp. 357-365.

Zhang, B. (2011): Effects of moisture evaporation (weight loss) on fracture properties of high performance concrete subjected to high temperatures, Fire Safety Journal, vol. 46, pp. 543-549.

Zhang, B., Bicanic, N., Pearce, C.J., and Balabanic, G. (2000): Residual fracture properties of normal-and-high-strength concrete subject to elevated temperatures, Magazine of Concrete Research, vol. 52, issue-2, pp. 123-136.

Zhang, J., and, Scherer, G. W. (2011): Comparison of methods for arresting hydration of cement, Cement and Concrete Research, vol. 41, pp. 1024-1036.

Zhang, S.P., and, Zong, L. (2014): Evaluation of Relationship between Water Absorption and Durability properties of Concrete Materials, Advances in Materials Science and Engineering, vol. 2014, Article ID 650373.

Zheng, J., and, Hryciw, R. D. (2016): Index Void Ratios of Sands from Their Intrinsic Properties, Journal of Geotech. Geoenviron. Eng., American Society of Civil Engineers, vol. 142(12).